December 2019

Controlling and Manipulating Microscopic Particles in Solution By Using Various Electric Field Geometries

Xavier Sacro Udad
University of Wisconsin-Milwaukee

CONTROLLING AND MANIPULATING MICROSCOPIC PARTICLES IN SOLUTION BY

USING VARIOUS ELECTRIC FIELD GEOMETRIES

by

Xavier S. Udad

A Dissertation Submitted in

Partial Fulfillment of the

Requirements for the Degree of

Doctor of Philosophy

in Chemistry

at

The University of Wisconsin-Milwaukee

December 2019

ABSTRACT

CONTROLLING AND MANIPULATING MICROSCOPIC PARTICLES IN SOLUTION BY
USING VARIOUS ELECTRIC FIELD GEOMETRIES

by

Xavier S. Udad

The University of Wisconsin-Milwaukee 2019
Under the Supervision of Jörg C. Woehl

Progress in micro- and nanotechnologies depends on our capability of manipulating and
interacting with microscopic particles and nanosize material. A promising approach
towards this goal is the use of electric fields, which are the dominant forces at the
molecular length scale. One technique for trapping nanoparticles in solution uses an
externally controlled electric field, generated by two electrode pairs, to counteract the
Brownian motion of a single, selected particle. Unlike other trapping tools, such as optical
tweezers or magnetic tweezers, this approach scales favorably with particle size, down
to the level of a single molecule. However, it depends on real-time position information
from fluorescence imaging and requires a fast, well-calibrated feedback system. The
approach taken in this thesis does not rely on this kind of external control; rather, we use
geometric patterns (corral traps) "etched" into an otherwise conductive layer to create
energy wells that are capable of trapping micro- and nanoscale particles as long as an
electric voltage is applied to the device. These energy wells create a stable trapping
potential that can keep a particle confined without the need for a feedback system. The

main trapping forces are either electrostatic or dielectrophoretic in nature, depending on whether DC or AC voltages are applied to the corral trap electrode. We investigate the influence of the geometric shape of the electric field on the electrostatic and dielephoretic trapping behavior of charged and uncharged polarizable particles, and compare the experimental results to finite-element simulations of the electrostatic and dielectrophoretic forces generated by different experimental setups and various symmetric and asymmetric metal patterns. Also, the influence of electric field-induced flow patterns in solution, such as electro-osmosis, are investigated theoretically. Aside from pure trapping, i.e. confinement of particles to the low-energy regions, we find that particles can also be manipulated to move in a particular direction, follow pathways or trails, diverge in different directions, converge in one direction, make 90° turns, and even perform circular loops by utilizing various shapes and patterns on a metal surface.

TABLE OF CONTENTS

LIST OF FIGURES

xvii

LIST OF ABBREVIATIONS

ABEL   anti-Brownian electrophoretic trap

AC   alternating current

DC   direct current

DNA   deoxyribonucleic acid

TMV   tobacco mosaic virus

UV   ultra-violet light

LIST OF SYMBOLS

k	Spring constant
k_B	Boltzmann's constant
ε_o	Vacuum permittivity
ε	Permittivity of substance
σ	Conductivity
U	Potential energy
ω	AC frequency
E	Electric field
Φ	Electric flux
q	Charge
ρ	Density
μ	Viscosity
F	Faraday's constant
R	Gas constant

ACKNOWLEDGEMENTS

This thesis is dedicated to my parents, for always believing in me.

Chapter 1

Introduction

1.1 History

There is a certain limit to the smallest object the human eye can see unaided, which is roughly 100 microns. This can be overcome with the use of microscopes. The microscope is an iconic scientific instrument used in making observations of systems that are too small for normal observation. While most words in the English language are derived from Latin, the word "micro" is actually Greek for "small" and the word "scope", also Greek, means "to look". For most of his existence, man was unaware of a world that existed just beyond the limits of his vision. As with all scientific progress, knowledge and insight proceeds in stages that build on each other. Below is a timeline of some key events in the development of the microscope.

2nd Century BC - Claudius Ptolemy described a stick appearing to bend in a pool of water, and accurately recorded the angles to within half a degree. This marks the first recorded study of refraction[1].

1st Century - Romans were experimenting with glass and found objects appeared larger when viewed through this new material[2].

12th Century - Salvino D'Armate from Italy made the first eye glass, providing the wearer with an element of magnification to one eye. However, whether D'Armate actually was the first eye glass maker is under dispute[3].

1590 - Two Dutch spectacle makers, Zacharias Jansen and his father Hans started experimenting by mounting two lenses in a tube, the first compound microscope[4].

1665 - Robert Hooke's book called *Micrographia* officially documented a wide range of observations through the microscope[5].

With the invention of the microscope, an entirely new level of reality was discovered. The first impulses were to simply observe. One such man was Robert Hooke. His book, Micrographia, must have seemed like an entirely alien world to the people of the time. It was the first significant work on microscopy.
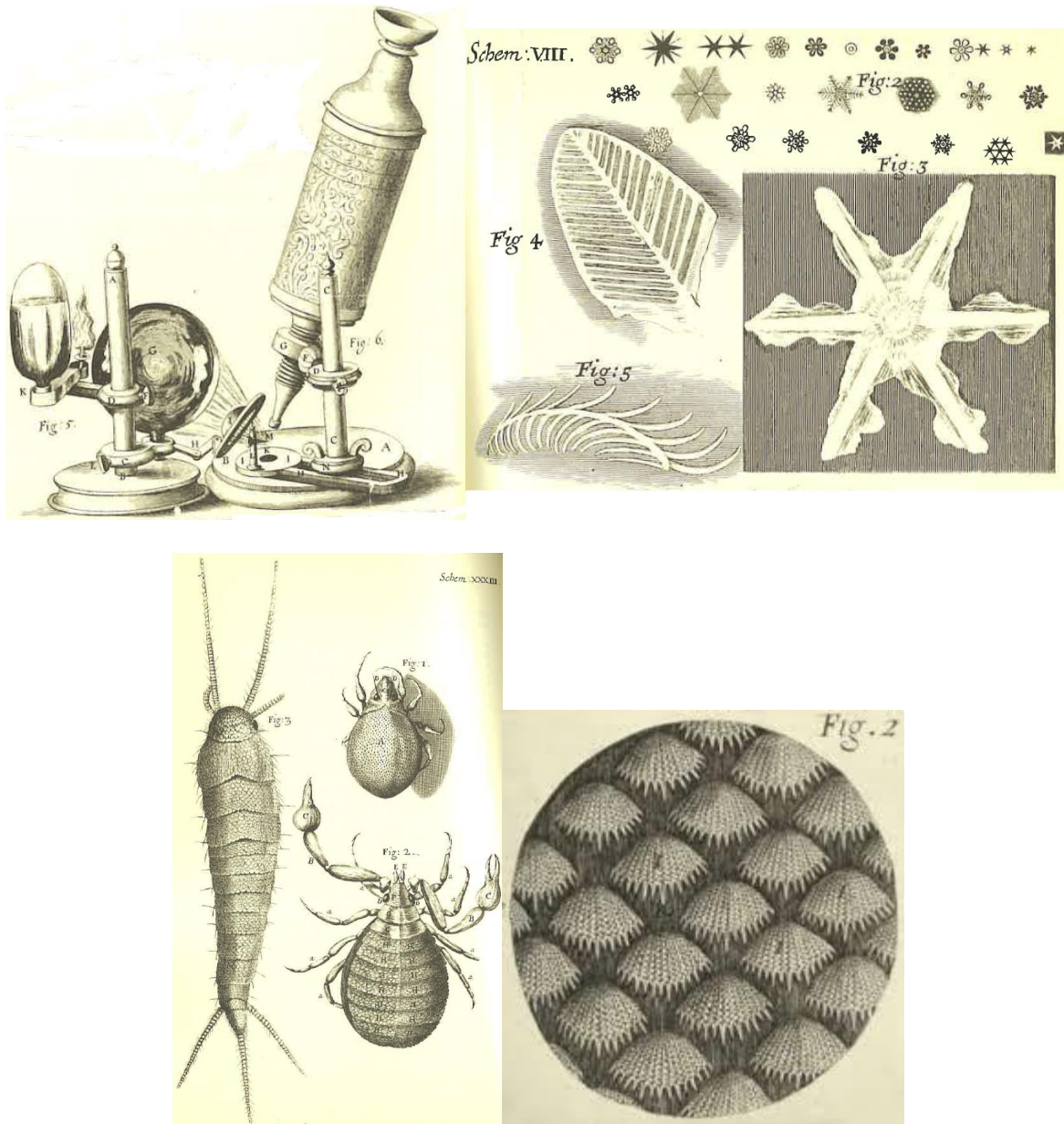
Figure 1.1 – Illustration of the microscope used by Robert Hooke and some of his observations[5].

Figure 1.2 – Image of Clarkia pulchella pollen[6, 7].

In 1827, a botanist by the name of Robert Brown observed a species of pollen, *Clarkia pulchella*, under a microscope[6]. The pollen displayed random erratic movements. Brown's initial thoughts were that it was due to some type of stamina or life force inherent to the pollen. Today we know that the erratic movement of microscopic particles in solution is due to the constant collisions of water molecules with the particle, which is appropriately called Brownian motion. Robert Brown made many important contributions to the science of botany. He contributed additional work on pollination and fertilization, taxonomy, physiology, and palynology. There was some contention as to whether Robert Brown was actually capable of seeing microscopic pollen[8]. But the contention was appropriately refuted with a convincing demonstration of the available optics of the time[9].

In 1909, Jean Baptiste Perrin mapped out the exact movements of more than 200 individual particles by hand[11]. He determined the motion was not due to the mass, density, or nature of the particles. He corroborated Albert Einstein's theoretical explanation of Brownian motion[10] which helped to solidify the idea of the particle nature of matter. Jean Baptiste Perrin won the Nobel Prize in 1926 in physics for his work on the discontinuous structure of matter. Now, in the modern age, man attempts to actually control and manipulate these microscopic particles. It is a significant leap from trying to control microscopic particles to trying to control nanoscopic particles, but it has been done.
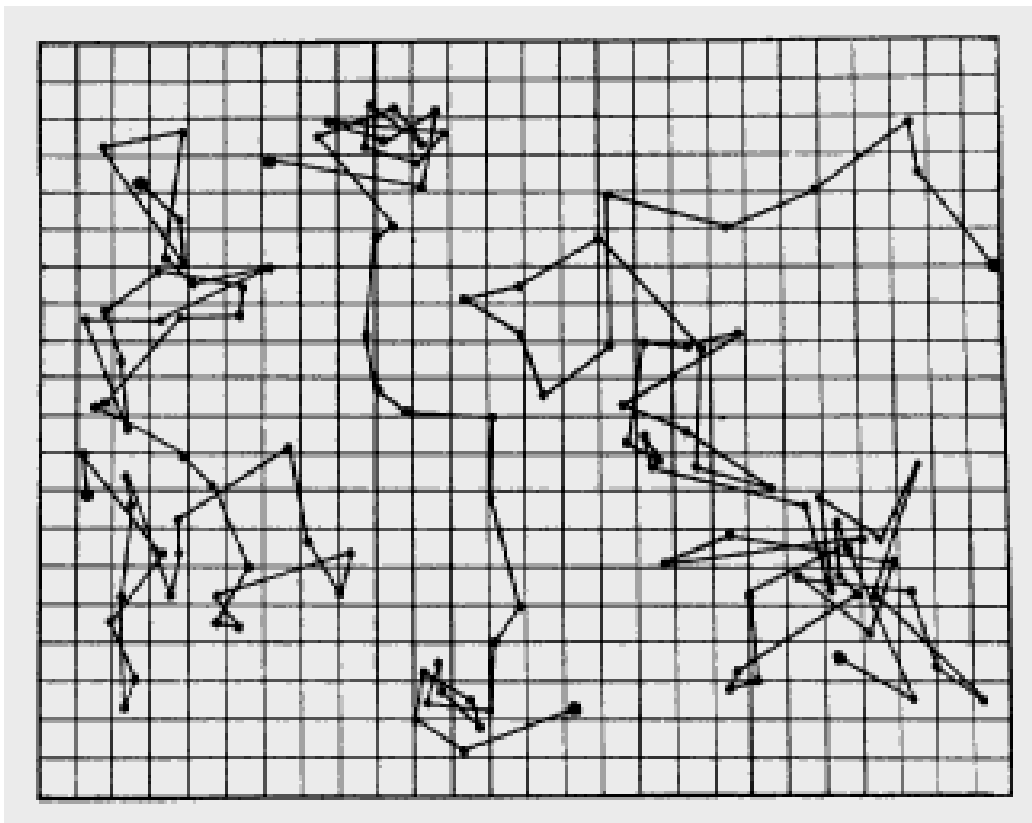
Figure 1.3 – Particle tracking performed by Jean Baptiste Perrin, painstakingly done by hand. The dots represent the particle positions at 30 second intervals. The radius of the particle is 0.52 microns. One division is 3.125 microns[11].

There are a few methods that enable interaction with single molecules; among them are microneedles, which can be used to measure the tensile strength of protein filaments[12], and atomic force microscopy, which combines the principles of the scanning tunneling microscope and a stylus profilometer[13]. The following sections will cover two methods for trapping particles, the ABEL trap and optical tweezers. The reason these two methods are covered is because they are most closely related to the method of manipulation used in this thesis.

1.2 The ABEL Trap

The ABEL trap, or anti-Brownian electrophoretic trap, was developed by Adam E. Cohen and W. E. Moerner in 2005[14]. It is composed of two pairs of electrodes, making a total of four electrodes, that are oriented in a "+" shape.
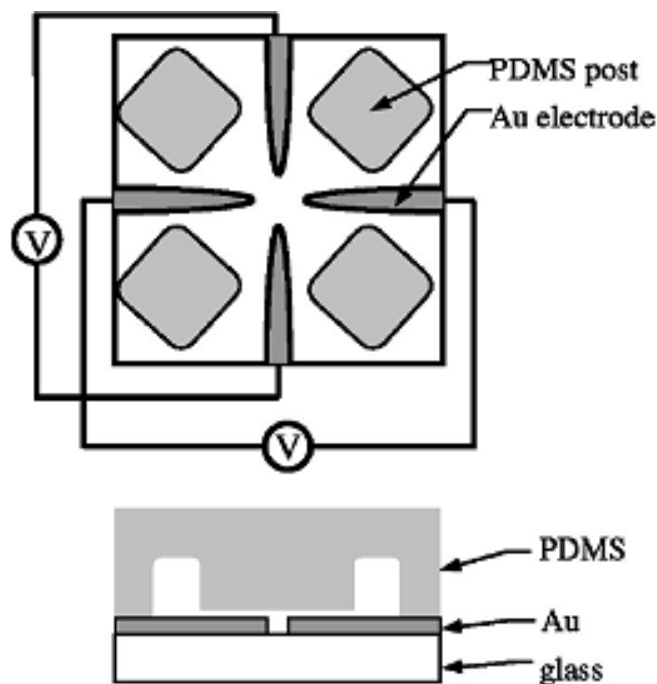
Figure 1.4 – A top view schematic of the ABEL trap and its view from the side[14].

6

The two electrodes of one pair are collinear, while the two pairs are perpendicular to each other and are integrated into two separate circuits that are independent of each other. Even though they are independent of each other, the two pairs of counter electrodes are programmed to work cooperatively. The spacing between one pair of counter electrodes can range from 3 to 15 micrometers. This configuration is capable of trapping a single charged nanoscale object with nanoscale resolution.

The general idea of the ABEL trap is electrophoresis which utilizes DC, direct current. When a voltage is applied to two electrodes immersed in solution, negatively charged particles migrate towards the positive electrode while positively charged particles migrate towards the negative electrode.
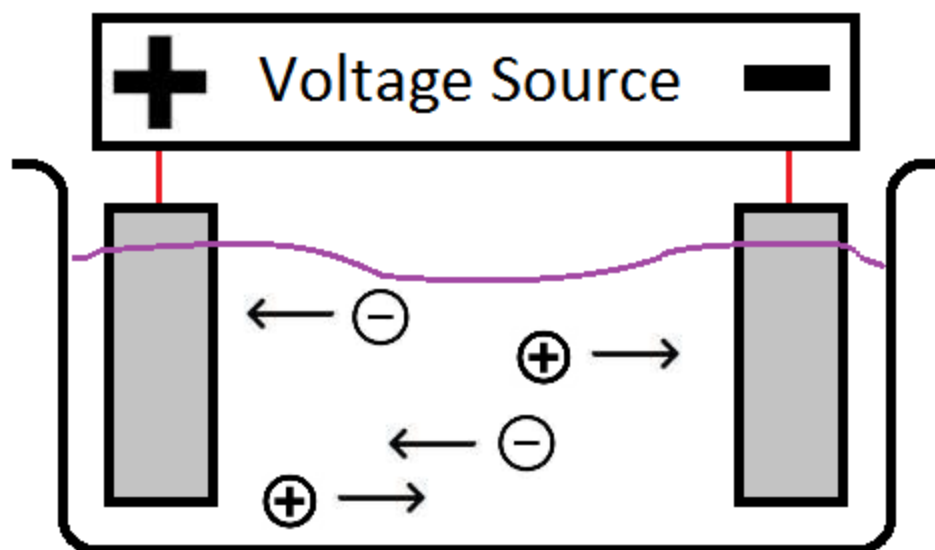
Figure 1.5 – The principle of electrophoresis. First observed in 1930 by Arne Tiselius[15].

When the sign of the voltage is switched, the polarity of the electrodes switch as well and a particle can change directions. Another pair of electrodes is implemented to

allow control of a particle in two dimensions instead of one. The charged particle is localized through its fluorescence signal and its physical location is continuously monitored. When a particle deviates from the center of the ABEL trap, an appropriate voltage is applied to exactly counteract the displacement of the particle and bring it back to the center. There are instances when no voltage is applied to either pair of electrodes while the system waits for appropriate information regarding the location of the particle. There are also instances when the sign of the voltage to one of the electrode pairs is switched. The amount of variables that must be controlled or known are quite extensive. Both the mass of the particle and the charge on the particle must be taken into account in order to apply the correct voltage. The ionic strength of the solution that the particle is in could potentially shield the particle from the effects of the electric fields which the electrodes generate. Since the particle is charged, it will primarily be surrounded by ions of the opposite charge. This primary shielding layer of ions will then be surrounded by another more diffuse layer of oppositely charged ions that are the same charge as the original particle. The feedback system has inherent timing, electrical, and circuit delays. These are the types of factors that must be taken into account with regards to the programming of the system. One of the disadvantages of the ABEL trap is that there is no control of the particle on the vertical axis, the particle is free to move up and down. As long as a charge can be conferred on a particle, it can be trapped with this method.
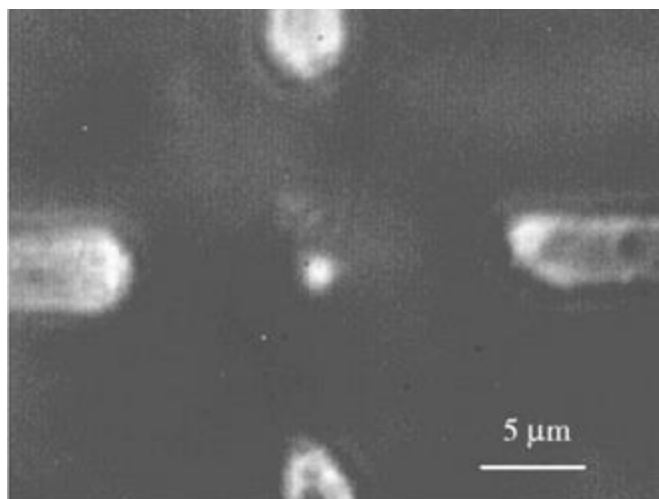
Figure 1.6 – Trapping of a 200 nanometer diameter particle under fluorescence imaging[14].

One of the more interesting experiments performed with the ABEL trap involved mannipulating the trajectory of a 200 nanometer diameter particle over the course of a minute; a total of 1800 positions were recorded as shown in Figure 1.7. Two of the data points that joined the eyes and mouth are not plotted.

Figure 1.7 – Trajectory of a particle manipulated to draw out a smiley face[14].

Despite the casual whimsy of manipulating a nanoparticle to travel the trajectory of a smiley face with a complicated programmed system of electrodes, circuits, microscopes, camera monitoring, and a continuous feedback loop, the implications of the figure are immense. This indicates that, with four electrodes, one can actually move the particle to a specific location and keep it there in the general area as long as it is within the confines of the four electrode system. It is not necessary to keep the particle in the center. If desired, the particle can be continuously confined off center. The particle can be kept in one location for a certain amount of time and then moved to another location and kept there as well. The velocity of the particle, when it is moved to a new location, can also be controlled. The particle can be made to move slowly or quickly to the new location depending on the magnitude and duration of the applied voltage. This is a very high degree of control and manipulation in the horizontal plane[14]. The ABEL trap has been used to study the photodynamics of fluorophores[16], conformational dynamics of proteins[17], and characteristics such as diffusivity and mobility of molecules[18].

1.3 Optical Tweezers

Another method for trapping micro or nano-particles is the use of optical tweezers[19]. The name of this method is somewhat misleading. A tweezer is a tool that is basically two curved levers connected together at one fixed end. The two ends that are not connected can be used to manipulate or pick up small objects. An optical tweezer is a single beam of light, not two beams of light as one might suspect, that can only trap one very particular type of particle; so this trapping method is highly limited, more so than the ABEL trap. This very particular type of particle must have some degree of transparency

and must have the ability to scatter light such as a microscopic glass sphere. There are also limits to the size of the particle this method can trap. Smaller particles require higher laser powers for stable trapping, which often leads to undesired local heating. Silica particles as small as 26 nm have been successfully trapped, but required 1.4 W of laser power. More typically, optical trapping is performed with microbeads in the micrometer range[19]. Trapping can also be affected by the degree of difference of the index of refraction of the particle relative to the index of refraction of the solution. However unlike the ABEL trap, the particle is not required to have a charge[19].
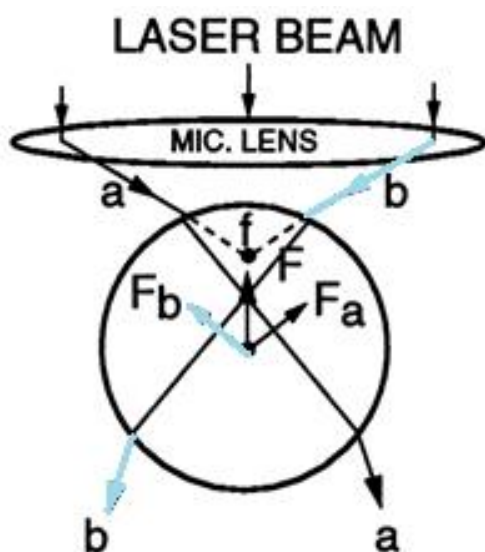
Figure 1.8 – Ray optics for the single-beam gradient force trap (optical tweezers). Small f is the focus of the laser. Small a and small b represent vectors of light that become refracted as they enter the particle and leave the particle. F_a and F_b represent the change in momentum of the particle. Large F is the resultant upward force of both F_a and F_b combined[23].

A laser beam is aligned through a focusing lens and an optically active particle is located at the focal point of the lens. Trapping results from the transfer of momentum of light photons as they pass through the particle. The orange billiard in Figure 1.9

corresponds to a quantity of photons of light and the billiard they collide with is the trapped particle. There are a few minor reflections that diminish the momentum transferred to the trapped particle by the light photons and the resultant angles are slightly different from the resultant angles of billiard balls colliding. There is also a significant difference in mass between the particle and light photons, but the three main vectors should adequately convey the idea.
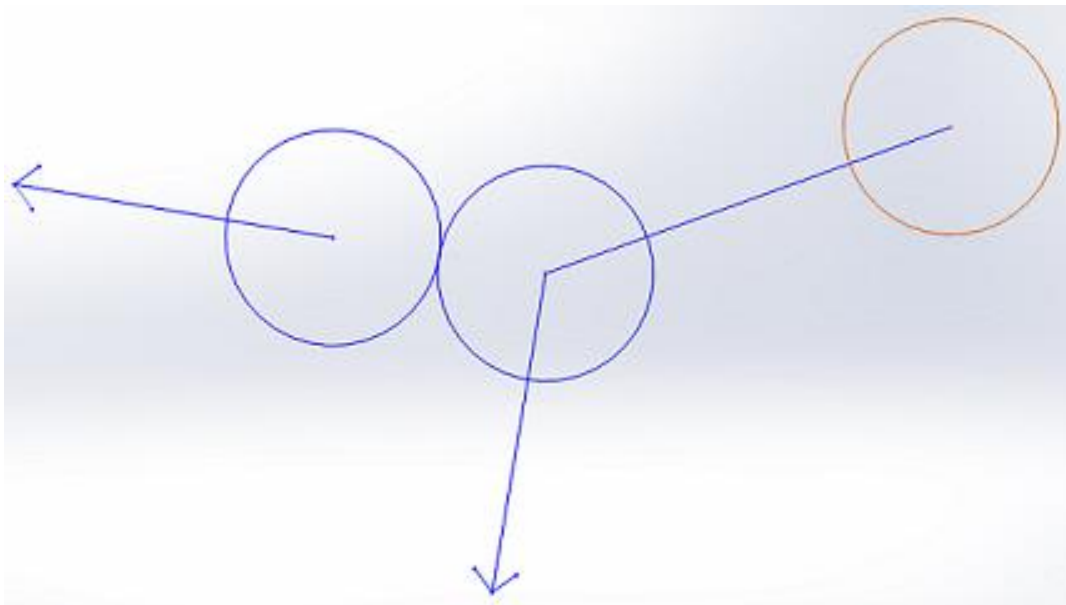
Figure 1.9 – How momentum is transferred and redirected with billiard balls. The orange circle represents the original position of one of the two billiards.

Since the incident beams of light coming from the laser are symmetric in all directions from the point of view of the trapped particle along the z axis, the overall force vector exerted on the particle is straight up towards the direction of light from the incoming laser beam.
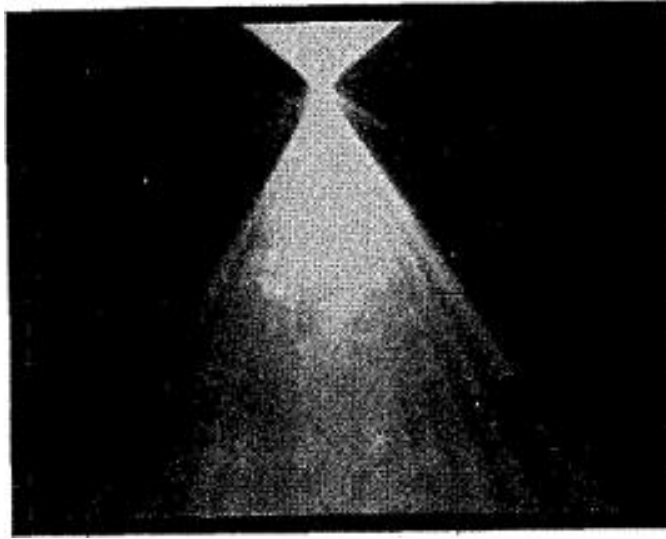
Figure 1.10 – Fluorescence imaging of a trapped 10 micrometer sphere in solution, showing the path of both incident and scattered light rays[19].

Some of the crucial factors for successful trapping are the index of refraction of the particle, the index of refraction of the medium, the wavelength of the source beam, the size of the focal spot of the beam, and the trapping laser's intensity. Possibly the most important factor to consider in the use of optical tweezers is the size of the particle itself. There are two particle regimes. A Rayleigh particle is a particle whose diameter is much smaller than the wavelength of light being used, while a Mie particle is a particle whose diameter is larger than the wavelength of light being used[20]. Optical trapping has advanced significantly and can now be used for nanofabrication[21] and simultaneous use of multiple optical traps is also being done[22]. One field that has benefitted from optical tweezers is biology. The use of infrared lasers significantly reduces trapping damage to biological cells to the point where the cells can even reproduce[24]. It has been used to elucidate the biomechanics of flagellar bacteria[25], and even to measure the force-extension relation of a DNA strand by linking one end of the strand to a glass substrate and the other end to a microscopic bead[26].

Another way to control and manipulate microscopic particles is to use various electric field geometries. These electric field geometries can be produced with thin metal layer patterns that are created with a technique known as lithography. Since the system involves very small solution quantities, microfluidics also play a factor. That is the focus of this thesis.

References for Chapter 1

1.   Mark A. Smith, *Ptolemy's Theory of Visual Perception – An English Translation of the Optics*, 1996, American Philosophical Society

2.   E. Marianne Stern, "Roman Glassblowing in a Cultural Context", 1999, *American Journal of Archaeology*, Vol 103, No 3, Pages 441-484

3.   Edward Rosen, "The Invention of Eyeglasses", 1956, *Journal of the History of Medicine and Allied Sciences*, Vol XI, issue 1, Pages 13-46

4.   lbert Van Helden, Sven Dupre, Rob van Gent, *The Origins of the Telescope*, 2010, Amsterdam University Press

5.   Robert Hooke, *Micrographia or Some Physiological Descriptions of Minute Bodies Made by Magnifying Glasses with Observations and Inquiries Thereupon*, 1665, The Royal Society, London

6.   Robert Brown, "A Brief Account of Microscopical Observations", 1827, The Royal Society of Denmark

7.   Philip Pearle, Brian Collett, Kenneth Bart, David Bilderback, Dara Newman, Scott Samuels, "What Brown Saw and You Can Too", 2010, *American Journal of Physics*, Vol 78, Issue 12, Pages 1278-1289

8.   Deutsch, D. H. "Did Robert Brown Observe Brownian Motion: Probably Not", 1991, *Scientific American*, 265:20

9.   Brian J. Ford, "Robert Brown, Brownian Movement, and Teethmarks on the Hatbrim", 1991, *The Microscope*, Vol 39, Pages 161-171

10. Albert Einstein, "Investigations on the theory of the Brownian Movement", 1926, Dover Publications

11. Jean Baptiste Perrin, *Annales de Chimie et de Physique*, 8th Series, September 1909, Ox Bow Press

12. Akiyoshi Kishino, Toshio Yanagida, "Force Measurements by Micromanipulation of a Single Actin Filament by Glass Needles", 1988, *Nature*, Vol 334, Pages 74-76

13. G. Binnig, C. F. Quate, "Atomic Force Microscope", *Physical Review Letters*, Vol 56, No 9, Pages 930-933

14.   Adam E. Cohen, W. E. Moerner, "Method for Trapping and Manipulating Nanoscale Objects in Solution", 2005, *Applied Physics Letters*, Vol 86, Issue 9, Pages 093109-1 to 093109-3

15.   Arne Tiselius, "The Moving Boundary Method of Studying the Electrophoresis of Proteins", 1930, *Inaugural Dissertation Upsala*

16.   Quan Wang, W. E. Moerner, "Lifetime and Spectrally Resolved Characterization of the Photodynamics of Single Fluorophores in Solution Using the Anti-Brownian Electrokinetic Trap", 2013, *Journal of Physical Chemistry*, Vol 117, No 16, Pages 4641-4648

17.   Samuel Bockenhauer, Alexandre Furstenberg, Xiao Jie Yao, Brian K. Kobilka, W. E. Moerner, "Conformational Dynamics of Single G Protein-Coupled Receptors in Solution", 2011, *Journal of Physical Chemistry*, Vol 115, No 45, Pages 13328-13338

18.   Quan Wang, W. E. Moerner, "An Adaptive Anti-Brownian Electrokinetic Trap with Real-Time Information on Single-Molecule Diffusivity and Mobility", 2011, *ACS Nano*, Vol 5, No 7, Pages 5792-5799

19.   A. Ashkin, J. M. Dziedzic, J. E. Bjorkholm, Steven Chu, "Observation of a Single-Beam Gradient Force Optical Trap for Dielectric Particles", 1986, *Optics Letters*, Vol 11, No 5, Pages 288-290

20.   Maria Dienerowitz, Michael Mazilu, Kishan Dholakia, "Optical Manipulation of Nanoparticles: A Review", 2008, *Journal of Nanophotonics*, Vol 2, Pages 1-32

21.   David G. Grier, "A Revolution in Optical Manipulation", 2003, *Nature*, Vol 424, Pages 810-816

22.   Jeffrey R. Moffitt, Yann R. Chemla, Steven B. Smith, Carlos Bustamante, "Recent Advances in Optical Tweezers", 2008, *Annual Review of Biochemistry*, Vol 77, Pages 19.1-19.24

23.   Arthur Ashkin, "Optical trapping and manipulation of neutral particles using lasers", 1997, *Proceedings of the National Academy of Science*, Vol 94, Pages 4853-4860

24.   A. Ashkin, J. M. Dziedzic, T. Yamane, "Optical trapping and manipulation of single cells using infrared laser beams", 1987, *Nature*, Vol 330 (24/31), Pages 769-771

25.   Richard M. Berry, Howard C. Berg, "Absence of a barrier to backwards rotation of the bacterial flagellar motor demonstrated with optical tweezers", 1997, *Proceedings of the National Academy of Science*, Vol 94, Pages 14433-14437

26.   Michelle D. Wang, Hong Yin, Robert Landlick, Jeff Gelles, Steven M. Block, "Stretching DNA with Optical Tweezers", 1997, *Biophysical Journal*, Vol 72, Pages 1335-1346

Chapter 2

Theory of Electrostatic and Dielectrophoretic Trapping

2.1 Electric Fields

Electromagnetism is the study of electricity and magnetism. At one point, they were thought of as being separate phenomena. In 1873, James Clerk Maxwell showed that electricity and magnetism are actually different manifestations of the same phenomenon[1]. He summarized electricity and magnetism in four simple, yet very elegant, equations. Maxwell's four equations unify the behavior of electric and magnetic fields[2]. For this thesis, only one of Mawell's equations is necessary; that being Gauss's Law, which describes the behavior of electric fields.

An electric field exerts a force on any object that has an electrical charge. If an object has no charge, it is not affected by an electric field. Electric fields are generated by single charges or charged objects or charged surfaces. An electric field exerts a force on a charge[15].

$$\vec{F} = q \cdot \vec{E}$$

q is a test charge placed in a location where the field is $\vec{E}$. The force exerted on the charge is the product of the charge and the electric field. This is the electric field's most useful property since forces can be used to push or pull, repulse or attract, an object. In this case, an electric field can push or pull an object with a charge. This property can also be used to derive Coulomb's Law. The field manifests itself as a force that pushes or pulls an object which has a charge.

To calculate an electric field, electric flux has to be defined[3].

$$\Phi \equiv \oint_S \vec{E} \cdot d\vec{A}$$

Φ is the electric flux, which can be thought of as the "flow" of the electric field through a closed surface S. $\vec{E}$ is the electric field and $d\vec{A}$ is an element of the surface S, defined as having a magnitude equal to the surface element's area and having a direction pointing outward and perpendicular to the surface element. Note that both $\vec{E}$ and $\vec{A}$ are vector quantities. Figure 2.1 shows electric field lines that are perpendicular to a surface.
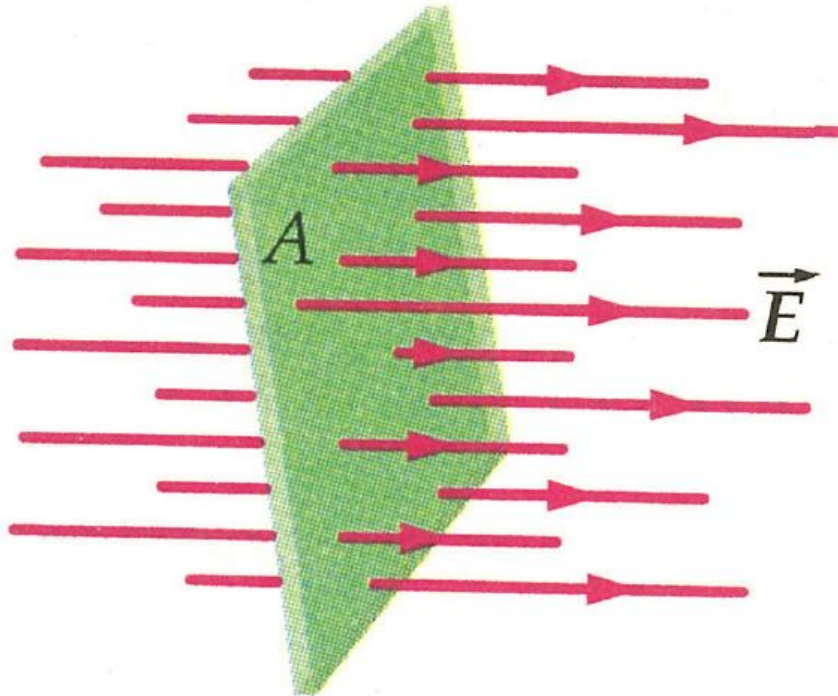
Figure 2.1 – Electric field lines of a uniform field that are perpendicular to the surface area A. The product is the electric flux through the surface[15].

Gauss's Law is

$$\Phi = \frac{\Sigma q}{\epsilon_0}$$

Σq is the sum of all charges enclosed within the surface S and ϵ_0 is the constant of vacuum permittivity, which is 8.85×10^{-12} F/m (Farad per meter). The two equations can then be set equal to each other.

$$\oint_S \vec{E} \cdot d\vec{A} = \frac{\Sigma q}{\epsilon_0}$$

2.2 Simple Electric Field Systems

The simplest example of an electric field is the field surrounding a single point charge. The field has spherical symmetry and only depends on the distance to the point charge.
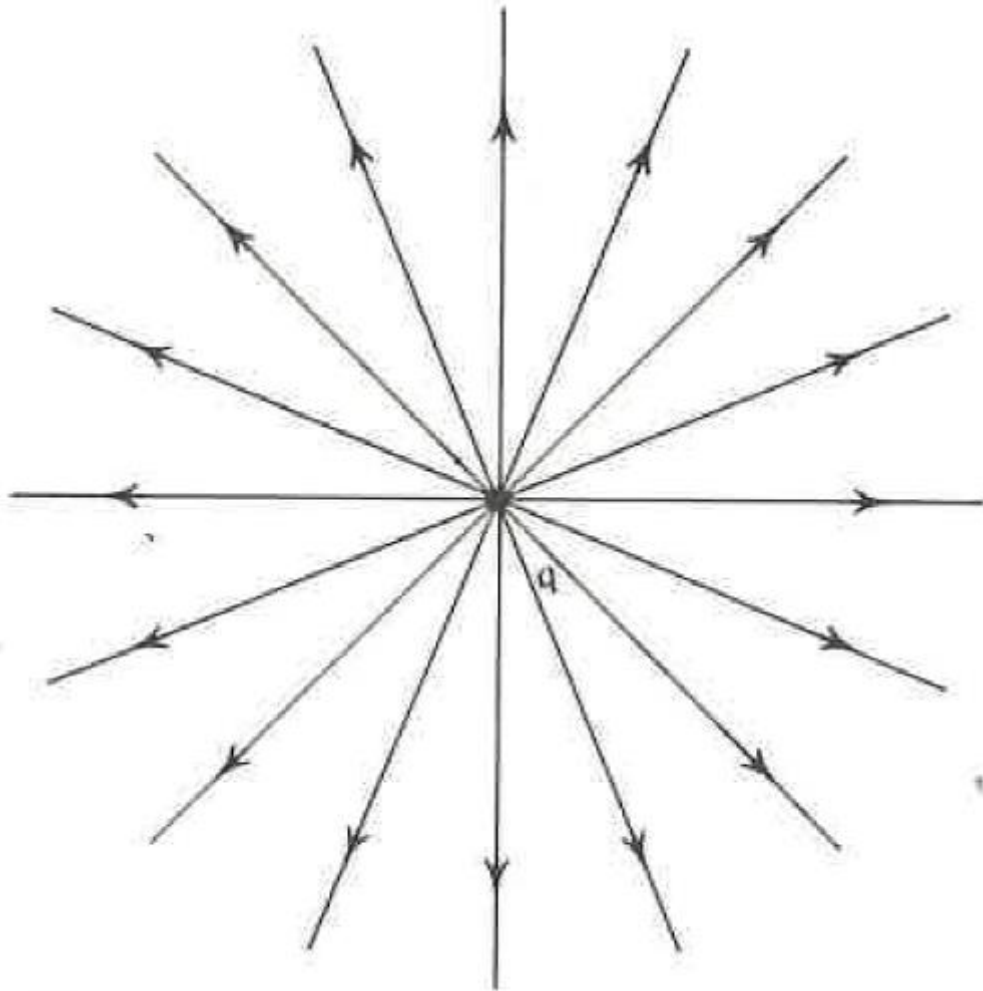
Figure 2.2 – Electric field generated by a single point charge. The field lines represent the force of attraction or repulsion generated by the single point charge q in the center[4].

To calculate the electric field at the location of the red dot in Figure 2.3 requires an application of Gauss's Law. The first step is to decide on an appropriate Gaussian surface. In this example, a sphere, with a radius that is equal to the distance of the red dot from the center would be appropriate as it allows us to make use of the symmetry of the system.
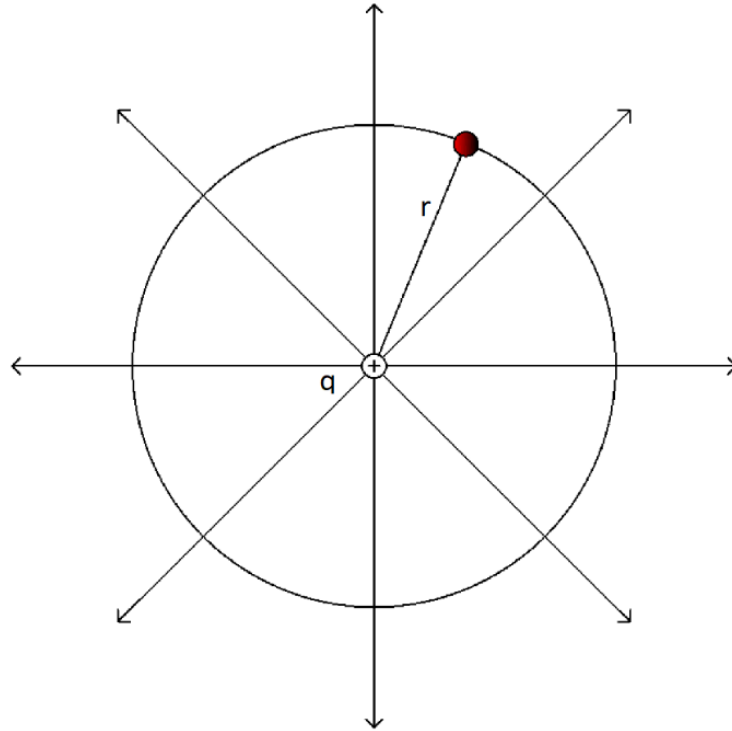
Figure 2.3 – A spherical Gaussian surface imposed on an electric field of a single point charge. The red dot represents the point where the electric field is calculated.

Even though both $\vec{E}$ and $\vec{A}$ are vector quantities, they both point in the same direction, namely outward from the center in all directions. In essence, the vectors are parallel and can be treated as scalar quantities since the relative angle between the two vectors is zero.

$$\oint_S E\, dA = \frac{\Sigma q}{\epsilon_0}$$

For reasons of symmetry, the electric field has the same magnitude at equal distances from the center. Therefore E can be treated as a constant and can be taken out of the integral. Since there is only one point charge, Σq is equal to q.

$$E \oint_S dA = \frac{q}{\epsilon_0}$$

This leads to

$$E A = \frac{q}{\epsilon_0}$$

Since the Gaussian surface is a sphere, the surface area of a sphere is $4\pi r^2$.

$$E \, 4\pi r^2 = \frac{q}{\epsilon_0}$$

The equation is then solved for E, the electric field.

$$E = \frac{q}{4\pi\epsilon_0 r^2}$$

Coulomb's Law, which describes the force that repels or attracts two particles that have an electrical charge, can then be expressed simply by factoring in the charge of a second particle[5].

$$F = \frac{q_1 q_2}{4\pi\epsilon_0 r^2}$$
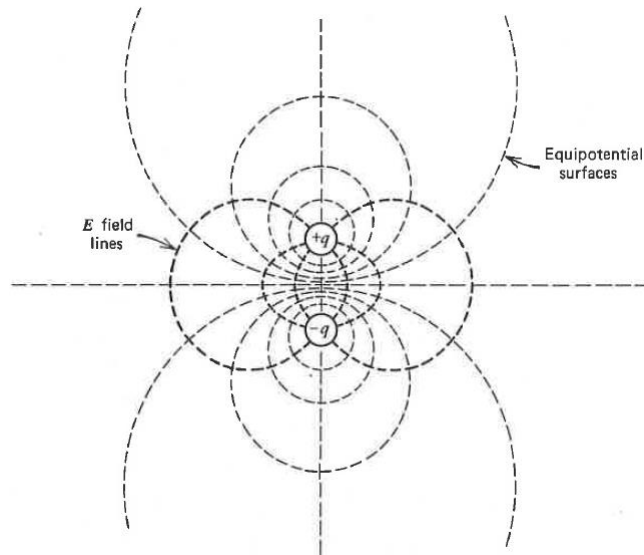
Figure 2.4 – Electric field lines and equipotential surfaces of two point charges[6].

The figure above shows the electric field lines of the simplest Coulombic system, two point charges separated by a certain distance. Despite being considered a simple system, the field lines and equipotential surfaces have a certain degree of complexity.

The figure below is the electric field for a parallel plate capacitor. In the center of the plates, away from the edges, the field lines are parallel and uniform. There are edge effects which distort the field at the edges of the parallel plates, making the field lines non-parallel and non-uniform[7].
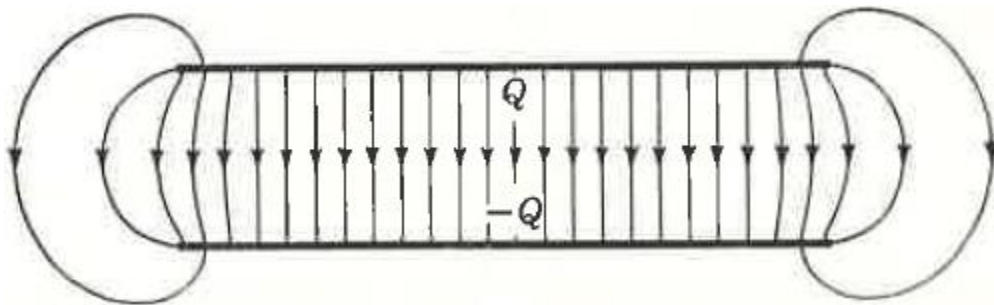
Figure 2.5 – The electric field of a parallel plate capacitor with edge effects[8].

In the figure below, the field lines actually extend to the surface of the opposite plate, they are drawn with a shorter length to indicate the direction of the field. An appropriate Gaussian surface for this system would be a cylinder, as it allows us again to exploit the symmetry of the field for its calculation.
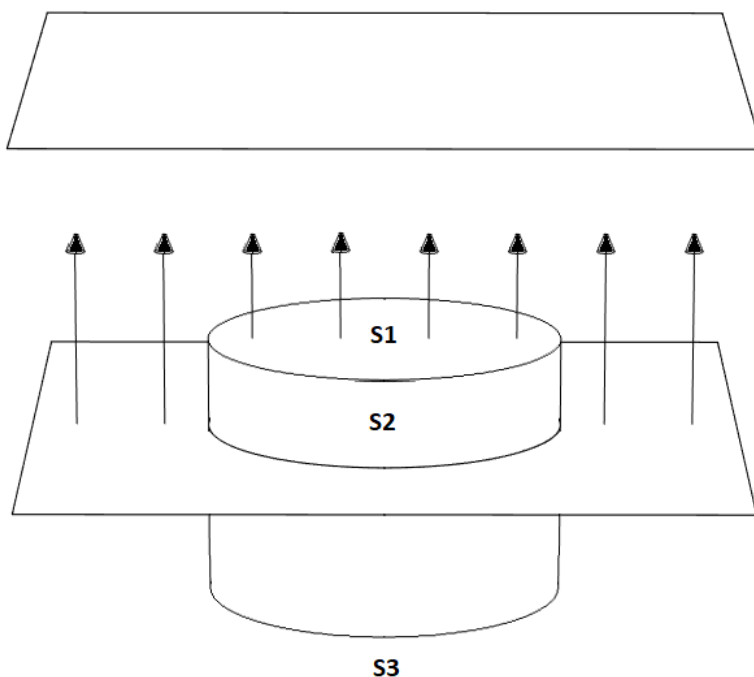
Figure 2.6 – A parallel plate capacitor with a cylinder as a Gaussian surface. While the parallel plates are depicted as finite, they actually extend to infinity. Only then can edge effects be completely ignored.

The cylinder has three surfaces labelled as S1, S2, and S3. S3 is simply the circular face of the cylinder opposite S1. The electric field at surface S3 is zero because it's not between the two plates. The electric field at surface S2 is also zero because any element $d\vec{A}$ on the surface of S2 is perpendicular to the direction of the electric field. Surface S1 is the only part of the cylinder that experiences an electric field. Surface S1 is a circular disk with a quantity of charges on it, we can define Σq as σ*A*, where σ is the

26

surface charge density and *A* is the area of the circular disk. The electric field and the

surface element vector d$\vec{A}$ are in the same direction, vector notation can be dropped.

$$\oint_S E\,dA = \frac{\sigma A}{\epsilon_0}$$

Since the electric field is the same at all points on the Gaussian surface and edge

effects are ignored since the parallel plates extend to infinity, *E* can be treated as a

constant and taken out of the integral.

$$E \oint_S dA = \frac{\sigma A}{\epsilon_0}$$

Integration leads to

$$E\,A = \frac{\sigma A}{\epsilon_0}$$

which simplifies to

$$E = \frac{\sigma}{\epsilon_0}$$

This result is the electric field of a parallel plate capacitor anywhere between the

two plates.

2.3 Finite Element Methods

Electric fields can also be calculated by solving Maxwell's equations numerically using the finite element method. One such program that uses the finite element method is COMSOL[9]. It is a physics simulation program capable of modelling numerous physical phenomenon such as mechanics, acoustics, fluid flow, heat transfer, etc. It is most widely used by engineers as it enables quick prototype simulation. It can be used to predict behavior of a theoretical system[10] or it can be used to model the behavior of a system that has already been observed experimentally. Using COMSOL to predict behavior is one of its best uses. This enables scientists and engineers to design systems theoretically first. And based on the results, the decision can be made whether or not to proceed with actually building the system. COMSOL performs calculations by using "meshes". Meshes are simply the sizes and the shapes that COMSOL overlays on the system's geometry in order to perform its calculations. Mesh size can be very large, these give the quickest results but are not always the best in terms of accuracy. The smaller the mesh size, the longer the calculations take but results are more accurate. Mesh size can be customized by the user.

All COMSOL simulations, here in Chapter 2 as well as in Chapter 5, were done with the following global parameters.

Electrode separation distance: 10 μm
Voltage assignment of bottom electrode: 10 V
Voltage assignment of top electrode: Ground
Modules for electrophoresis and dielectrophoresis: AC/DC (Select Electrostatics)
Modules for electro-osmosis: Fluid Flow (Select "Single-Phase Flow" then
　　"Creeping Flow")

The following are the COMSOL notations used for the electric field simulations.

Electric potential in 2D or 3D (1 input field): V
Electric field in 2D (2 input fields): es.Ex, es.Ey
Electric field in 3D (3 input fields): es.Ex, es.Ey, es.Ez

The following are the notations used for the dielectrophoretic field simulations.

Dielectrophoretic potential in 2D: log((es.Ex)^2+(es.Ey)^2)
Dielectrophoretic potential in 3D: log((es.Ex)^2+(es.Ey)^2+(es.Ez)^2)
Dielectrophoretic field in 2D: d((es.Ex)^2+(es.Ey)^2,x)
                              d((es.Ex)^2+(es.Ey)^2,y)
Dielectrophoretic field in 3D: d((es.Ex)^2+(es.Ey)^2+(es.Ez)^2,x)
                              d((es.Ex)^2+(es.Ey)^2+(es.Ez)^2,y)
                              d((es.Ex)^2+(es.Ey)^2+(es.Ez)^2,z)

The following are the notations used for the electro-osmosis simulations.

Electro-osmotic velocity potential in 2D: log(spf.U)
Electro-osmotic velocity field in 2D: u, v

All potentials display as a color gradient. Only one input field is required. All fields can either be displayed as arrows or lines. Fields require separate x and y component inputs for 2D; and separate x, y, and z component inputs for 3D. Dielectrophoresis and electro-osmosis have not yet been discussed.

The figures below and in the following pages are COMSOL simulations of the three previously discussed electrical field systems; a single point charge, two point charges, and two finite parallel plates.
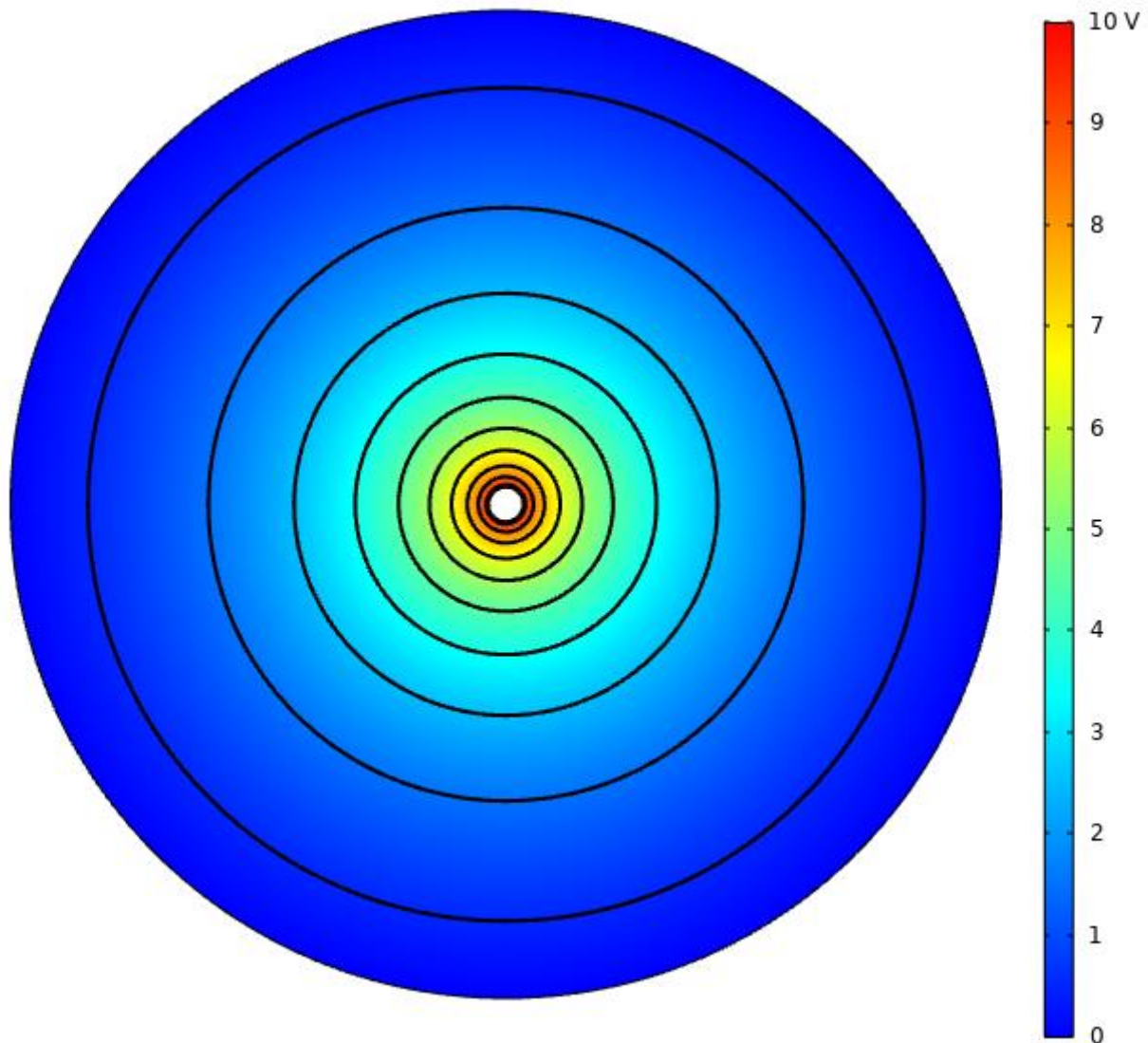
Figure 2.7 – Charge intensity gradient of a point charge. It should be noted that COMSOL cannot actually handle point charges. The simulation was done by defining a small inner circle assigned with a potential of 10V and a large outer circle assigned as ground. Although the result is given as a potential, the qualitative results are exactly the same as a point charge.
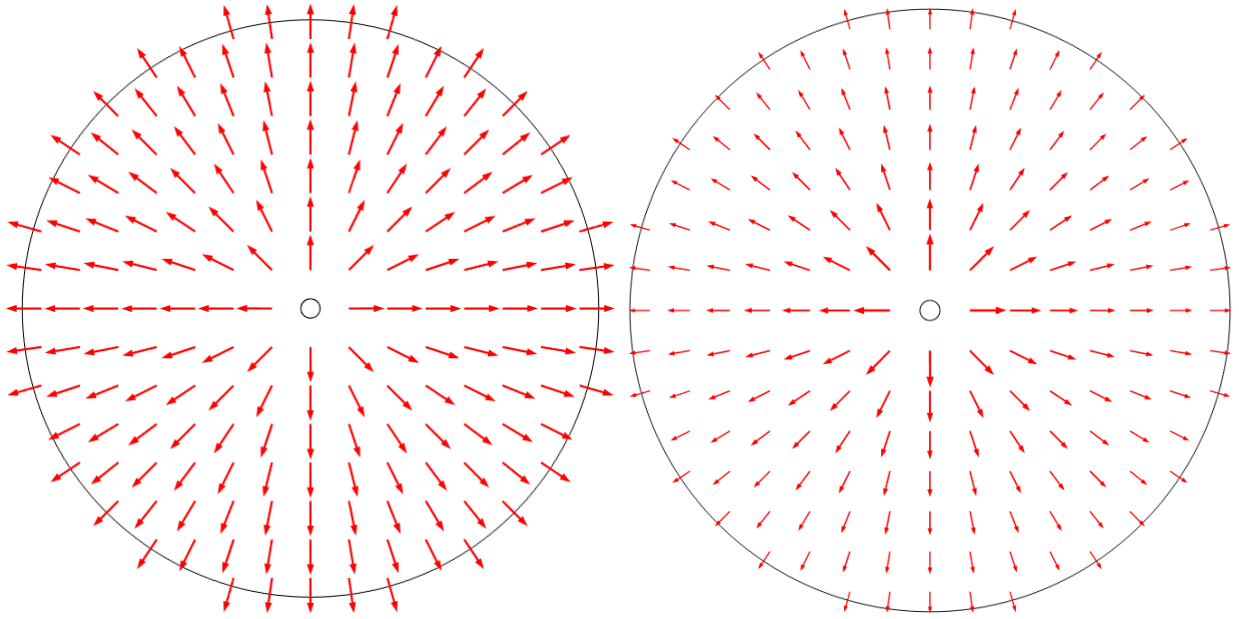
Figure 2.8 – Left image, the electric field of a single point charge depicted as normalized arrows. Normalized arrows only indicate the direction of the field. Right image, the electric field depicted with logarithmic arrows. In addition to indicating the direction of the field, the size of the arrows indicate the magnitude of the force the field will exert on another charged particle at the location of the base of the arrow.
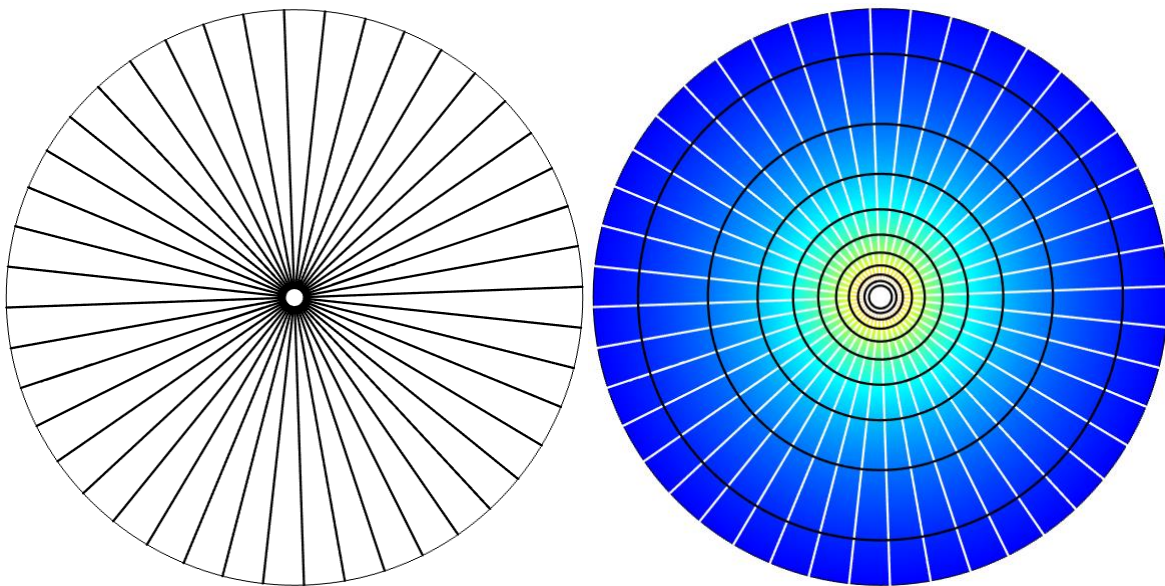
Figure 2.9 – Left image, the electric field of a single point charge depicted with equivalent field lines instead of arrows. Right image, the charge intensity and the electric field on the same graph.
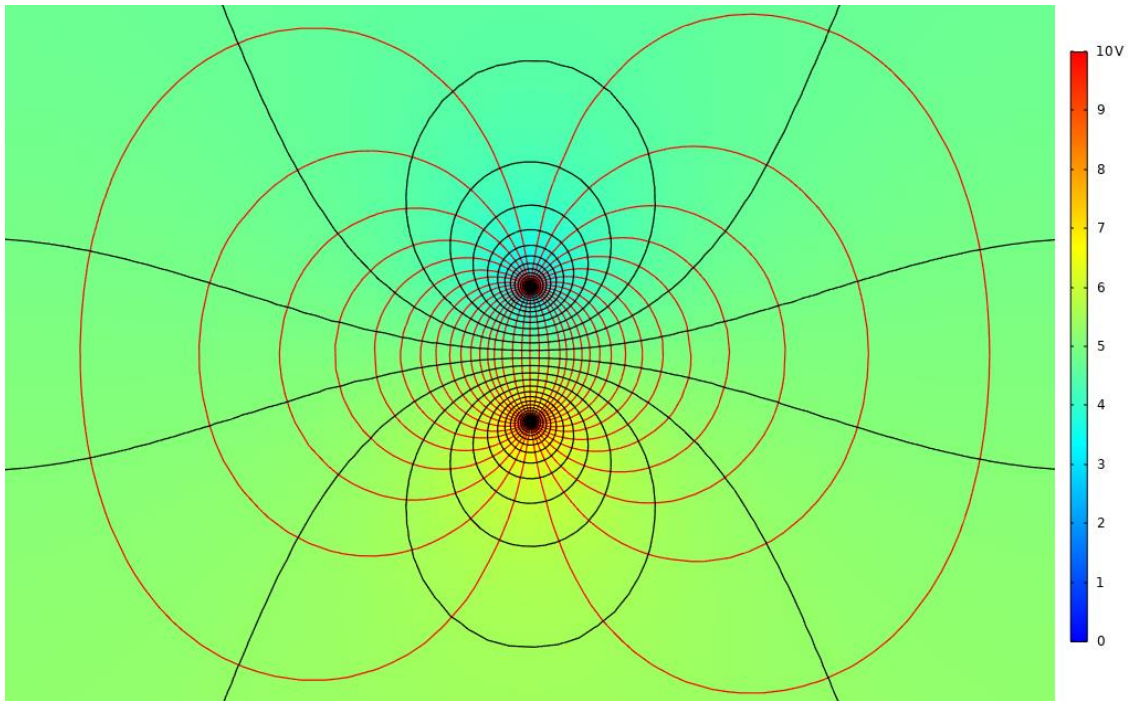
Figure 2.10 – Charge intensity and electric field of two opposite point charges expressed as a potential and as lines.
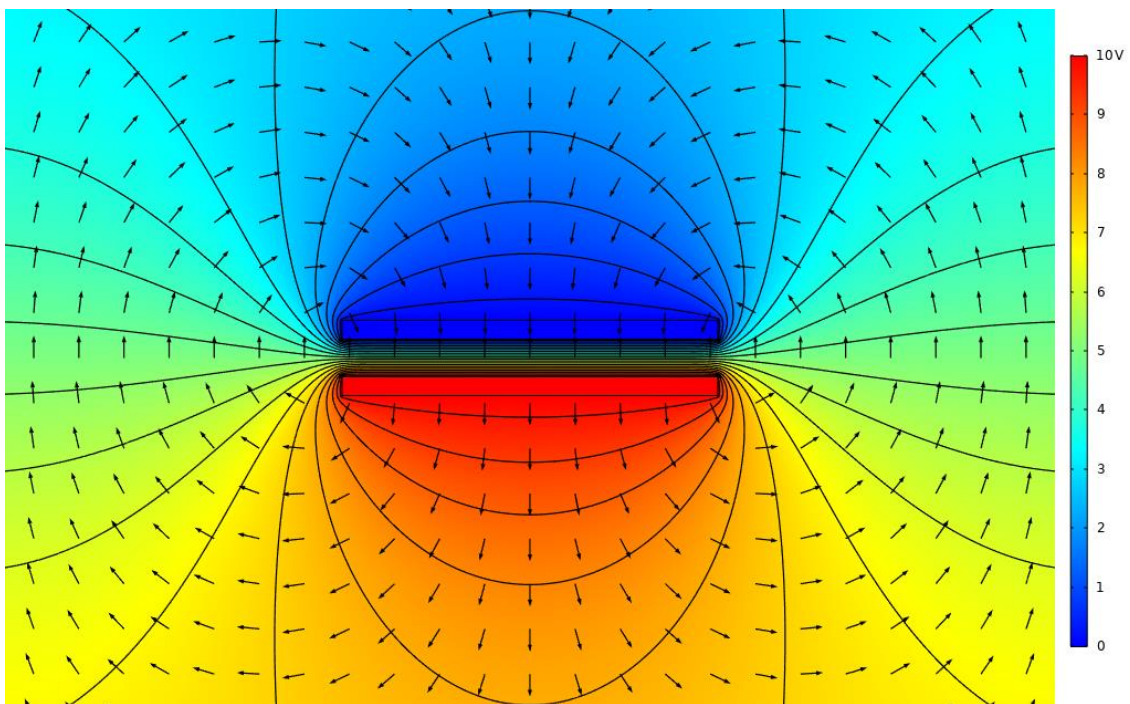
Figure 2.11 – The potential and electric field of two finite parallel plates. The bottom plate is assigned as 10V and the top plate is assigned as ground.

2.4 The Corral Trap
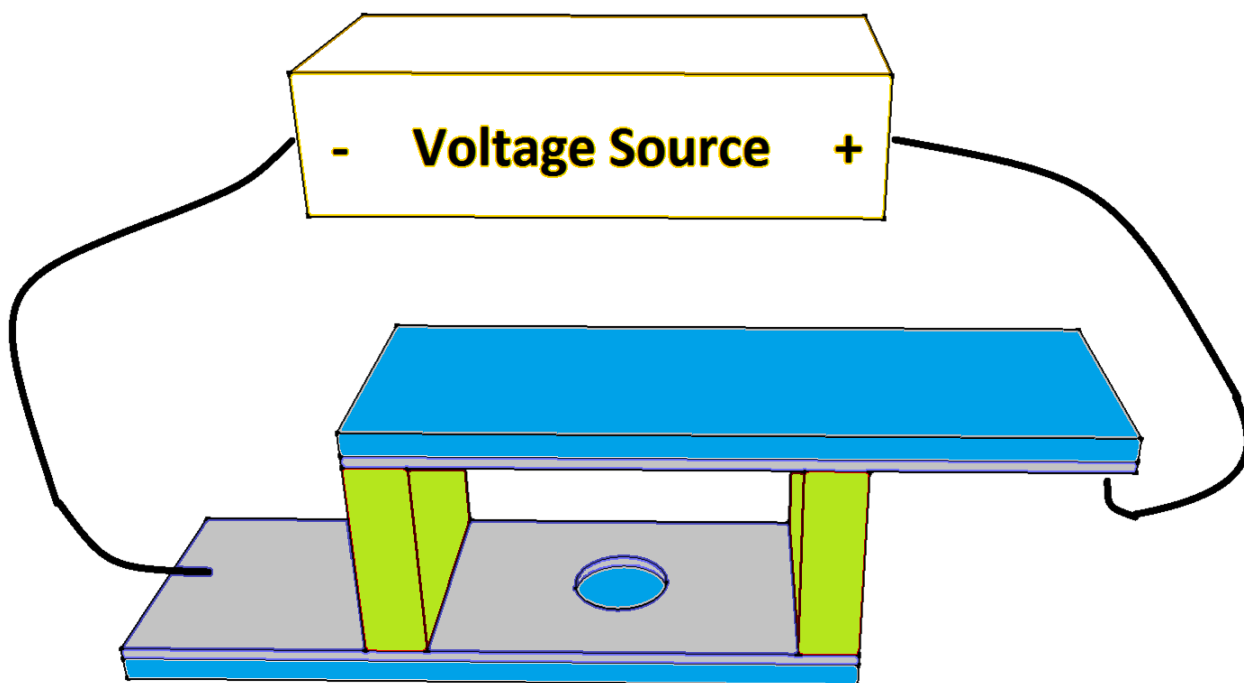
Figure 2.12 – Basic schematic of the corral trap. Blue is glass, gray is metal, and green is a non-conductive layer used to prevent the two electrodes from coming into contact and to keep them at a fixed known distance.

Chapter 1 introduced two ways that particles can be trapped, the ABEL trap and optical tweezers. Both have disadvantages. The ABEL trap uses a feedback system to monitor the particle's position, hence there is no stable trapping potential. Optical tweezers can only trap transparent particles, and high laser intensities can damage the particle. The idea behind the corral trap is to apply a restoring force to a particle, similar to the ABEL trap, that is stable and "built into" the setup. Figure 2.12 shows the basic schematic of the corral trap[16] (the image is not to scale, it is only meant to convey the main features of the system). It consists of two electrodes that are two parallel plates with a circular area devoid of metal in the middle of one of the bottom plate. The green, non-

conductive layer has two purposes. It prevents the electrodes from coming into contact with each other, thereby preventing an electrical short. It also keeps the electrodes at a known, fixed distance.

Figure 2.13 in the following page shows the geometry of the system used for COMSOL simulations. The overall width of the system is 60 microns, the diameter of the corral is 40 microns, and the electrode separation distance is 10 microns. The thickness of the metal layer of the bottom electrode is 15 nm. The thickness of the metal layer for the top electrode is also 15 nm, but this does not need to be taken into account for COMSOL simulations. The bottom electrode is assigned a potential of 10V, while the top electrode is assigned as ground. As can be seen from the fourth image of Figure 2.13, which depicts the electric field created by the corral trap, the field is not uniform across the trap.
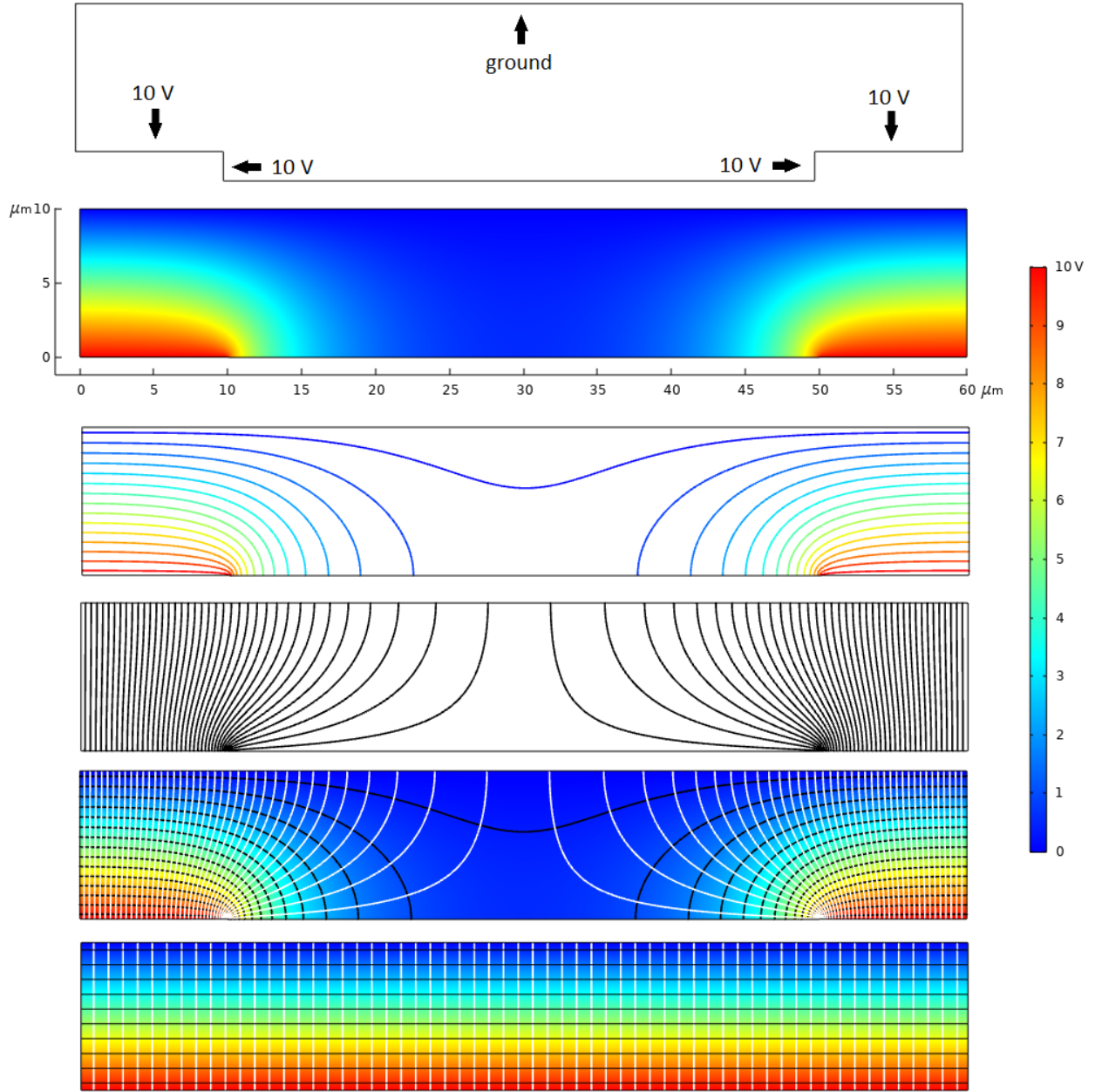
Figure 2.13 – Top image, the exaggerated two dimensional geometry of the corral trap which conveys the location of the rim. Second image: electrostatic potential. Third image: equipotential lines. Fourth image: electric field. Fifth image: composite. Bottom image: electric field of featureless metal surfaces for comparison.

The COMSOL results shown in Figure 2.13 can be used to predict the behavior of charged particles in solution. Consider the potential gradient; if a particle is negatively charged and the bottom electrode is negatively charged as well, a particle located within

the red regions will experience a strong repulsive force and will move towards the blue regions. If a particle is located outside the corral and a voltage is applied, it will simply move straight up towards the top electrode. If a particle is located inside the corral and a voltage is applied, it will go towards the center and up, the region where a particle will experience the least amount of repulsive force. The void of the corral trap thus creates a potential well, which is clearly seen in the second image.
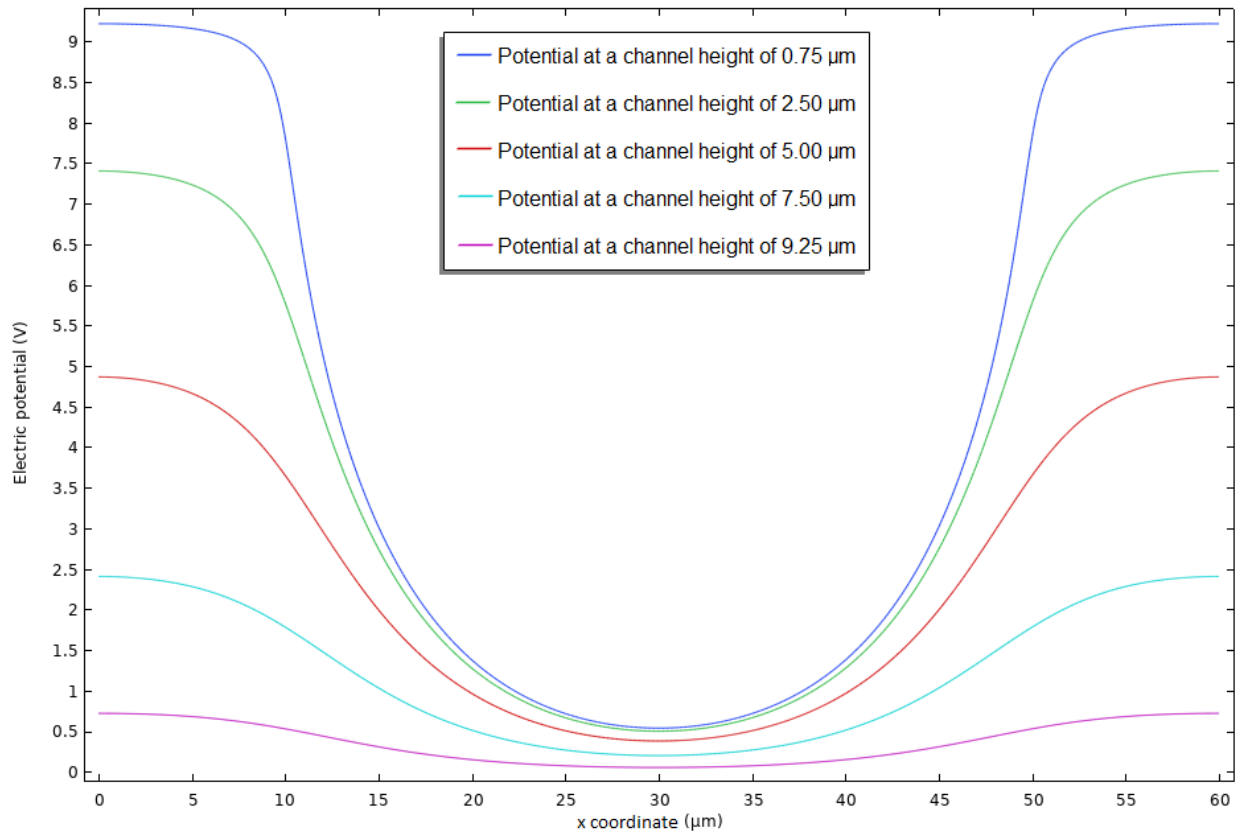
Figure 2.14 – Potential profiles of the corral trap based on the channel height with an electrode separation distance of 10 μm.

Figure 2.14 shows the potential profiles of the corral trap based on the channel height with an electrode separation distance of 10 μm. The blue line is the potential at a height of 0.75 μm. The reason this height was chosen and not 0.00 μm is because the

majority of experimental results were obtained with beads having a radius of 0.75 μm. The dark blue line has the most pronounced well. The difference in potential is dramatic relative to the rim of the corral and the center of the corral. The graph shows that, regardless of height, all potential profiles generally converge to the relatively same low value at the center of the corral trap. This indicates the center of the corral has the lowest energy relative to other areas of the corral and will therefore be favored by a particle; the result is electrostatic trapping.

The electric field is an indication of the exact pathway a point charge will actually follow once voltage is applied and the electric field is brought into existence. A point charge will move along a given field line. Microscopic particles, however, are not zero dimensional points. They are finite and have dimension and volume. Therefore they are affected by multiple field lines and will not follow the exact pathway of a single field line.

The images on the following page depict the electric field of the corral trap with arrows instead of lines. A charged particle located at the base of any arrow will experience a force, attractive or repulsive, based on the charge of the particle and the signs of the electrodes, in the direction of the arrow.
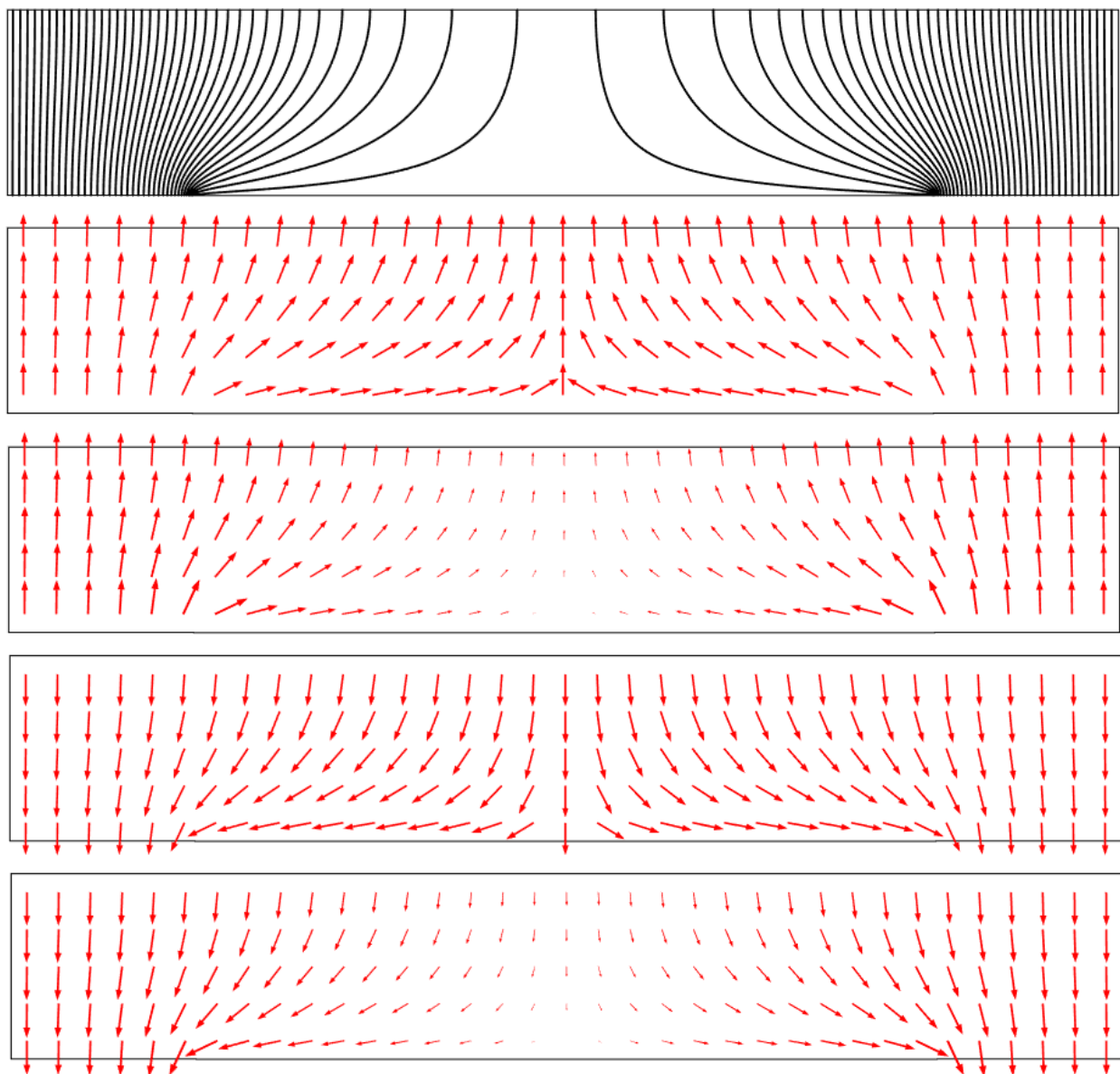
Figure 2.15 – Top image: electric field of the corral trap with lines. Second image: electric field as arrows if the bottom electrode is negative and top electrode is positive. Arrows are normalized. Third image: logarithmic arrows. Fourth image: electric field if the bottom electrode is positive and top electrode is negative. Arrows are normalized. Bottom image: logarithmic arrows.

By visualizing the electric field, the behavior of charged particles can now be theoretically predicted. As can be seen from the images, the field is not as strong in the middle of the corral. The strongest force, whether it be attractive or repulsive, is exerted

at the rim of the corral; and the field is the weakest inside the corral. If the the bottom

electrode and the particle are oppositely charged, it is inside the corral where the particle

would experience the least repulsion and thus move to inside the corral and towards the

top.
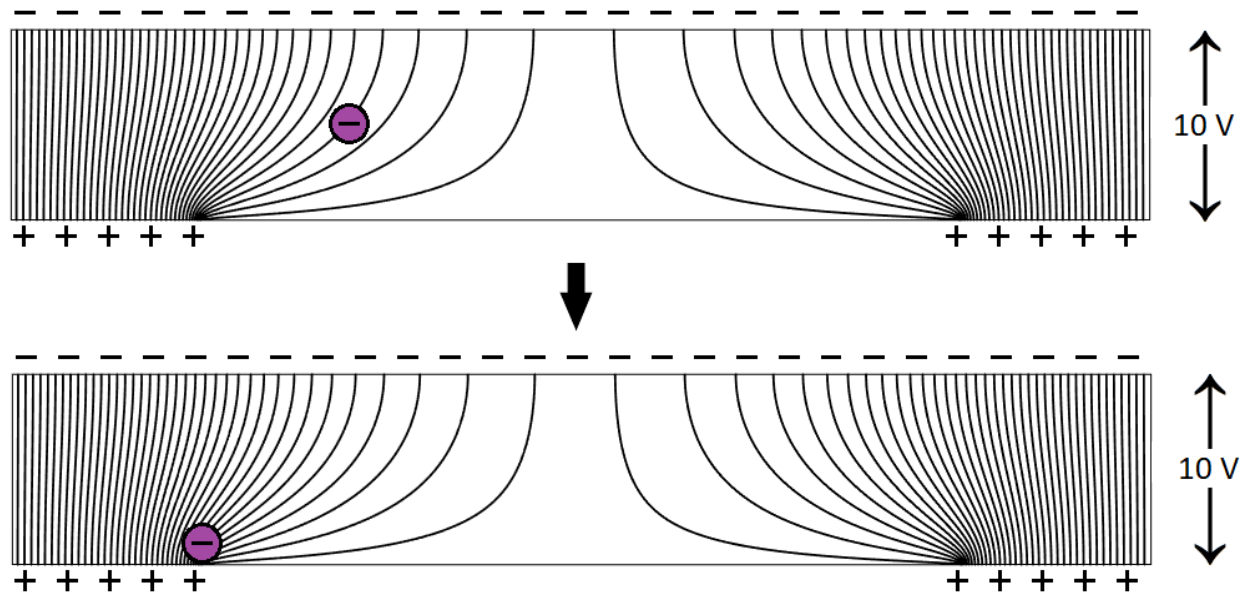
Figure 2.16 – Assuming a particle is negatively charged, rim trapping is the result of setting the bottom electrode to positive. This is the same result if a particle is positive and the bottom electrode is set to negative.

Figure 2.16 is an illustration of rim trapping. The bead is initially located arbitrarily

within the corral itself and equidistant from both the top and bottom electrodes. Once the

voltage is applied the bead is attracted to the rim, where it will finally be trapped. Figure

2.17 on the following page illustrates corral trapping. Once the voltage is applied, the

bead ends up at the top electrode and directly above the center of the corral trap.
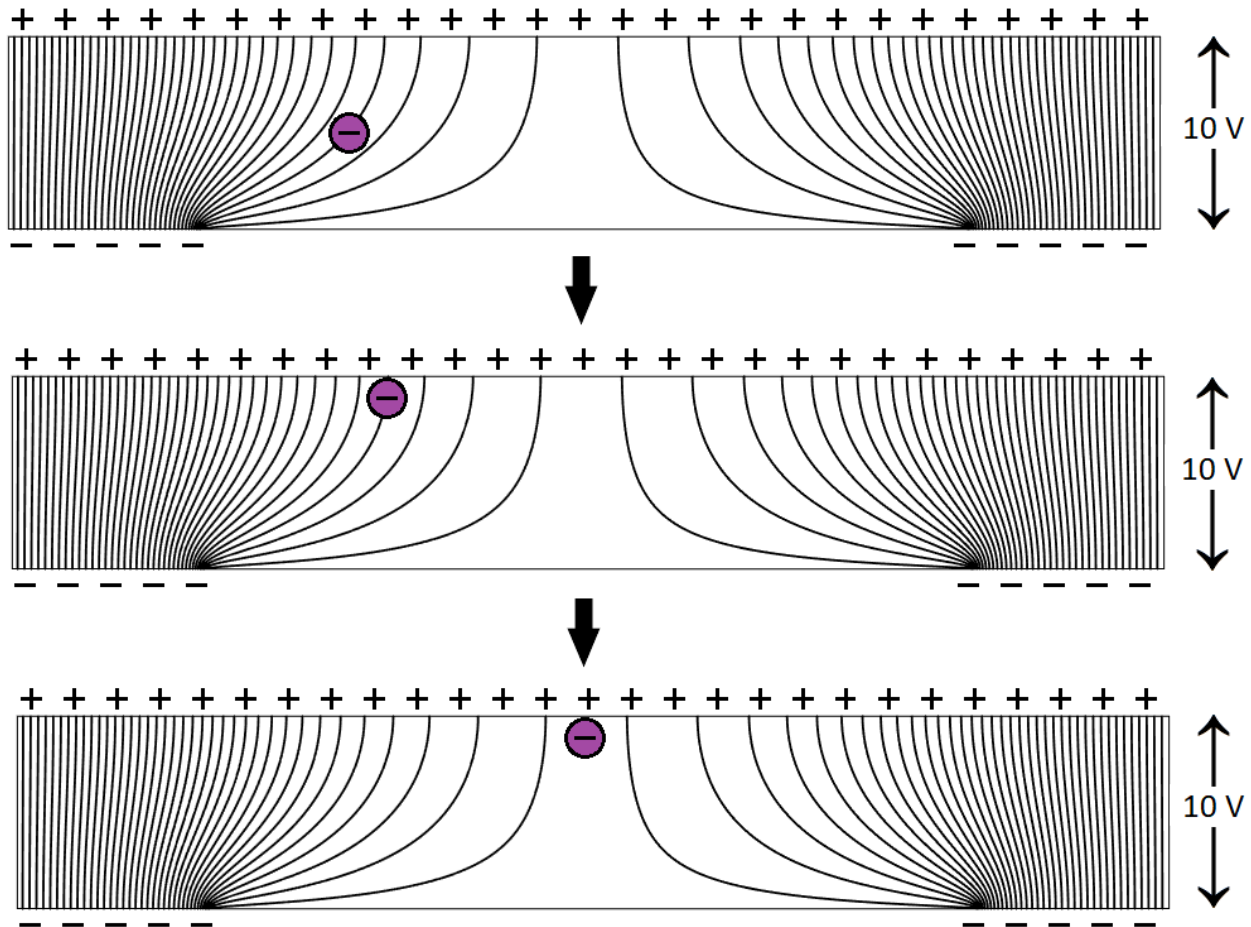
Figure 2.17 – Assuming a particle is negatively charged, corral trapping is the result of setting the bottom electrode to negative. This is the same result if a particle is positive and the bottom electrode is set to positive.

2.5 The Corral Trap In Three Dimensions

COMSOL is also capable of visualizing results in 3D. The calculations are a bit more intensive and require significantly more computational time. Results can appear muddled and unclear if too many arrows or lines are used for visualization purposes. Deciding on the proper number of arrows or lines so that results are reasonably interpretable requires some care. However, 3D does have some advantages over 2D in that representations of the system can be completely visualized, but 2D representations

are definitely easier to read. While circular corral traps are symmetric, non-symmetric metal shapes such as rectangles, squares, or triangles must be modeled in 3D.
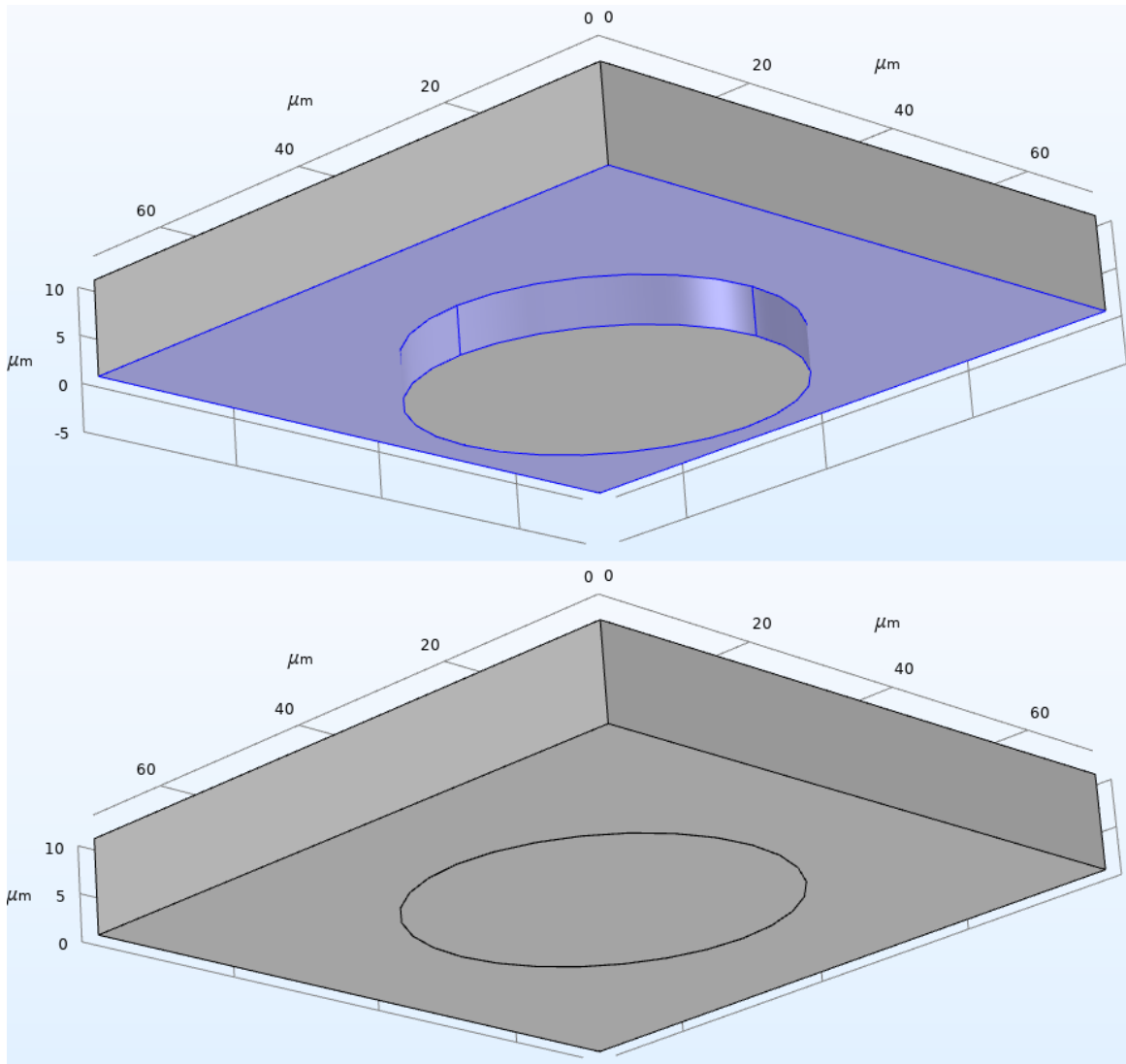
Figure 2.18 – Exaggerated geometry and scaled geometry of the corral trap in 3D.

Figure 2.18 shows both the exaggerated and scaled geometry of the corral trap in 3D. Voltages are assigned to the surfaces that are highlighted in purple in the top image. The top surface of the system's geometry, not visible, is assigned as ground.
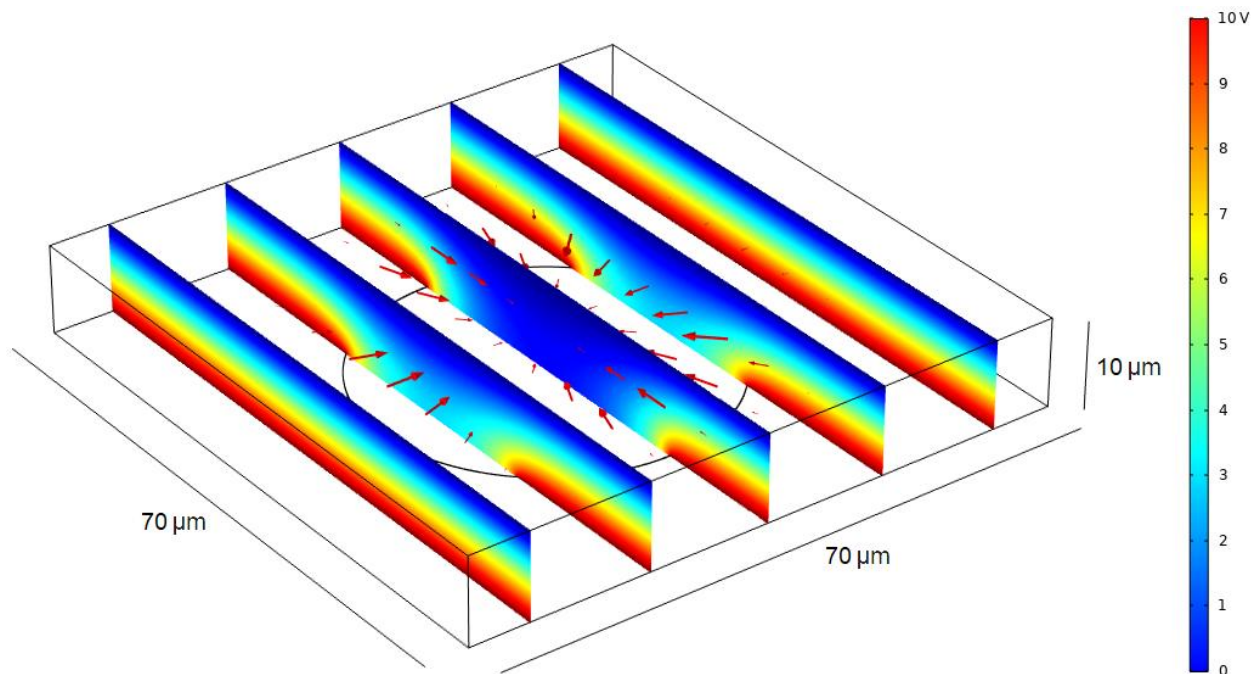
Figure 2.19 – Potential slices of the three dimensional corral trap.

In Figure 2.19, the corral trap is shown with slices at equal and set intervals. The middle slice goes through the corral trap where its well size is maximum. The potential well can be clearly seen. The two slices on either side of the middle have a smaller well size, and the remaining two have no well at all. The figure above shows how the well size varies as a function of the distance from the center. Since this is a three dimensional representation, the shorter well size of the outer slices also has the effect of pushing particles to other parallel slices where the well size is larger, namely towards the middle slice. It should be noted that a charged particle located outside the corral cannot be trapped; it must already be within the corral when the voltage is applied.
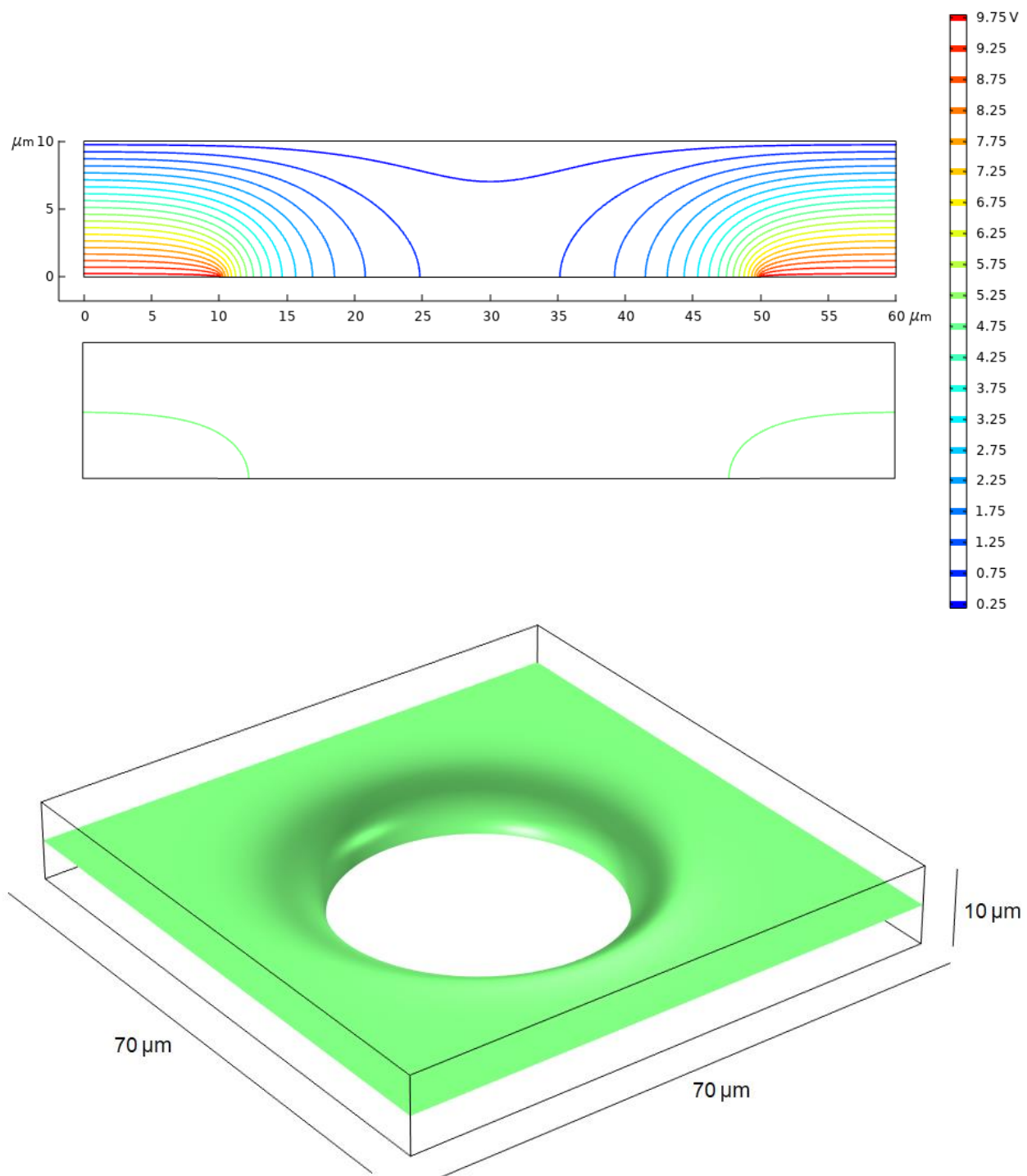
Figure 2.20 – Top image, 20 potential profiles. Middle image, a single potential. Bottom image, that single potential depicted as a three dimensional isosurface.

In Figure 2.20 on the previous page, a single equipotential line is chosen and fully rotated in three dimensions. This is known as an isosurface; the potential is the same anywhere on this surface. A particle with energy equivalent to the surface can freely move or diffuse anywhere on the surface. If the particle loses or gains energy, it will move up or down to a different isosurface. Mentally visualizing an axiosymmetric 2D plot into a 3D image may not necessarily be an easy connection to make, which is one of the distinct advantages of COMSOL's 3D visualization capabilities. When a single potential is rotated in 3D, the basic geometry is that of a well. It is inside this well that a particle can be confined if that particle has less energy than the isosurface. The figure on the following page shows a single system depicted with four isosurfaces and how they vary depending on the value of the associated electrostatic potential. The diameter of the well is larger when the potential is large and gets smaller as the potential decreases.
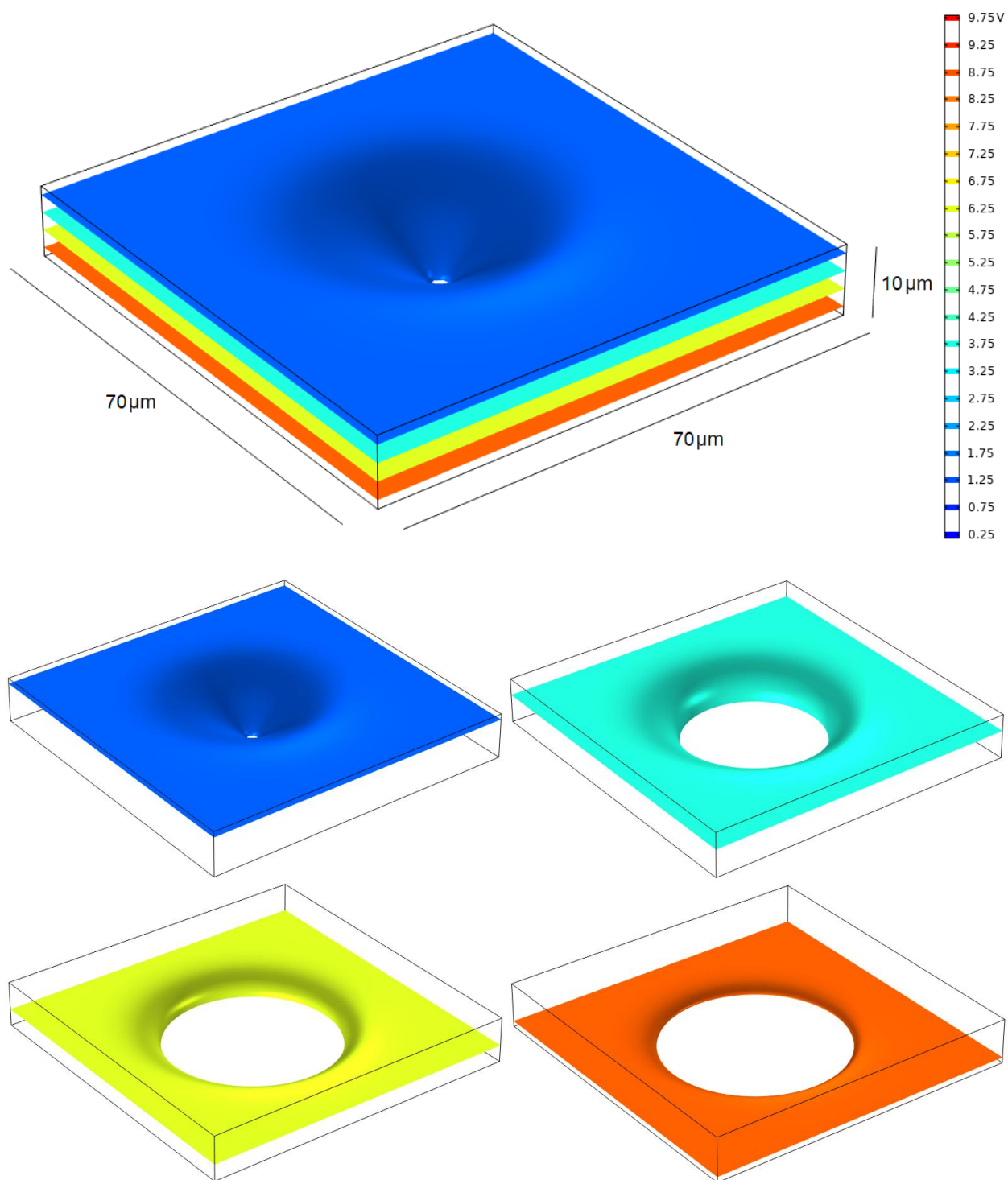
Figure 2.21 – Isosurface images of the corral trap shown separately with the master image at the very top.
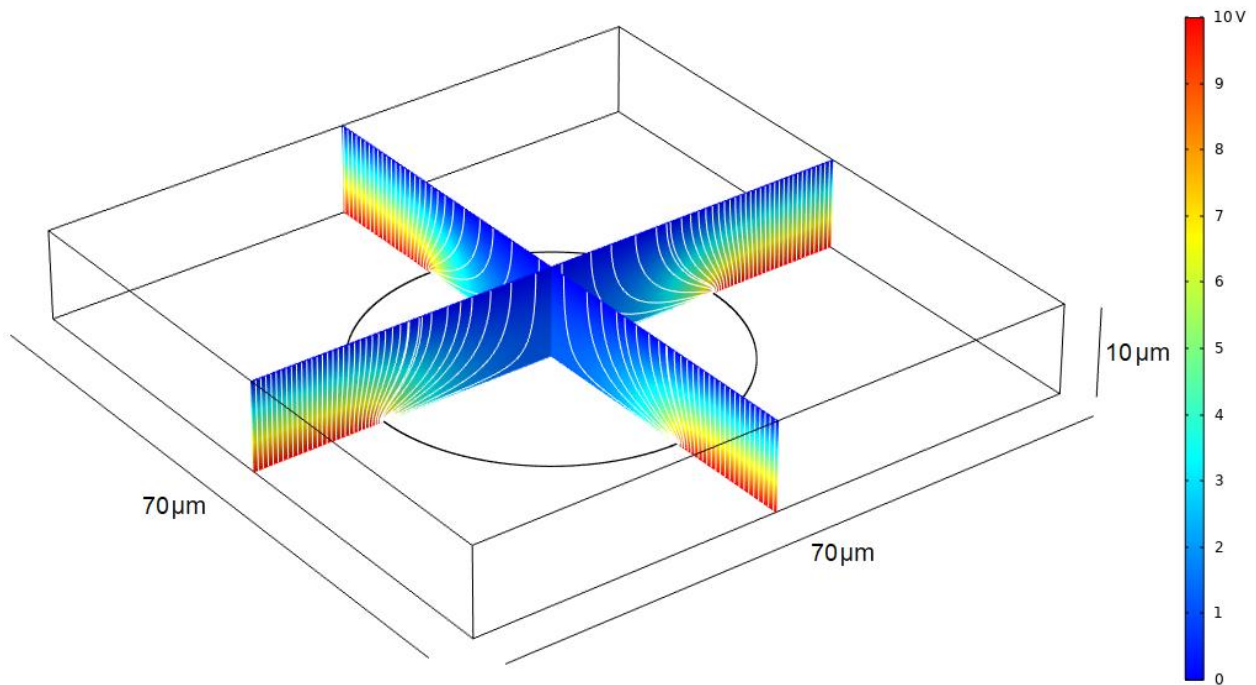
Figure 2.22 – The axio-symmetric 3D electric field, shown with white lines, depicted on two perpendicular slices.

If three dimensional force fields are visualized using lines, the results can often be confusing. Some aspects of COMSOL's visualization capabilities do lack some specifics. But for now, the best option is to display key individual slices. The understood implication when depicting fields as lines is that line density is directly proportional to the force of the field. Outside the corral trap, the lines are the most dense, and the field is therefore the strongest. Inside the corral trap, the lines are more spread out and less dense and the field is weak. Alternatively, arrows can be used to convey information about the strength of the electric field.

2.6 Dielectrophoresis

Dielectrophoresis is an electrokinetic phenomenon that occurs when a charged or uncharged polarizable particle, is placed under the influence of a non-uniform electric

field[11]. To which extent a particle can become polarized depends entirely on the material the particle is made of, and is described by the material's dielectric constant $\mathcal{E}_r$ (relative permittivity). Dielectrophoresis leads to a force that pushes the particle in a certain direction. A uniform electric field is simply an electric field with perfect symmetry where all field vectors are parallel and of the same magnitude, whereas a non-uniform field has a distortion.

It's important to make the distinction that while a non-uniform field can have a distortion, it can still have a certain degree of symmetry. The corral trap is considered non-uniform but it is also axio-symmetric around the center of the corral. Low field density occurs in areas where field lines are far apart and high field density occurs in areas where the field lines are highly concentrated. In the case of the corral trap, high field density occurs at the rim of the corral and low field density occurs in the middle of the corral.
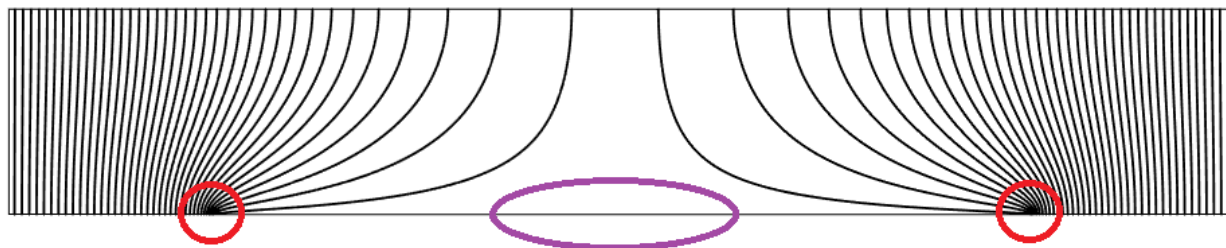
Figure 2.23 – Red indicates areas of high field density, purple indicates areas of low field density.

Dielectrophoresis was first observed in 1951 by Herbert A. Pohl[12, 22]. When the polarizability of the particle is greater than the solution, the non-uniform field exerts greater forces on the particle. When the solution is more polarizable than the particle, the non-uniform field exerts greater forces on the solution. Dielectrophoresis is not readily

47

understandable upon first exposure to the topic. The key to the dielectrophoretic effect is the gradient of the electric field. In Figure 2.24 below, the electrodes consist of a pin at the center and a ring as the outer radius. The field lines are more densely packed and closer together the closer a particle is to the center. This field line density concentrates polarization charges in the particle to areas of the particle where the field line density is greatest, hence the particle becomes polarized and can therefore be affected by the electric field.
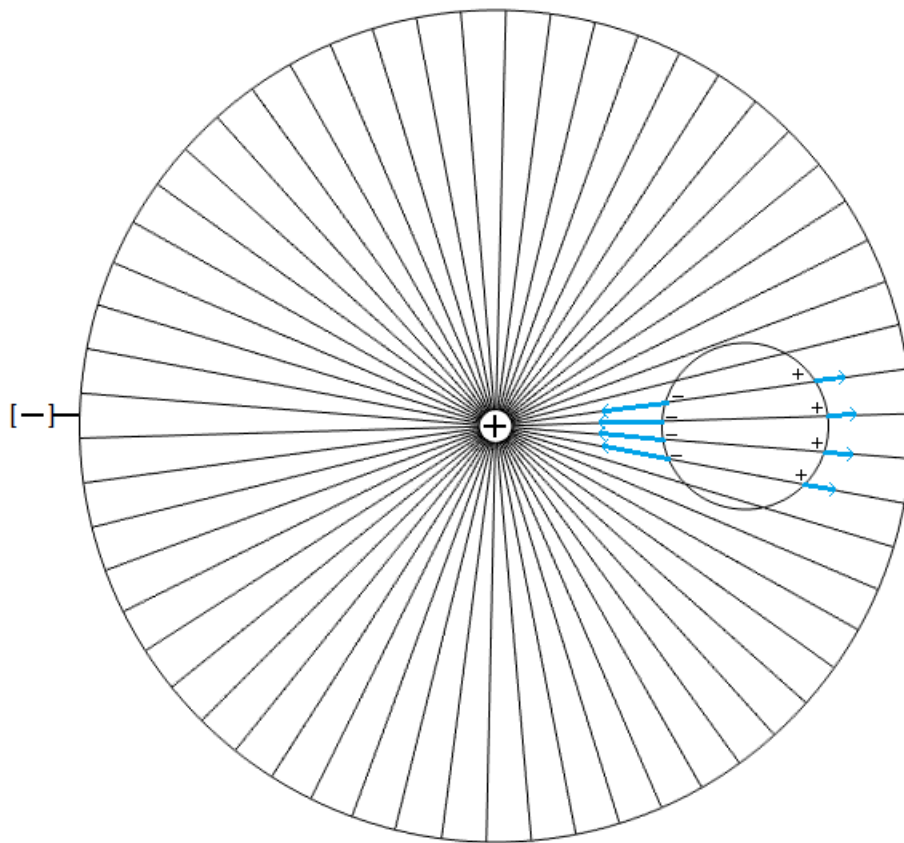
Figure 2.24 – Image of dielectrophoretic field lines acting on a particle. The system consists of a pin electrode in the center and a ring electrode as the outer radius with a particle in between the two. Field line density is greater in the left area of the particle and more spread out in the right area of the particle[12].

The dielectrophoretic force can actually depend on the shape of the particle. The tobacco mosaic virus, also called TMV, is shaped like a rod and not a sphere. If the particle is aligned with the field the dielectrophoretic force can be written as[20]

$$\mathbf{F}_{\text{DEP}} = \frac{\pi a^2 b}{3} \epsilon_m \text{Re}\left\{\frac{\epsilon_p^* - \epsilon_m^*}{\epsilon_m^*}\right\} \nabla |\mathbf{E}|^2$$

a is the radius of the rod and b is the half-length. ε_p^* and ε_m^* are the complex permittivities of the particle and the medium. Re is the real part of the ratio of the difference of the complex permittivities and the medium complex permittivity. The complex permittivities are defined as[21]

$$\varepsilon^* = \varepsilon - i\frac{\sigma}{\omega}$$

ε is the permittivity, σ is the conductivity, i is the imaginary unit, and ω is the AC frequency. Permittivity itself is defined as[24]

$$\varepsilon = \varepsilon_r \varepsilon_o$$

ε_r is relative permittivity and ε_o is vacuum permittivity. ε_r can be thought of as the dielectric constant of the substance or medium.

All the experiments performed for this thesis were done with spherical particles and not rods. The dielectrophoretic force which acts on a spherical and uniformly polarizable particle that is exposed to a non-uniform field of certain symmetry is described by this equation[13].

$$F_{DEP} = 2\pi\varepsilon_m r^3 Re\left[K\left(\omega\right)\right] \nabla \left|E_{rms}\right|^2$$

ε_m is the permittivity of the solution the particle is in, r is the radius of the particle, and $\nabla|E_{rms}|^2$ is the gradient of the non-uniform electric field squared. If the electric field is uniform with no gradient, this factor becomes a zero vector; hence there is no dielectrophoresis in a uniform field. Permittivity is the ability of a substance to store electrical energy. The higher the permittivity of a substance, the more polarizable it is; therefore permittivity and polarizability are directly related. Since dielectrophoresis is directly proportional to r^3, this implies smaller particles might be harder to trap.

The factor of "Re[K(ω)]" is the equation below and is known as the real part of the Clausius-Mossotti factor[14].

$$Re\left[K\left(\omega\right)\right] = \frac{(\varepsilon_p - \varepsilon_m)(\varepsilon_p + 2\varepsilon_m) + \frac{(\sigma_p - \sigma_m)(\sigma_p + 2\sigma_m)}{\omega^2}}{(\varepsilon_p + 2\varepsilon_m)^2 + \left(\frac{\sigma_p - 2\sigma_m}{\omega}\right)^2}$$

This factor introduces a few more parameters. ε_p is the permittivity of the particle, σ_p is the conductivity of the particle, σ_m is the conductivity of the solution, and ω is the frequency of the electrical current. Conductivity is the ability of a substance to facilitate

electron flow. The frequency of a current is only relevant with regards to AC, alternating current; frequency would be considered zero in the case of DC.

The real part of the Clausius-Mossotti factor can be simplified in certain cases[14].

$$Re\,[K\,(\omega)] = \frac{(\sigma_p - \sigma_m)}{(\sigma_p + 2\sigma_m)} \quad \text{when } \omega \to 0$$

$$Re\,[K\,(\omega)] = \frac{(\varepsilon_p - \varepsilon_m)}{(\varepsilon_p + 2\varepsilon_m)} \quad \text{when } \omega \to \infty$$

In cases of low frequency for the current, the conductivities of the particle and solution become the predominant factor; while in cases of high frequency, the permittivities become more important. There are also more specific sub-cases. When "ε_p is less than ε_m" AND "σ_p is greater than σ_m", Re[K(ω)] is positive at low frequency and negative at high frequency. When "ε_p is greater than ε_m" AND "σ_p is less than σ_m", Re[K(ω)] is negative at low frequency and positive at high frequency. The frequency at which Re[K(ω)] is zero is known as the crossover frequency, hence the exact same particle can display BOTH positive dielectrophoresis and negative dielectrophoresis depending on the frequency. The result of positive dielectrophoresis is that the particle will move to areas of high field density. For negative dielectrophoresis, the particle will move to areas of low field density[14]. In the case of the corral trap, areas of high field density occur at the rim and areas of low field density occur in the middle.

Prior to calculating the dielectrophoretic field, the electric field squared must be calculated. Since crucial information can also be gleened from the electric field squared, the topic merits discussion. The electric field squared is a type of potential that is the

source for the dielectrophoretic force, just like the electrostatic potential is the source for the electrostatic field.

The dielectrophoretic force itself is proportional to the gradient of the electric field squared.

$$F_{\mathrm{DEP}} \propto \nabla \, |E_{\mathrm{rms}}|^2$$

Hence the dielectrophoretic field derives from the square of the electric field, which can be used to visualize the dielectrophoretic forces and "energies" for the corral trap.
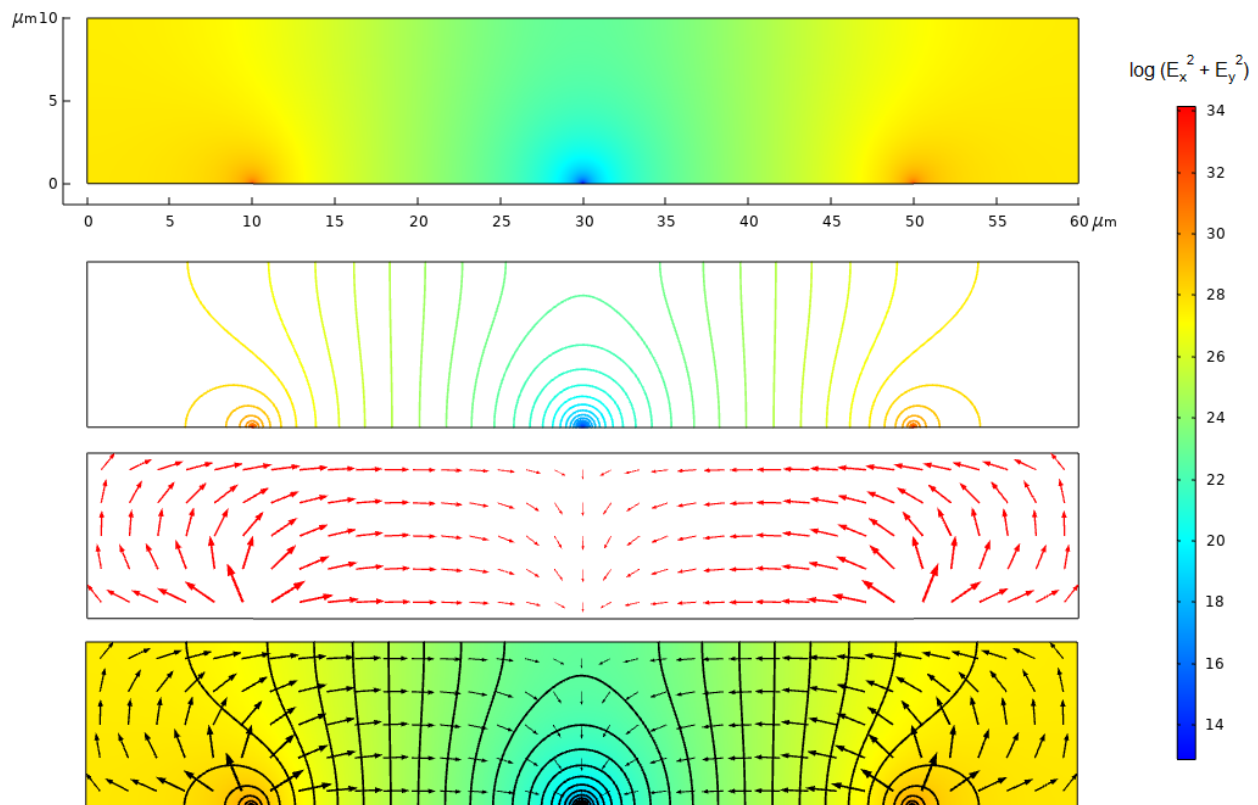
Figure 2.25 – Top image, the dielectrophoretic potential depicted as a logarithmic of the electric field squared. Second image, equipotential lines. Third image, negative dielectrophoreis shown with logarithmic arrows. Bottom image, composite.

Figure 2.25 in the previous page depicts all potentials, lines, and fields associated with dielectrophoresis. There are similarities to the potentials, lines, and fields due to electrostatics. The dielectrophoretic potential is depicted in the top image. There are areas of high potential, shown in red, and areas of low potential, shown in blue. Dielectrophoretic particles will move to one of these areas depending on whether the particle experiences positive or negative dielectrophoresis. The second image displays lines of equipotential. The third image displays the dielectrophoretic field itself, in this case, negative dielectrophoresis is shown. The bottom image is a composite and it can be seen that the dielectrophoretic field is always perpendicular to the lines of equipotential.

According to these simulations, one of the differences between the electric field and the dielectrophoretic field is that a dielectrophoretic particle can also be trapped if it is located outside of the corral but within reasonable proximity to the rim. A particle might display a type of looping behavior while under dielectrophoresis. Although there is some degree of upward or downwar tilt, most of the forces within the corral are directionally parallel to both electrodes except at the rim or in the center. Similar to to the electric field force, the strongest dielectrophoretic force is experienced at or near the rim.

In the case of electrostatics, when the electrostatic potential is plotted based on channel height, the result is a "U" shape potential. This was previously shown in Figure 2.14. If the same calculation is done for the dielectrophoretic potential, the well looks different. Figure 2.26 on the next page shows this well, it is the logarithm of the electric field squared based on the channel height.
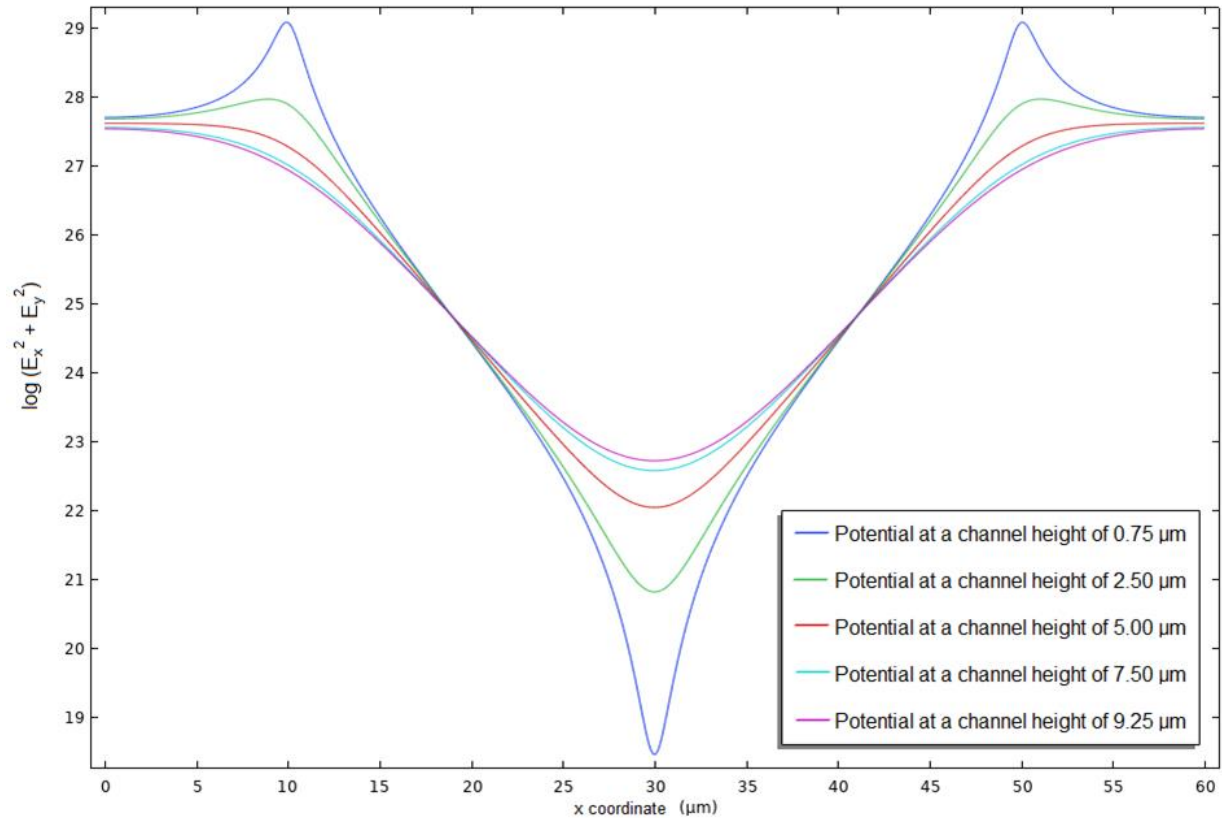
Figure 2.26 – The profiles of the dielectrophoretic potential based on channel height for the case of negative dielectrophoresis with an electrode separation distance of 10 µm. The center of the corral has the lowest potential.

The profile for a channel height of 0.75 µm is the most interesting, there is an absolute minimum at the center of the corral and an absolute maximum at both of the rims. There are also relative minimums outside of the corral. Outside of the corral or inside of the corral would be the preferred areas where a bead would move to in order to minimize its energy. The profile at a channel height of 5.00 µm starts to look more similar to the electrostatic potential profile, since there is only a minimum and no absolute maximums. Figure 2.27 on the next page shows the case for postivie dielectrophoresis. The lowest potential occurs at the rim, so this is the most likely location where a particle

will be found. For a particle to be located at the center of the corral would require a relatively large amount of energy.
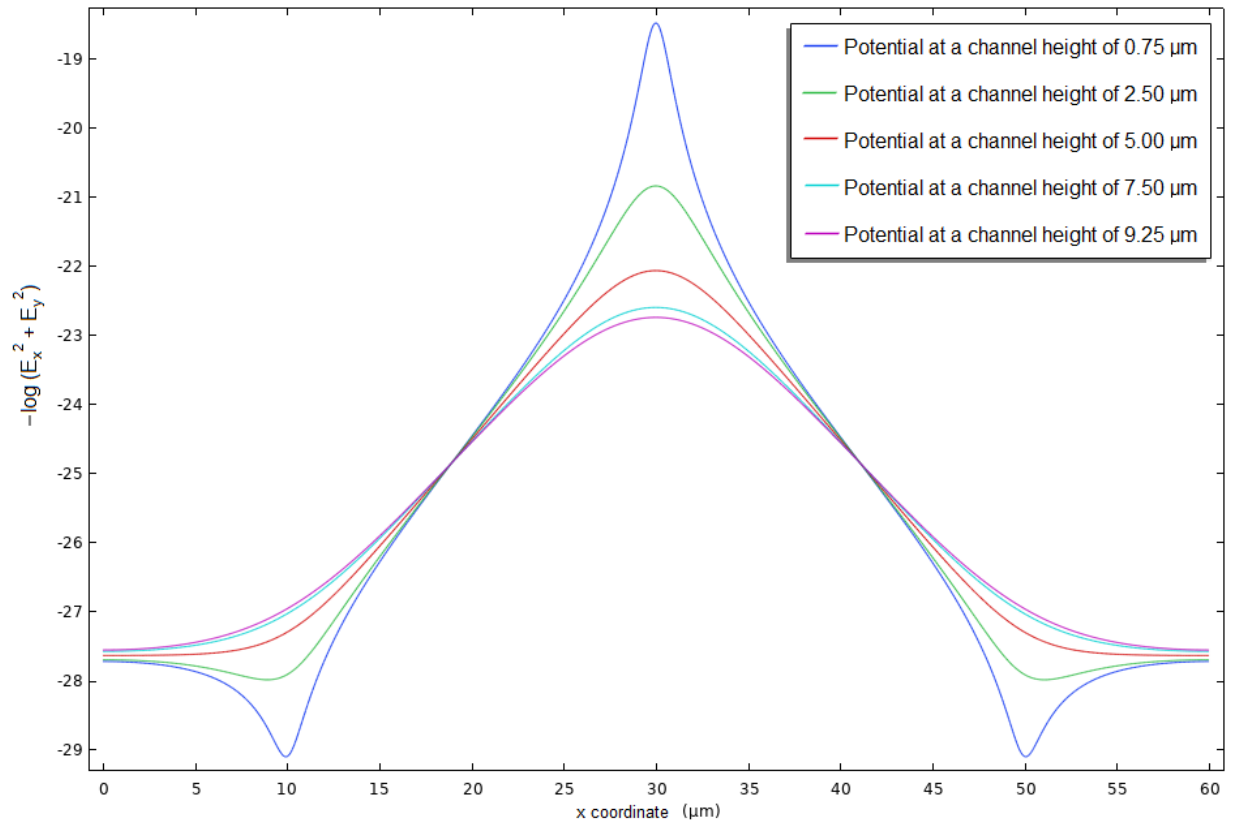
Figure 2.27 – The profiles of the dielectrophoretic potential based on channel height for the case of positive dielectrophoresis with an electrode separation distance of 10 µm. The rim of the corral has the lowest potential.
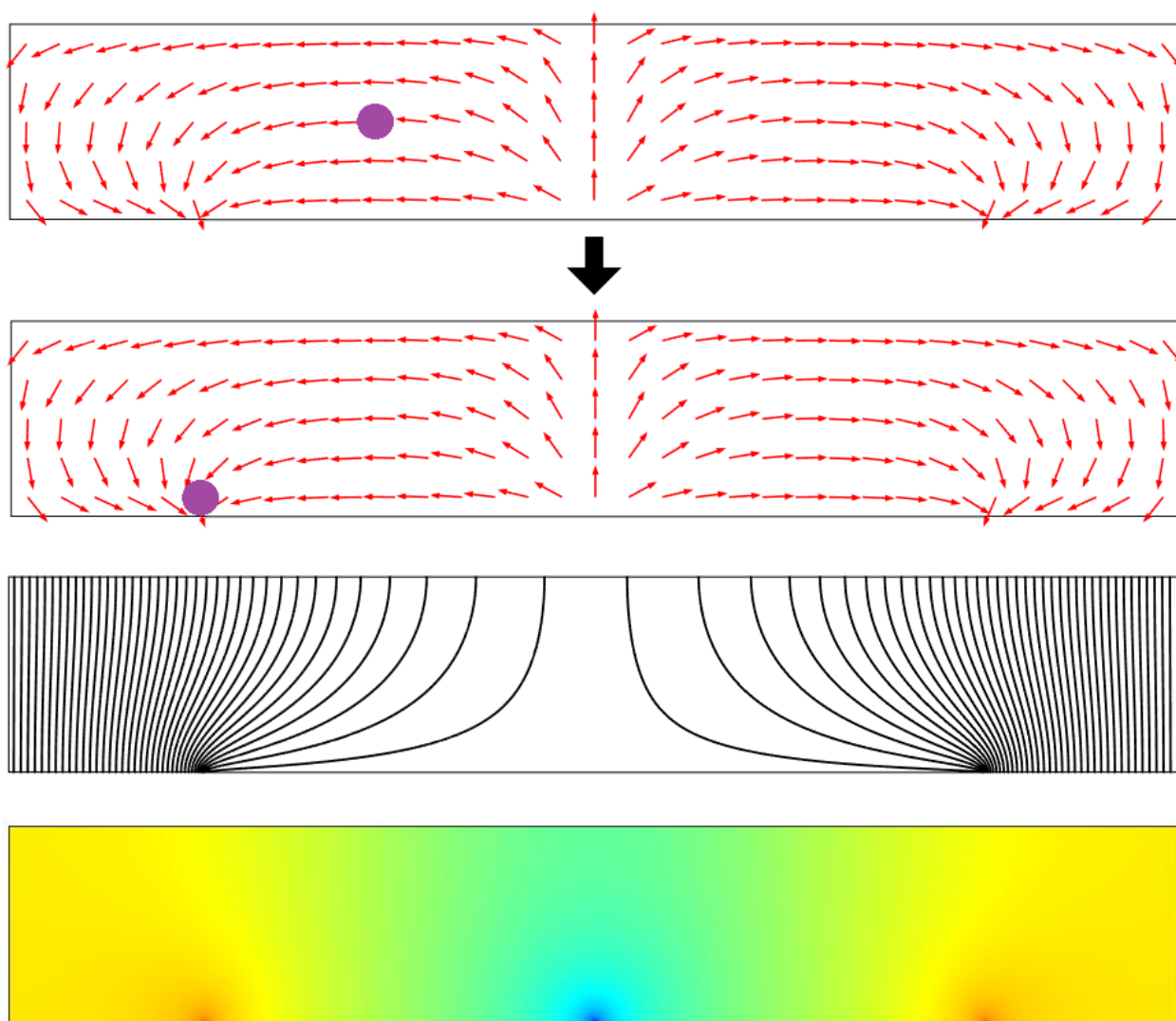
Figure 2.28 – Top two images, positive dielectrophoresis. Bead moves to the rim of the corral. Third image, electric field. Bottom image, electric field squared.

An illustration of the phenomenon itself is shown in Figure 2.28, for the case of positive dielectrophoresis. A bead arbitrarily located within the diameter of the corral will then move towards the rim of the corral when a voltage is applied. With regards to the electric field, the particle will move to areas of high field density (areas with compact electric field lines). With regards to the electric field squared, the particle will move to areas of high potential (orange)[23].

Negative dielectrophoresis is shown in Figure 2.29 below. A bead will move towards the center of the corral. With regards to the electric field, this corresponds to areas of low field density (areas with no electric field lines). With regards to the electric field squared, this corresponds to areas of low potential (blue)[23].
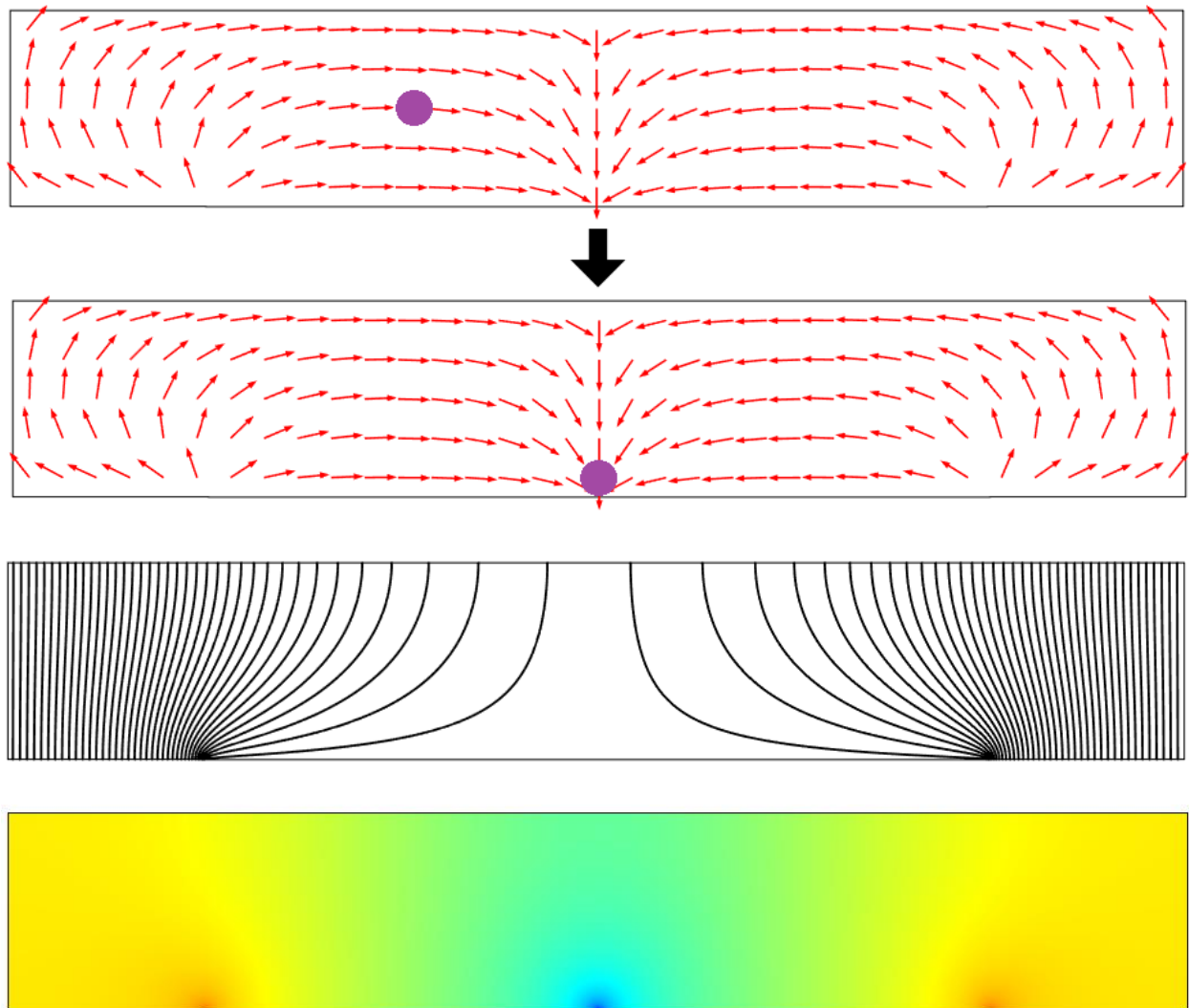
Figure 2.29 – Top two images, negative dielectrophoresis. Bead moves to the center of the corral. Third image, electric field. Bottom image, electric field squared.

The dielectrophoretic field can also be depicted in three dimensions, Figure 2.30 below. Similar to how the electric field was previously displayed, only two key slices are shown since the field is axio-symmetric.
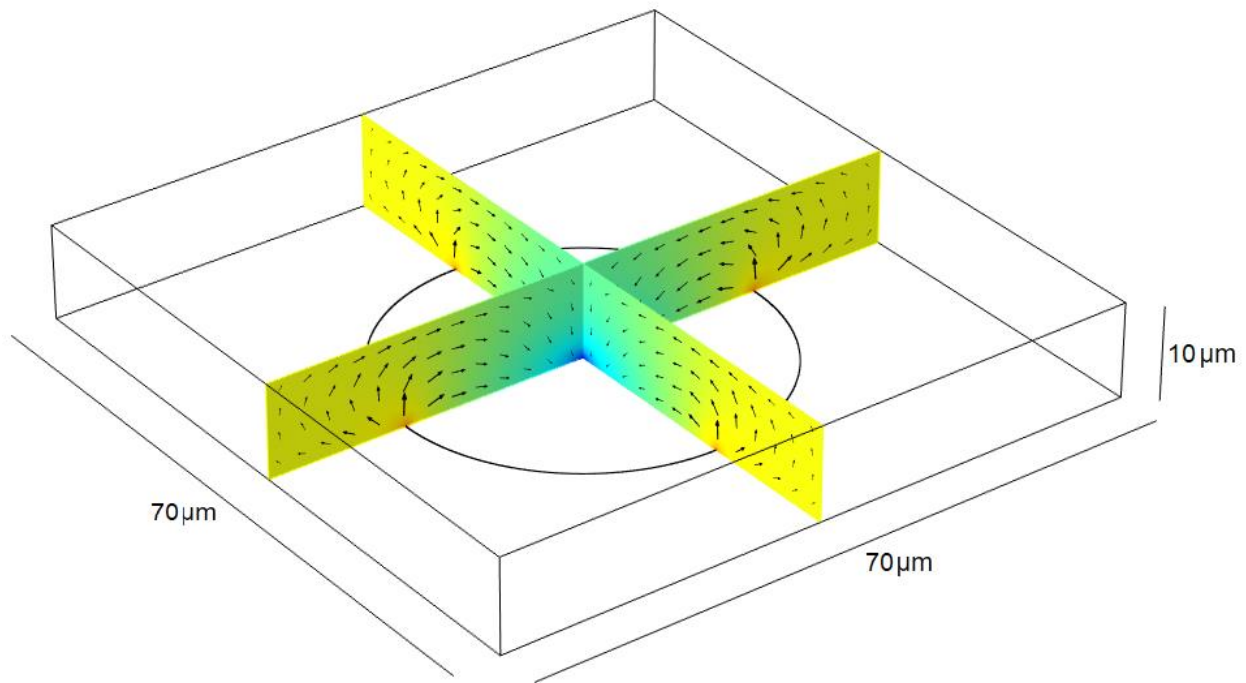
Figure 2.30 – The negatve dielectrophoretic field shown with two perpendicular slices.

The main advantage of dielectrophoresis is that it does not degrade the electrodes to the extent that electrophoresis does. Dielectrophoresis can have manly useful applications particularly in the field of microfluidic system. Dielectrophoresis can be used for separating and sorting particles[25-28]. It can also be used for trapping particles[29-34], nanotube assembly[35], purification[36], and even characterization[37].

2.7 Optical Trapping of Rayleigh Particles is Similar to Diectrophoresis

In Chapter 1.3, optical tweezers was discussed but it entailed only one type of particle, namely Mie particles. Mie particles are much larger than the wavelength of light being used, and trapping is mainly due to light refraction within the particle and the transfer of momentum from light to the particle. The other regime is known as Rayleigh particles, the particles are much smaller than the wavelength of light being used. Because the particle size is smaller than the wavelength of light being used, light refraction inside the particle is considered negligible. Instead, small objects develop an electric dipole moment in response to the light's electric field. Since a polarized particle will move to areas of high electric field density, namely the laser's focus, the optical trapping of Rayleigh particles is similar to positive dielectrophoresis. The force due to the gradient of the laser is shown below[17].

$$F_{\text{grad}} = -\frac{n_b^3 r^3}{2}\left(\frac{m^2 - 1}{m^2 - 2}\right)\nabla E^2$$

Similar to dielectrophoresis, the laser's gradient force exerted on the particle is dependent on the gradient of the electric field squared, ∇E^2. In the case of normal dielectrophoresis, the force is also dependent on the permittivities and conductivities of the particle and the solution, as well as the AC frequency. In the case of optical trapping, it is dependent on the index of refraction of the particle, n_b, and the index of refraction of the medium, m. It is also dependent on the radius of the particle, r. Smaller particles will be harder to trap. In the case of normal dielectrophoresis, both positive and negative

dielectrohoresis can be observed simply by changing the AC frequency. With regards to optical trapping of Rayleigh particles, the gradient force is always directed towards the highest field intensity (laser focus) unless the index of refraction of the particle or the medium are adjusted accordingly. The index of refraction of the medium could be changed if a solution gradient was introduced. Because different shaped laser profiles can have various electric field densities, small particles can be sorted and manipulated with lasers using dielectrophoretic principles since different electric field geometries could be created with different laser profiles.
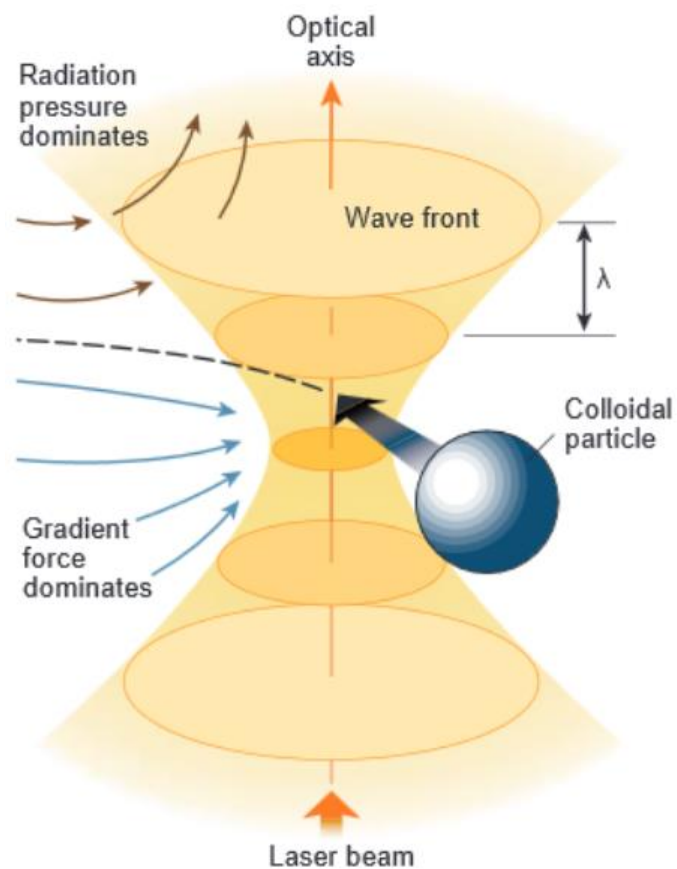
Figure 2.31 – Optical trapping of Rayleigh particles.

2.8 Electro-Osmosis

Electrophoresis and dielectrophoresis are two forces which can affect the trapping of particles. Another significant force which can affect the trapping of particles is electro-osmosis. Electro-osmosis is the movement of liquid relative to a stationary charged surface induced by an applied electric field[18]. Since electro-osmosis involves the movement of liquid, the equations governing the behavior of liquids must be considered first. A fluid is defined as a substance that is a continuum and not made up of discrete particles. Both liquids and gases can be treated as fluids. The equations that describe the behavior of fluids in Euclidean space are known as the Navier-Stokes equations[19]. They are analogous to Newton's second law of motion when applied to fluids. The Navier-Stokes equations can be used to model numerous phenomenon such as weather, ocean currents, water flow in a pipe, air flow around a wing, etc., and they are widely used in computer animation. The equations take into account velocity, pressure, density, and viscosity of the fluid. Calculations for fluid behavior can be simplified if certain assumptions are made. If a fluid is treated as incompressible, then density is constant and changes in density would be zero. The flow of a non-viscous fluid does not slow down due to friction, so the viscosity would be zero. If a fluid is treated as a Newtonian fluid, viscosity remains constant. As a general rule to model reality, fluid density and fluid viscosity are kept constant. If density and viscosity are constant, the equations can be solved for velocity and pressure.

Shown below are the Navier-Stokes equations for a fluid with constant density and constant viscosity[19].

$$\rho\left(\frac{\partial u}{\partial t} + u\frac{\partial u}{\partial x} + v\frac{\partial u}{\partial y} + w\frac{\partial u}{\partial z}\right) = \rho f_x - \frac{\partial p}{\partial x} + \mu\left(\frac{\partial^2 u}{\partial x^2} + \frac{\partial^2 u}{\partial y^2} + \frac{\partial^2 u}{\partial z^2}\right)$$

$$\rho\left(\frac{\partial v}{\partial t} + u\frac{\partial v}{\partial x} + v\frac{\partial v}{\partial y} + w\frac{\partial v}{\partial z}\right) = \rho f_y - \frac{\partial p}{\partial y} + \mu\left(\frac{\partial^2 v}{\partial x^2} + \frac{\partial^2 v}{\partial y^2} + \frac{\partial^2 v}{\partial z^2}\right)$$

$$\rho\left(\frac{\partial w}{\partial t} + u\frac{\partial w}{\partial x} + v\frac{\partial w}{\partial y} + w\frac{\partial w}{\partial z}\right) = \rho f_z - \frac{\partial p}{\partial z} + \mu\left(\frac{\partial^2 w}{\partial x^2} + \frac{\partial^2 w}{\partial y^2} + \frac{\partial^2 w}{\partial z^2}\right)$$

There are quite a few variables so here is what they all represent.

x, y, z – fluid coordinates along its respective axis in three dimensions

u, v, w – velocity of the fluid along its respective axis in three dimensions

ρ – density of the fluid

p – pressure of the fluid

μ – viscosity of the fluid

f_x, f_y, f_z – an arbitrary force applied to the fluid along its respective axis

To make the equations solvable, the following condition must also be met.

$$\frac{\partial u}{\partial x} + \frac{\partial v}{\partial y} + \frac{\partial w}{\partial z} = 0$$

If the arbitrary force is gravity, the Navier-Stokes equations simplify as folows:

$$\rho\left(\frac{\partial u}{\partial t}+u\frac{\partial u}{\partial x}+v\frac{\partial u}{\partial y}+w\frac{\partial u}{\partial z}\right)= \quad -\frac{\partial p}{\partial x}+\mu\left(\frac{\partial^2 u}{\partial x^2}+\frac{\partial^2 u}{\partial y^2}+\frac{\partial^2 u}{\partial z^2}\right)$$

$$\rho\left(\frac{\partial v}{\partial t}+u\frac{\partial v}{\partial x}+v\frac{\partial v}{\partial y}+w\frac{\partial v}{\partial z}\right)= \quad -\frac{\partial p}{\partial y}+\mu\left(\frac{\partial^2 v}{\partial x^2}+\frac{\partial^2 v}{\partial y^2}+\frac{\partial^2 v}{\partial z^2}\right)$$

$$\rho\left(\frac{\partial w}{\partial t}+u\frac{\partial w}{\partial x}+v\frac{\partial w}{\partial y}+w\frac{\partial w}{\partial z}\right)=\rho g \quad -\frac{\partial p}{\partial z}+\mu\left(\frac{\partial^2 w}{\partial x^2}+\frac{\partial^2 w}{\partial y^2}+\frac{\partial^2 w}{\partial z^2}\right)$$

In concise vector form, the Navier-Stokes equations can be summarized as such.

$$\rho\left(\partial_t \mathbf{v}+(\mathbf{v}\cdot\nabla)\mathbf{v}\right)=\rho\mathbf{f}-\nabla p+\mu\nabla^2\mathbf{u}$$

The Navier-Stokes equations due to electro-osmosis can then be derived, shown below[18].

$$\rho\left(\partial_t \mathbf{v}+(\mathbf{v}\cdot\nabla)\mathbf{v}\right)= \quad -\rho_{el}^{eq}\nabla\phi-\nabla p+\mu\nabla^2\mathbf{u}$$

The first term on the right side of the equation is the force due to electro-osmosis, everything else is the same as in the general form of the Navier-Stokes equations. There are two ρ's in the equation. The one on the left side is the density of the fluid, the one on

the right side is the equilibrium charge density of a charged surface of the system. $-\nabla\Phi$

is the electric field. Like electrophoresis and dielectrophoresis, electro-osmosis is also

dependent on the geometry of the electric field. The electro-osmotic velocity field of the

fluid in a corral trap system is shown in Figure 2.32. Results were obtained with COMSOL.

The slight asymmetry of the velocity gradient is due to COMSOL requiring a fluid inlet and

fluid outlet for its calculations.
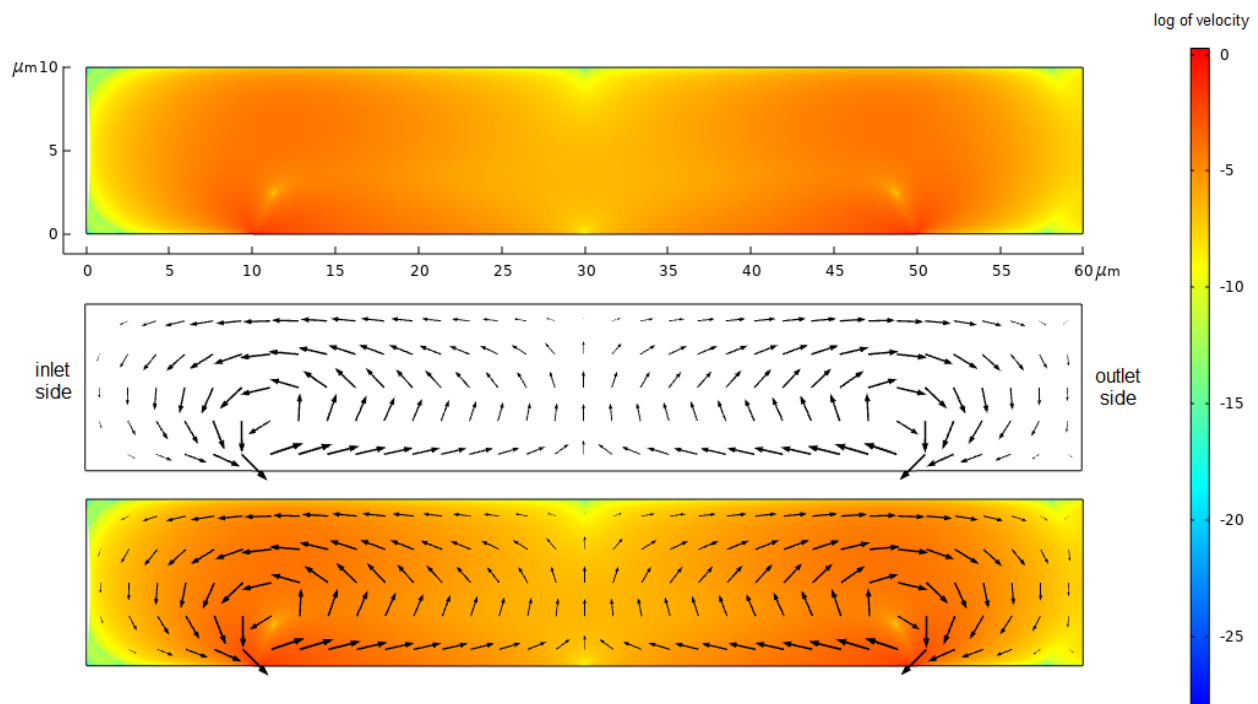
Figure 2.32 – Top image, velocity gradient due to electro-osmosis of the fluid. Middle image, electro-osmotic velocity field depicted with logarithmic arrows. Bottom image, composite.

There is a circular looping behavior that occurs at the rims of the corral. With

regards to the fluid within the corral's diameter, the general direction of fluid flow is

upward; with fluid near the bottom electrode flowing inward towards the center and fluid

near the top electrode flowing outward towards the rims.

In summary there are three main forces that can affect corral trapping to varying degrees; electrophoresis, dielectrophoresis, and electro-osmosis. These three forces give rise to their appropriate fields; the electric field, the dielectrophoretic field, and the electro-osmotic velocity field. The degree to which these forces can affect trapping are likely influenced by experimental conditions. All three fields are shown in Figure 2.33 below.
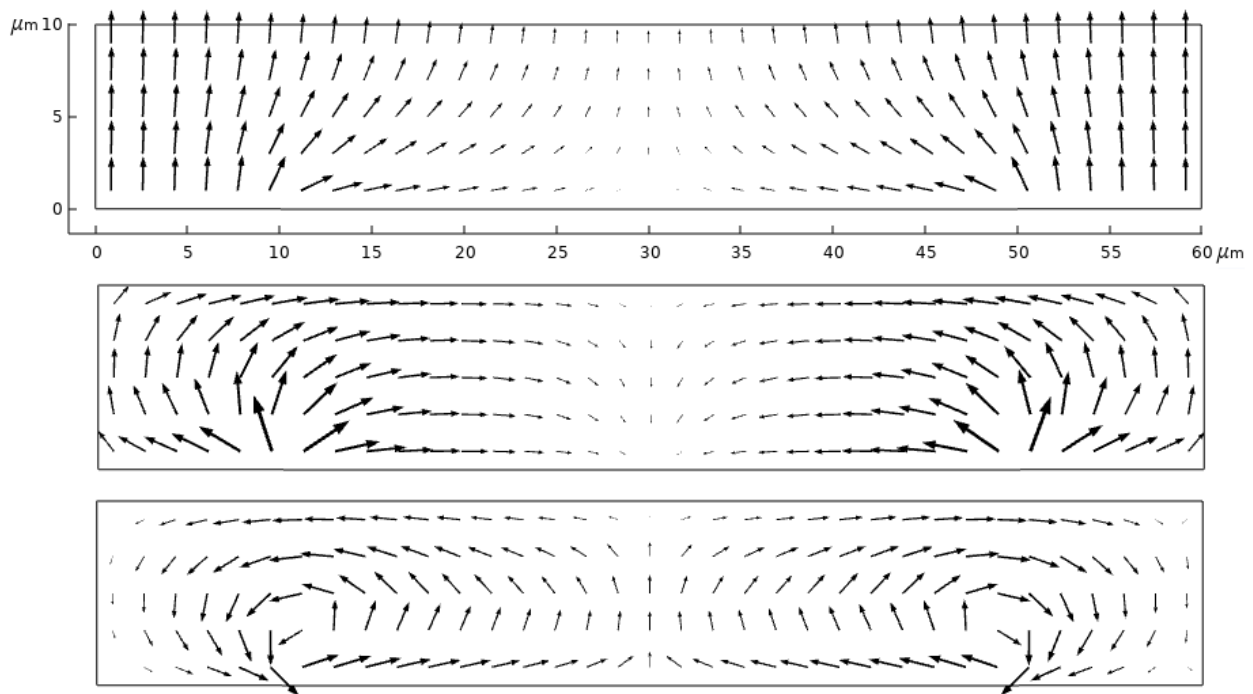
Figure 2.33 – Summary of all fields that can affect corral trapping. Top image, electric field. Middle image, dielectrophoretic field. Bottom image, electro-osmotic velocity field. All arrows are logarithmic.

References for Chapter 2

1.   James Clerk Maxwell, *A Treatise on Electricity and Magnetism*, 1873

2.   Julian Schwinger, Lester L. DeRaad Jr., Kimball A. Milton, Wu-Yang Tsai, *Classical Electrodynamics*, 1998, Perseus Books, Reading, Massachusetts

3.   Carl Friedrich Gauss, "Theoria Attractionis Corporum Sphaeroidicorum Ellipticorum Homogeneorum Methodo Nova Tractate", 1877, *Werke*, Volume V, Page 1

4.   Charles A. Holt, *Introduction to Electromagnetic Fields and Waves*, 1963, John Wiley & Sons, New York

5.   A. Z. Capri, P. V. Panat, *Introduction to Electrodynamics*, 2002, CRC Press, Boca Raton, Florida

6.   Arthur Dearth Moore, *Electrostatics And Its Applications*, 1973, John Wiley & Sons, New York

7.   Ralph P. Winch, *Electricity And Magnetism*, 1963, Prentice-Hall, Englewood Cliffs, New Jersey

8.   Henry G. Booker, *An Approach To Electrical Science*, 1959, McGraw-Hill Book Company, York, Pennsylvania

9.   COMSOL Multiphysics Modeling Software
     COMSOL, Inc.
     www.comsol.com

10. Javier L. Baylon-Cardiel, Blanca H. Lapizco-Encinas, Claudia Reyes-Betanzo, Ana V. Chavez-Santoscoy, Sergio O. Martinez-Chapa, "Prediction of Trapping Zones in an Insulator-Based Dielectrophoretic Device", 2009, *Royal Society of Chemistry*, Vol 9, Pages 2896-2901

11   Herbert A. Pohl, *Dielectrophoresis*, 1978, Cambridge University Press, Cambridge

12. Herbert A. Pohl, "The Motion and Precipitation of Suspensoids in Divergent Electric Fields", 1951, *Journal of Applied Physics*, Vol 22, No 7, Pages 869-871

13. Ronald Pethig, "Review Article – Dielectrophoresis: Status of the Theory, Technology, and Applications", 2010, *Biomicrofluidics*, Vol 4, Pages 022811-1 to 022811-35

14. Swagatika Dash, Swati Mohanty, "Dielectrophoretic Separation of Micron and Submicron Particles: A Review", 2014, *Electrophoresis*, Vol 35, Pages 2656-2672

15. Paul A. Tipler, Gene Mosca, *Physics for Scientists and Engineers Sixth Edition*, 2008, W. H. Freeman and Company, New York

16. Christine A. Carlson, *Development of the Electrostatic Corral for the Trapping of Single Molecules in Solution*, 2010, PhD Thesis, Department of Chemistry, University of Wisconsin-Milwaukee

17. A. Ashkin, J. M. Dziedzic, J. E. Bjorkholm, Steven Chu, "Observation of a single-beam gradient force optical trap for dielectric particles", 1986, *Optics Letters*, Vol 11, No 5, Pages 288-290

18. Henrik Bruus, *Theoretical Microfluidics*, 2008, Oxford University Press, Oxford

19. Edward J. Shaughnessy, Ira M. Katz, James P. Schaffer, *Introduction to Fluid Mechanics*, 2005, Oxford University Press, Oxford

20. Hywel Morgan, Michael P. Hughes, Nicolas G. Green, "Separation of Submicron Bioparticles by Dielectrophoresis", 1999, *Biophysical Journal*, Vol 77, Pages 516-525

21. C. Zhang, K. Khoshmanesh, A. Mitchell, K. Kalantar-zadeh, "Dielectrophoresis for manipulation of micro/nano particles in microfluidic systems", 2010, *Analytical Bioanalytical Chemistry*, Vol 396, Pages 401-420

22. Herbert A. Pohl, *Dielectrophoresis: the behavior of neutral matter in nonuniform electric fields*, 1978, Cambridge University Press, Cambridge

23. Arun T. J. Kadaksham, Pushpendra Singh, Nadine Aubry, "Dielectrophoresis of nanoparticles", 2004, *Electrophoresis*, Vol 25, Pages 3625-3632

24. Ian Mills, Tomislav Cvitas, Klaus Homann, Nikola Kallay, Kozo Kuchitsu, *Quantities, Units and Symbols in Physical Chemistry*, 1993, IUPAC, Blackwell Science, Oxford

25. Peter R. C. Gascoyne, Jody Vykoukal, "Particle separation by dielectrophoresis", 2002, *Electrophoresis*, Vol 23, Pages 1973-1983

26. Jason G. Kralj, Michael T. W. Lis, Martin A. Schmidt, Klavs F. Jensen, "Continuous Dielectrophoretic Size-Based Particle Sorting", 2006, *Analytical Chemistry*, Vol 78, Pages 5019-5025

27. Jianpinig Fu, Pan Mao, Jongyoon Han, "Nanofilter array chip for fast gel-free biomolecule separation", 2005, *Applied Physics Letters*, Vol 87, Pages 263902-1 to 263902-3

28. M. D. Vahey, J. Voldman, "An Equilibrium Method for Continuous-Flow Cell Sorting Using Dielectrophoresis", 2008, *Analytical Chemistry*, Vol 80, Pages 3135-3143

29. N. G. Green, H. Morgan, Joel J. Milner, "Manipulation and trapping of sub-micron bioparticles using dielectrophoresis", 1997, *Journal of Biochemical and Biophysical Methods*, Vol 35, Pages 89-102

30. Ralph Holzel, Nils Calander, Zackary Chiragwandi, Magnus Willander, Frank F. Bier, "Trapping Single Molecules by Dielectrophoresis", 2005, *Physical Review Letters*, Vol 95, Pags 128102-1 to 128102-4

31. Liming Ying, Samuel S. White, Andreas Bruckbauer, Lisa Meadows, Yuri E. Korchev, "Frequency and Voltage Dependence of the Dielectrophoretic Trapping of Short Lengths of DNA and dCTP in a Nanopipette", 2004, *Biophysical Journal*, Vol 86, Issue 2, Pages 1018-1027

32. W. Andre Germishuizen, Christoph Walti, Rene Wirtz, Michael B. Johnston, Michael Pepper, A. Giles Davies, Anton P. J. Middelberg, "Selective dielectrophoretic manipulation of surface-immobilized DNA molecules", 2003, *Nanotechnology*, Vol 14, Pages 896-902

33. Lifeng Zheng, Shengdong Li, James P. Brody, Peter J. Burke, "Manipulating Nanoparticles in Solution with Electrically Contacted Nanotubes Using Dielectrophoresis", 2004, *Langmuir*, Vol 20, Pages 8612-8619

34. Sreeja B. Asokan, L. Jawerth, R. Lloyd Carroll, R. E. Cheney, S. Washburn, R. Superfine, "Two-Dimensional Manipulation and Orientation of Actin-Myosin Systems with Dielectrophoresis", 2003, *Nano Letters*, Vol 3, No 4, Pages 431-437

35. Zhuo Chen, Zhongyun Wu, Lianming Tong, Huapu Pan, Zhongfan Liu, "Simultaneous Dielectrophoretic Separation and Assembly of Single-Walled Carbon Nanotubes on Multigap Nanoelectrodes and Their Thermal Sensing Properties", 2006, *Analytical Chemistry*, Vol 78, Pages 8069-8075

36. Xianming Liu, John L. Spencer, Alan B. Kaiser, W. Mike Arnold, "Selective purification of multiwalled carbon nanotubes by dielectrophoresis within a large array", 2006, *Current Applied Physics*, Vol 6, Issue 3, Pages 427-431

37. Haibo Li, Yanan Zheng, Demir Akin, Rashid Bashir, "Characterization and Modeling of a Microfluidic Dielectrophoresis Filter for Biological Species", 2005, *Journal of Microelectromechanical Systems*, Vol 14, No 1, Pages 103-112

Chapter 3

An Electrokinetic Survey

3.1 Infinite Possibilities

The following is an overview of methods that have been used to trap or manipulate particles by electrokinetic forces, and are therefore relevant for the work presented in this thesis. All manner of electrokinetic behavior is possible depending on the electrode patterns, electrode shapes, electrode designs, conductive system geometry, non-conductive system geometry, solution ion concentration, inherent nature of the particle itself, solution direction and flow, size and volume of system, implementation of light and optics, etc. The research possibilities of field geometries and their interactions with various parameters are endless. This chapter is a survey of some methods that have been explored through experimentation from other researchers.

3.2 Electrodeless Dielectrophoresis of Single- and Double-Stranded DNA[1]
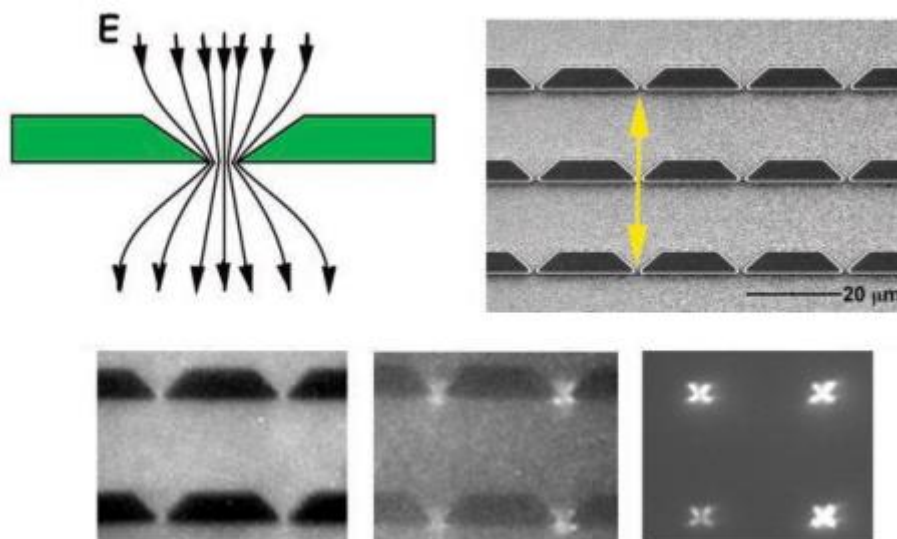
Figure 3.1 – Top left, the geometry of the electric field as it flows through a non-conductive physical restriction. Top right, the constriction array etched out of quartz. Bottom row, images of trapped DNA. They are visualized with epifluorescence[1].

The title of the article is somewhat misleading. The mechanism used to trap DNA is not an electrode, but rather a non-conductive physical restriction. However, electrodes are still required to generate the electric field itself. The physical restrictions distort the field and create a gradient. The highest field density occurs at the restriction, therefore positive dielectrophoresis could be used to trap particles at the restrictions. The constriction array is etched out of quartz. The yellow arrows in the top right image indicate the direction of the applied electric field. The advantage of this method is that trapping can be achieved at low AC frequencies. If metallic trapping structures were used, which would function as electrodes, electrolysis would occur and degrade the electrodes. The bottom row of images shows the trapping trend, left to right, of higher frequency to a lower frequency and of short DNA strands to longer DNA strands.

3.3 Evaluation of the Potential for Using Dielectrophoresis to Separate Minerals[2]
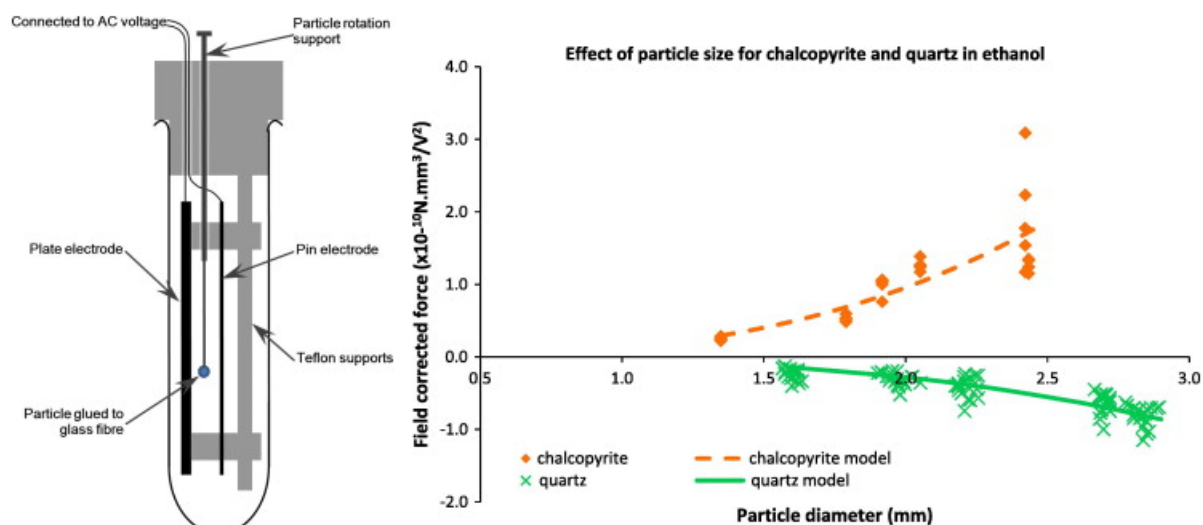
Figure 3.2 – Left image, schematic of system. Right image, dielectrophoretic force experienced by particle based on the particle's size[2].

This is not a separation or a type of trapping, but rather to test if dielectrophoresis could be used to potentially separate minerals. Chalcopyrite particles and quartz particles were tested. The schematic indicates that one electrode is a flat plate and the other is a thin pin. The thin pin would experience the highest field density due to its smaller volume relative to the flat plate electrode. A mineral particle is suspended between the two electrodes on a flexible glass fiber. A dielectrophoretic particle will move towards one of the two electrodes. The dielectrophoretic force experienced by the particle based on the size of the particle was measured. The larger the particle size, the greater the dielectrophoretic force it experiences. Under identical conditions, chalcopyrite always underwent positive dielectrophoresis while quartz always underwent negative dielectrophoresis. This indicates dielectrophoretic separation of substances is possible based on the nature of the substance itself.

3.4 Microfluidic System for Dielectrophoretic Separation Based on a Trapezoidal Electrode Array[3]
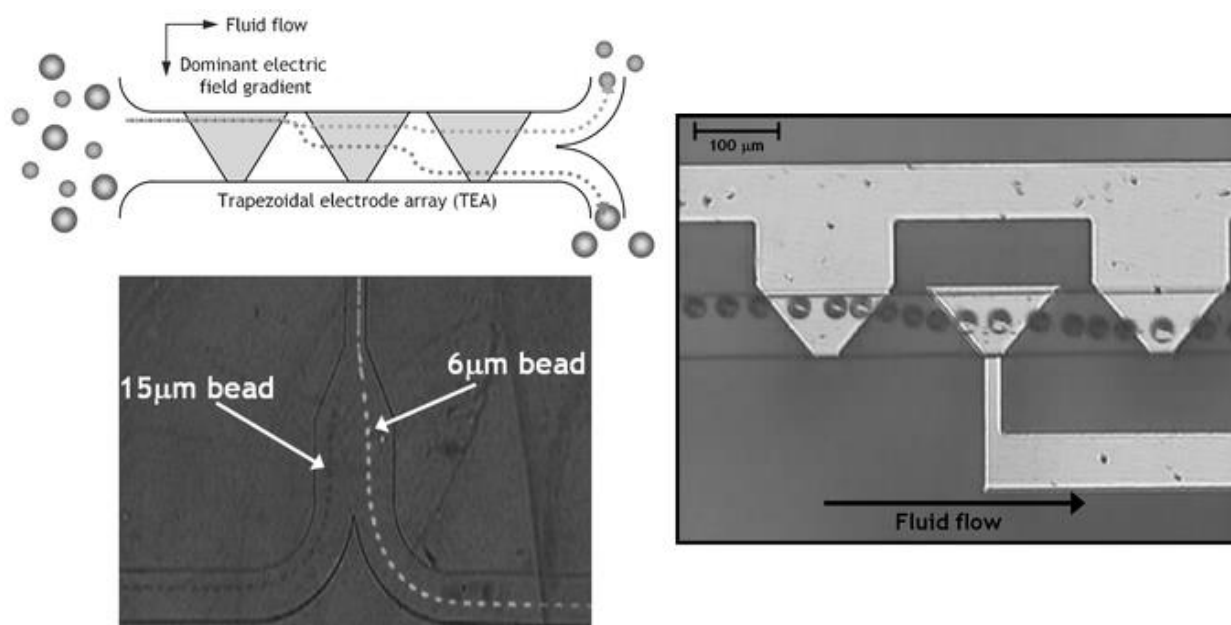
Figure 3.3 – Top left, system schematic. Gray areas are metal. Right image, electrical schematic indicating trapezoids alternate between electrodes. Electrodes are also co-planar. Bottom left, separation of beads based on their properties as well as size[3].

The metal surfaces of this system are trapezoidal in shape. The electrical schematic shows that the trapezoids alternate between electrodes. Since the shape of the electrodes are not truly trapezoidal, the shape of the trapezoid is imposed by the use of a microfluidic channel. With a trapezoid, one side has shorter length and the opposing side has longer length. The system has both metallic trapezoids and non-metallic trapezoids. There would be greater field density at the shorter length of the non-metallic trapezoid and lower field density at the longer length of the non-metallic trapezoid. Particles will either move towards the longer length of the non-metallic trapezoid or the shorter length of the non-metallic trapezoid based on their inherent properties.

3.5 Dielectrophoresis: An Assessment of its Potential to aid the Research and Practice of Drug Discovery and Delivery[4]
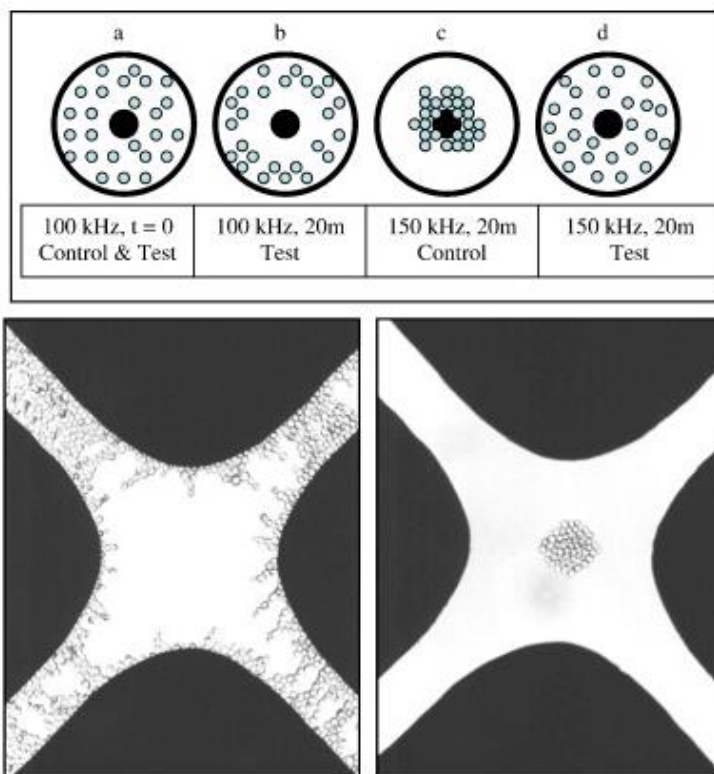
Figure 3.4 – Top image, dielectrophoretic effects using a pin and ring electrode system. Bottom images, yeast cells exhibiting dielectrophoretic behavior under a quadrupole electrode system. A quadrupole electrode system requires two voltage sources[4].

For the top image, both control and test cells are randomly distributed between the pin and ring electrodes at time zero. After 20 minutes of incubation with an apoptosis-inducing drug, all cells move away from the pin and move towards the ring. Apoptosis is cell death, so the cell's normal functions have ceased. The apoptosis-inducing drug is capable of altering the dielectrophoretic properties of cells. With an increase in AC frequency, only the control cells are attracted to the pin electrode and only the test cells become randomly distributed again.

74

3.6 Dielectrophoretic Filter for Separation and Recovery of Biological Cells in Water[5]
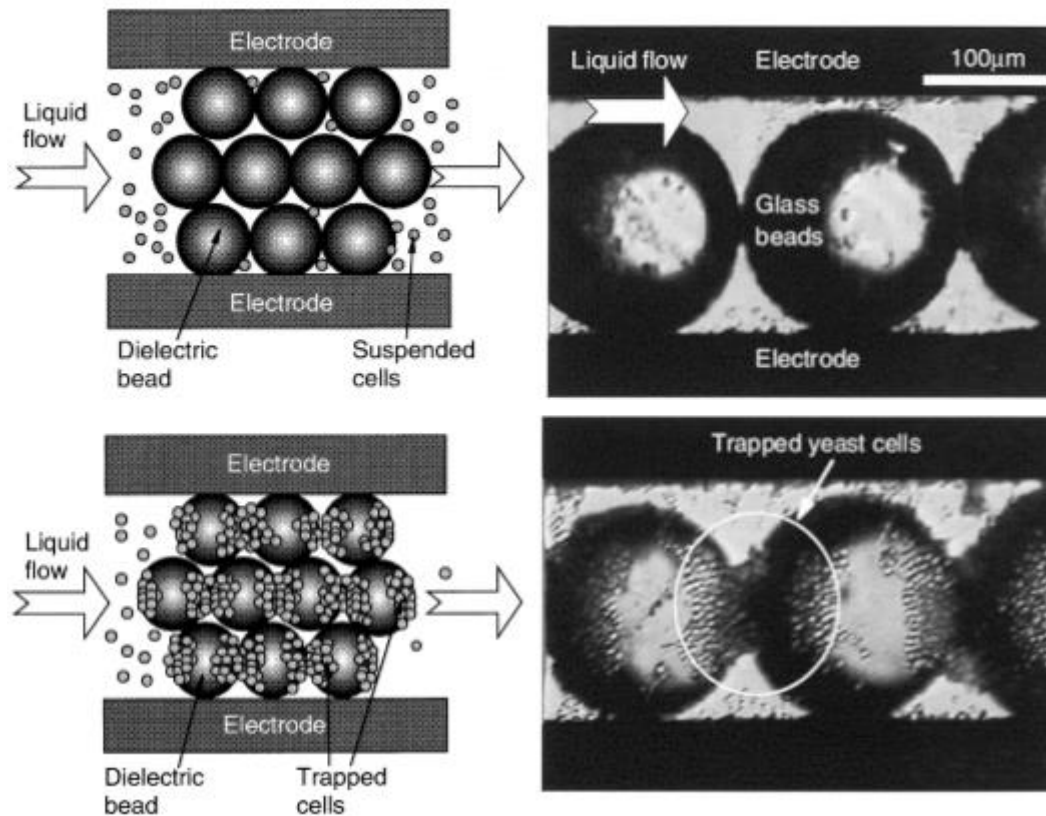
Figure 3.5 – Top left, voltage is off. Bottom image, voltage is on. Right images, the trapping of yeast cells[5].

The principle for a dielectrophoretic filter involves the use of dielectric glass beads that are located between the top and bottom electrode. While the voltage is off, biological cells are capable of flowing through the gaps of the beads. Once voltage is applied, biological cells become attracted to the beads. This principle could be used simply for general filtration and purification of water, which is always useful; but the main focus is the recovery of biological cells. Biological cells are recovered by allowing the beads to flow out of the channel.

3.7 Continuous Cell from Cell Separation by Traveling Wave Dielectrophoresis[6]
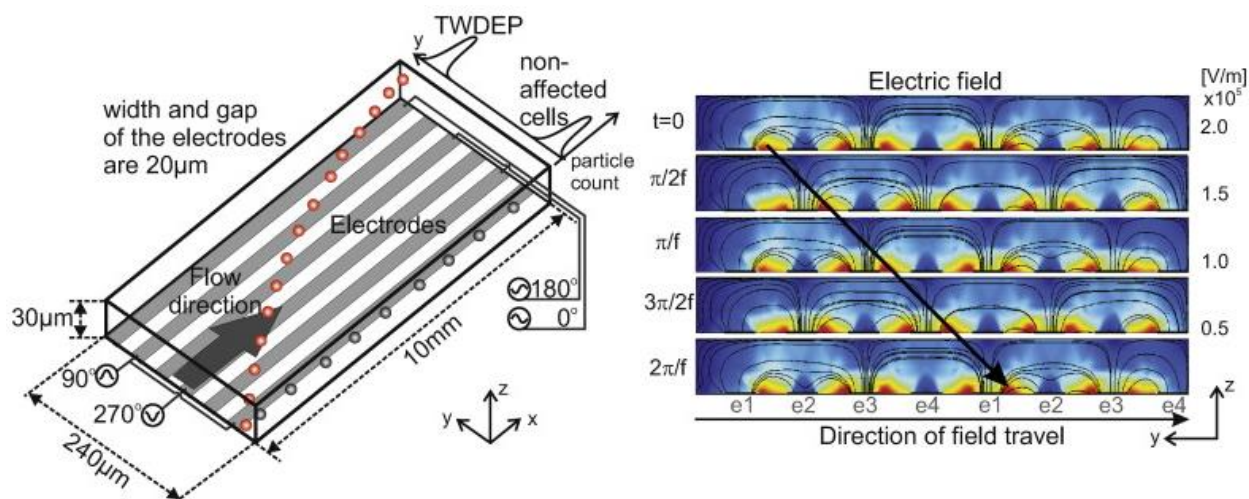
Figure 3.6 – Left image, electrical schematic. Right image, snapshots of the traveling wave as it goes from electrode to electrode[6].

The system is made up of parallel, rectangular strips of metal. The traveling wave dielectrophoretic force is perpendicular to solution flow direction. A traveling wave is attained by phase shifting the AC frequency. A phase shift describes the degree to which two alternating quantities reach their maximum, minimum, or zero values; the schematic indicates there are four voltage sources. If two identical AC frequencies reach their maximum, minimum, and zero values simultaneously; they are both in phase. A 90° phase shift means that one frequency will reach its maximum 90° after the first frequency. The traveling wave perpetuates through the electrodes and simultaneously exerts dielectrophoretic forces on particles. The left image shows that a gray particle unaffected by dielectrophoresis maintains its original trajectory, while a red particle that is affected by dielectrophoresis moves toward a different trajectory, thereby enabling separation.

3.8 Dynamic Holographic Optical Tweezers[7]
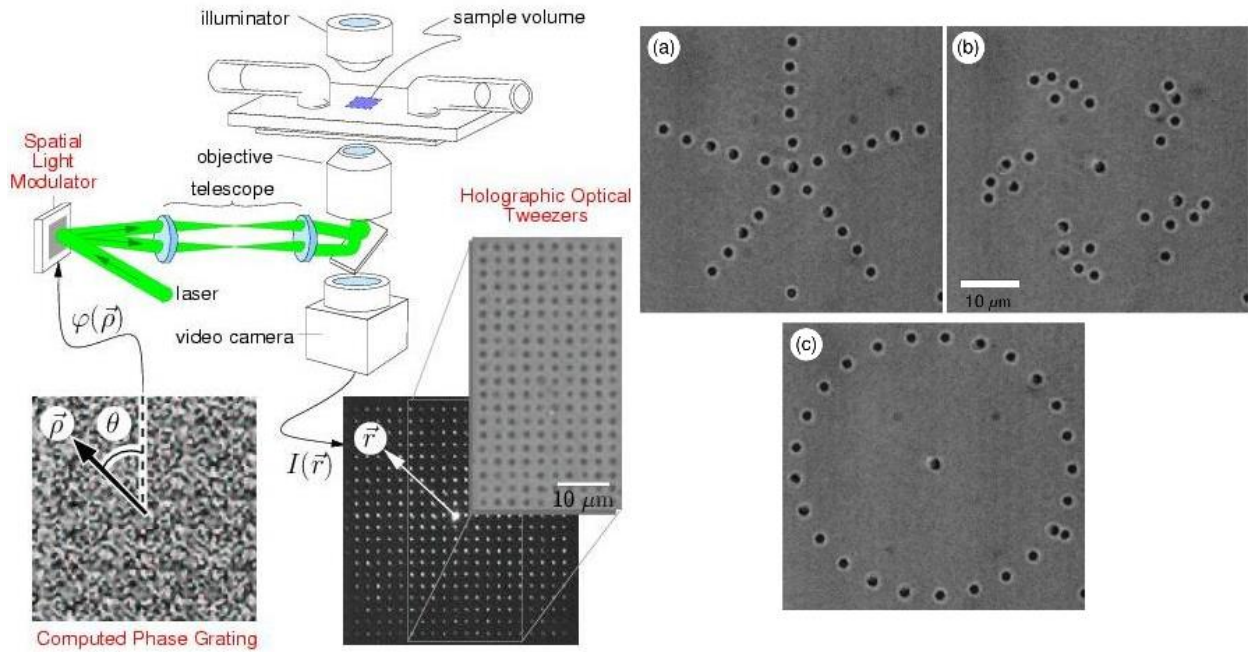
Figure 3.7 – Left image, schematic for dynamic holographic optical tweezers. Right images, silica spheres manipulated with dynamic holographic optical tweezers[7].

A dynamic holographic optical tweezer utilizes the same principle as a conventional optical tweezer. This system incorporates a computer-designed diffractive optical element which splits a single laser beam into several separate beams. Images show the beads initially configured in a star pattern, the very same beads are then configured into different patterns. Such a system uses custom programming to control the way the single laser beam is split. There is likely to be a trade-off with how many separate beams the diffractive element can make while still being able to effectively trap particles with each beam. The spheres are not simply confined and stationary, they are actually moved around.

3.9 Fabrication Of Linear Colloidal Structures For Microfluidic Applications[8]
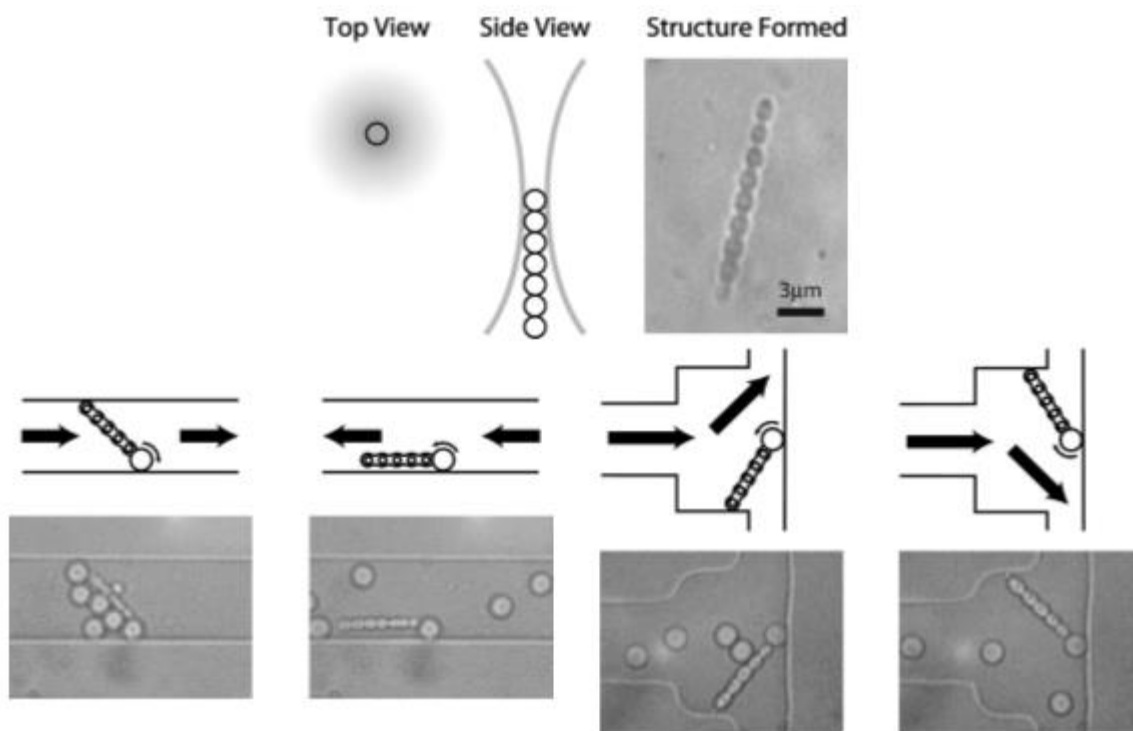
Figure 3.8 – Top image, linear polymerization of silica spheres. Bottom images, the linear polymerized spheres used a type of valve[8].

The top image shows how silica spheres are polymerized with an optical trap. The mechanism is interesting in that aligning the spheres linearly is done with the optical trap and polymerizing the spheres is also done with the same said optical trap. The linear chain of polymerized silica spheres is then also maneuvered into a microfluidic channel with the optical trap and also held in place with the optical trap. Such a setup requires fine computer-controlled motors and mechanisms to maneuver the optical trap around along with the linear structures. The bottom images show how the linear structure can be used as a type of valve. Opening and closing the valve is done with solution flow.

3.10 Microfluidic Control Using Colloidal Devices[9]
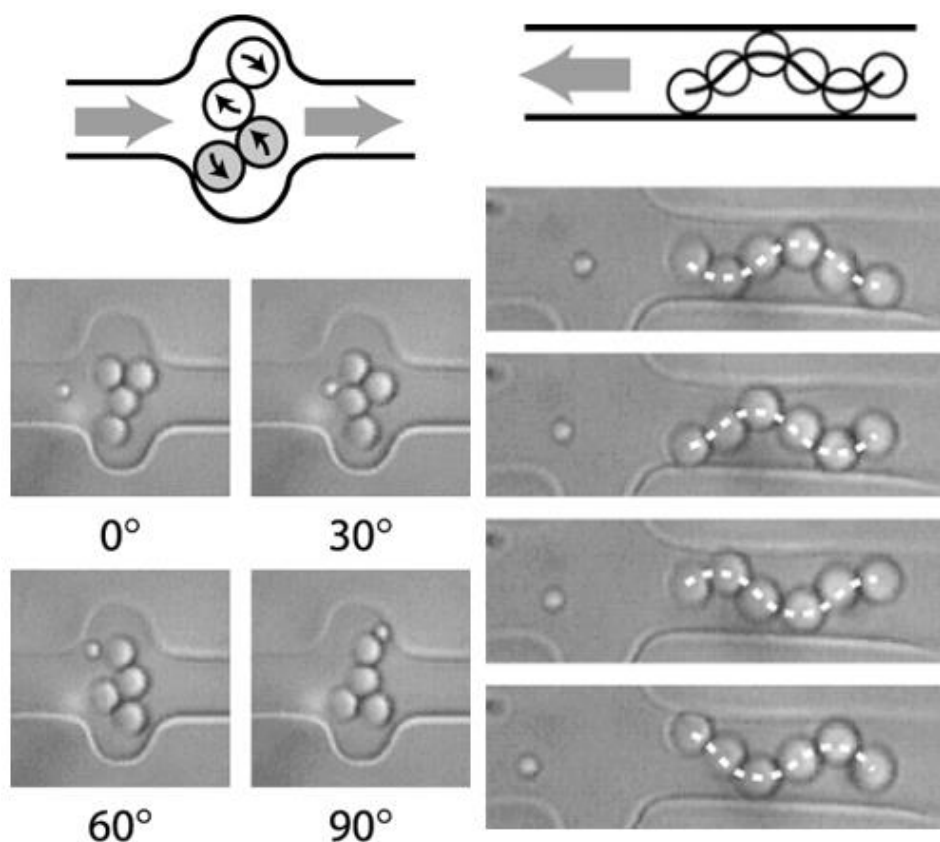
Figure 3.9 – Left image, a gear pump. When one gear turns, the other turns as well. Right image, a peristaltic pump. The single tracer bead gradually advances to the left[9].

These two designs are pumps that induce the movement of beads. The images on the left show a gear pump. The images on the left illustrate lobe movement, the top pair of beads rotate clockwise which forces the bottom pair of beads to rotate counter-clockwise; they essentially function as gears. The motion of the gears results in pushing a smaller tracer bead along the channel. The images on the right show the undulating snake-like motion of a string of beads. The result is similar to the gear pump, a small tracer bead is pushed further along the channel. The system on the left utilizes four optical traps to manipulate the beads. The system on the right uses six optical traps.

3.11 Structure of Optical Vortices[13]
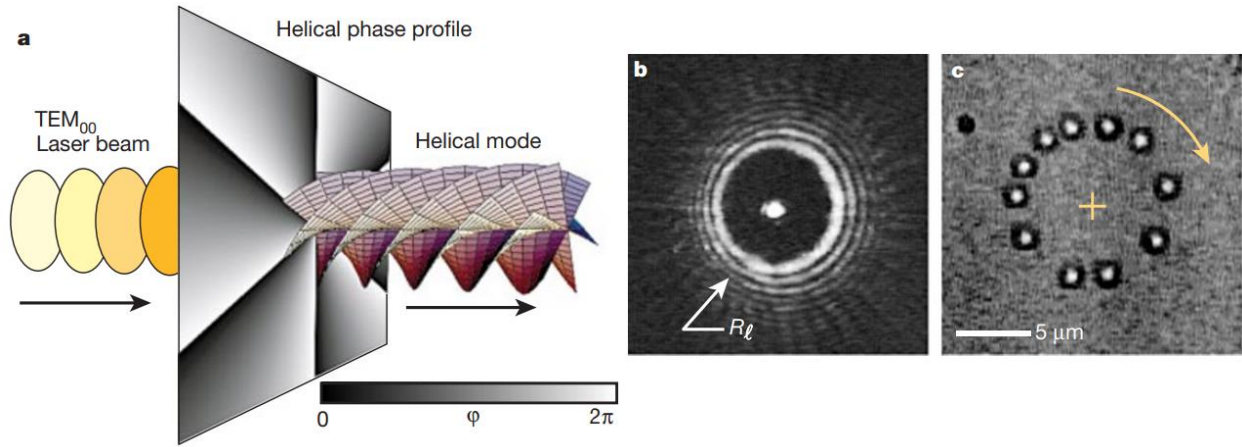
Figure 3.10 – This experiment shows the result of imposing a phase shift on an optical tweezer. Instead of being trapped in the center, a particle will rotate in a circular pattern[12,13].

In this experiment, an optical trap is modified. Trapping is still the result, but this time a beam of light is created that has a helical wavefront. This is achieved by utilizing a phase mask. Beams with a helical wavefront focus to rings instead of points. In the left image of Figure 3.10 above, the helical mode is achieved with a spatial light modulator (SLM). The middle image is the optical vortex. The right image is a time-lapse composite of a single colloidal sphere traveling around the optical vortex.

The pitch of the helical wavefront is the degree of the helice's steepness or shallowness. The radius of the optical vortex is proportional to its pitch; the greater the pitch, the greater the optical radius. Since the laser wavefront is dynamically controlled by a spatial light modulator, dynamically changing the wavefront also dynamically changes its electric field. This could potentially lead to other types of dielectrophoretic manipulation with lasers.

3.12 Microscopic Particle Manipulation via Optoelectronic Devices[10]
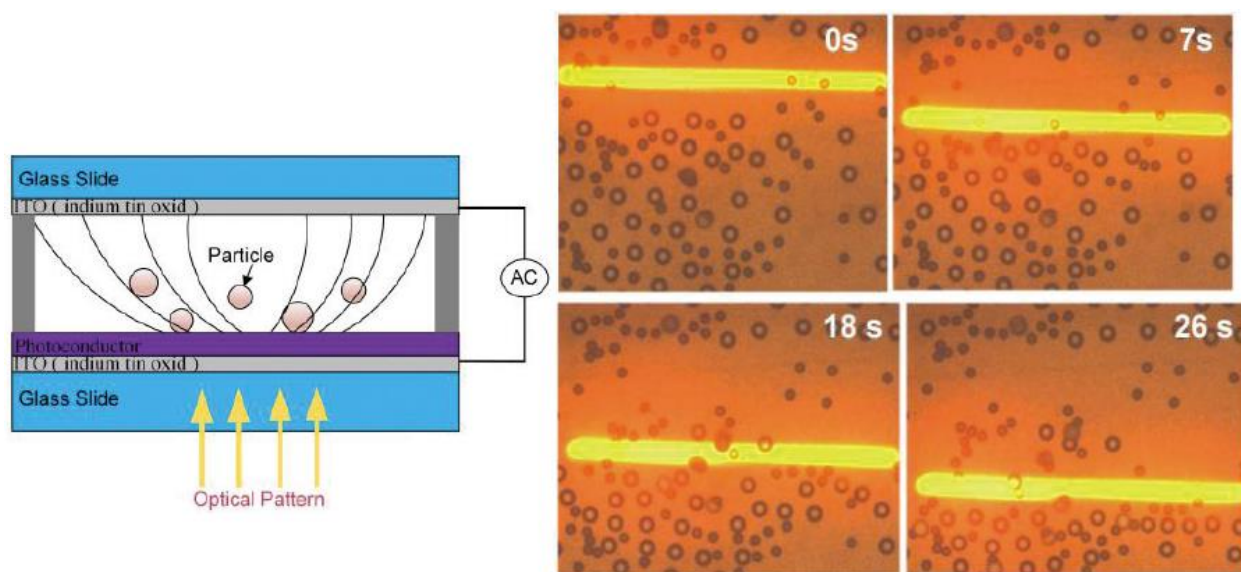
Figure 3.11 – Left image, schematic for optically induced dielectrophoresis. Right image, a dielectrophoretic light pattern is moved up and down and displaces beads[10].

The system consists of two electrodes, one on top of the other. The new element is a photoconductive layer that covers the entire surface of the bottom electrode, indicated with purple in the left image. It is non-conductive, the layer becomes conductive when light is shined upon it. If the entire surface is illuminated, the entire surface becomes conductive. But instead of illuminating the entire surface, it can be illuminated with specific light patterns such as small circles, which essentially function similar to corral traps. With this technique, designing patterns on the metal layer isn't even necessary since patterns could easily be created with light instead. However, this technique could conflict with imaging methods that involve fluorescence. Not only can patterns be created with programmable convenience, patterns can be changed during the experiment itself.

3.13 Optically-Induced Dielectrophoretic Technology for Particles Manipulation and Separation[11]
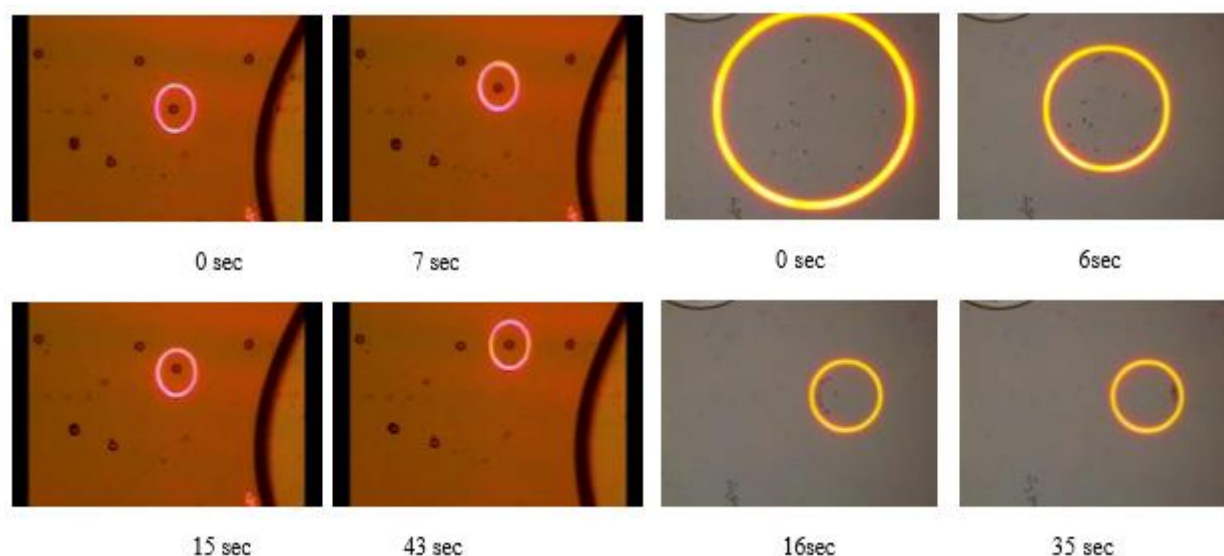
Figure 3.12 – Left image, physical manipulation of a bead using optically-induced dielectrophoresis. Right image, concentrating beads by diminishing the size of the ring[11].

The examples above are functionally ring-shaped electrodes, which do not behave exactly the same way as a corral. With a corral trap, trapping is attained with negative dielectrophoresis due to the metal void of the corral trap. With a ring electrode, trapping is done with positive dielectrophoresis. Using an actual metal ring electrode would require wiring that would not be exposed to the solution. One advantage of optically-induced dielectrophoresis is that this wiring would not be necessary. The left images show a bead being moved up and down. It is the light pattern itself that is moved up and down, while the bead stays confined inside it. The right images show a concentration technique. The diameter of the ring electrode is initially very large and is gradually diminished over time. The result is that the beads become more concentrated.

3.14 Fast AC Electro-Osmotic Micropumps with Nonplanar Electrodes[15]
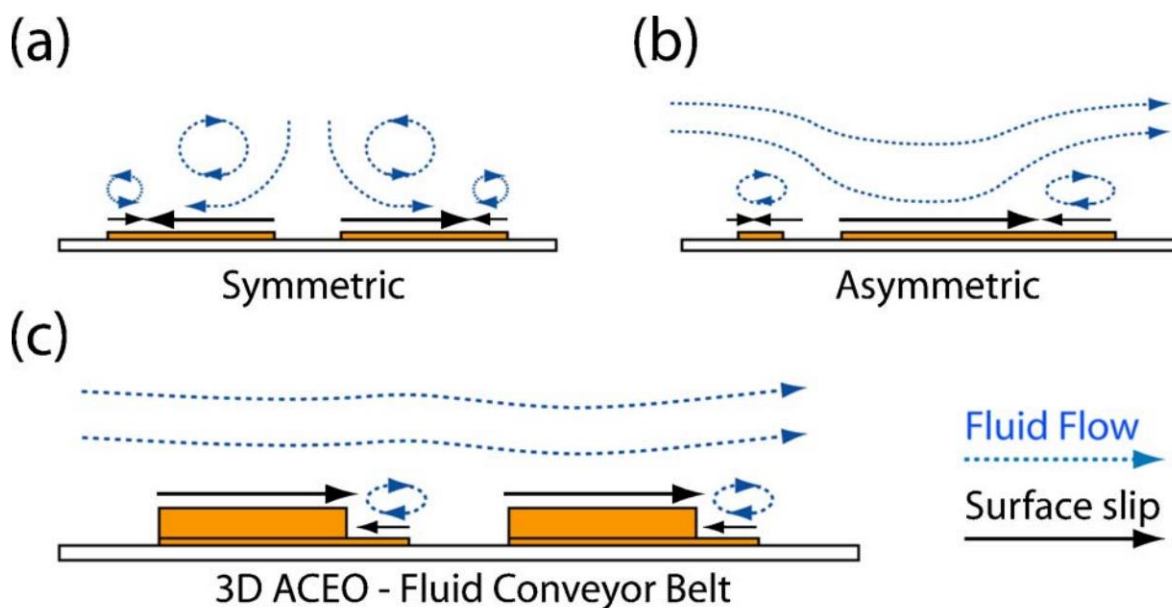
Figure 3.13 – Types of fluid flow created by different electrode configurations[15].

While this experiment is not specifically about trapping, it does deal with creating solution flow in microfluidic systems. Corral trapping and any other type of bead manipulation would be implemented in microfluidic systems and micropumps would provide a means to move beads to the desired corral traps. In the top left image of Figure 3.13, the electrodes are symmetric and does not create an overall unidirectional flow. In the top right image with asymmetric electrodes, there are minor vortices but this configuration does create unidirectional flow of solution. In the bottom image, a step in the electrode is created which results in higher fluid flow velocities. This step could easily be created with a two-step metal deposition process and appropriate masking for each step. An electrode configuration could potentially be devised to trap particles solely using electro-osmosis. The particle would not have to be charged or polarized.

3.15 Dielectrophoresis Switching with Vertical Sidewall Electrodes for Microfluidic Flow Cytometry[16]
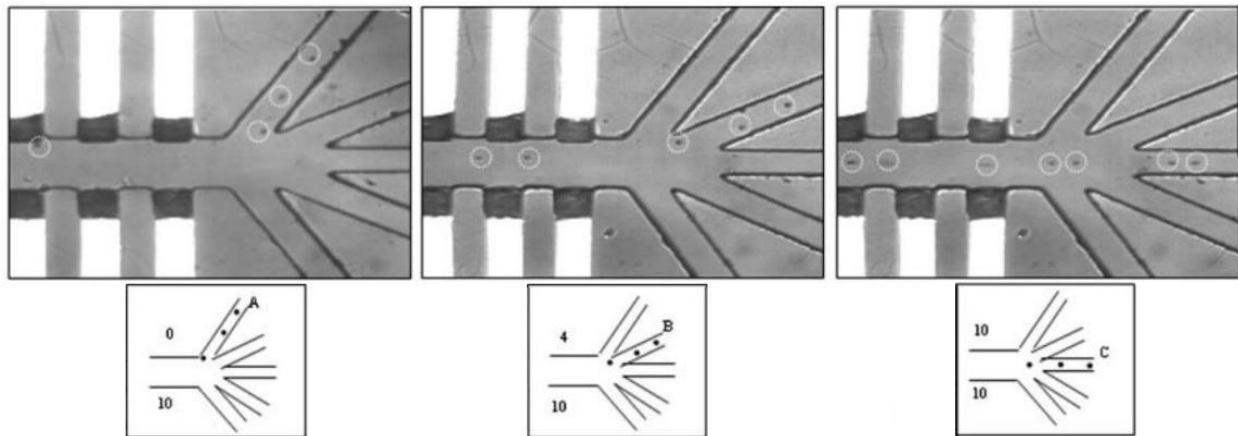
Figure 3.14 – The six dark rectangular shapes are electrodes. Beads flowing in solution are circled in white. Solution flow direction is left to right. Left images, if the bottom three electrodes are set to 10 V and the top three electrodes are set to 0 V, the beads will exit out of the top channel. Middle images, bottom three electrodes are set to 10 V and the top three electrodes are set to 4 V, the beads will exit out of the second channel from the top. Right images, all electrodes are set to 10 V, the beads will exit out of the middle channel.

Both the top and bottom sets of electrodes have three more electrodes to the left of the visible electrodes, so they are not seen in the images. The top and bottom sets of electrodes are on two separate circuits. The top set of electrodes create a dielectrophoretic field towards the bottom set of electrodes, similarly the bottom set of electrodes create a dielectrophoretic field toward the top set electrodes. By varying the voltages the beads can be maintained at a certain equilibrium position along the channel pathway. If the top set of electrodes is set at a higher voltage than the bottom set of electrodes, the beads will be closer to the bottom set of electrodes. If both sets of electrodes have the same voltage magnitude, the bead will be exactly midway between the two sets of electrodes.

References for Chapter 3

1.   Chia-Fu Chou, Jonas Tegenfeldt, Olgica Bakajin, Shirley Chan, Edward Cox, Nicholas Darnton, Thomas Duke, Robert Austin, "Electrodeless Dielectrophoresis of Single- and Double-Stranded DNA", 2002, *Biophysical Journal*, Vol 83, No 4, Pages 2170-2179

2.   G. R. Ballantyne, P. N. Holtham, "Evaluation of the Potential for using Dielectrophoresis to Separate Minerals", 2014, *Minerals Engineering*, Vol 55, Pages 75-79

3.   Sungyoung Choi, Je-Kyun Park, "Microfluidic System for Dielectrophoretic Separation based on Trapezoidal Electrode Array", 2005, *Lab on a Chip*, Vol 5, Pages 1161-1167

4.   Ronald Pethig, "Dielectrophoresis: An Assessment of its Potential to Aid the Research and Practice of Drug Discovery and Delivery", 2013, *Advanced Drug Delivery Reviews*, Vol 65, Issues 11-12, Pages 1589-1599

5.   Junya Suehiro, Guangbin Zhou, Manabu Imamura, Masanori Hara, Dielectrophoretic Filter for Separation and Recovery of Biological Cells in Water", 2003, *IEEE Transactions on Industry Applications*, Vol 39, No 5, Pages 1514-1521

6.   Sander van den Driesche, Vivek Rao, Dietmar Puchberger-Enengl, Wojciech Witarski, Michael J. Vellekoop, "Continuous Cell from Cell Separation by Traveling Wave Dielectrophoresis", 2012, *Sensors and Actuators B: Chemical*, Vol 170, Pages 207-214

7.   Jennifer E. Curtis, Brian A. Koss, David G. Grier, "Dynamic Holographic Optical Tweezers", 2002, *Optics Communications*, Vol 207, Issues 1-6, Pages 169-175

8.   Alex Terray, John Oakey, David W. M. Marr, "Fabrication of Linear Colloidal Structures for Microfluidic Applications", 2002, *Applied Physics Letters*, Vol 81, No 9, Pages 1555-1557

9.   Alex Terray, John Oakey, David W. M. Marr, "Microfluidic Control Using Colloidal Devices", 2002, *Science*, Vol 296, Issue 5574, Pages 1841-1844

10.   Xiaolu Zhu, Yifei Yang, *Microscopic Particle Manipulation via Optoelectronic Devices*, 2017, InTech

11.   Hsiu-Hsiang Chen, Wan-Ting Tien, Hsin-Hsiang Lo, Chun-Chuan Lin, Jyh-Chern Chen, "Optically-Induced Dielectrophoretic Technology for Particles Manipulation and Separation", 2013, *8th Interational Microsystems Packaging Assembly and Circuits Technology Conference (IMPACT)*

12. K. T. Gahagan, G. A. Swartzlander Jr., "Trapping of low-index microparticles in an optical vortex", 1998, *Journal of the Optical Society of America*, Vol 15, No 2, Pages 524-534

13. Jennifer E. Curtis, David G. Grier, "Structure of Optical Vortices", 2003, *Physics Review Letters*, Vol 90, No 13. Pages 133901-1 to 133901-4

14. Xiayan Wang, Chang Cheng, Shili Wang, Shaorong Liu, "Electroosmotic Pumps and their Applications in Microfluidic Systems", 2009, *Microfluidics and Nanofluidics*, Vol 6, Issue 2, Pages 145-162

15. John Paul Urbanski, Todd Thorsen, Jeremy A. Levitan, Martin Z. Bazant, "Fast ac electro-osmotic micropumps with nonplanar electrodes", 2006, *Applied Physics Letters*, Vol 89, pages 143508-1 to 143508-3

16. Lisen Wang, Lisa Flanagan, Noo Li Jeon, Edwin Monuki, Abraham P. Lee, "Dielectrophoresis switching with vertical sidewall electrodes for microfluidic flow cytometry", 2007, *Lab on a Chip*, Vol 7(9), Pages 1114-1120

Chapter 4

Methods

4.1 Materials

The main materials used to fabricate the electrodes are standard 1" x 3" microscope slides, 1" x 1" microscope coverslips, 10.5 mm x 22 mm microscope coverslips, acetone, methanol, isopropanol, ultra-pure water (water that has a resistivity of 18.2 MΩ·cm), S1813 (positive photoresist), SU8 2002 (negative photoresist), MF-321 (positive photoresist developer), SU8 Developer (negative photoresist developer), PG Remover (photoresist remover), professional mask (designed with a CAD program), tungsten filament, and Nichrome (60% Ni, 16% Cr, 24% Fe alloy) metal wire and Au/Pd (60%:40%) metal wire for deposition of the metal layers. All lithography chemicals are from Microchem (www.microchem.com). All filaments and metal wires are from Ted Pella (www.tedpella.com). The professional mask was first designed with Draftsight (www.3ds.com), which is a CAD program that exists in both a free version and a professional version; the free version is more than adequate for mask design. The design was then fabricated into a mask by Photo Sciences, Inc (www.photo-sciences.com). The required instrumentation includes a sonicator, spin-coater, oven, lithography UV aligner, ultra-pure water filtration system, and metal deposition system.

4.2 Glass Cleaning Process

The glass cleaning process involves a series of sonications of the glass in various organic solvents[1]. Sonication is simply the application of sound energy and is achieved with a sonicator bath. The slides are placed on a mold, which is then submerged in a beaker of organic solvent for sonication. The mold is used to orient the slides vertically and ensures that the largest possible surface area of the slide is exposed to solvent. The

sonication instrumentation used for these experiments has only one setting, "on". The process involves three solvents.

1) Acetone for 15 minutes at a temperature of 35°C

2) Methanol for 15 minutes at a temperature of 35°C

3) Isopropanol for 15 minutes at a temperature of 35°C

The cleaning process is done to remove any type of residual substances left behind by the manufacturing of the glass slides or coverslips, as well as remove incident particulate matter or dust. The process ensures a relatively clean glass surface with which further lithography and metal deposition can be performed.
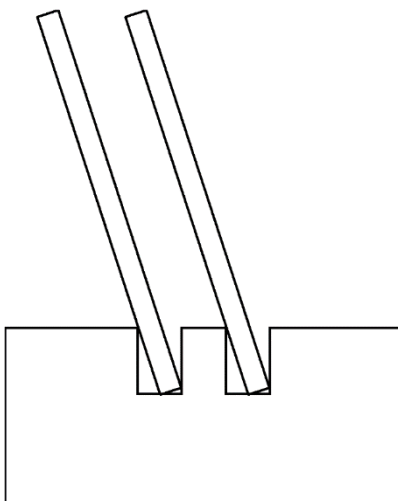
Figure 4.1 – During sonication, glass slides are oriented to be as vertical as possible by the use of a mold to ensure maximum surface exposure to cleaning solvents.

After sonication with isopropanol is finished, the slides are immediately dried with compressed and filtered N_2 gas. Each slide is kept submerged in the isopropanol until

89

drying is performed. Only the surface where metal is intended to be deposited on is dried with N_2 gas, this is of course the top surface. The idea is to blast the top surface with nitrogen gas and to remove the isopropanol as quickly as possible to prevent the isopropanol from drying out on the surface. If the isopropanol is allowed to evaporate, this will leave behind residual material. Soluble substances remain dissolved in the solvent and gradually become more concentrated as the amount of solvent decreases; this results in areas of the glass surface contaminated with accumulated residual material when the solvent fully evaporates. The size of this residual material could potentially be orders of magnitude larger than the fabrication scale of the electrodes or of a microfluidic flowcell. The bottom surface is not directly dried with nitrogen gas. Drying only the top surface with nitrogen gas creates enough resulting air currents that incidentally reach the bottom surface and are also adequate enough to dry the bottom surface. The purpose of keeping the slides submerged in solvent until the last possible moment is to ensure minimal exposure to atmosphere and dust particles.
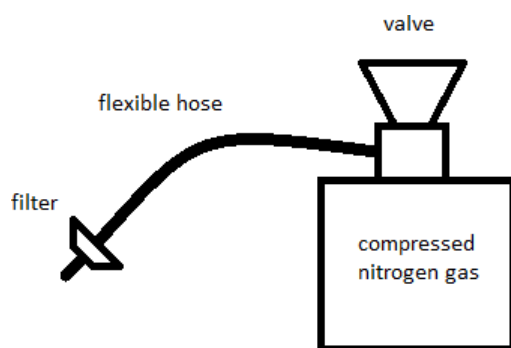
Figure 4.2 – Nitrogen gas, compressed through a filter, is used for many of the cleaning steps and intermediate steps to remove dust or particulate matter.

Nitrogen gas used directly from compressed N_2 cylinders often contain small amounts of oil or other lubricants; and as a precautionary measure, a filter is attached at the end of the nitrogen gas outlet. Since only the top surface of the glass material is dried directly, residual material can often be observed to form on the bottom surface of the glass substrate as the isopropanol evaporates. This is generally not a concern, since only the top surface of the glass substrate is where metal deposition and lithography will be performed.

4.3 Application of HMDS Primer

After cleaning, the glass is exposed to HMDS (hexamethyldisilazane). HMDS is a chemical primer used before spincoating that renders the substrate hydrophobic and functions as an adhesion promoter for photoresist[2]. The glass substrates and an open bottle of liquid HMDS are both enclosed within a confined space by using a plastic container. The plastic container is simply turned upside down. Liquid HMDS vaporizes and bonds to the surface of the glass. This process is done for 20 minutes and performed in the hood. This results in a single molecular layer of HMDS that has bonded to the glass, which enables the photoresist, applied later, to better adhere to the surface. The priming setup is shown in figure 4.3 on the following page.
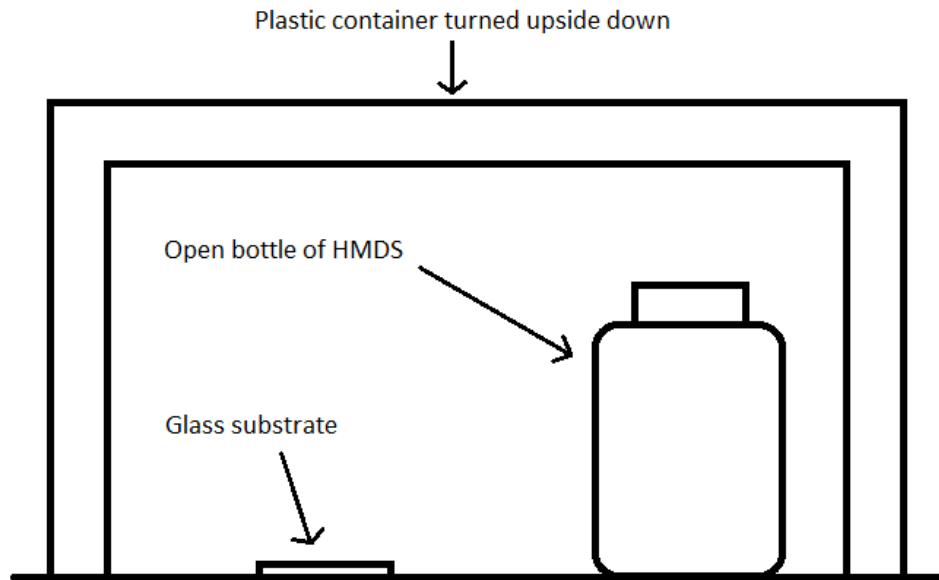
Figure 4.3 – Setup for HMDS exposure to the glass substrates. This is performed in a chemical hood.

4.4 Application Of Photoresist

The general purpose of photolithography is to create a desired pattern of a thin polymer film onto a substrate surface. These organic polymers are known as photoresists and can polymerize or break apart when exposed to heat or UV light. The first known documented use of photoresist was during the 1820s[3]. A man by the name of Nicephore Niepce invented the first photoresist which utilized a type of asphalt. Interestingly enough, he is also credited with being the inventor of photography. The asphalt that Niepce used was coated on glass and became less soluble when it was exposed to light. This technique enabled its use primarily as a printing plate. The development of modern photolithography occurred in the 1950s when Jay W. Lathrop and James R. Nall were tasked by the U. S. military to find a way to reduce the size of electronic circuits inside the limited space of a proximity fuse[4]. A proximity fuse is a fuse that denotes an explosive when the distance to a target becomes smaller than a predetermined value. Lathrop and

Nall were able to fabricate a miniaturized integrated circuit using photolithography. Photolithography would then lead to the development of microchips.

Photoresists are typically spin-coated onto a substrate, such as glass or silicon. The faster the photoresist is spin-coated, the thinner the layer it will be. Different formulations of photoresist will give different thicknesses depending on its composition and the rotational speed of the spin-coater. The desired thickness of the photoresist also depends on design goals. Prior to spin-coating, the glass is cleaned with compressed nitrogen gas to remove any dust particles that may be on the surface. The glass is held in place on the spin-coater by applying a vacuum to the bottom surface. Immediately after spin-coating, photoresists are baked at elevated temperatures to remove any undesired solvent.
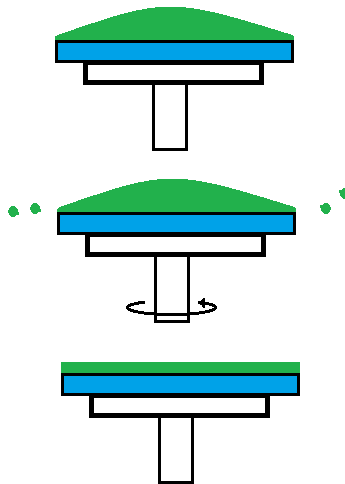
Figure 4.4 – Spincoating of photoresist. Blue is glass, green is photoresist. HMDS layer between the glass and the photoresist is not shown. The result is a flat, even layer of photoresist.

Masks are then used to cover areas of the photoresist to allow patterning. There are two types of photoresist, positive and negative. Negative photoresists create patterns

that are complementary to the mask pattern used, while positive photoresists yield patterns like the mask pattern used. This must obviously be taken into consideration when designing a mask. A common negative photoresist is SU8, which is often used to create permaent structures, such as the walls of a microfluidic channel. Positive photoresists are not intended to be permanent as they are often used for further patterning during processes such as metal deposition. It is important to work with photoresist only under yellow light conditions to prevent polymerization or to prevent depolymerization.

The higher the rotational speed, the thinner the photoresist layer will be. Most spin-coaters can be programmed allowing for different spin speeds and spin duration; varying acceleration speeds and deceleration speeds can be programmed and used in multi-step processes of acceleration and deceleration. The sequence for spincoating S1813 is the following:

1) Duration: 10 seconds, Speed: 500 rpm, Ramp: 500

2) Duration: 30 seconds, Speed: 4000 rpm, Ramp: 1000

3) Duration: 0 seconds, Speed: 0 rpm, Ramp: 500

The sequence for spincoating SU8 2002 is the following:

1) Duration: 10 seconds, Speed: 500 rpm, Ramp: 136

2) Duration: 30 seconds, Speed: 3000 rpm, Ramp: 272

The figures below show direct manufacturer data that relate the spin speed to the final thickness of the photoresist layer, and again demonstrates that the faster the spin speed, the thinner the layer will be and vice-versa.
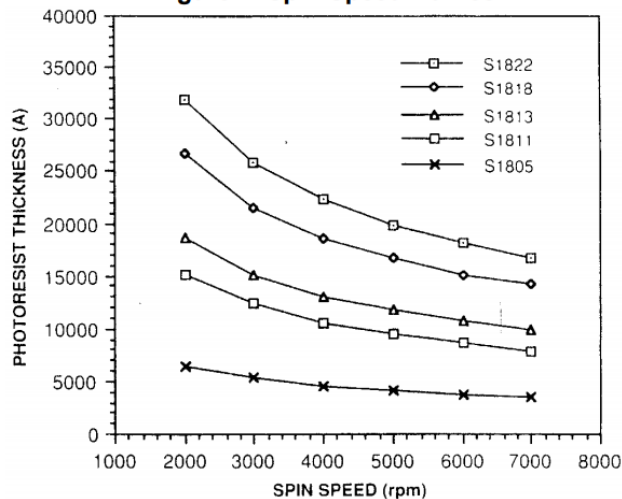
Figure 4.5 – Manufacturer data relating photoresist thickness to spin speed of various S1800 series formulations. If S1813 is spincoated at 4,000 rpm; the resulting photoresist layer will be 13,000 angstroms thick (1.3 μm)[5].
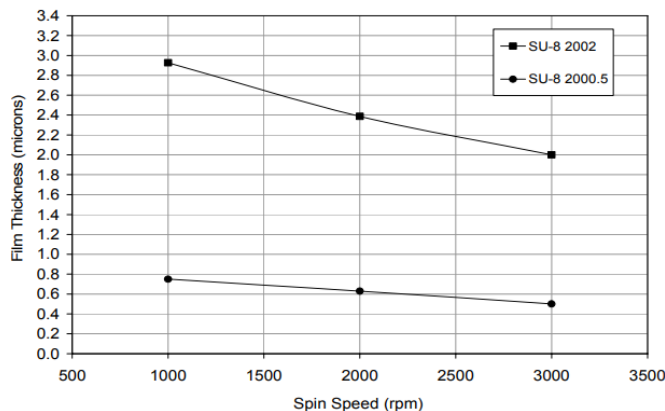
Figure 4.6 – Manufacturer data relating photoresist thickness to spin speed of SU8 2000 series. If SU8 2002 is spincoated at 3000 rpm, a photoresist layer of 2 μm will be obtained[6].

The main difference between positive and negative photoresist is that positive photoresist must be baked at an elevated temperature, 115 °C, for 10 minutes. This is to remove any unwanted solvent as well as to actually polymerize the photoresist. Negative photoresist is baked at 95 °C for two minutes, in order to remove unwanted solvent but not to polymerize the photoresist.

4.5 UV Exposure

Photoresist is then properly masked for corral traps and exposed to UV light for 5 seconds using a professional UV aligner. Numerous photoresists were spin-coated on glass substrates; the first sample was exposed for 2 seconds, the second sample was exposed for 3 seconds, the third sample was exposed for 4 seconds, up to 15 seconds. An exposure time of 5 seconds gave the best results as verified by visual inspection under a microscope.

Positive photoresist protected by the mask stays polymerized, while photoresist not protected by the mask breaks down. After UV exposure, the glass substrate is then submerged in developer chemical, MF-321. The substrates are manually agitated with tweezers while they are submerged, which aids in photoresist removal. Once all of the de-polymerized photoresist is removed, the substrate is left in the developer for an additional 45 seconds. The substrate is then immediately submerged in ultra-pure water for two minutes. Ultra-pure water is defined as water having a resistance value of 18.2 MΩ·cm, and can be obtained from any type of ultra-pure water filtration system. While the use of S1813 in this thesis is straightforward, it can also be used as a sacrificial layer to

create more complicated structures[7]. The general process, and differences, between the two types of photoresists are illustrated below.
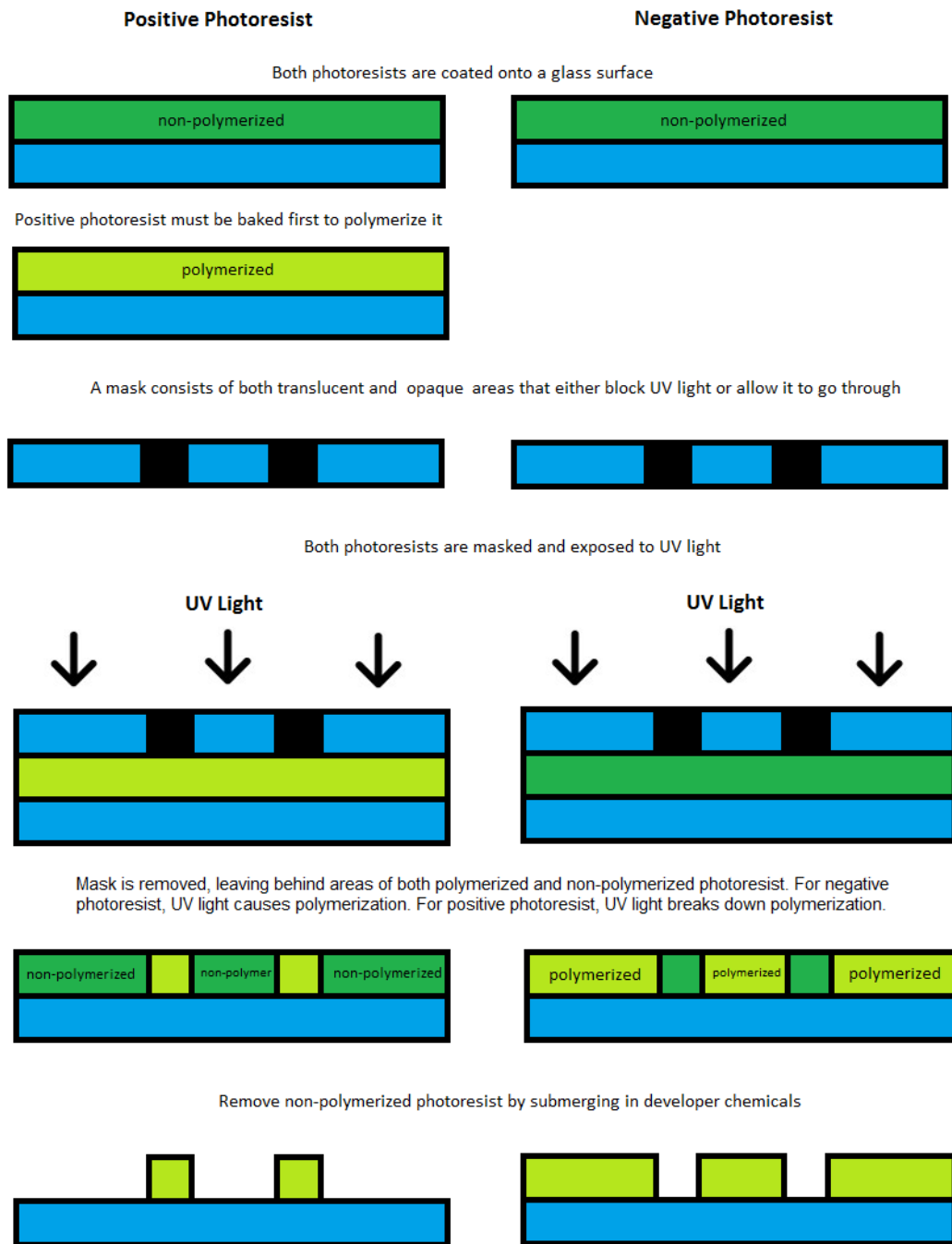
Figure 4.7 – The main differences between positive and negative photoresist. Green areas are photoresist and gray areas are glass. HMDS layer between glass and photoresist not shown.

Traditional lithography is done with a photomask, which is a thin sheet of lime-glass that is patterned with chromium metal, which is the method used in this thesis. Photomasks have advanced to the point where they are conformable[8]. There are photomasks that actually use fluid, instead of chromium, to absorb light[9]. Phase-shift photomasks utilize constructive and destructive light interference to fabricate structures on the nano-scale[10]. Although significantly advanced, the fabrication of masks is still somewhat costly and attempts have been made with using microfiche as a photomask[11].

For micro-scale patterns, a professional UV aligner is required. A normal light source will emit photons with uniform density in all directions. When placed next to a flat surface, such as a layer of photoresist on a glass substrate, the area directly beneath the light source will have the greatest photon density and areas further away will have lesser photon density; resulting in uneven UV exposure of the photoresist. The main advantage of a professional UV aligner is that it produces straight, collimated light that illuminates an area evenly; therefore all areas of the photoresist have equal UV exposure. Non-collimated light will also result in distorted patterns not intended by the mask.
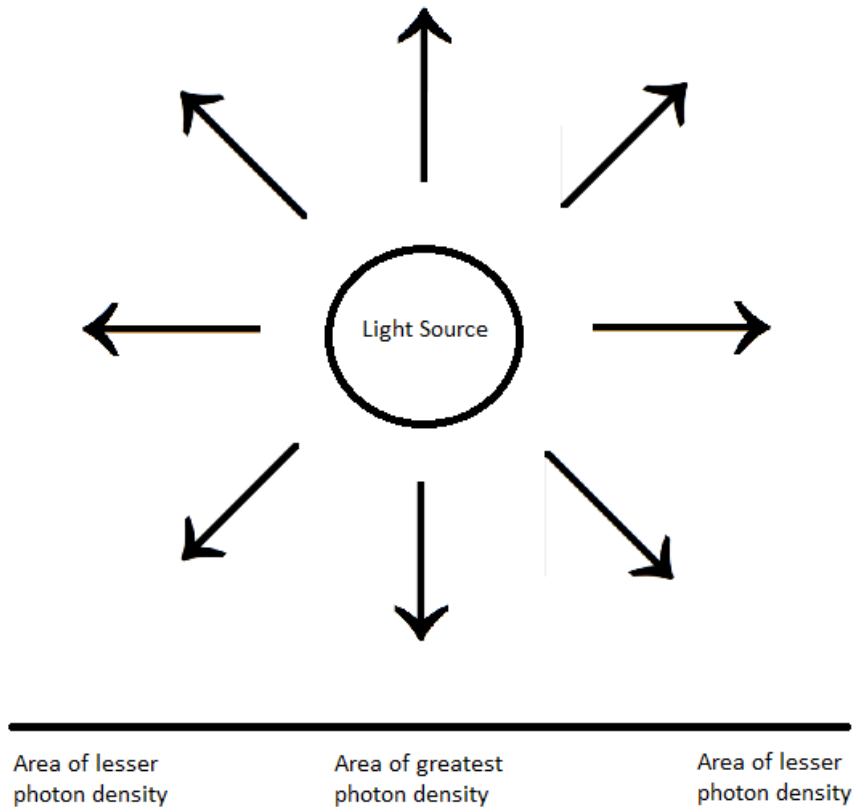
Figure 4.8 – Photon density of a flat surface based on its location relative to a normal light source. The result is uneven light exposure.
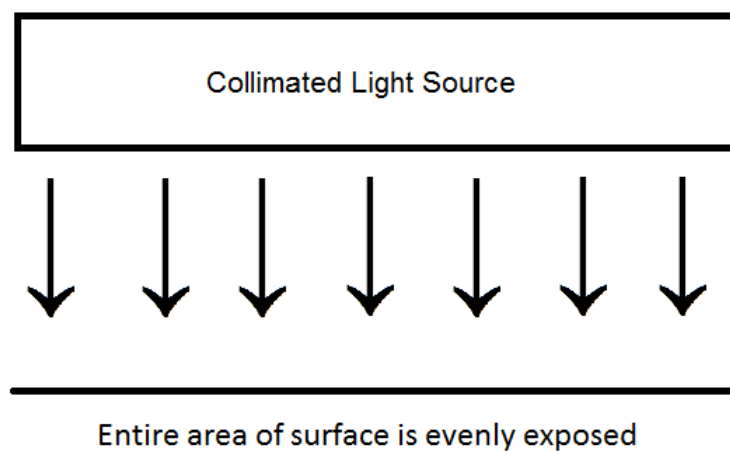
Figure 4.9 – Even light exposure on a flat surface due to a collimated light source.

4.6 Metal Deposition

After the photoresist has been exposed and developed, the next step is to deposit two layers of metal over the photoresist: 7.5 nm of nichrome first which acts as a wetting layer to promote adhesion, followed by 7.5 nm of Au/Pd as a cover layer. Metals can be purchased as pellets or wires and the deposition can be done with either a cup or filament. If a filament is used, the wire can be bent in the shape of a "u" and simply hung on the filament. If a cup is used, the common form is a pellet which is placed inside the cup.
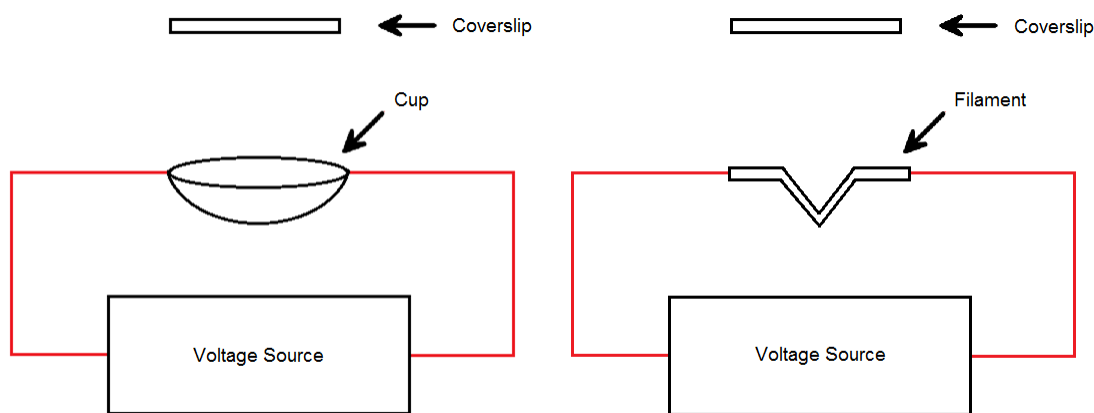
Figure 4.10 – Schematic for metal deposition. Metal deposition can be done with a cup or v-shaped filament.

If the deposition instrumentation does not provide a way to determine the thickness of metal being deposited, a simple mathematical relation can be used to calculate the amount of metal needed for evaporation[1].

$$m = \rho\, t \cdot (4\,\pi\, d^2)$$

m = the mass of metal required in grams

t = the desired thickness of the metal layer to be deposited in centimeters

ρ = the density of the metal being deposited in grams/centimeters^3

d = the distance from the metal source to the glass substrate in centimeters

If the desired thickness of a nichrome metal layer is 7.5 nm (7.5 x 10^{-7} cm) and the distance from the nichrome to the glass substrate is 10 cm, the required amount of nichrome metal to be evaporated would be 0.00792 grams using a density of 8.4 g/cm^3.

$$m = (8.4 \text{ g/cm}^3)(7.5 \times 10^{-7} \text{ cm})(4\,\pi\,(10 \text{ cm})^2)$$

$$m = 0.00792 \text{ grams}$$

The assumption of this calculation is that a filament is used and not a cup. When a filament is used, the metal wire first melts and becomes a roughly spherical drop of molten metal that hangs on the bottom of the "V" of the filament. As more voltage is put into the filament, the molten metal vaporizes in all directions. When a cup is used, most of the vaporization is directed upward; so the equation would have to be altered by a certain factor to take this into account.

If the radius of the wire is known, the wire length to cut can be calculated by using dimensional analysis and cancelling out units.

$$\text{wire length} = \frac{m}{\rho\,\pi\,r^2}$$

m = mass of metal from previous calculation in grams

ρ = density of metal in grams/centimeter^3

r = radius of wire in centimeters

Using the values from the previous example, this would mean that the length of wire to cut is 1.9 cm if the radius of the wire is 0.0127 cm.

$$\text{wire length} = \frac{0.00792 \text{ g}}{(8.4 \text{ g/cm}^3) \, (\pi) \, (0.0127 \text{ cm})^2}$$

wire length = 1.9 cm

The result of the deposition process is illustrated on the next page in Figure 4.12. Although two layers of metal are deposited, only one layer is shown for the sake of simplicity. Once the two layers of metal are deposited, the photoresist can be removed with PG Remover or acetone. The glass substrate is submerged in PG remover (or acetone) and then sonicated for 2 minutes. It is crucial to orient the substrate horizontally, not vertically, during this first sonication with the photoresist side facing up and exposed to photoresist remover. Visual inspection of sonication results under a microscope indicate that a horizontal orientation results in cleaner photoresist removal. This would imply that the motion of sonication is horizontal.

Figure 4.11 – Glass slide submerged in photoresist remover and oriented horizontally during sonication.

The substrate is then sonicated in isopropanol for 8 minutes while using the mold to orient the substrate vertically. Lastly, the substrates are dried with nitrogen gas. Instead of lithography, circular corral traps can also be made using spherical microscopic glass beads. The beads are deposited directly on the glass substrate. After metal deposition, the beads are removed by sonication. The main disadvantage to using beads is that there is no control over where the corral traps will appear, the placing of corral traps will be random.
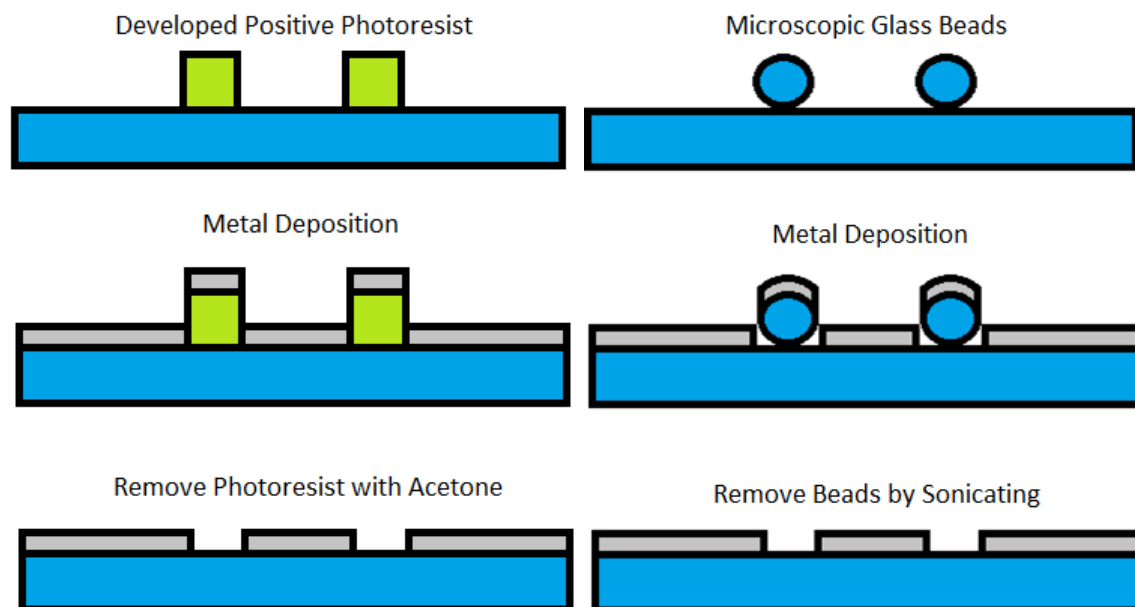
Figure 4.12 – Metal deposition process for making corral traps with positive photoresist or spherical microscopic glass beads[1].

Throughout the entire process, exposure to dust or other particles in the air are kept at a minimum. Ideally, an actual clean room should be used for the entire process. A clean room simply reduces the number of ambient particles in the air through the use of filters and controlled air flow[12]. Unfortunately, the main UWM campus does not have

such a facility. However, the Water Campus of UWM has clean room facilities where UV exposure was performed.
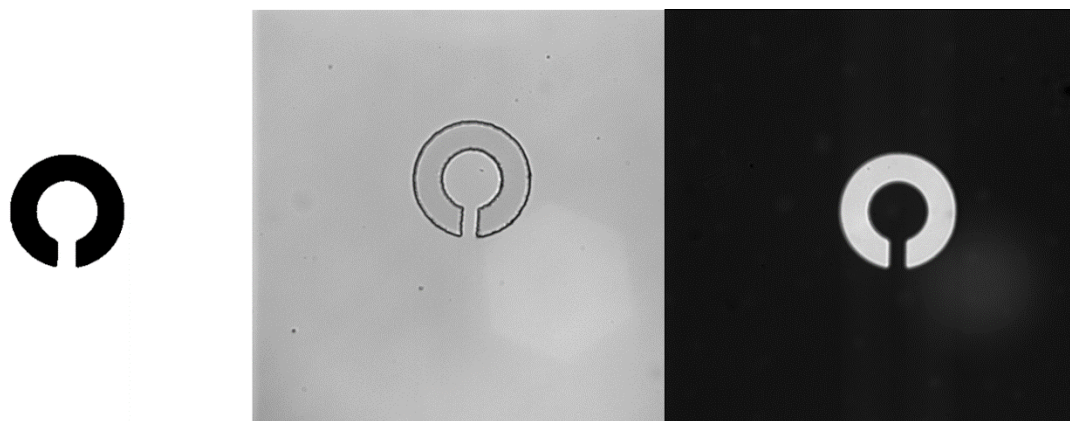
Figure 4.13 – Various stages of lithography. The left image is the mask itself, namely chromium metal patterned onto soda-lime glass. The middle image is the photoresist after it has been baked, masked, exposed to UV light, and submerged in developer chemical. The right image is the resulting metal pattern after metal deposition and photoresist removal; the dark area is the metal layer, the light area is glass.

Since the top electrode has no metal patterns on it, the fabrication is relatively easier; the slides only need to be cleaned and then metal deposition is performed. After metal deposition for the top electrode, the electrodes are placed in isopropanol and sonicated for 10 minutes. The mold is used to orient the electrodes vertically. After sonication the electrodes are dried with nitrogen gas. As a side note, patterns can also be made on the top electrode if desired simply by following the same procedure for the bottom electrode.

4.7 Putting Spacers On The Bottom Electrode

The final step is to create spacers on the bottom electrode which will create a consistent, well-defined gap between the bottom and top electrodes. This is done with

negative photoresist, SU8 2002. There are many formulations of SU8. For these experiments, SU8 is simply employed as a spacer to prevent the electrodes from coming into contact with each other; but its use can be highly sophisticated and is capable of fabricated multi-layer structures and channels[13]. The thermal and mechanical properties of SU8, such as tensile strength, glass-transition behavior, and stability, have been characterized based on the influence of processing conditions[14].

The SU8 2002 is spin-coated on the bottom electrode. Parameters for spin-coating SU8 2002 are repeated here:

1) Duration: 10 seconds, Speed: 500 rpm, Ramp: 136
2) Duration: 30 seconds, Speed: 3000 rpm, Ramp: 272

After spin-coating, the electrode is placed in the oven at 95 $^{\circ}$C for 2 minutes. Since the spacers are "relatively" large structures, a professional UV aligner is not necessary and a crude hand-made UV light source is used instead, Figure 4.14 on the following page. Since precision is not crucial for making the spacers, rectangular strips of common aluminum foil are used for masking. A professional UV aligner can of course be used if desired. The light sources are simple blacklights that can be purchased from Amazon (www.amazon.com). Optimal exposure time was determined experimentally by spin-coating numerous samples of photoresist and exposing them to the blacklights from a range of 1 minute to 10 minutes. A 5 minute exposure time gave the best results.
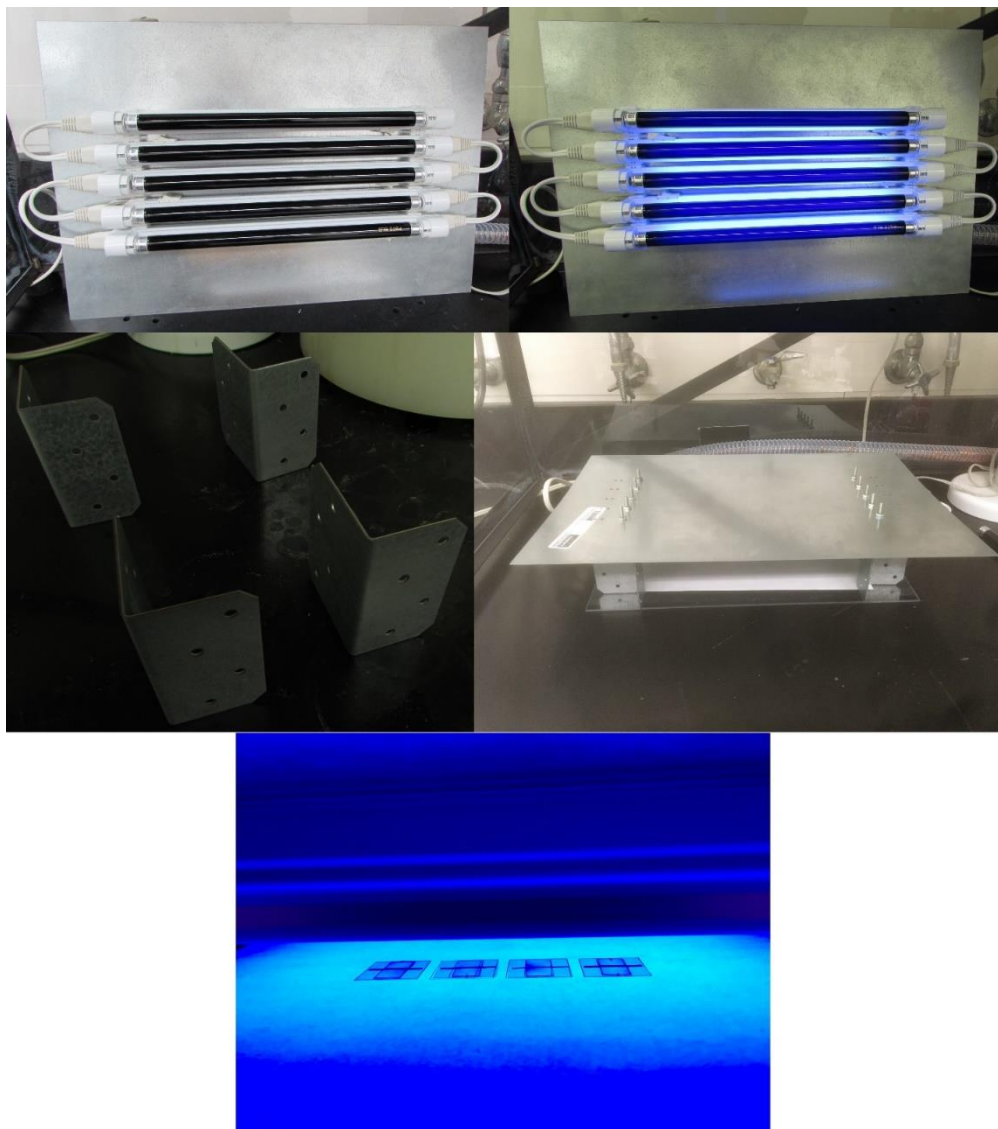
Figure 4.14 – A hand-made UV light source. The left middle image are metal bracers, 2.5 inches high, that keep the UV light source horizontal and above the substrates.

Crude lithography does have advantages and disadvantages. The main advantage is speed and convenience. Since the main purpose of the spacers is to keep the electrodes from coming into contact and they don't affect the electric field, they don't need to have very straight edges. There will often be curves along the spacer wall that protrude inward toward the channel or outward toward the developed photoresist, Figure 4.15 on the following page shows this to be the case.
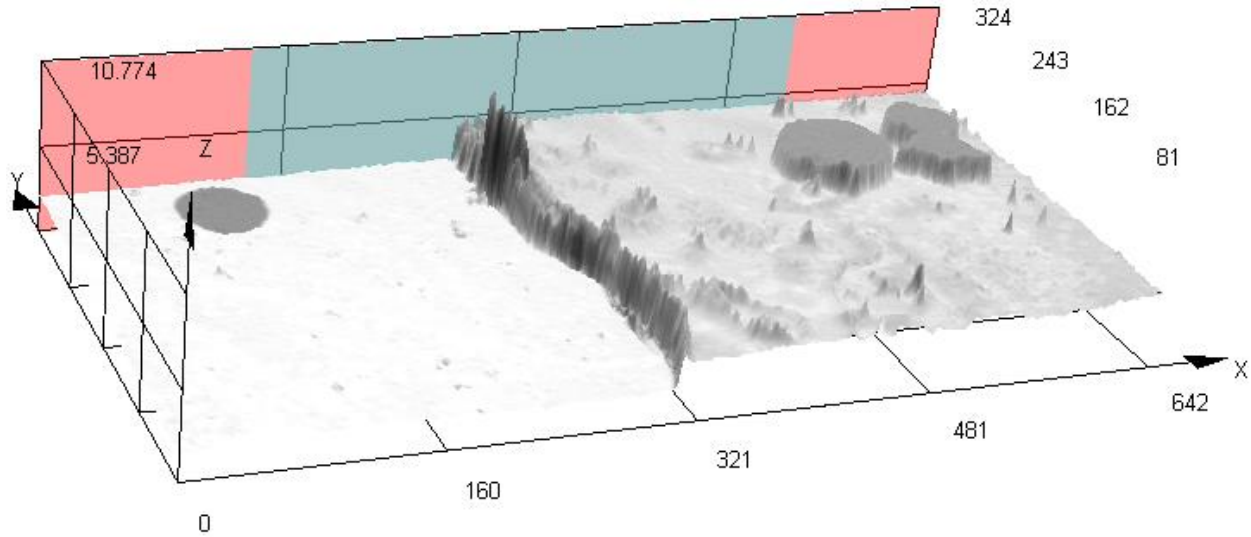
Figure 4.15 – Three dimensional profile of the SU8 2002 spacer taken with 3D laser confocal microscopy. The area on the left is the electrode surface. The area on the right is the spacer.

One thing that 3D laser confocal microscopy has revealed is that the SU8 spacer layer can generally range from 1 µm to 5 µm thick, consistency is difficult to attain. This may actually be due to the fact that crude lithography has always been used for the spacers and not a professional UV aligner. This inconsistency could be directly tied to crude lithography since the light is not collimated and there is uneven UV exposure of the photoresist. Another observation, particularly when electrode patterns are close to the spacer wall, is that the non-straight edges of the spacer wall can cause erratic bead flow. The non-straight edges of the spacer wall might also affect solution/bead flow in the middle of the channel, but probably to a lesser degree.

After UV exposure, the electrodes are placed in the oven a second time at 95 °C for 2 minutes. Since SU8 2002 is a positive photoresist, it polymerizes when it is exposed to UV light; therefore areas of the photoresist that are protected by the mask remain non-polymerized. The final step consists in removing the non-polymerized photoresist by

submerging in SU8 developer for 2 minutes. Then the substrates are submerged in isopropanol for 4 minutes and then dried with nitrogen gas. The general procedure is outlined in Figure 4.16.

Negative photoresist is spin-coated over the corral traps

Mask is placed on top

Assembly is exposed to UV light

Areas not protected by the mask become polymerized

Non-polymerized photoresist is removed by submerging in developer
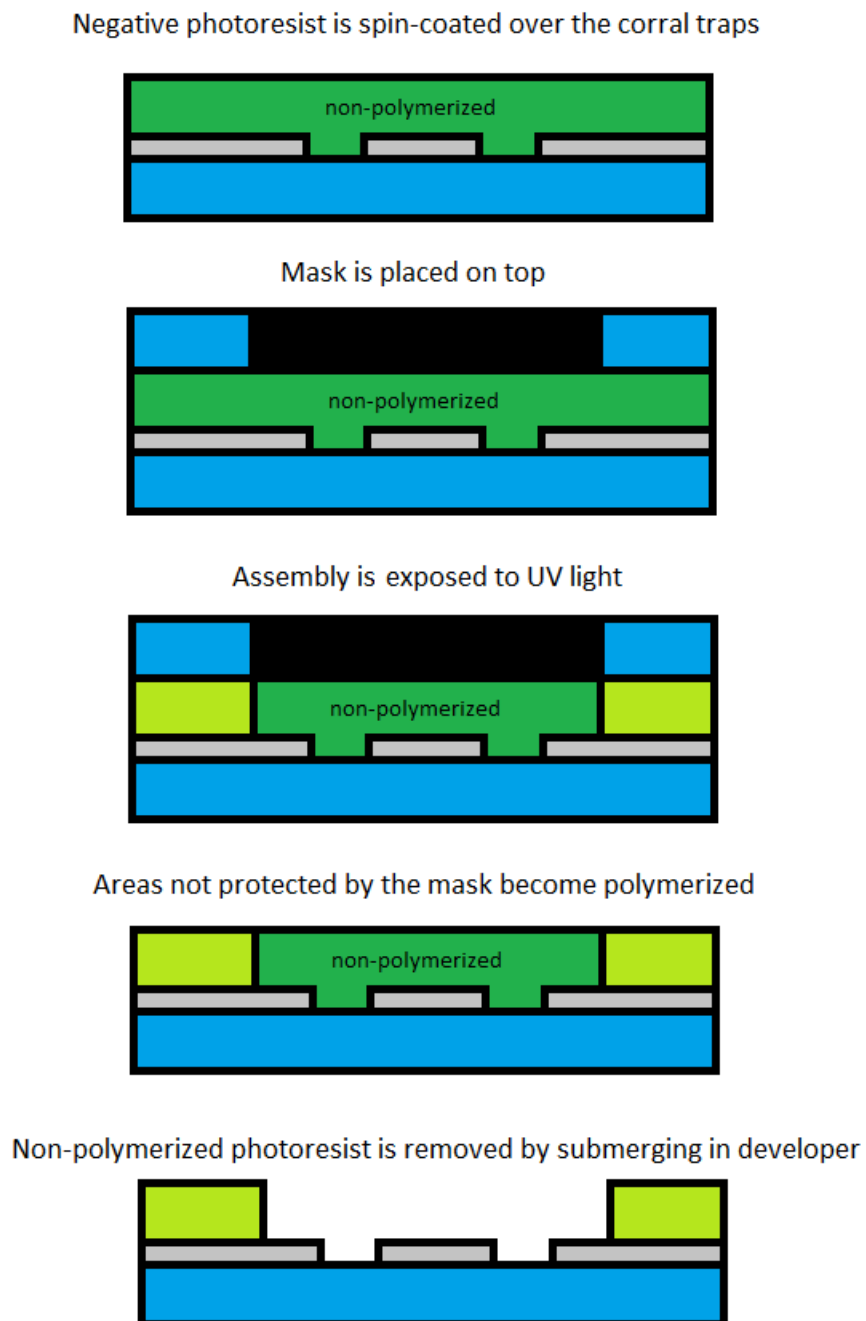
Figure 4.16 – General procedure for putting spacers on the bottom electrode.

Experiments can now be conducted with any type of microscope/camera setup, an AC/DC voltage source, and microscopic polystyrene beads. It is generally a good idea to dilute the vendor stock solution of beads with de-ionized water or ultra-pure water. Recommended dilutions are 1:10, 1:100, 1:1000, etc; by volume.

Summary For Bottom Electrode Fabrication:

1) Sonicate glass substrates in acetone for 15 minutes at 35 °C using the mold

2) Sonicate in methanol for 15 minutes at 35 °C

3) Sonicate in isopropanol for 15 minutes at 35 °C

4) Dry with compressed nitrogen gas

5) Enclose both glass substrates and an open bottle of HMDS with a plastic container for 20 minutes in the hood

6) Turn off main lights and turn on yellow lights to use the spincoater

7) Cover entire surface of glass substrate with photoresist S1813 using an eye-dropper

8) Spincoat with the following parameters:

    a) Duration: 10 seconds, Speed: 500 rpm, Ramp: 500

    b) Duration: 30 seconds, Speed: 4000 rpm, Ramp: 1000

    c) Duration: 0 seconds, Speed: 0 rpm, Ramp: 500

    d) These steps are already programmed in and can be quickly recalled by selecting "Program T"

9) Bake at a temperature of 115 °C for 10 minutes, this corresponds to a dial setting of "9.25" for the oven

10) Place in opaque containers (little black boxes)

11) Main lights can now be turned on

12) Mask glass substrates for corral trap placement and expose to UV light for 5 seconds with professional aligner; duration is the only parameter that needs to be set

13) Place in opaque containers

14) Turn off main lights and turn on yellow lights

15) Submerge in MF-321 developer under the hood

16) Agitate the glass substrates with tweezers until all of the non-polymerized photoresist is visibly removed from the surfaces, duration of this step is variable and based on personal judgement

17) Allow the glass substrates to stay submerged in developer for an additional 45 seconds

18) Submerge in ultra-pure water for 2 minutes (water with a resistivity value of 18.2 MΩ·cm)

19) Dry with compressed nitrogen gas

20) Main lights can now be turned on

21) Place in opaque containers

22) Deposit a 7.5 nanometer layer of Nichrome (60% Ni, 16% Cr, 24% Fe alloy) metal

23) Deposit a 7.5 nanometer layer of Au/Pd (60%:40%) metal

24) Sonicate the glass substrates in acetone for 2 minutes; make sure the glass substrates are oriented horizontally, not vertically; do not set a temperature

25) Sonicate in isopropanol for 8 minutes, orient the glass substrates vertically using the mold, do not set a temperature

26) Dry with compressed nitrogen gas

27) Turn off main lights and turn on yellow lights to use the spincoater

28) Cover entire surface of glass substrate with photoresist SU8 2002

29) Spincoat with the following parameters:

   a) Duration: 10 seconds, Speed: 500 rpm, Ramp: 136

   b) Duration: 30 seconds, Speed: 3000 rpm, Ramp: 272

   c) These steps are already programmed in and can be quickly recalled by selecting "Program S"

30) Bake at a temperature of 95 °C for 2 minutes, this corresponds to a dial setting of "7" for the oven

31) Mask glass substrates for spacer placement and expose to UV light for 5 minutes with crude lithography using the hand-made UV light source

32) Bake glass substrates again at a temperature of 95 ºC for 2 minutes, this corresponds to a dial setting of "7" for the oven

33) Submerge in SU8 Developer for 2 minutes, agitate with tweezers for 5 seconds

34) Submerge in isopropanol for 4 minutes, agitate with tweezers for 5 seconds

35) Dry with compressed nitrogen gas

Summary For Top Electrode Fabrication:

1) Sonicate glass substrates in acetone for 15 minutes at 35 ºC using the mold

2) Sonicate in methanol for 15 minutes at 35 ºC

3) Sonicate in isopropanol for 15 minutes at 35 ºC

4) Dry with compressed nitrogen gas

5) Deposit a 7.5 nanometer layer of Nichrome (60% Ni, 16% Cr, 24% Fe alloy) metal

6) Deposit a 7.5 nanometer layer of Au/Pd (60%:40%) metal

7) Sonicate in isopropanol for 10 minutes using the mold, do not set a temperature

8) Dry with compressed nitrogen gas

9) If patterns on the top electrode are desired as well, ignore this summary and follow the same procedure for bottom electrode fabrication up to step 26 instead

List of Instrumentation and Equipment

1) Sonicator

  Bransonic Ultrasonic Cleaner
  Model 1510R-DTH
  Branson Ultrasonics Corportation

2) Spin-Coater

  Spin Processor
  Model WS-400B-GNPP/LITE/10K
  Laurell Technologies Corporation

3) Oven

  Isotemp Oven
  Model 506G
  Fisher Scientific

4) Lithography UV Aligner

  Mask Aligner
  Model MJB4
  Suss MicroTec

5) Ultra-Pure Water Filtration System

  Arium 611
  Model Arium 611VF
  Sartorius Ag Gottingen

6) Metal Deposition System

  Edwards Coating System
  Model E306A
  Edwards Vacuum

7) 3D Laser Confocal Microscope

  Olympus LEXT
  OLS4100
  Olympus

8) Yellow Lightbulbs (to prevent photoresist polymerization during spin-coating)

    Bug Light
    Model 98001693
    PC 97495
    General Electric

9) Blacklights (UV light source used for crude lithography)

    8 Watt Flourescent T5 Blacklight 12"
    Model 15516-F8T5/BLB
    Eiko

References for Chapter 4

1. Christine A. Carlson, *Development of the Electrostatic Corral for the Trapping of Single Molecules in Solution*, 2010, PhD Thesis, Department of Chemistry, University of Wisconsin-Milwaukee

2. Akira Kawai, Junko Kawakami, "Wetting Analysis of Hydrophobic Substrate Treated by HMDS Primer", 2007, *Journal of Photopolymer Science and Technology*, Vol 20, No 6, Pages 815-816

3. C. Grant Willson, Ralph R. Dammel, Arnost Reiser, "Photoresist materials: A Historical Perspective", 1997, *Proceedings of SPIE*, Vol 3049

4. Jay W. Lathrop, "The Diamond Ordnance Fuze Laboratory's Photolithographic Approach to Microcircuits", 2013, *IEEE Annals of the History of Computing*, Vol 35, Issue 1, Pages 48-55

5. "Shipley: Microposit S1800 Series Photo Resists", http://microchem.com/PDFs_Dow/S1800.pdf

6. "SU-8 2000: Permanent Epoxy Negative Photoresist Processing Guidelines", http://microchem.com/pdf/SU-82000DataSheet2000_5thru2015Ver4.pdf

7. In-Hyouk Song, Pratul K. Ajmera, "Use of a Photoresist Sacrificial Layer with SU-8 Electroplating Mould in MEMS Fabrication", 2003, *Journal of Micromechanics and Microengineering*, Vol 13, Pages 816-821

8. Seokwoo Jeon, Etienne Menard, Jang-Ung Park, Joana Maria, Matthew Meitl, Jana Zaumseil, John A. Rogers, "Three-Dimensional Nanofabrication with Rubber Stamps and Conformable Photomasks", 2004, *Advanced Materials*, Vol 16, No 15, Pages 1369-1373

9. Chihchen Chen, Danny Hirdes, Albert Folch, "Gray-Scale Photolithography using Microfluidic Photomasks", 2002, *Proceedings of the National Academy of Sciences*, Vol 100, No 4, Pages 1499-1504

10. Gillian A. M. Reynolds, Roger H. French, Peter F. Carcia, C. C. Torardi, Greg Hughes, D. J. Jones, M. F. Lemon, M. Reilly, L. Wilson, C. R. Miaso, "TiSi-Nitride Attenuating Phase-Shift Photomask for 193 nm Lithography", 1998, *Proceedings of SPIE*

11. Tao Deng, Joe Tien, Bing Xu, George M. Whitesides, "Using Patterns in Microfiche as Photomasks in 10-um-Scale Microfabrication", 1999, *Langmuir*, Vol 15, Pages 6575-6581

12.   W. Whyte, *Cleanroom Technology: Fundamentals of Design, Testing and Operation*, 2010, John Wiley & Sons, West Sussex, United Kingdom

13.   A. del Campo, C. Greiner, "SU-8: A Photoresist for High-Aspect-Ratio and 3D Submicron Lithography", 2007, *Journal of Micromechanics and Microengineering*, Vol 17, Pages R81-R95

14.   Ru Feng, Richard J. Farris, "Influence of Processing Conditions on the Thermal and Mechanical Properties of SU8 Negative Photoresist Coatings", 2002, *Journal of Micromechanics and Microengineering*, Vol 13, Pages 80-88

Chapter 5

Experimental Results

5.1 Determination of Image Dimensions at Different Magnifications

The camera used for these experiments generates images with a size of 512 pixels x 512 pixels. The microscope used is capable of 10x, 40x, and 100x magnifications. A calibration ruler, with 10 micron divisions, was used to determine the image dimensions at each magnification.
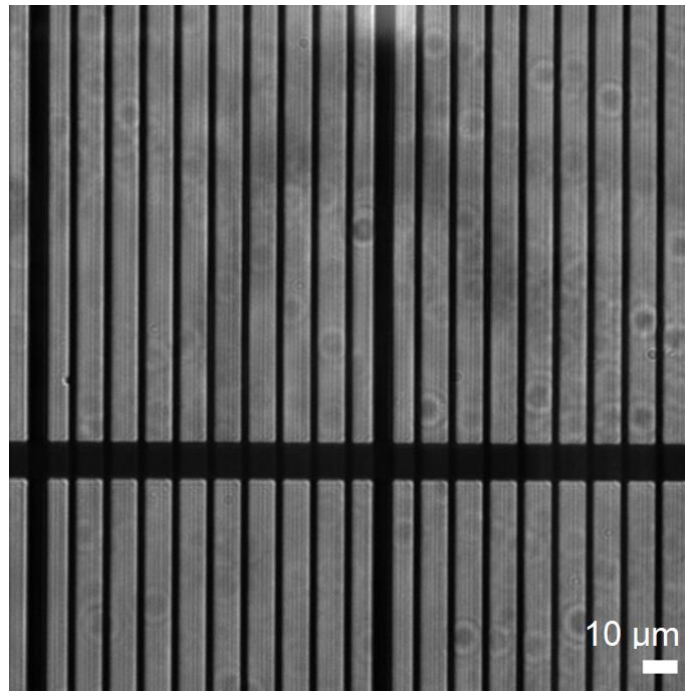
Figure 5.1 – An image of the calibration ruler at 40x magnification. The calibration ruler has minor divisions of 10 microns and major divisions of 100 microns.

Images were taken and loaded into the MATLAB programming environment[6]. MATLAB is software that has built in tools, applications, and even its own programming language for numerical and mathematical analysis. A simple command, "ginput(2)", will return x and y pixel coordinates of two points on an image that are input by the user with mouse-clicks.
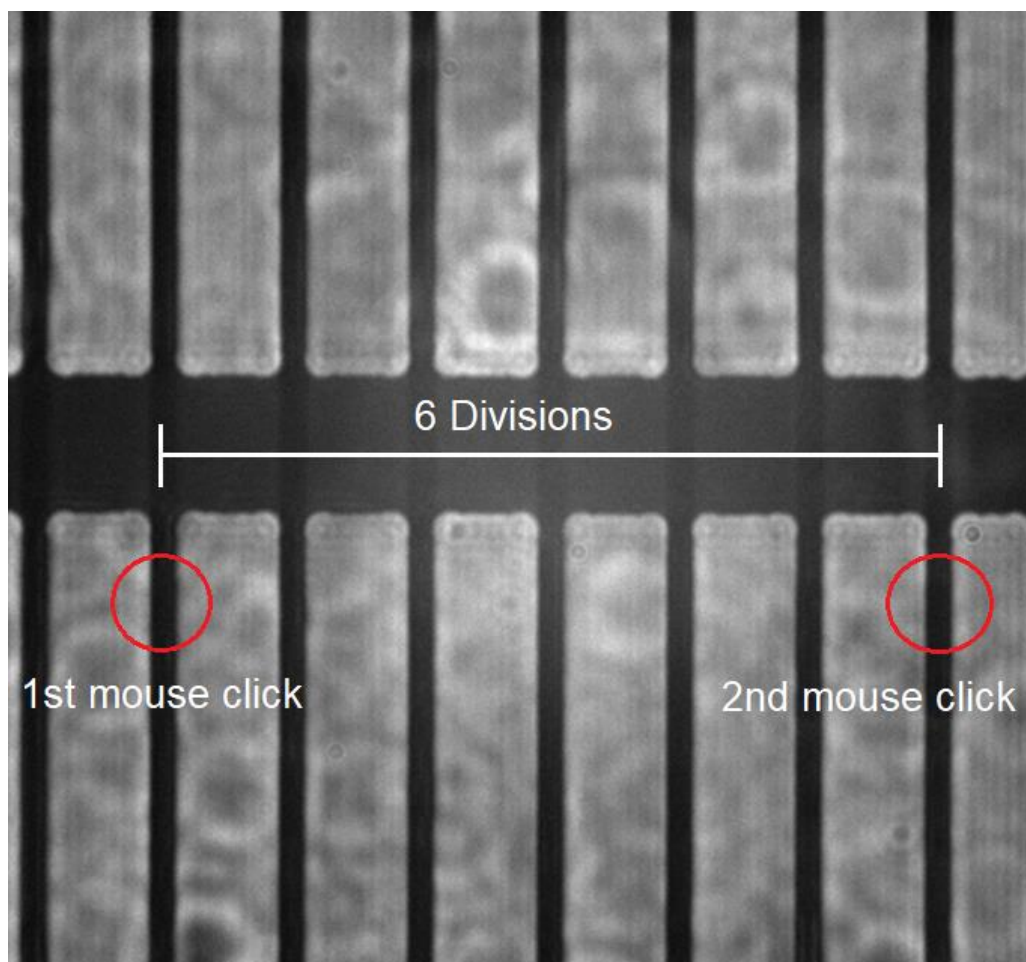
Figure 5.2 – The pixel coordinates of the two points, circled in red, are determined with MATLAB commands. Pixel dimensions can be easily determined by correlating pixel coordinates to the known distance of the 6 divisions.

Using these image manipulation commands and precise pixel locations under the MATLAB programming interface, the following image dimensions for the camera were determined.

Magnification	Full Image Dimensions	Perceived Pixel Dimensions
10x	795 μm x 795 μm	1.55 μm x 1.55 μm
40x	199 μm x 199 μm	0.388 μm x 0.388 μm
100x	79.5 μm x 79.5 μm	0.155 μm x 0.155 μm

5.2 Corral Trapping with DC Voltages

Trapping with DC has proven difficult to duplicate with reasonable consistency; however, there have been isolated instances of success. In these isolated instances, the trapping works extremely well and there are never any indications that electrolysis is taking place, despite the expectation that electrolysis should occur since the experimental set-up involves two electrodes. These isolated successes also indicate that there are possibly crucial parameters that have not been taken into consideration, or that the parameters already taken into consideration need more refinement.

Electrolysis, the decomposition of water into oxygen gas and hydrogen gas due to an applied voltage, is expected to occur at around 1.23 V or higher based on the standard reduction potential values that can be found in general chemistry textbooks[7]. The half-reactions in acid are

Anode (oxidation) $2\,H_2O\,(l) \rightarrow O_2\,(g) + 4\,H^+\,(aq) + 4\,e^-$ $E^o = -1.23$ V

Cathode (reduction) $2\,H^+\,(aq) + 2\,e^- \rightarrow H_2\,(g)$ $E^o = 0.00$ V
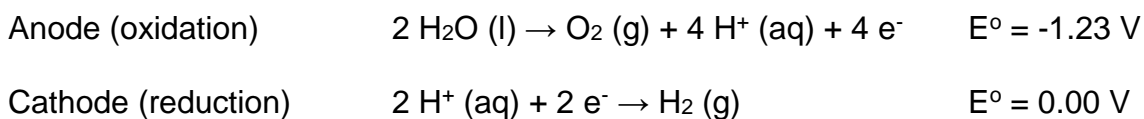
In basic solution, the half-reactions for electrolysis are

Anode (oxidation) $2\,OH^-\,(aq) \rightarrow \tfrac{1}{2}\,O_2\,(g) + H_2O\,(l) + 2\,e^-$ $E^o = -0.40$ V

Cathode (reduction) $2\,H_2O\,(l) + 2\,e^- \rightarrow H_2\,(g) + 2\,OH^-\,(aq)$ $E^o = -0.83$ V
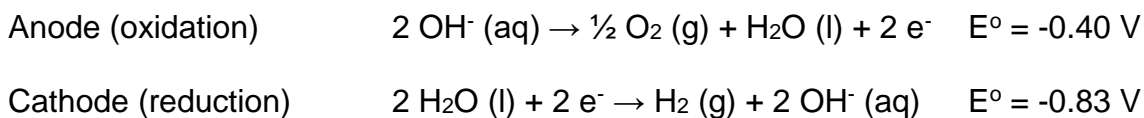
The expected potential for electrolysis is also 1.23 V in basic solution.

Water is also capable of autoprotolysis under neutral conditions.

Anode (oxidation) $2\ OH^-\ (aq) \rightarrow \frac{1}{2}\ O_2\ (g) + H_2O\ (l) + 2\ e^-$ $E^o = -0.40$ V

Cathode (reduction) $2\ H^+\ (aq) + 2\ e^- \rightarrow H_2\ (g)$ $E^o = 0.00$ V
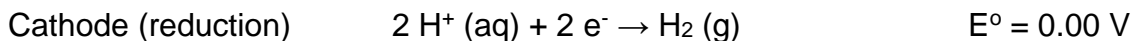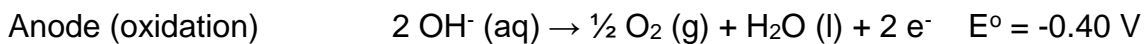
If the two reactions are combined, the result is

$2\ H^+\ (aq) + 2\ OH^-(aq) \rightarrow H_2O\ (l) + \frac{1}{2}\ O_2\ (g) + H_2\ (g)$ $E^o = -0.40$ V
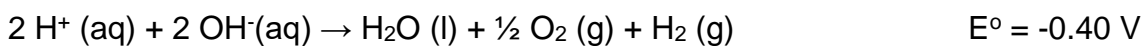
The Nernst equation is then used to calculate the resulting potential[7].

$$E_{cell} = E^o - \frac{RT}{nF}\ln Q$$

The number of transferred electrons is 2, and the concentrations of both H^+ and OH^- are 1 x 10^{-7} M under neutral conditions. R is the gas constant and the value used is 8.314 J/(mol K). T is Kelvin room temperature. And F is Faraday's constant which is 96485 C/mol.

$$E_{cell} = -0.40\ V - \frac{(8.314\ J/mol\ K)\ (298\ K)}{(2)\ (96485\ C/mol)}\ \ln \frac{1}{(1\ x\ 10^{-7})^2\ (1\ x\ 10^{-7})^2} = -1.23\ V$$

The result is the same even in neutral conditions.

In the cases where corral trapping with DC has been successful, the voltage has exceeded 1.23 V. It is possible that electrolysis is occurring off-screen and simply not occurring in the chosen observed area.
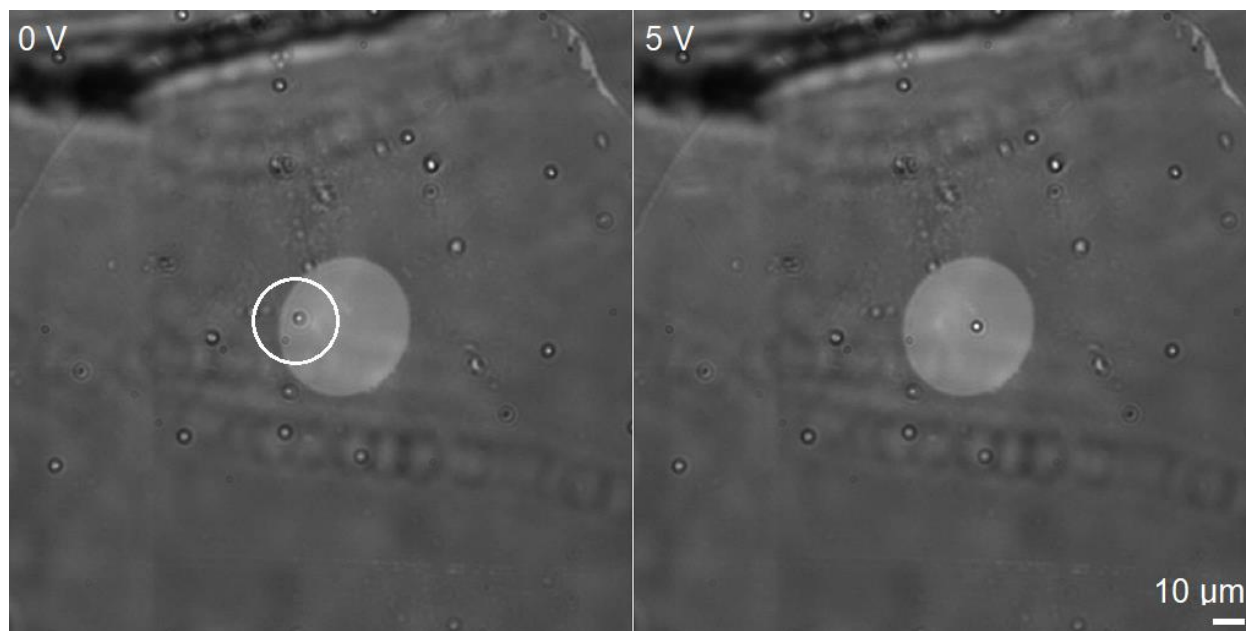
Figure 5.3 – Corral trapping with DC at 40x magnification. Left, voltage is off. White circle indicates the bead to be trapped. Right, voltage is turned on and the bead becomes trapped in the center of the corral.

Figure 5.3 shows the trapping of a 2.0 µm diameter polystyrene bead in a 40 um diameter corral trap at an applied voltage of 5 V. The bead is functionalized with COOH groups and is negatively charged due to their deprotonated carboxy groups in a pH 8.0 NaOH buffer. The experimental set-up is basically the same as Figure 2.15. A small sample of bead solution, 1 µL, is deposited directly on the bottom electrode with a pipette and then the counter electrode is placed on top. In order for trapping to occur, the bead must already be within the diameter of the corral. If the bead is initially located outside of the corral, trapping is not possible.
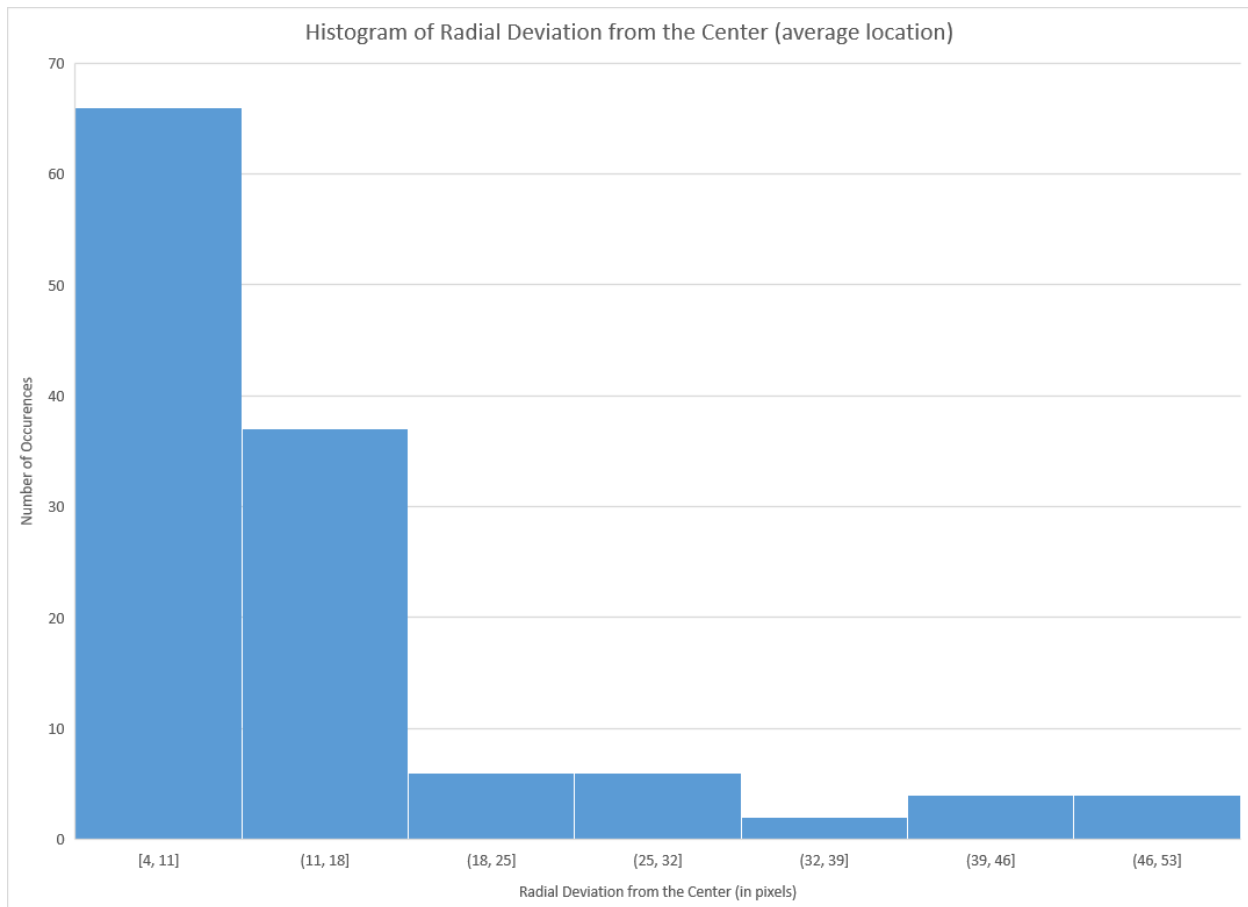
Figure 5.4 – Histogram of the radial deviation of the particle from average location in pixels. Average radial deviation is 14 pixels. Since the pixel dimensions are 0.388 microns x 0.388 microns, this corresponds to an average displacement of 5.38 microns. Standard deviation, σ, is 1.45 microns.

Figure 5.4 shows the magnitude of the radial deviation of the particle relative to the average location. Pixel displacements were determined manually. The x coordinate of the center was determined by taking the average of all the x values of the particle's location. The y coordinate of the center was done the same way. The radial deviation, r, was then calculated.

$$r = \sqrt{(x - x_o)^2 + (y - y_o)^2}$$

The average radial deviation is 5.38 microns. The standard deviation, σ, is 1.45 microns. Based on the histogram of Figure 5.4, the particle is mostly found within 11 pixels from the center, which is 4.3 μm.

A Gaussian curve describes a probability distribution function[4] that can be expressed as

$$g(x) = \frac{1}{\sigma\sqrt{2\pi}} e^{-\frac{1}{2}((x-\mu)/\sigma)^2}$$

Since the average value, μ, is referenced as zero, we can simplify the Gaussian to be

$$g(x) = \frac{1}{\sigma\sqrt{2\pi}} e^{-\frac{1}{2}(x/\sigma)^2}$$

A Boltzmann distribution describes the probability, p_i, that a system will be in a certain state, i, as a function of the state's energy and temperature[5].

$$p_i = \frac{1}{Q} e^{-\varepsilon_i/(kT)} \quad \text{where} \quad Q = \sum_{j=1}^{\infty} e^{-\varepsilon_j/(kT)}$$

ε = energy of the system in joules

k = Boltzmann's constant; 1.38 x 10⁻²³ J/K

T = temperature in Kelvin

Since the potential profiles of Figure 2.18 show parabolic behavior, Hooke's law can be used as a one dimensional model for the corral trap[3]. Hooke's law describes the behavior of a linear spring. When a spring is stretched outward, the spring itself will exert an inward force to restore the spring to its rest length. This is the restoring force of the spring and is designated as negative, which is opposite the direction of the force required to stretch the spring out.

$$F = -kx$$

k is the spring constant with units of N/m, and x is the displacement of the spring with units of meters. Force is the negative gradient of the potential energy U.

$$F = -\frac{dU}{dx}$$

These equations are set equal to each other.

$$-\frac{dU}{dx} = -kx$$

Separation of variables and integrating leads to

$$U = \tfrac{1}{2} kx^2$$

This is the potential energy of a spring.

If the corral trap is modeled with Hooke's law, both the trap stiffness, k, and the restoring force of the trap, F, can be calculated from positional data of the trapped particle if the probability of the Boltzmann distribution is equated with the probability of the Gaussian curve.

$$\frac{1}{Q} e^{-\varepsilon_i/(kT)} = \frac{1}{\sigma\sqrt{2\pi}} e^{-\frac{1}{2}\,(x/\sigma)^2}$$

The exponential factors can be equated to each other. The normalization factors can be ignored since there is no dependence on x.

$$e^{-\varepsilon_i/(kT)} = e^{-\frac{1}{2}\,(x/\sigma)^2}$$

Applying the natural log to both sides leads to

$$-\varepsilon_i/(kT) = -\frac{1}{2}\,(x/\sigma)^2$$

The potential energy of a spring is $U = \frac{1}{2}\,kx^2$. The original k is given a "B" subscript to designate it as Boltzmann's constant and to distinguish it from the new k.

$$\left(-\frac{1}{2}kx^2\right)/(k_B T) = -\frac{1}{2}\,(x/\sigma)^2$$

Solving for k results in

$$k = \frac{k_B T}{\sigma^2}$$

Using $k_B = 1.38 \times 10^{-23}$ J/K, $T = 298$ K for room temperature, and $\sigma = 1.45 \times 10^{-6}$ meters, the trap stiffness is

$k = 1.96$ nN/m

Using $\sigma = 1.45 \times 10^{-6}$ meters for the x displacement and Hooke's law being "$F = -kx$", the restoring force of the spring at a deviation of 1σ from its average position is

$F = -2.84$ fN

5.3 Corral Trapping with AC Voltages

Figure 5.5 shows that the corral trap displays two main behaviors which correspond to negative dielectrophoresis and positive dielectrophoresis if AC voltages are applied. Corral trapping, or center trapping, is the result of negative dielectrophoresis and rim trapping is the result of positive dielectrophoresis. Under corral trapping, beads become confined in the center of the corral. The beads are not completely immobilized; however, they are confined in their movement. Under rim trapping, beads become

confined on the rim of the corral. Movement is much more restricted as the beads are confined directly to the rim, so the beads stay at a constant distance away from the center of the corral. The images below were processed with "ImageJ" software[1]. It is a public domain image processing program.
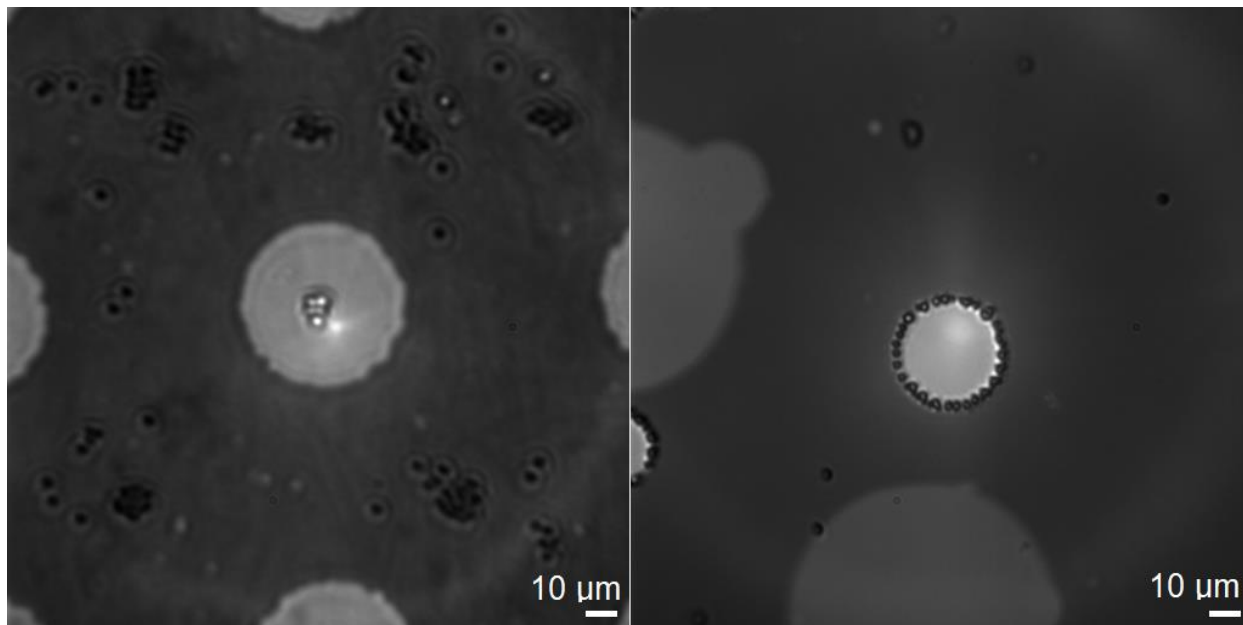
Figure 5.5 – The two main types of corral trap behavior. Left image, corral trapping of a few beads. Right image, rim trapping of numerous beads.

The beads that are corral trapped look different from the beads that are rim trapped. Since the images are focused on the rim of the corral which is located on the bottom electrode, the beads that are rim trapped are in focus and have a smaller diameter than the beads which are corral trapped; these beads are located near the bottom electrode. The corral trapped beads are out of focus and have larger diameters and are, therefore, further away from the bottom electrode. The beads in this instance are non-functionalized 1.5 micron diameter polystyrene beads that are electrically neutral, therefore they should not be affected by Coulombic forces. Polystyrene beads become

polarized under a non-uniform field so they are affected by the dielectrophoretic field. The observed experimental behavior does directly correlate with theoretical COMSOL simulations based on the metal pattern and the resulting fields that are generated. The beads end up in the center of the corral if there is negative dielectrophoresis. The center of the corral has the least electric field density and also the smallest values of E^2. The beads end up on the rim if there is positive dielectrophoresis. The rim of the corral has the highest electric field density and also the highest values of E^2.

Figure 5.6 below shows the corral trapping of a single bead at 10 V and 1 kHz AC. The adjacent image shows 300 location points of the bead over an interval of 43 seconds. The tracking was done with an ImageJ plugin called "Manual Tracking"[2]. The plugin assigns the pixel dimensions of the image based on the user input. The images are advanced frame by frame after the location of the particle is manually determined by the user with a point-and-click interface.
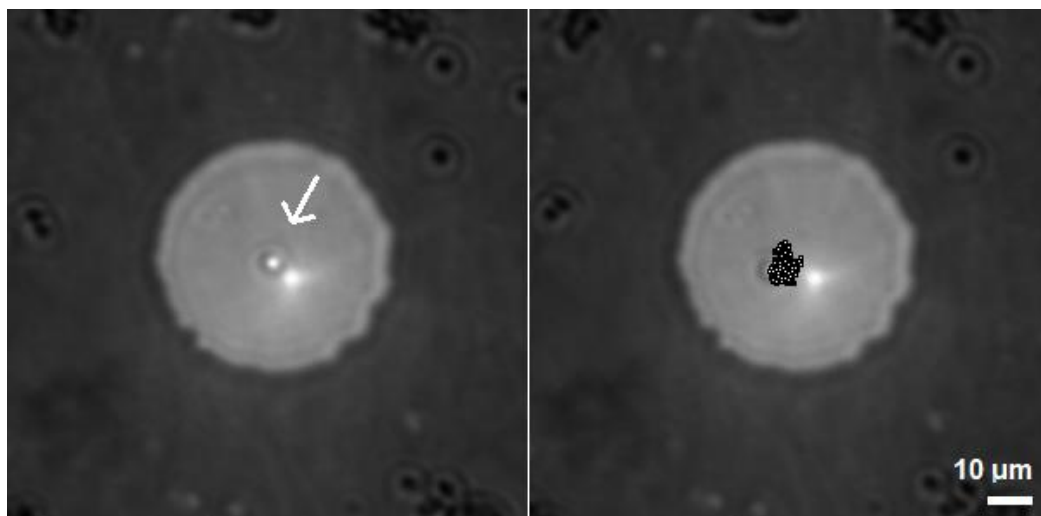
Figure 5.6 – Left, a single corral trapped bead indicated with an arrow. The bright spot next to the bead is an illumination artifact. The corral trap is 50 microns in diameter. Right, superposition of 300 location points over a time interval of 43 seconds.

When dielectrophoresis under AC conditions are used, the dielectrophoresis potential near the surface of the bottom electrode is clearly non-parabolic (Figure 2.26); three sharp points can be observed at the trap center and trap edges. If the dielectrophoresis potential at a y value of 5 μm or more is considered, it resembles more and more a parabola. Since the beads are not in focus while they are corral trapped under dielectrophoresis, they would be above the surface of the bottom electrode and so the potential at a y value of 0 μm would not apply. So a Hooke's law approximation could be done, assuming the beads are around 5 μm or more above the surface of the bottom electrode. Figure 5.7 below shows the radial displacement of the bead relative to the average location.
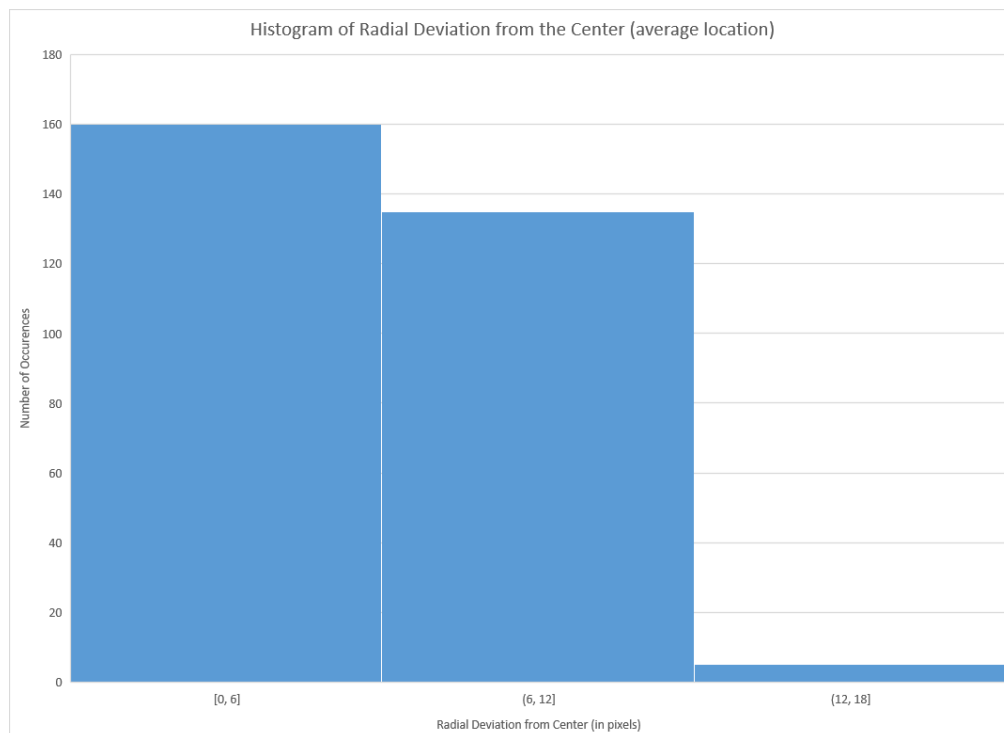
Figure 5.7 – Histogram of the radial deviation of the particle from the center of the corral (average location) in pixels. Average displacement is 6.0 pixels, this corresponds to 2.33 microns since the perceived pixel dimensions are 0.388 microns x 0.388 microns.

130

The data is analyzed similarly to the corral trapping done with DC. The results are summarized below.

	DC	AC
Current	DC	AC
Voltage	5 V	10 V
Frequency	N/A	1.0 kHz
Magnification	40x	40x
Bead material	polystyrene	polystyrene
Bead diameter	2.0 microns	1.5 microns
Functionalization	COOH	None
Solution	pH 8.0 NaOH	18.2 MΩ·cm resistivity water
Corral diameter	40 microns	50 microns
Electrode separation distance	unknown	unknown
Average radial deviation	5.38 microns	2.33 microns
σ (standard deviation)	1.45 microns	0.95 microns
k (trap stiffness)	1.96 nN/m	4.56 nN/m
Restoring force of corral	-2.84 fN	-4.33 fN

5.4 Rim Trapping

Rim trapping, as previously shown in Figure 5.5, is the result of positive dielectrophoresis; beads become trapped in areas of high electric field density, near the rim of the corral. Rim trapping greatly restricts the mobility of the bead. Assuming the corral is isolated and perfectly circular, the bead is confined to a constant distance away from the center. However, the bead is free to move in either direction along the rim, with the direction being mostly dictated by the direction of the solution flow. The bead will stop moving when the direction of solution flow is perpendicular to the tangent of the circle along the rim where the bead is at. Hypothetically, if a single bead is rim-trapped; the bead could be made to travel in a complete circle along the rim simply by changing the

direction of the solution flow. The solution flow would have to be sufficient enough to move

the bead, but not too strong so as to dislodge the bead.
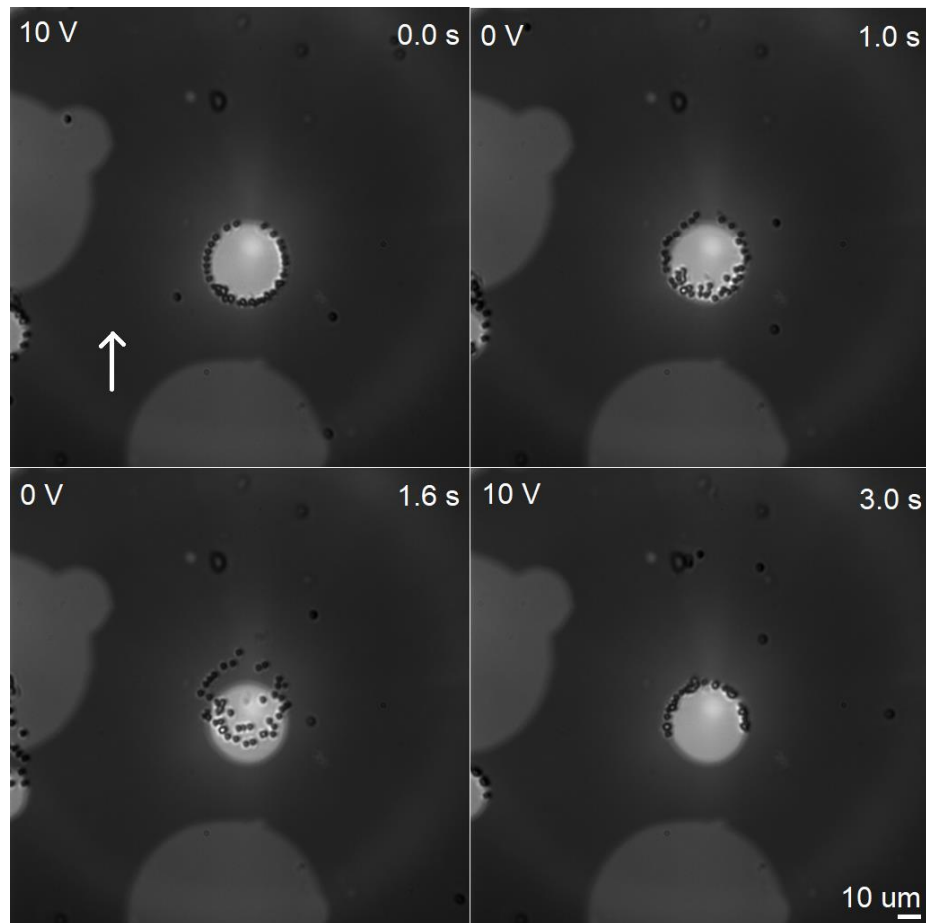
Figure 5.8 – Top left, beads are rim trapped. Arrow indicates direction of solution flow. Top right, voltage is turned off and beads travel upward since solution flow is in the upward direction. Bottom left, voltage is still off and beads continue upward. Bottom right, voltage is turned on and beads become rim trapped again.

Rim trapping has two other observed behaviors that occur as a result of changing

the frequency: rim expansion/contraction and rim looping. The parameters to replicate

these behaviors consistently have not been precisely determined, but they do occur with

reliable frequency. Rim expansion/contraction is first achieved with rim trapping, shown

in Figure 5.9. The frequency is then lowered and the diameter of the ring of beads expands outward. The beads must therefore experience some type of outward force uniformly away from the center that is dependent on the AC frequency. After expanding outward to a certain degree, the beads remain stationary. Lowering the frequency again results in greater outward expansion. If the frequency is brought back up to the original frequency, the beads move inward and become rim trapped again.
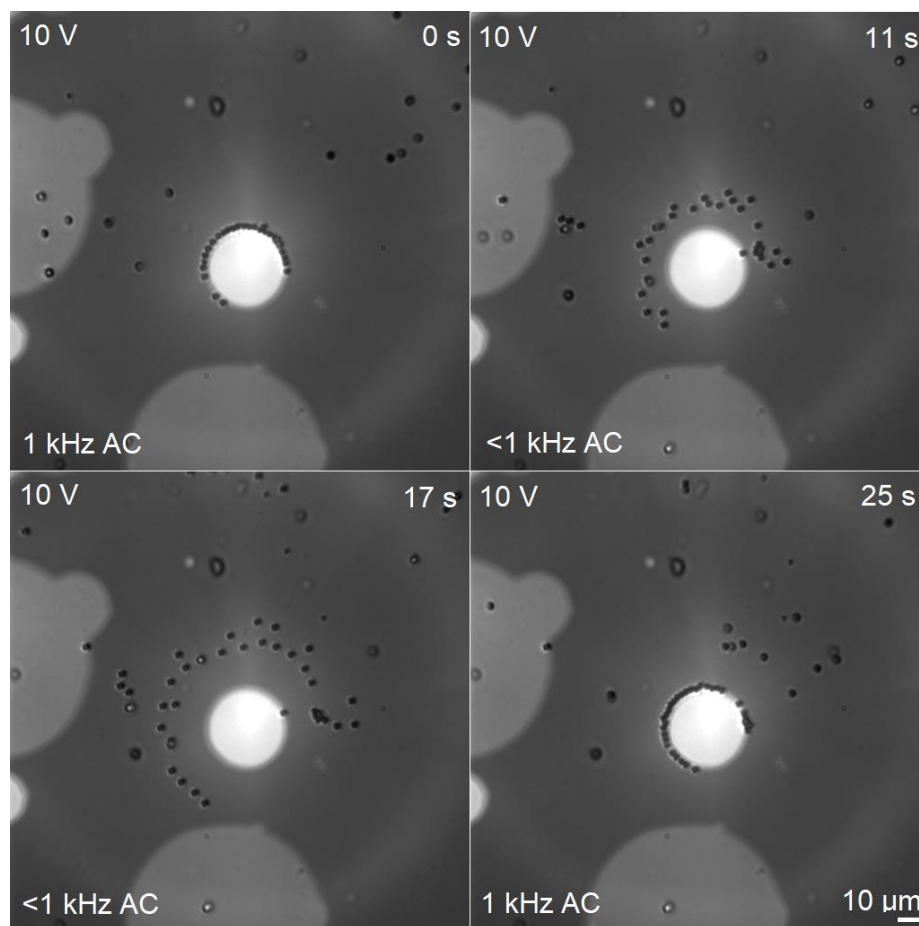
Figure 5.9 – Top left, beads are rim trapped. Top right, AC frequency is decreased and beads expand outward. Bottom left, frequency is decreased further and beads expand outward even more. Bottom right, frequency is brought back up to the initial frequency and the same beads move inward and become rim trapped again.

The other observed behavior is rim looping, shown in Figure 5.10 below. The beads are confined to the area around the rim. The beads then move in a circular loop that is perpendicular to the tangent of the rim and perpendicular to the plane of the corral trap. Looping behavior is not apparent in still images, therefore showing a sequence of images would not be helpful. The direction of looping has proven difficult to ascertain, so both possible directions are shown in the following figures. The thickness of the rim in Figure 5.11 is exaggerated to clarify where the looping occurs. If the center of the corral is used as a reference point, a bead directly on the rim would experience an initial force directed outward away from the center or an initial force directed inward towards the center. The acquisition frame rate of the images is very low, only 7 frames per second. This low frame rate is the reason why discerning the direction of looping has been difficult. Performing a frame by frame analysis results in the bead either being inside the corral or outside the corral. With a faster acquisition frame rate, the direction of looping could more easily be determined.
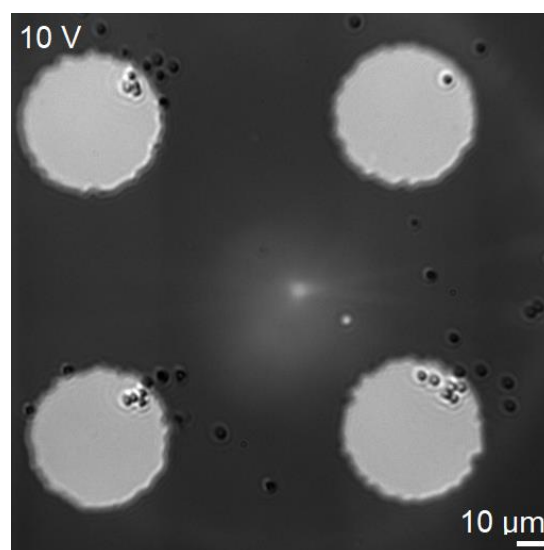
Figure 5.10 – Rim looping.

Figure 5.11 – The possible directions of looping behavior. The thickness of the rim is exaggerated.

This behavior is observed while using AC, which does not correspond to either positive dielectrophoresis or negative dielectroporesis. However, it does correspond well to the electro-osmotic velocity field, Figure 2.32. The frequency at which this behavior occurs would have to be the change-over frequency, the frequency which makes the Clausius-Mossatti factor zero. When the Clausius-Mossatti factor is zero, there should be neither positive or negative dielectrophoresis.

5.5 Grid Trapping

The behavior of a single isolated corral is interesting in and of itself; but additional behavior is observed if there is a grid of corrals, behavior that would not exist otherwise. Figure 5.12 shows subsequent images of corral trapping using a grid. The top left image is the system before the application of voltage, beads in random motion can be observed throughout. In the top right image, voltage has already been applied; electrokinetic behavior is observed and bead patterns start to form. Beads line up in straight lines and form a grid of squares. In the bottom left image, the voltage is still on. Since this is a grid

135

of corrals and not a single isolated corral, two types of trapping occur. The first type is one that has already been described, namely bead confinement within the corral. The second type occurs outside the corral, circled in red.
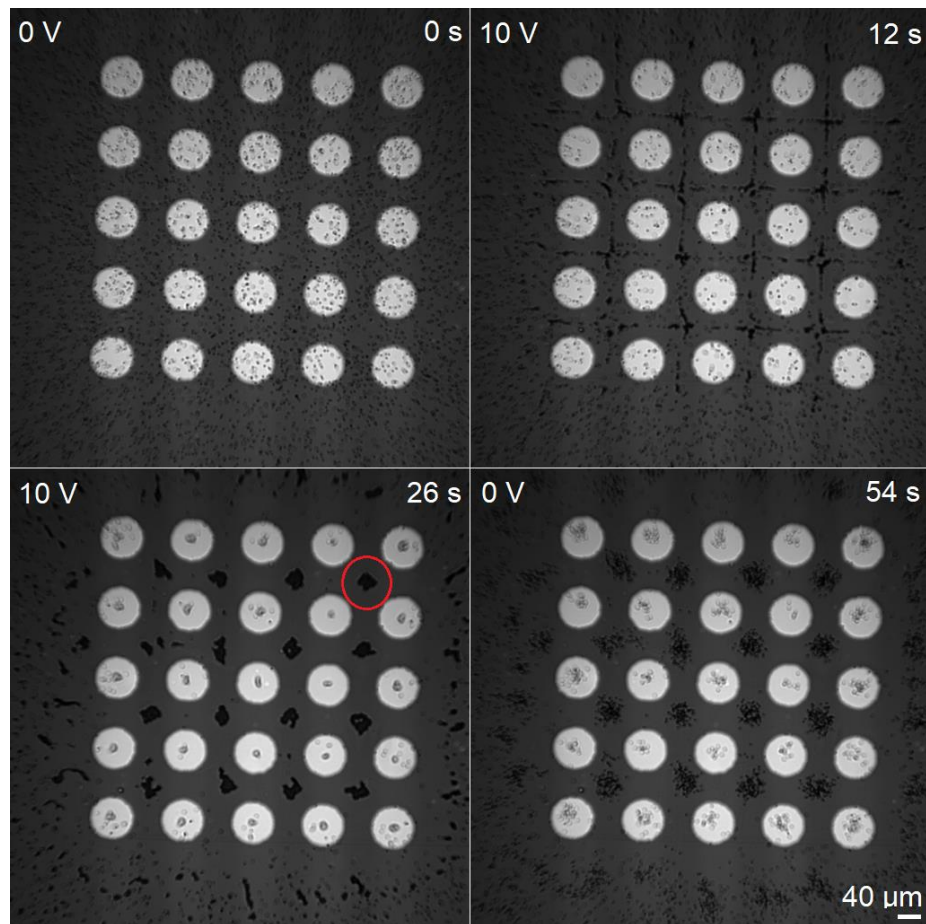
Figure 5.12 – Grid of corral traps at 10x magnification. Corralling is clearly visible inside the circles in the bottom left image. The red circle indicates another type of trapping that occurs simultaneously.
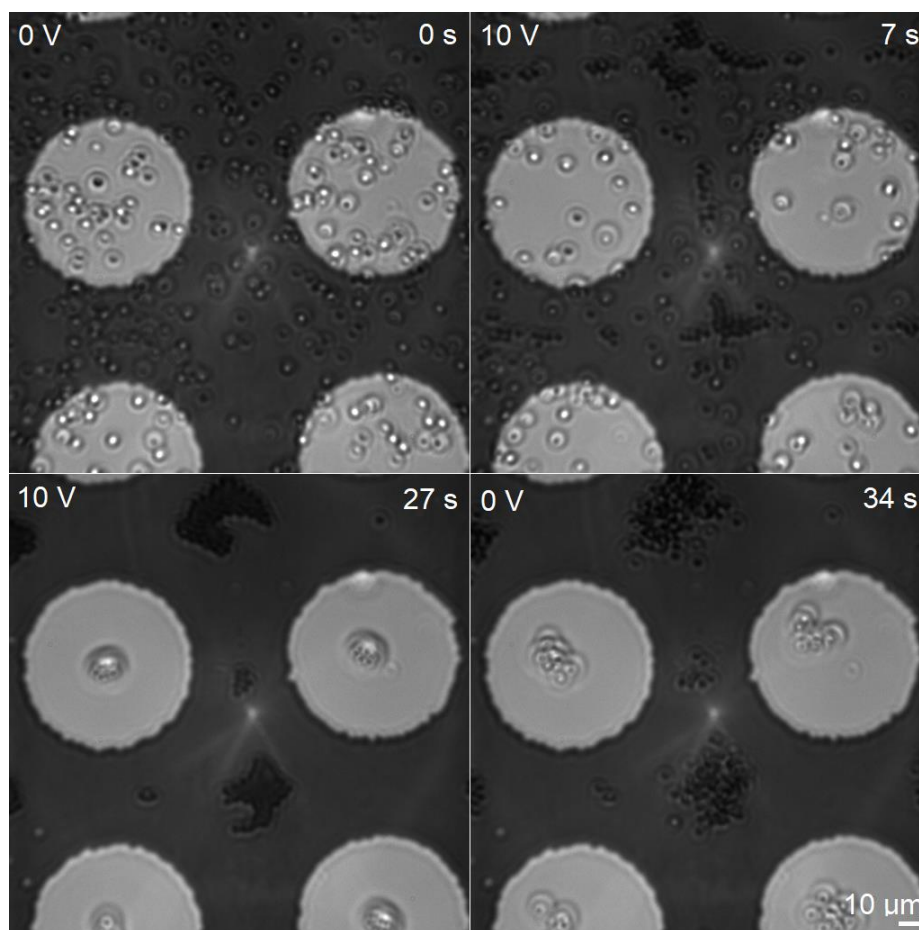
Figure 5.13 – Close up of a grid of corrals at 40x magnification.

Another case is shown in Figure 5.13, where the corrals are 70 microns in diameter and 40 microns apart from each other both horizontally and vertically; diagonally, they are 86 microns apart. The same behavior is observed. Initially the voltage is off and beads only display Brownian motion. The beads then begin to form straight lines that form a grid of squares around each corral. The lines eventually disappear and beads become trapped between the corrals. Since the corral creates a potential well capable of trapping particles, this would imply there exists another potential well between the corral traps that is also capable of trapping particles.
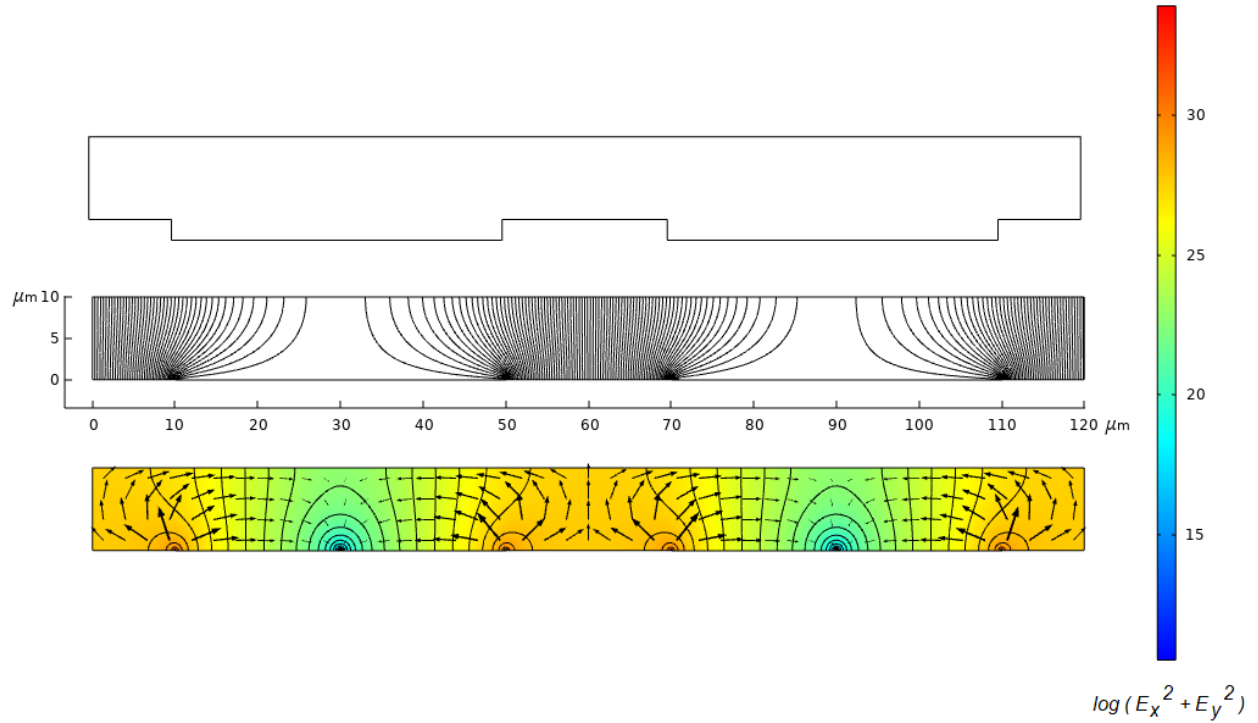
Figure 5.14 – Top, exaggerated dimensions to indicate where the rims of the corral traps are. Middle, the electric field of a two dimensional slice of two corrals side by side. Bottom, the dielectrophoretic potential and the dielectrophoretic field.

In order to investigate this observed behavior, COMSOL simulations of a corral trap array were performed. The dielectrophoretic potential, bottom image in Figure 5.14, shows there is a well between the two corrals. While the well is not an absolute minimum potential, it is a relative minimum potential that exists between the two corrals. The bottom row of arrows which are between the two corrals of the bottom image, show that they point outward and away from the rims of the corrals and towards the midpoint between the rims of the corrals. Since this is only a two dimensional image; trapping would occur in three places, inside the corrals and in between the corrals. Figure 5.15 on the next page shows how the slices of Figure 5.14 would appear in an actual grid. The figure also shows the dielectrophoretic field of the slices that are between the corrals and that also

go through the center of the grid. The slices that go through the center of the grid indicate the behavior of the beads that form the straight lines.
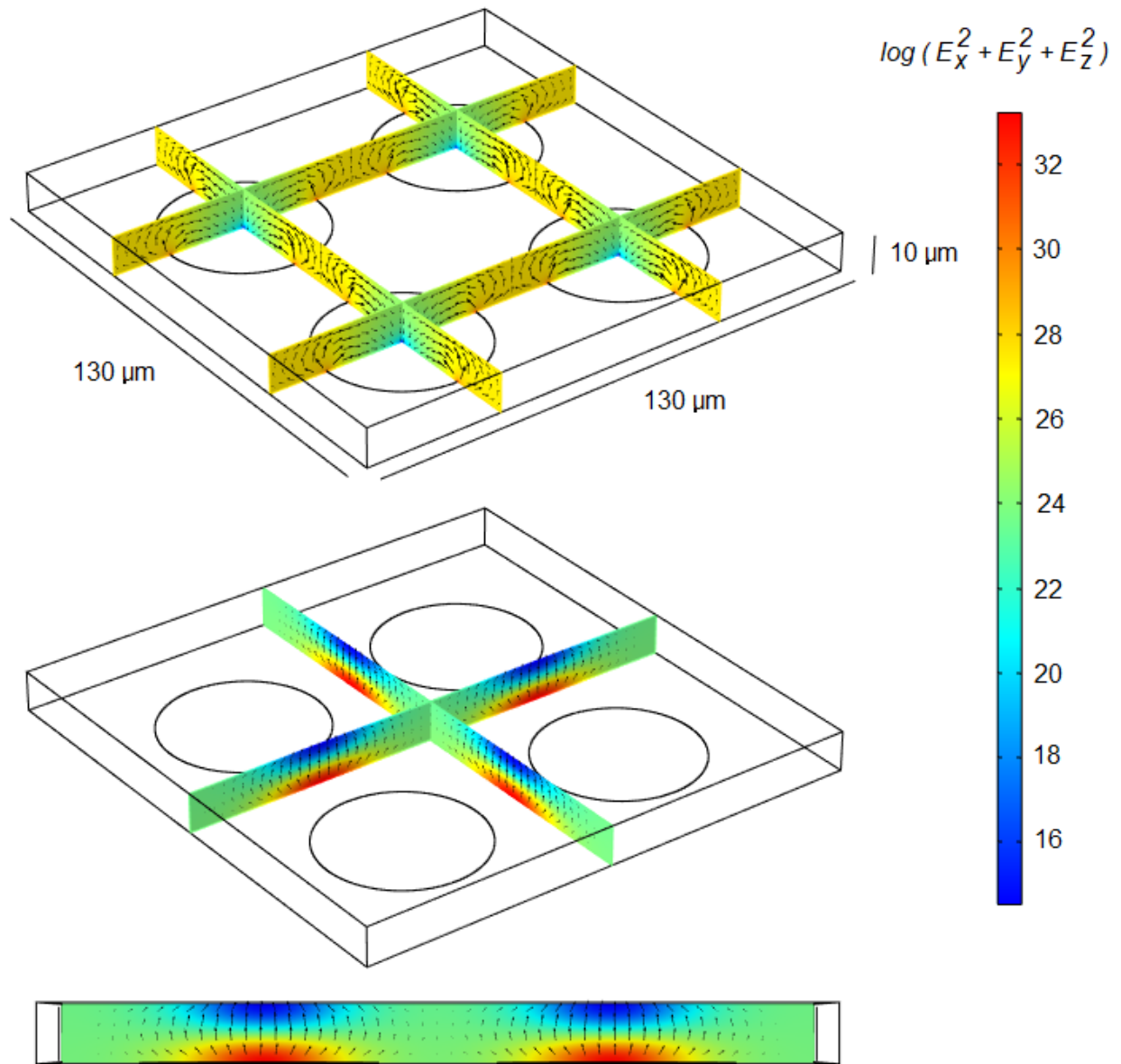
Figure 5.15 – The negative dielectrophoretic fields of specific slices of a grid of corrals.

There are discrepancies between the simulations and the actual experimental results. The experimental results of Figure 5.13 shows that the beads which form straight

lines are on the surface of the bottom electrode since they are in focus. The bottom image of the dielectrophoretic field of Figure 5.15 indicates the beads would be pushed up towards the top electrode and so should appear out of focus. If electro-osmosis is taken into consideration, Figure 5.16 shows that the beads which form straight lines between the corrals would be pushed downward towards the surface of the bottom electrode. This occurs at the 60 µm *x* coordinate mark, exactly midway between the two corral traps. While definite conclusions cannot be made, it is possible that electro-osmosis can be a contributing factor to beads located between the corral traps.
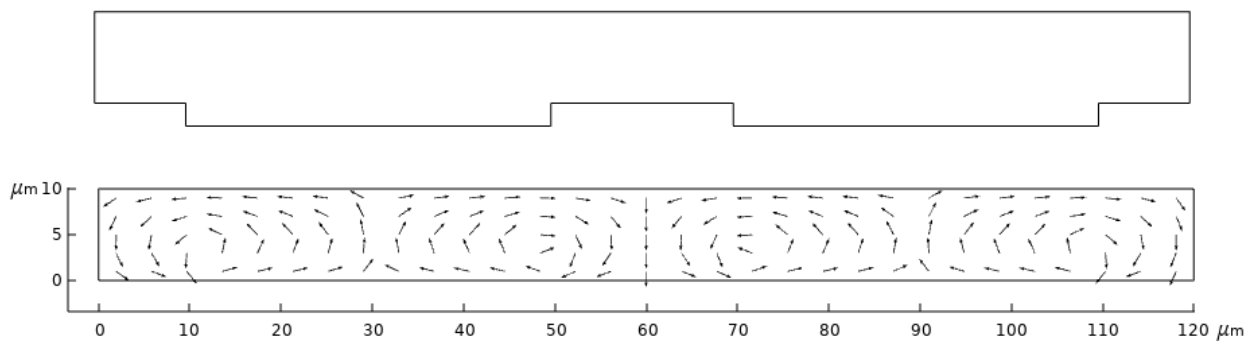
Figure 5.16 – The electro-osmotic velocity field for a grid of corrals.
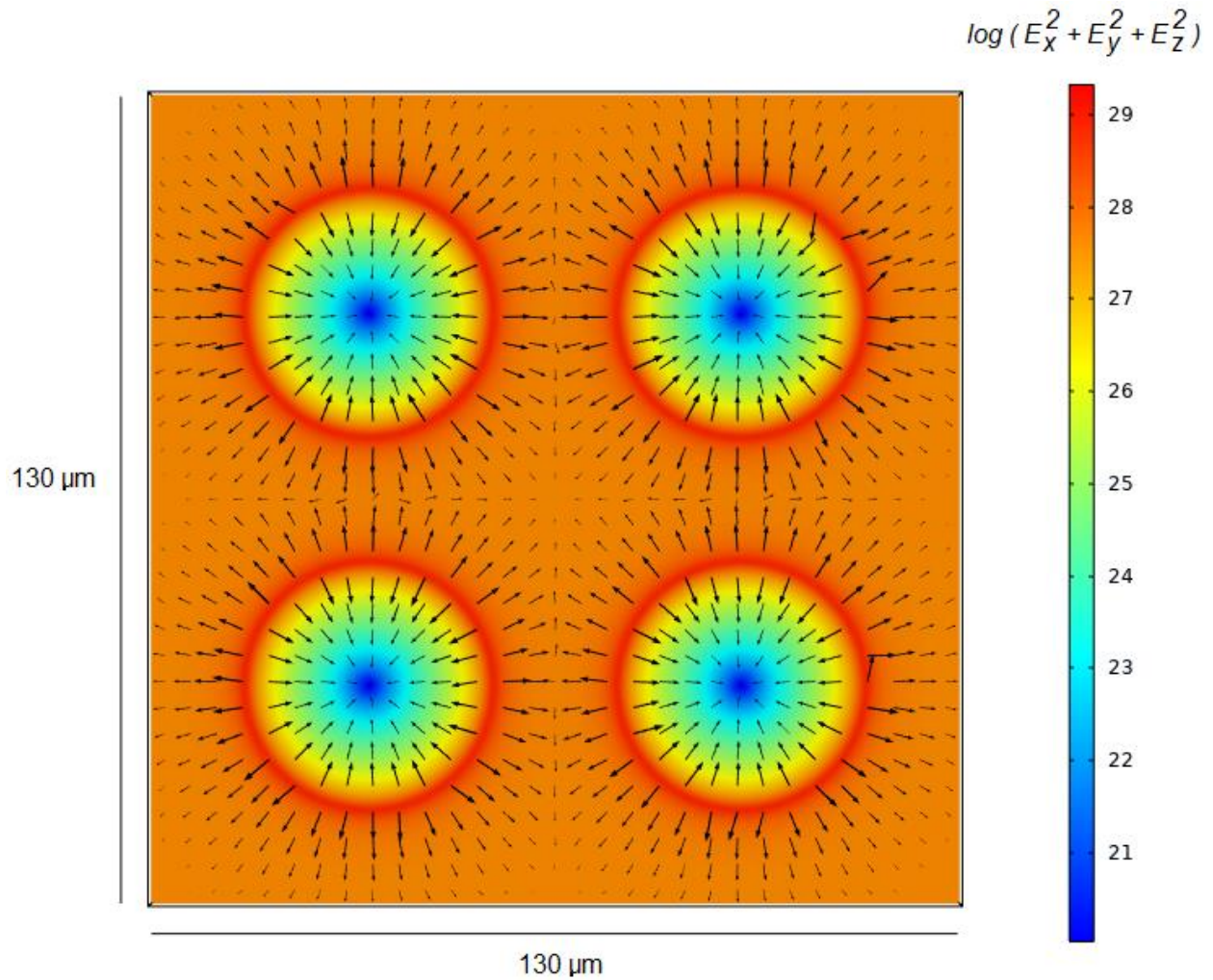
Figure 5.17 – The negative dielectrophoretic force vectors of the corral trap grid viewed from the top, calculated for a horizontal plane that is 0.75 µum above the surface of the bottom electrode.

When the dielectrophoretic field is shown as arrows and viewed from the top, the arrows do orient themselves at angles that form a square grid and create linear pathways for the beads to follow. The field shown in Figure 5.17 is close to the surface of the bottom electrode, so the trapping that occurs between the corrals will only happen to beads that are at or close to the surface of the bottom electrode. The field explains all of the observed behavior for a grid; the trapping inside a corral, the beads forming straight lines, and the trapping between the corrals.

$log(E_x^2 + E_y^2 + E_z^2)$
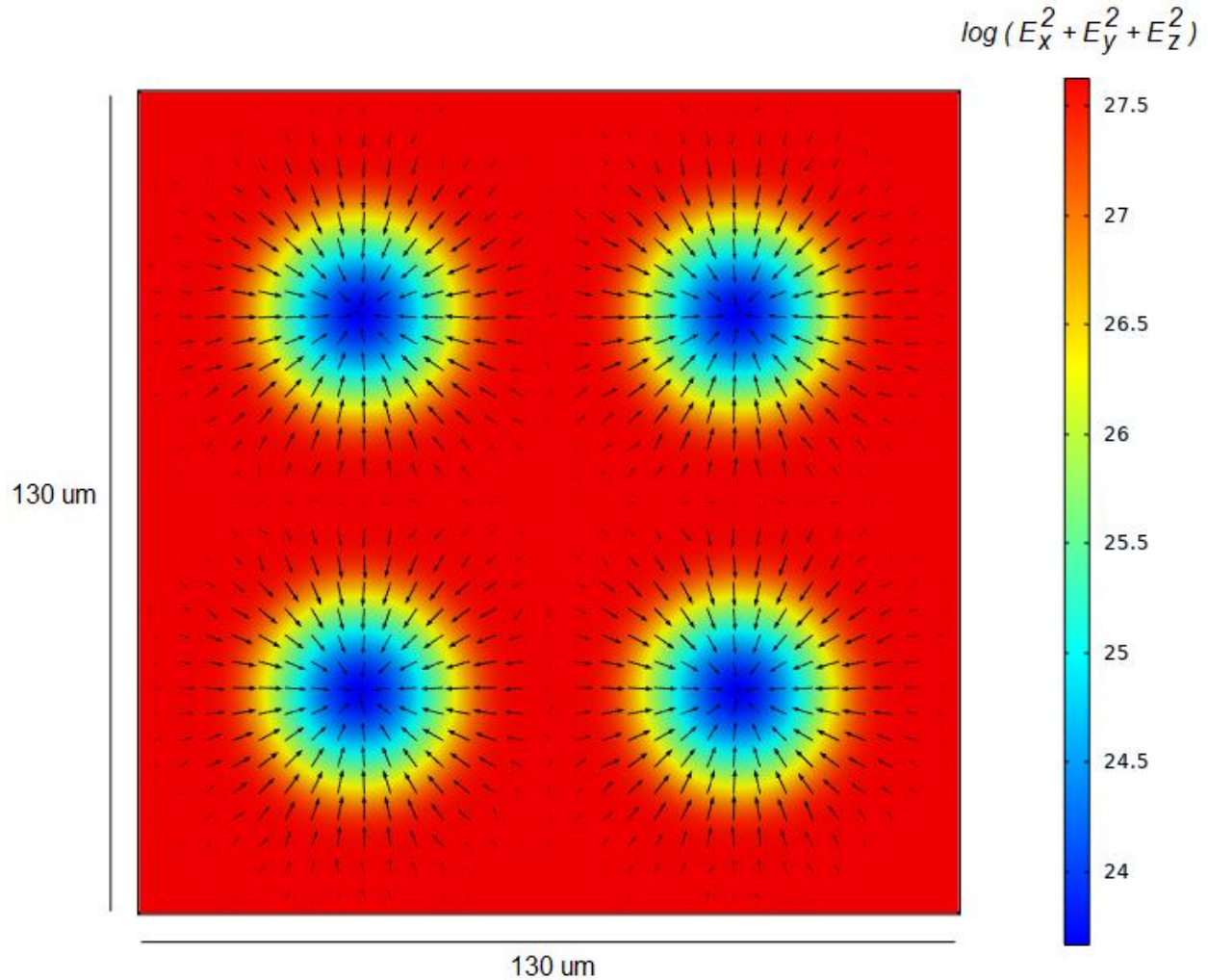
Figure 5.18 – The negative dielectrophoretic force vectors exactly midway between the bottom and the top electrodes. It is 5 µm above the bottom electrode and 5 µm below the top electrode.

Figure 5.18 is the dielectrophoretic field midway between the bottom and top electrodes. The arrows are given the same scale factor as the arrows in Figure 5.17, so direct comparisons can be made. What is most apparent is that the diameter of corralling is much larger above the surface of the bottom electrode than it is near the surface of the bottom electrode. A particle located outside the corral can become corral trapped as long as it is within a reasonable distance away from the rim; this isn't the case near the surface of the bottom electrode where the bead must be inside the corral. Another phenomenon

shown by the vector shield is that trapping between the corrals doesn't occur at the middle

horizontal plane either.
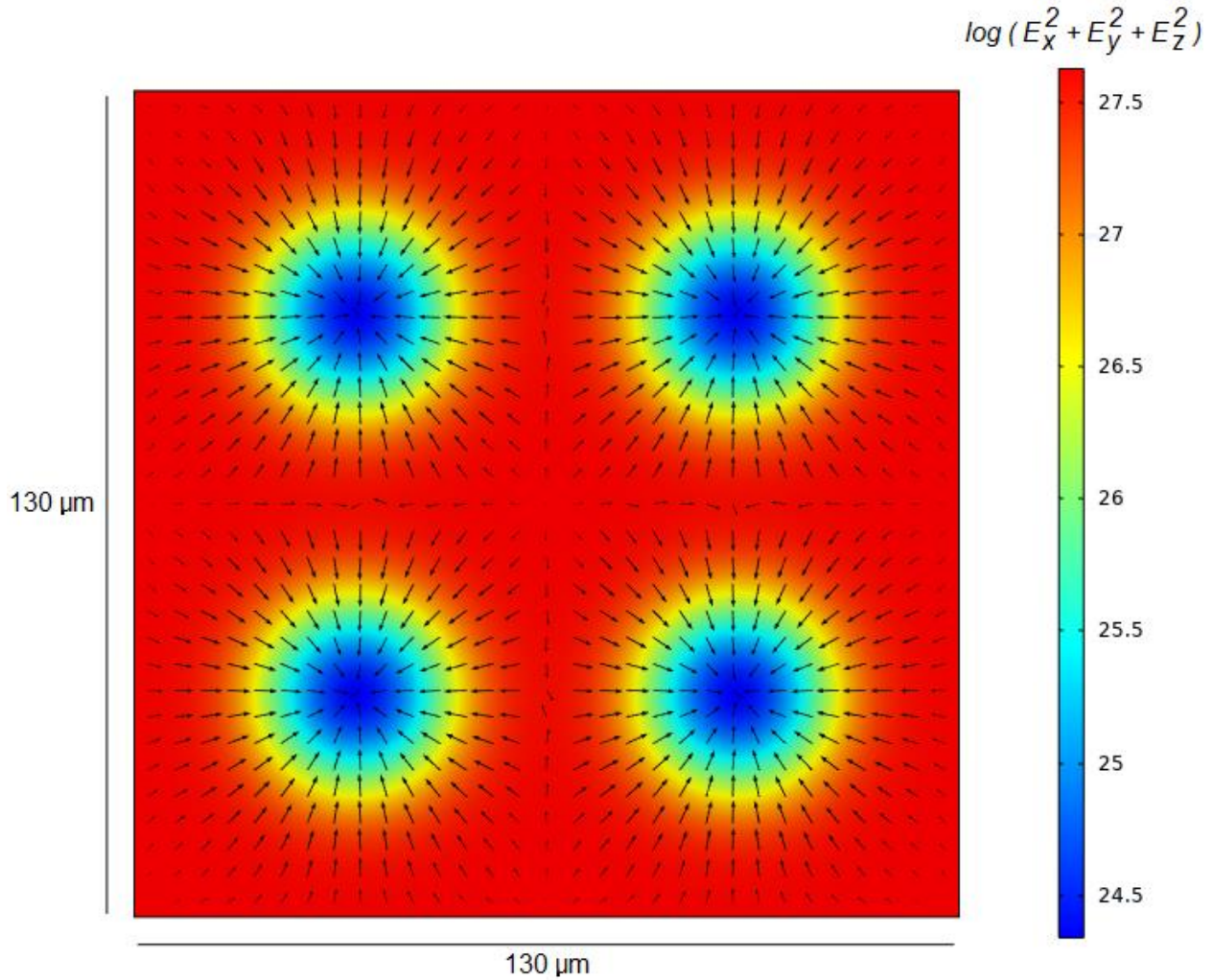
Figure 5.19 – The negative dielectrophoretic force vectors 0.75 µm below the surface of the top electrode.

Figure 5.19 shows the field that beads experience if they are close to the surface

of the top electrode. The straight lines between the corrals are present but this time they

point in the opposite direction when compared to the field close to the bottom electrode.

Again, this is an indication that a bead will behave differently depending on where it is

located on the vertical z axis. A bead could potentially go in one direction if it is located

close to the bottom electrode, and in the opposite direction if it is located close to the top

electrode.
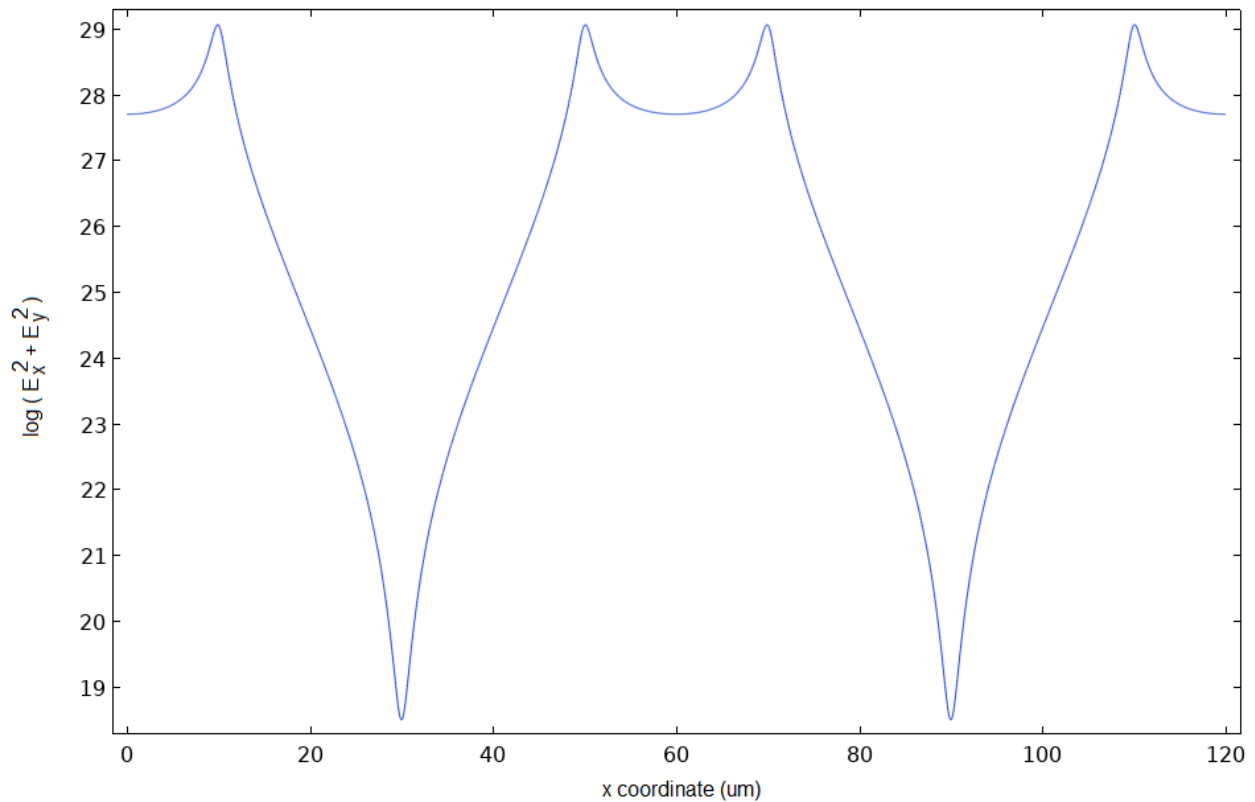
Figure 5.20 – The log of the electric field squared potential relative to the x coordinate of a corral grid. The potential is calculated at 0.75 µm above the surface of the bottom electrode.

Lastly, Figure 5.20 above shows the log of the dielectrophoretic potential of a corral

grid. The lowest potentials are the corral trap centers, which occur at 30 µm and 90 µm.

There is also a relative minimum between the corral traps which occurs at 60 µm. This

indicates beads will go to these areas of low potential.

5.6 Pushing Beads in a Particular Direction with a "V" Shape

A bead can be pushed in a particular direction by using a "V" shape. A bead will start from the sharp end of the "V" and move towards the wide end of the "V"; all the while, staying relatively equidistant from both sides of the "V". While this is the main behavior, it should be noted that the experiments performed do not involve a single isolated "V". There are adjacent "V"s and adjacent "V"s that point in opposite directions. Admittedly, this pattern was done out of curiosity; the resulting bead behavior was unexpected.
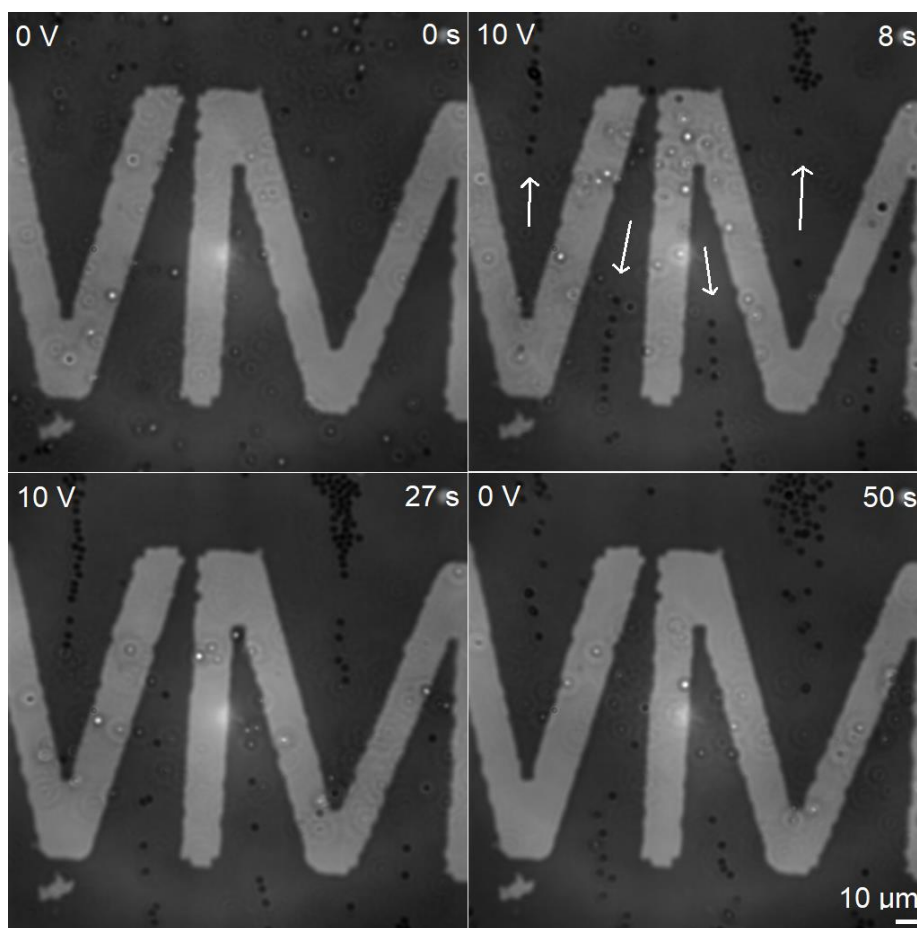
Figure 5.21 – If a metal pattern is in the shape of a "V", beads will travel from the tip of the "V" to the opening of the "V". Direction of bead motion is indicated with white arrows when the voltage is on.

145
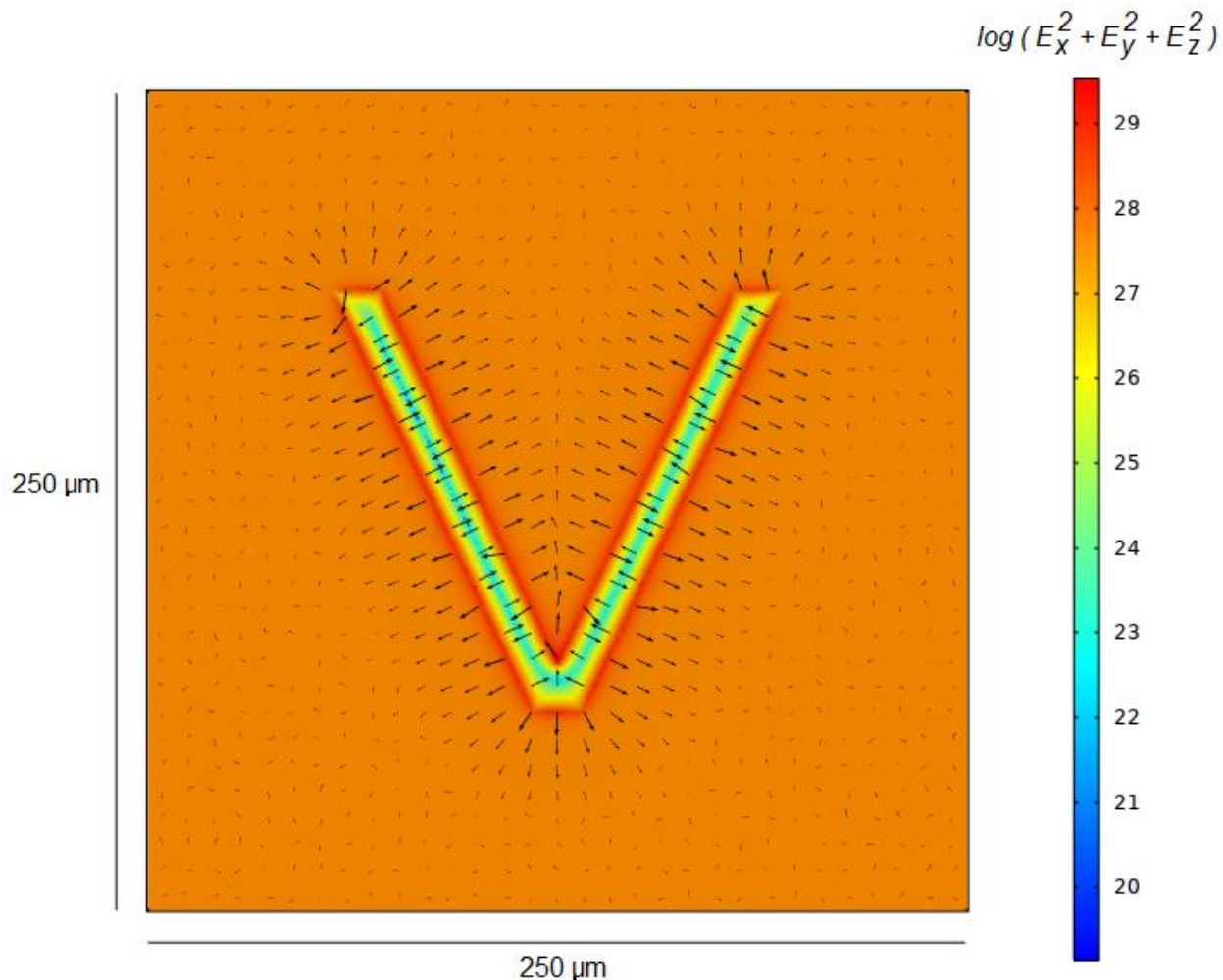
Figure 5.22 – The negative dielectrophoretic force vectors 0.75 μm above the surface of the bottom electrode. Vertical arrows that point upward can be seen that bisect the middle of the "V". The sides of the "V" also push the bead towards the bisector.

While this was not investigated experimentally, it is likely that the degree of sharpness of the "V" has an effect on the bead velocity. If all experimental conditions were the same, a very wide "V" would likely push the bead slower than a very narrow "V". A series of "V"s in a linear horizontal sequence, with varying degrees of sharpness, could potentially be used as a type of separation for particles with different dielectrophoretic properties.
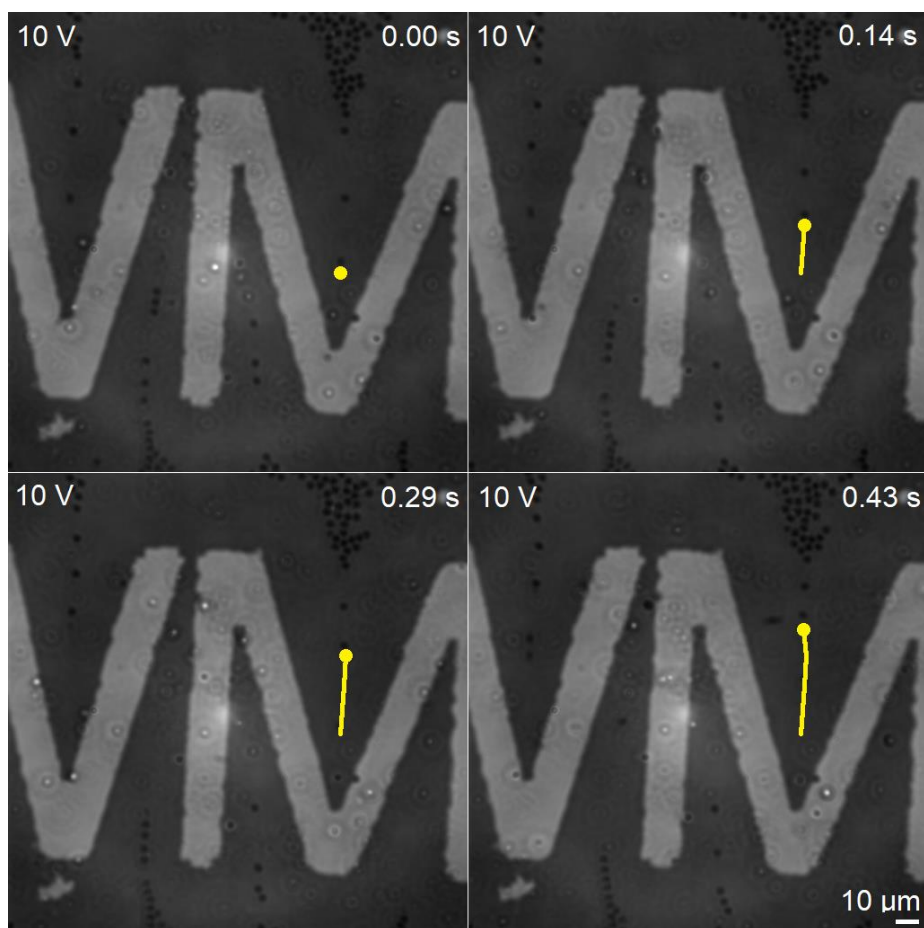
Figure 5.23 – Particle tracking of one bead. This solution has high bead concentration (1:10 dilution of the vendor stock), therefore it has high ion concentration, and therefore it has high conductivity. The bead has an average velocity of 105 microns/sec.

One of the parameters appearing in the calculation of the dielectrophoretic force is the conductivity of the solution. This means the conductivity can have an effect on the magnitude of the dielectrophoretic force. Generally the higher ion concentration a solution has, the greater the conductivity. Polystyrene beads were diluted with ultra-pure water from the vendor stock solution with ratios of 1:10, 1:100, and 1:1000.

All experiments were performed with the same dilutions of the vendor stock bead solution. The conductivities of the various dilutions were measured for one experiment.

Measurements were also made for ultra-pure water and pH 10 NaOH solution for comparison.

Dilution	Conductivity	Resistivity
1:10	10.0 µS/cm	
1:100	3.1	
1:1000	2.9	
ultra-pure water	2.0	18.2 MΩ·cm
pH 10 NaOH solution with ultra-pure water	11.2	

The experiment shown in Figure 5.23 was done with high bead concentration. The vendor stock solution contains substances to keep the polystyrene beads stable or extend shelf-life, and substances may be present that are involved during the manufacturing process of the beads. A solution with high bead concentration would contain a high number of ions which would lead to high conductivity. With the use of particle tracking, the bead velocity was determined to be 105 microns/sec for the high bead concentration solution. Figure 5.24 on the next page shows the particle tracking of a single bead in a low bead concentration solution. The average velocity of the bead was found to be 2.4 microns/sec.
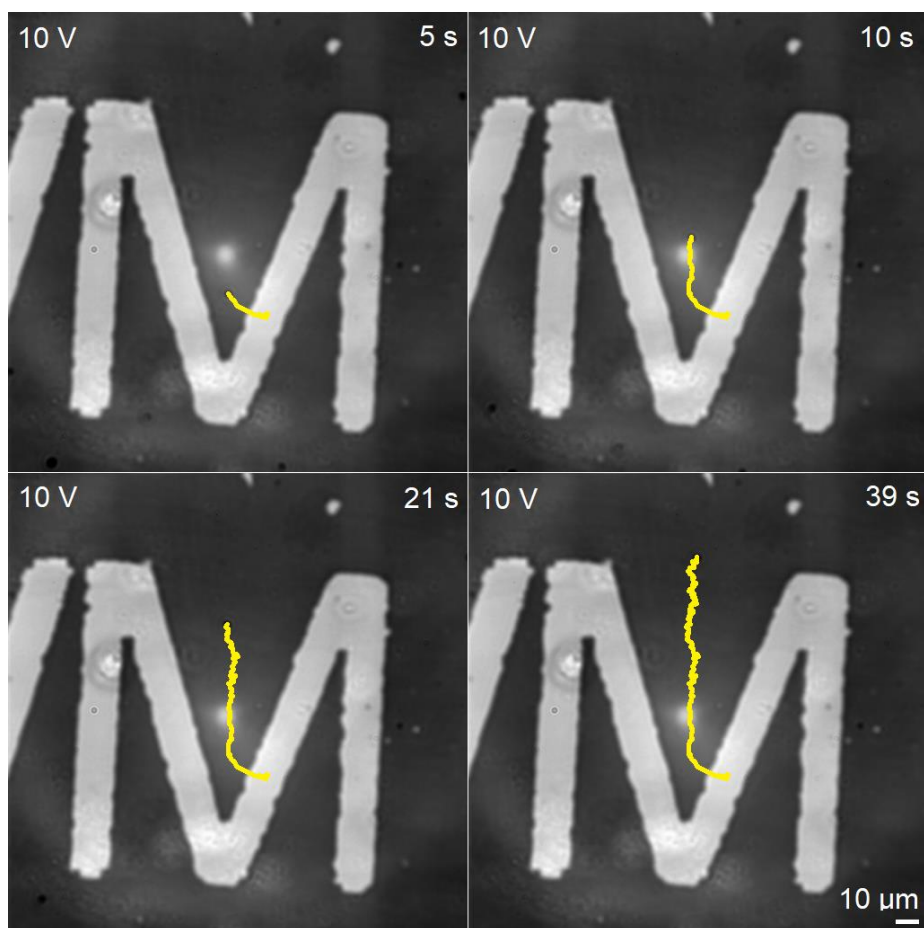
Figure 5.24 – This bead solution has low bead concentration (1:100 dilution of the vendor stock), therefore low ion concentration, and therefore low conductivity. Particle tracking results in an average bead velocity of 2.4 microns/sec.

Figure 5.25 shows the first few frames of the same experiment shown in Figure 5.24. One of the goals of this research is to obtain adequate Z axis data of the bead's physical location in order to fully understand the effects of the electric field's geometry as it influences particles. While the data at this point is qualitative, the bead's appearance could possibly be correlated to the bead's height along the Z axis. If it is certain that the bead is on the surface of the top electrode and the electrode separation distance is known; then the bead's appearance could be correlated to its height. If the bead is on the surface of the bottom electrode, its appearance would also be distinct. The general trend

149

is that the size of the brightness of the inner portion of the bead gradually diminishes as the bead comes into focus. It will start off as a bright spot then gradually change into a black spot.
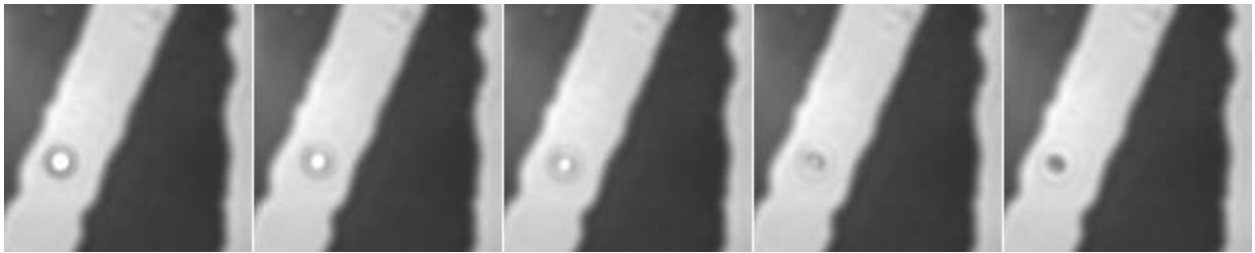
Figure 5.25 – Images of a single 1.5 µm diameter bead as the electric field pushes it downward, from the surface of the top electrode towards the surface of the bottom electrode, along the vertical Z axis.

5.7 Two Rectangles Side By Side Can Induce A 90º Turn

If two rectangles are parallel along the longer side of each other, a 90º turn is observed at the ends of the rectangles. A single rectangle by itself will not display this behavior. When the voltage is turned on, a bead will move perpendicular to the longer side of each rectangle towards the midpoint between the rectangles. The bead will then move parallel to the longer side of each rectangle towards the ends of each rectangle. Figure 5.26 below shows the path a bead will take.
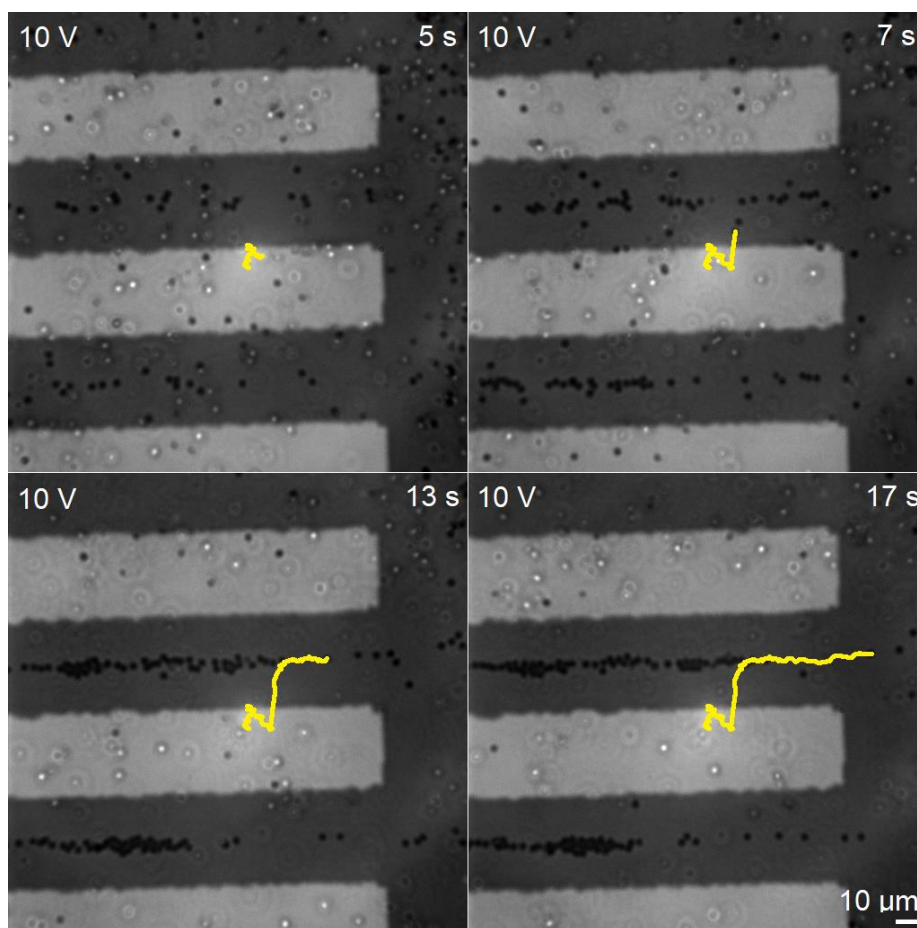
Figure 5.26 – Particle tracking of a single bead. The yellow line indicates the successive motion of the particle.
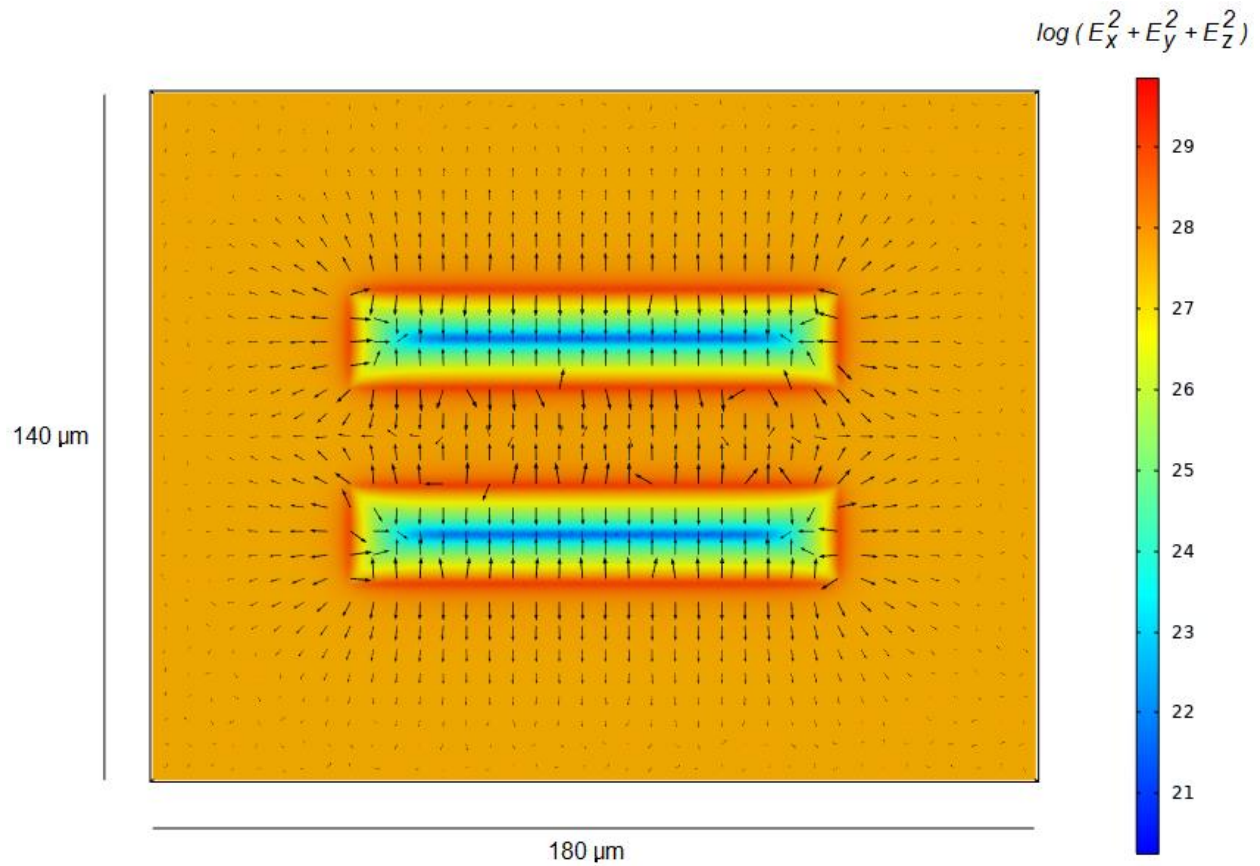
Figure 5.27 – The negative dielectrophoretic field 0.75 µm above the surface of the bottom electrode.

Figure 5.27 shows there are forces which are perpendicular to each other towards the ends of the rectangles. The middle row of vectors that are between the two rectangles vary in magnitude, they are largest towards the ends and smaller in the middle. The fact that they are smaller in the middle indicates the beads in this area will not experience a significant force to push them in a perpendicular direction relative to the direction of their original motion. Experiments show that beads in the middle will eventually move towards the ends, but they do so very slowly.

5.8 Star Trapping

The star trap has a symmetric void in the middle so trapping in this area is expected. The area of the middle void is larger than the area of the spokes of the star, therefore the middle void will have the lower electric field density when compared to the spokes. What is interesting is that the spokes of the star act as pathways for beads to follow.
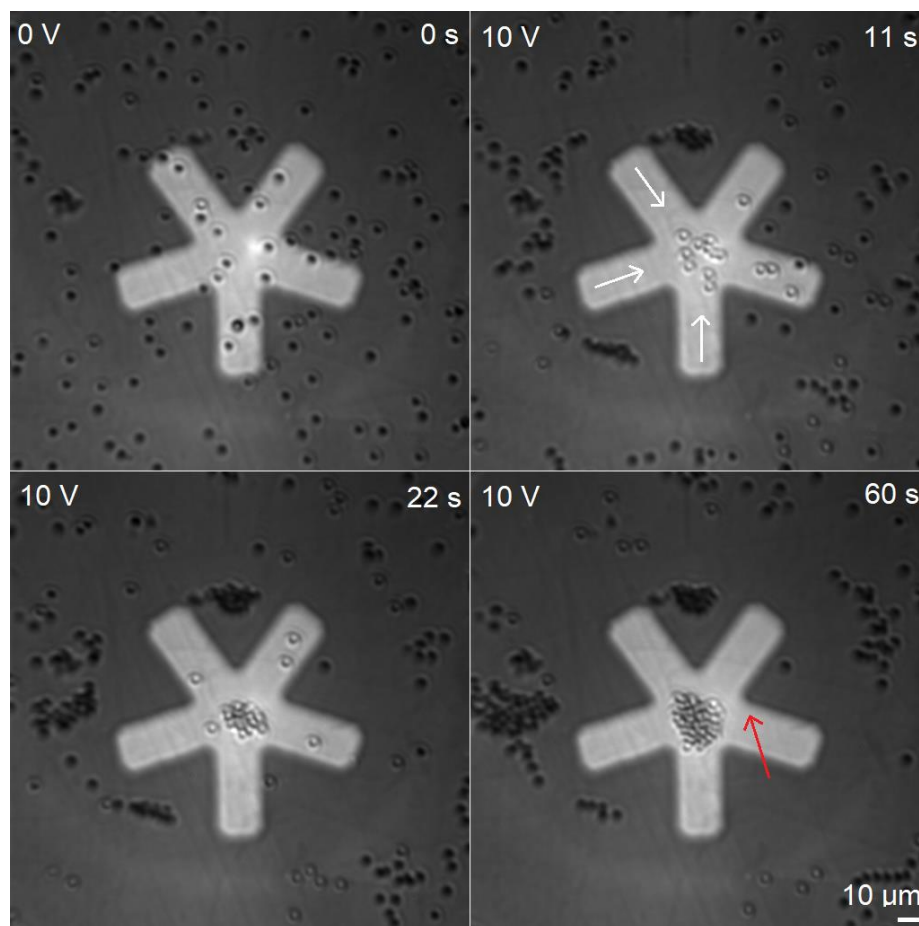
Figure 5.28 – Star trapping. Top left, voltage is off. Top right, voltage is turned on and beads follow the pathway of the spokes of the star indicated with white arrows. Bottom left, beads accumulate in the center. Bottom right, voltage is still on. Red arrow indicates where some beads travelling down the spoke of the star can escape prior to reaching the center.
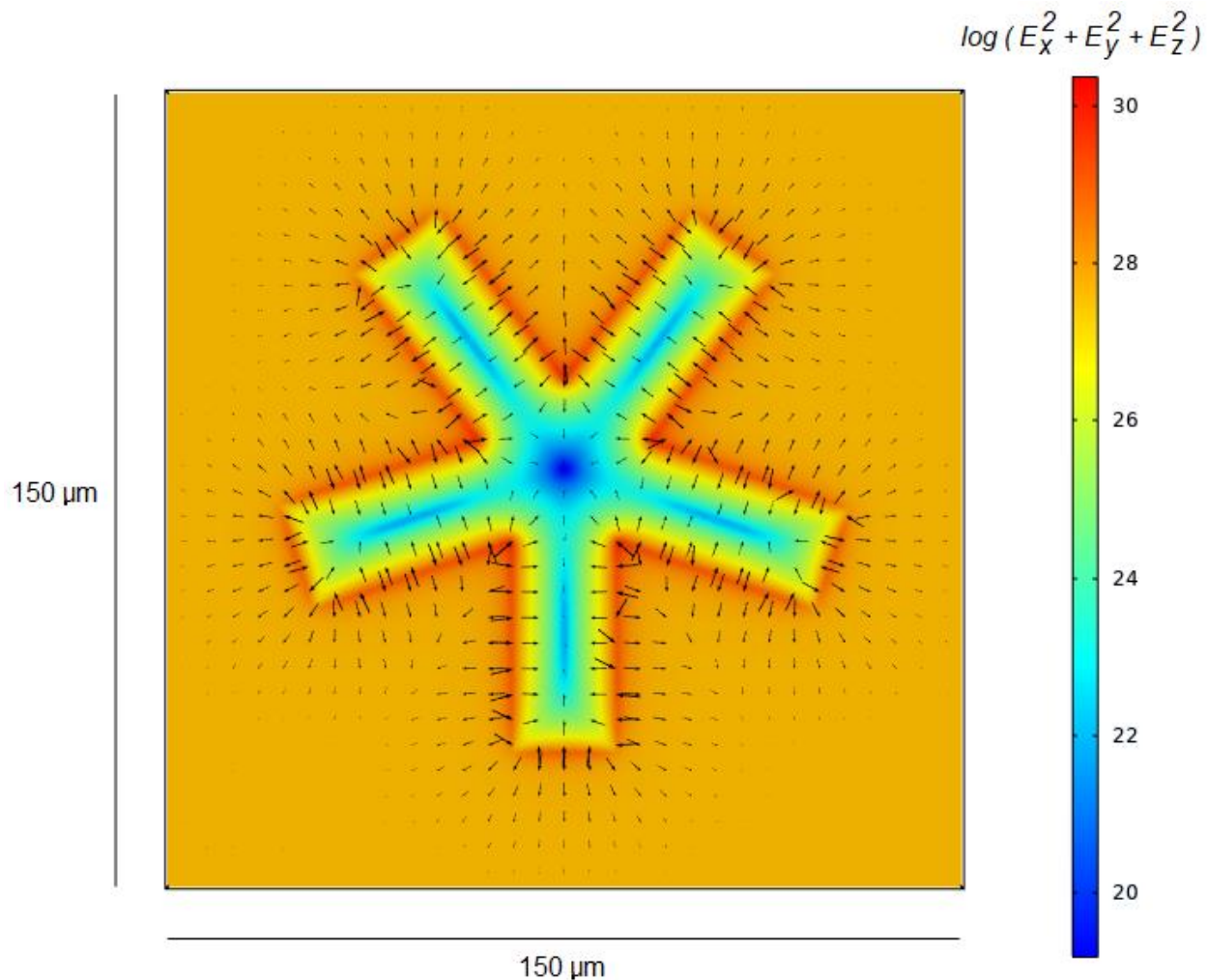
Figure 5.29 – The negative dielectrophoretic field 0.75 µm above the surface of the bottom electrode.

Only particles that are close to the surface of the bottom electrode are capable of escaping the star trap. The red arrow in Figure 5.28 indicates where beads can escape. The areas of the star trap that are not the spokes or the middle are essentially "V"s, and this behavior was discussed previously in Chapter 5. Figure 5.29 shows that the vector field of one of these "V"s is similar to the vector field that was shown in Figure 5.22. It is possible that the sharpness of the "V"s increases the probability of escape. The beads that escape are generally in focus.
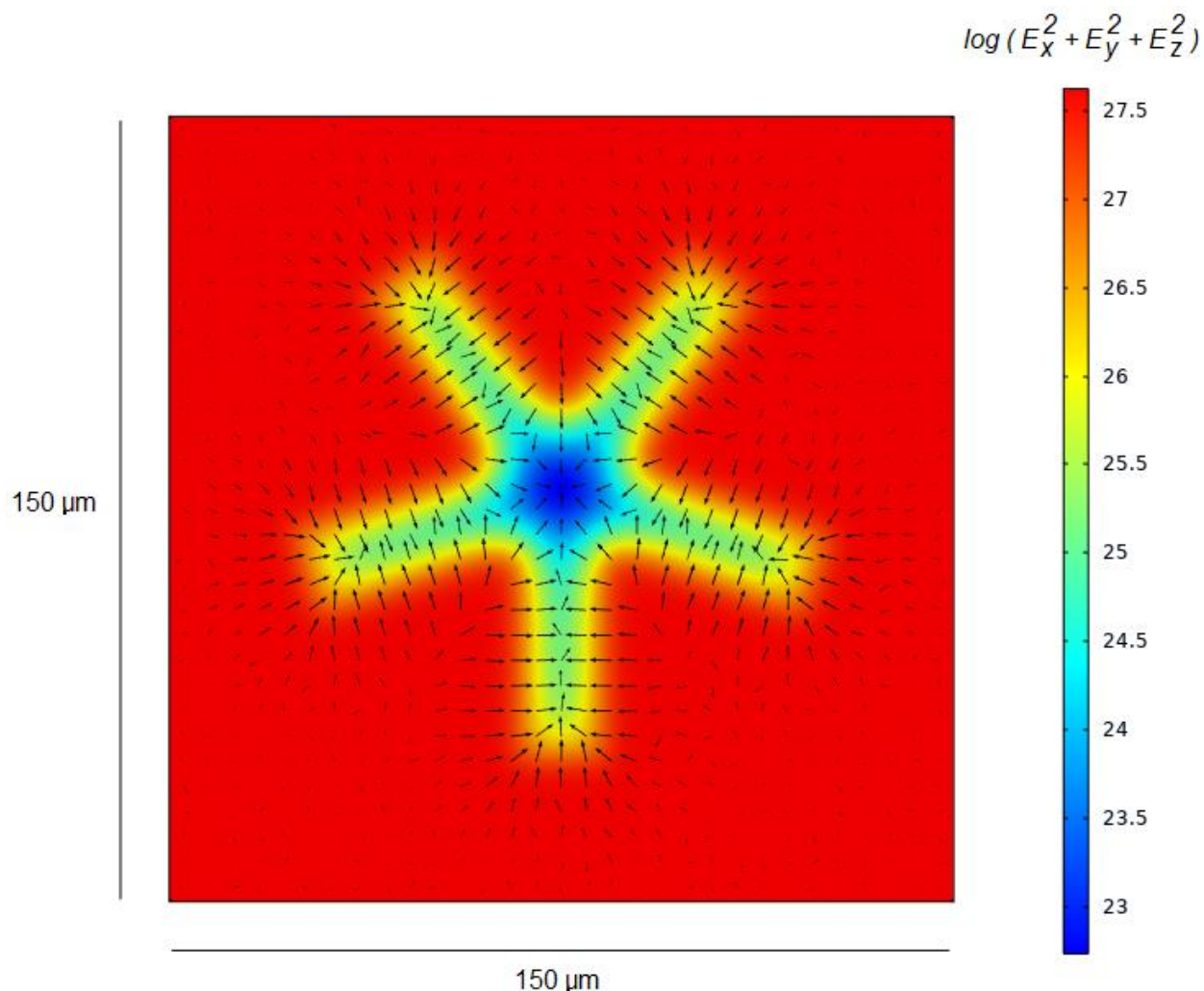
Figure 5.30 – The negative dielectrophoretic field exactly midway between the bottom and top electrodes. It is 5 µm above the bottom electrode and 5 µm below the top electrode.

The vector field shown in Figure 5.30 shows that trapping would be the expected result. There are also vectors that keep the bead inside the pathway and also push the bead along the pathway towards the center. Since this occurs midway between the bottom and top electrodes, the beads that are corralled are out of focus. They look different from the beads that escape, which are in focus. A general observation is that beads will go from small void areas of metal to larger void areas of metal. In the case of

the star trap, the small void areas are the pathways and the large void area is the center of the star. Bead pathways can be made in two ways; with voids as shown by the star trap and with metal strips as shown by the two adjacent rectangles in Chapter 5.7.
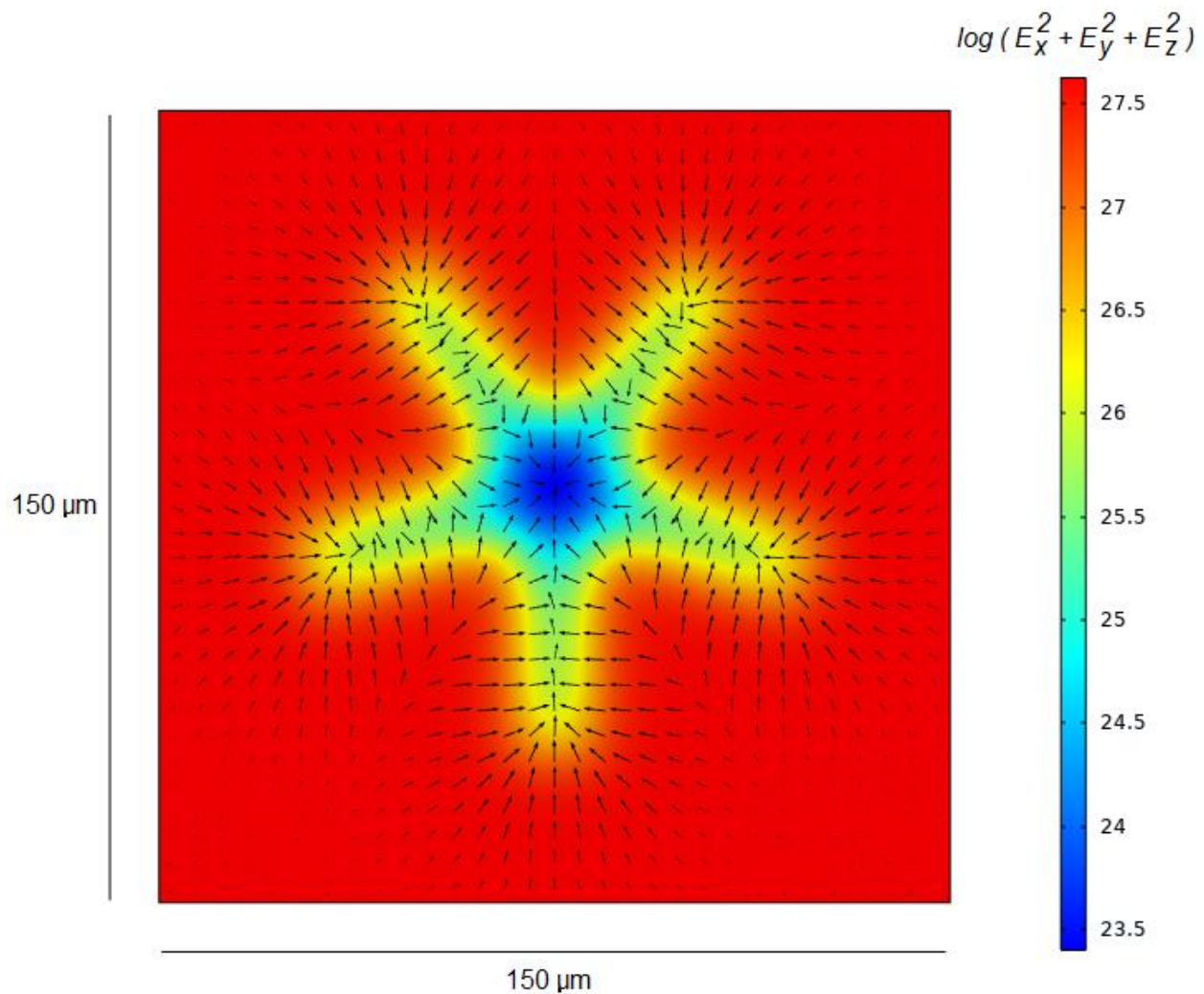
Figure 5.31 – The negative dielectrophoretic field 0.75 um below the surface of top electrode.

The dielectrophoretic field close to the surface of the top electrode, shown in Figure 5.31, is not drastically different from the field midway between the two electrodes. Corralling diameter simply extends outward a little more.

5.9 The Inverted Corral Trap

The inverted corral trap can be described as a concentric circular metal pattern within a corral trap that is connected with the metal surface of the electrode via a thin strip of metal that functions as an electrical bridge. Since the metal pattern is different from a simple corral trap, the dielectrophoretic field will be different. The beads should display different behaviors due to the metal bridge and possibly similar behaviors because it is circular. Figure 5.32 on the following page shows the trapping of beads. This is different from the corral trap in that trapping occurs over the metal surface, whereas trapping with a corral occurs over the metal void. A unique behavior of the inverted corral trap is that the beads can be released in the direction of the metal bridge by lowering the AC frequency. Of course, bead release in the flow direction can also be achieved simply by turning off the voltage.
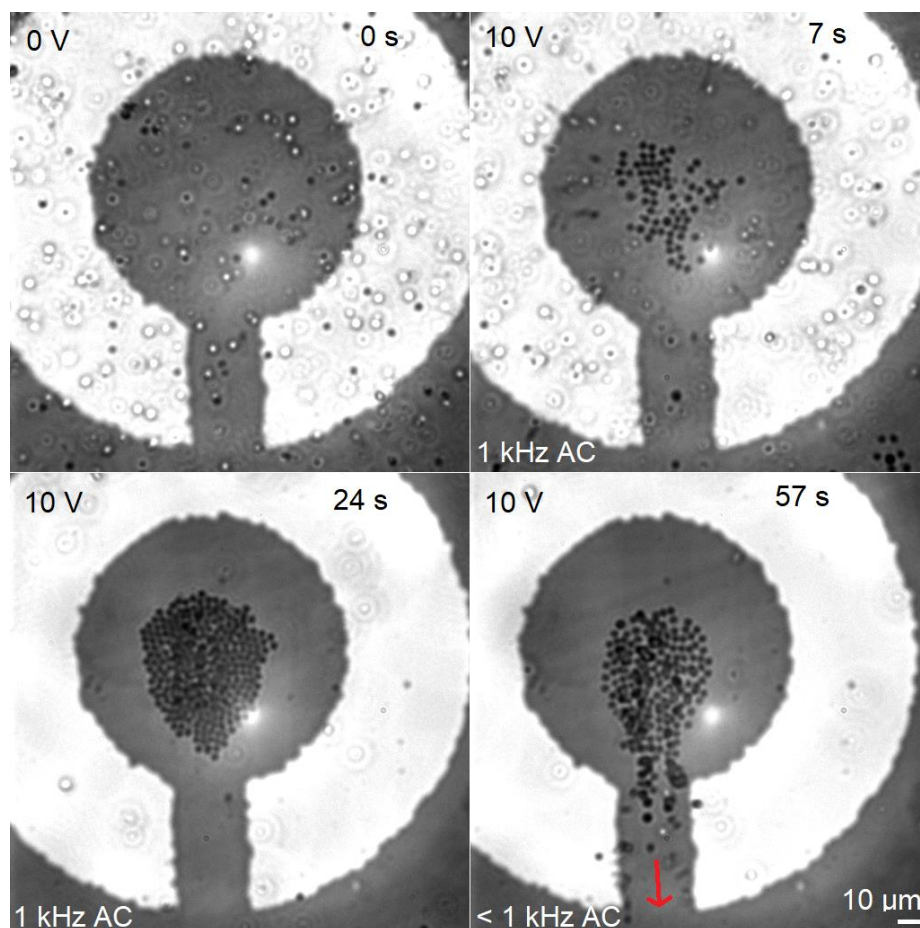
Figure 5.32 – Trapping and releasing of beads with the inverted corral trap. Top left, voltage is off. Top right, voltage is on. Bottom left, voltage has been on for an extended amount of time. Bottom right, AC frequency is lowered and beads escape in the direction of the metal bridge.

Beads that are trapped by this particular pattern have a solid dark color and are in focus, so this occurs near the surface of the bottom electrode. Figure 5.33 on the following page shows the vector field of this pattern. The central metal area, while not the area of lowest dielectrophoretic potential, is at a relatively low potential. In actuality, it is similar to the trapping that occurs with a grid of corrals. The grid of corrals can be thought of an inverted corral trap with four metal bridges instead of one.

158
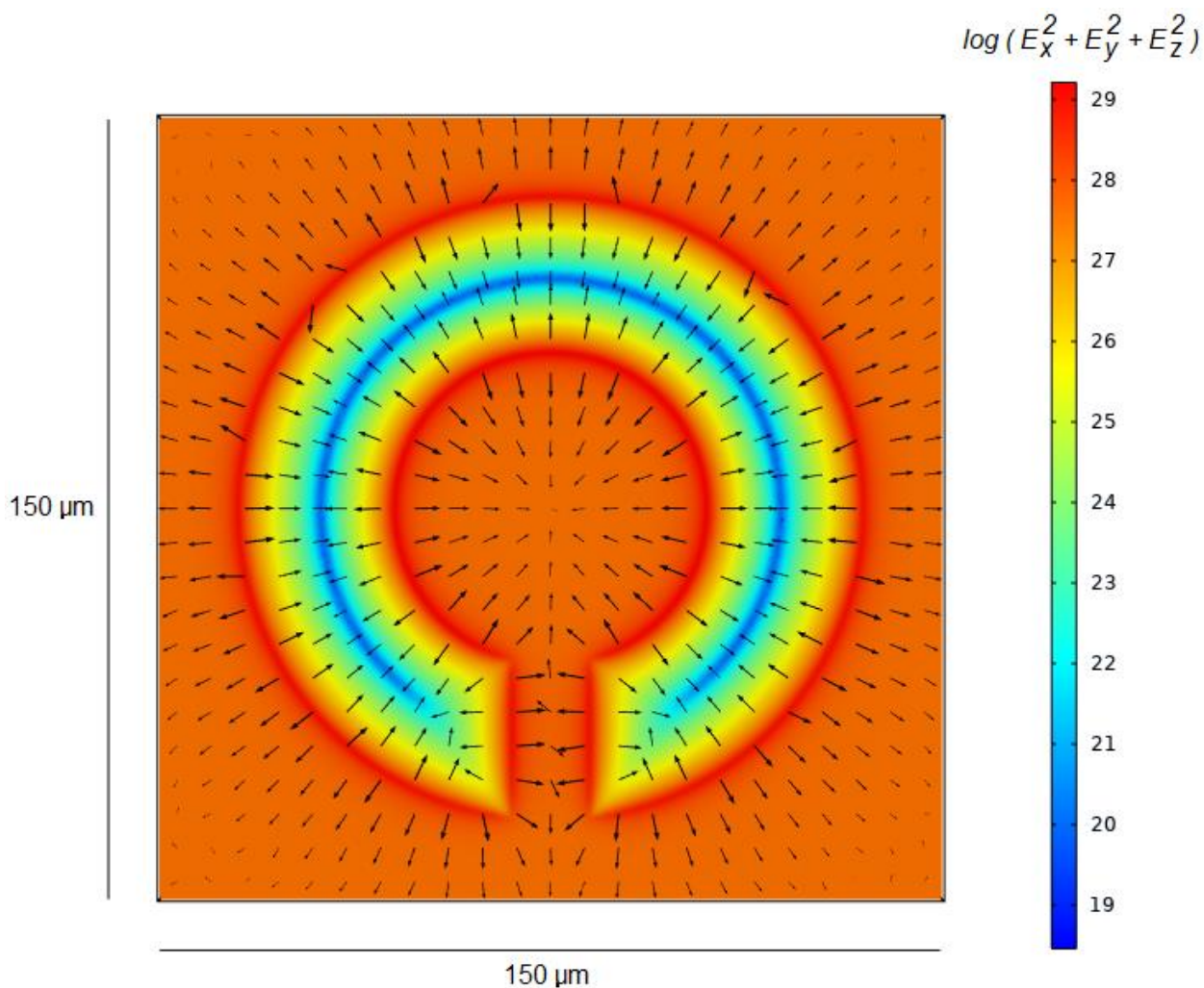
Figure 5.33 – The dielectrophoretic field 0.75 µm above the surface of the bottom electrode.

Figure 5.34 on the following page shows a sequence of corral traps. In the top left image, the voltage is off and only Brownian motion is observed. In the top right image, the voltage is turned on and beads become trapped. The beads are not trapped perfectly in the center of the corral, they appear to be skewed towards the direction of the metal bridge. In the bottom left image, the voltage is still on and beads accumulate. In the bottom right image, the voltage is turned off and the beads diffuse.
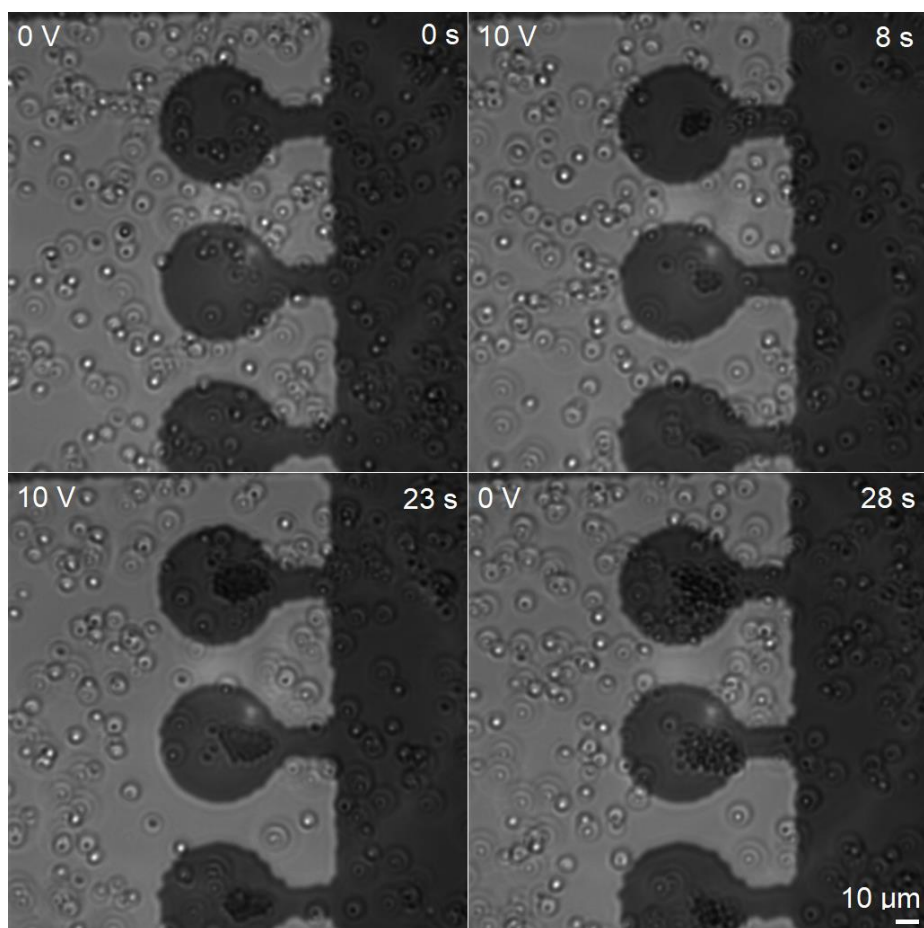
Figure 5.34 – Three inverted corral traps in sequence. Perhaps this configuration can be used for filtering, sorting, or separating different types of particles by varying the diameters of each inverted corral. Beads could potentially be released separately as well depending on the AC frequency.

5.10 Determining The Electrode Separation Distance

Getting consistent electrokinetic behavior has been problematic. Corralling can be observed in one set of electrode pairs; and despite using all of the same electrical settings, the same behavior isn't observed when using a different set of electrode pairs. One of the reasons for this is not being able to replicate a consistent separation distance between the two electrodes each time. However, at the very least, it is possible to know the separation distance each time. There are two requirements. The first is to rigidly set

160

the electrode separation distance by gluing the two electrodes together to keep them in place. The next requirement is implementing fine mechanical motors into the microscope system that can raise or lower the sample stage in discrete known increments, or raise and lower the focus if the stage is stationary.
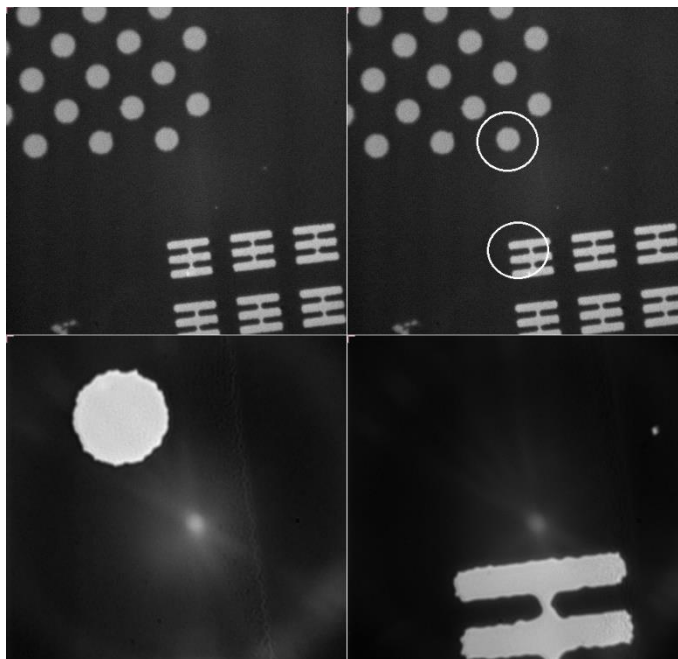
Figure 5.35 – Patterns used to determine the separation distance between the top and bottom electrode. The patterns circled in white are used to determine the separation distance. Separation distance is 28.5 microns for this particular flowcell.

In Figure 5.35, an area is selected that has patterns on both the top and bottom electrodes. The patterns have to be in relatively close proximity to each other. The top two images are at 10x and the bottom two images are at 40x. The circles are located on the bottom electrode while the rectangular shapes are on the top electrode. The first step is to manually focus on the circles. Then move the focus horizontally until the rectangular shapes appear in the field of view, they will first appear blurry at this point. The final step is to incrementally raise the sample until the rectangular shapes come into focus. If 57

increments were used to bring the rectangular shapes into focus, and each increment was 0.5 microns; then the distance between the two electrodes is 28.5 microns (57 x 0.5 = 28.5) since this was performed with a dry flowcell.

Flowcells were fabricated that were determined to have electrode separation distances of 9.0, 11.0, and 28.5 microns. Circular coralling trapping was not observed for the flowcells with 9.0 and 11.0 micron separation distances, while circular corral trapping was observed for the 28.5 micron separation distance. In retrospect, it is likely all successful corralling in the past was probably at or near this electrode separation distance. This does imply that corralling with AC is not possible at really small separation distances. But separation distance is not the only factor to consider. Corralling might still be possible at small distances if other parameters are changed. It is also possible that the flowcells with 9.0 and 11.0 micron separation distances may have inadvertently been fabricated with unintentional short circuits.

References for Chapter 5

1.   ImageJ
        ImageJ Software
        https://imagej.nih.gov/ij/

2.   Fabrice Cordelieres, "Manual Tracking" Plugin, Institut Curie, Orsay,
        France 2004 – https://imagej.nih.gov/ij/plugins/track/track.html

3.   Robert Hooke, *De Potentia Restitutiva, or of Spring. Explaining the Power of
        Springing Bodies*, 1678, London

4.   Donald A. McQuarrie, *Physical Chemistry A Molecular Approach*, 1997, University
        Science Books

5.   David W. Ball, *Physical Chemistry 2E*, 2013, Wadsworth Cengage Learning

6.   MATLAB
        Mathworks
        www.mathworks.com

7.   Darrell D. Ebbing, *General Chemistry 4th Edition*, 1993, Houghton Mifflin Company,
        Boston

Chapter 6

Future Experiments

6.1 Use of The Point Spread Function to Extract Vertical Z Axis Data

The point spread function is the image pattern of a microscopic object relative to its location above or below the plane of focus[1]. There are additional factors that determine the object's image pattern, not just the object's vertical location. One factor is the index of refraction of the solvent itself. In the case of polystyrene beads, the solvent is generally water. The ion concentration of the solution also plays a factor as this will alter the index of refraction of the solution. Since microscopy generally involves the use of glass slides or coverslips, the index of refraction and the thickness of the glass coverslip will also alter the point spread function. And lastly, there will be a certain immersion medium, such as air, between the microscope objective and the glass surface. At minimum, there will be three mediums to account for; immersion medium, glass, and solution.
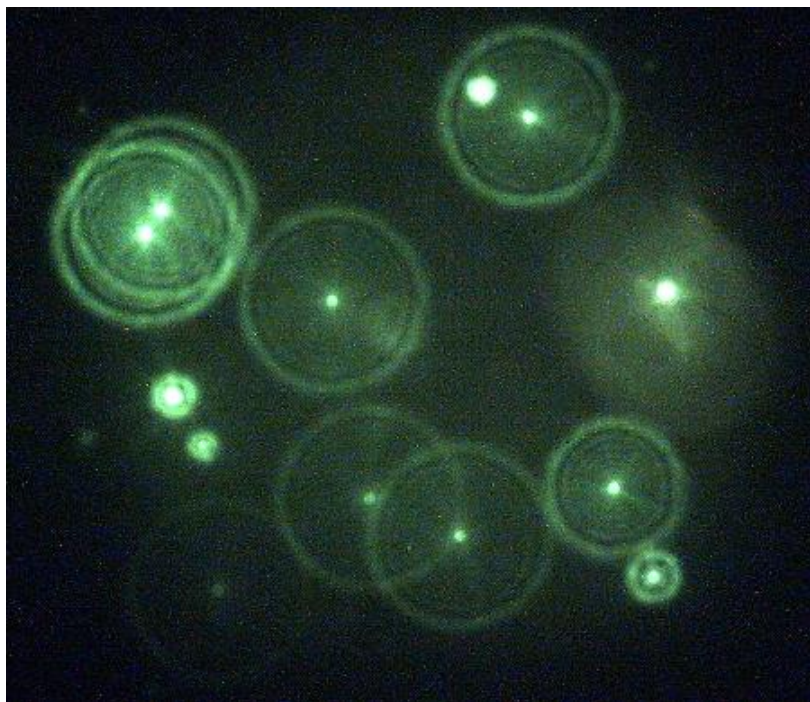
Figure 6.1 – The point spread function of 2.0 μm diameter fluorescing beads. The different diameters indicate the beads are at different z heights.

Figure 6.1 shows polystyrene beads that are functionalized with a fluorescent molecule known as Cy3. The beads are excited with a laser tuned to the absorption band of the functionalized bead. Since an excited state is higher in energy than a ground state, Cy3 will eliminate this excess energy through non-radiative decay channels or by fluorescing. The Cy3 will release photons that are longer in wavelength than the wavelength of the light of the initial excitation laser.

The figure shows point spread function slices of beads at various z locations. The smallest diameters are beads that are in focus, while the largest diameters are the most out of focus and consequently the furthest away from the plane of focus. Therefore the point spread function can be used as an indicator of a bead's height location relative to the vertical z axis. By correlating the diameter of the point spread function to a particle's height location on the z axis, three-dimensional data can be obtained from experiments.

Under bright-field imaging, three distinct point spread functions have been discerned for a particle, shown in Figure 6.2. The plane of focus is the metal pattern which corresponds to focusing on the bottom electrode, therefore the focus is manually adjusted until lines or edges of the metal patterns become clearly defined and show the strongest contrast. Beads that are closest to the bottom electrode appear as solid, non-opaque black dots. These generally have the smallest diameters, an example is circled in red. Beads that are farthest away appear as two rings, one inside the other. These generally have the largest diameters and would be closest to the top electrode, an example is circled in blue. A bead that is somewhere in between appears to have an outer ring with a certain degree of brightness in the center; an example is circled in white. These of course have diameters that are somewhere in between.
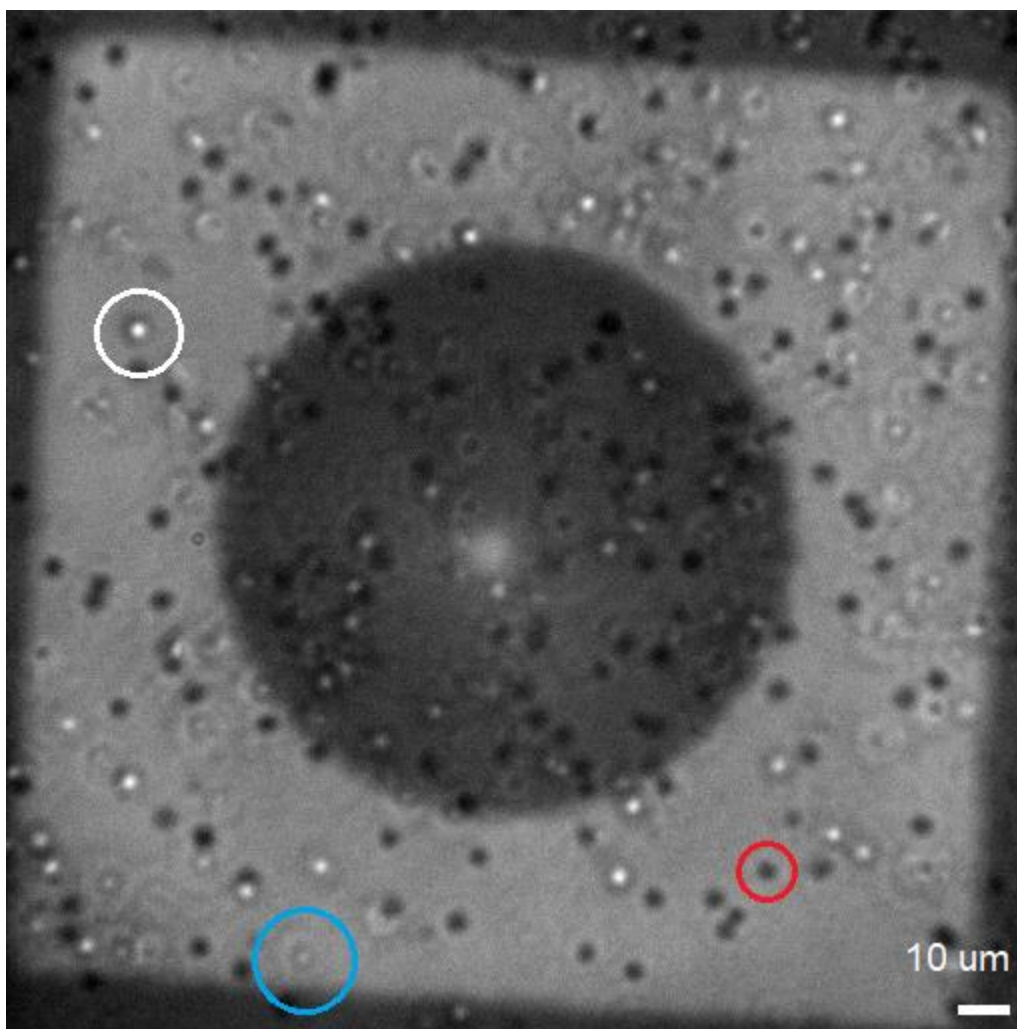
Figure 6.2 – The point spread function of beads under non-fluorescent, bright-field imaging. Bead circled in red is located near the bottom electrode. Bead circled in white is between the top and bottom electrode. Bead circled in blue is near the top electrode.

One experimental result of Chapter 5.10 showed that the separation distance between the top and bottom electrode could be determined if distinct patterns were placed on both electrodes. The idea was to focus on a pattern on the bottom electrode and then utilize a fine motor system that will incrementally adjust the height of the objective lens until patterns on the top electrode come into focus. Since the incremental height change is known, the height change is multiplied with the number of times the height change was performed, which gives the electrode separation distance.

The image of a bead with the smallest diameter would correspond to the bead being at the surface of the bottom electrode. The image of a bead with the largest diameter would correspond to the bead being at the surface of the top electrode. The diameters between the smallest diameter and the largest diameter would mean that the bead is somewhere in-between the two electrodes. It would be tempting to assume that the varying degrees of the bead's diameter is linearly correlated to its height along the vertical Z axis. In reality, the relationship of the diameter of a bead's point spread function relative to its distance away from the plane of focus is not linear.

Theoretically, getting x, y, and z coordinates of a bead is possible. The remaining problem would be to image a bead that is directly on the surface of the bottom electrode, and then image a bead that is directly on the surface of the top electrode. Experimental images of the bead located on the bottom electrode, which would have the smaller diameter, and images of the bead located on the top electrode, which would have the larger diameter, could then be correlated to a theoretical model for the point spread function. Z data could then be extrapolated from experiments. Figure 6.3 on the next page shows the experimental result of having metal patterns on both the bottom and the top electrodes. Circles are on the bottom electrode and triangles are on the top electrode. Aside from showing that corralling is possible with a triangle, it also shows that both surfaces can affect beads if there are patterns on them.
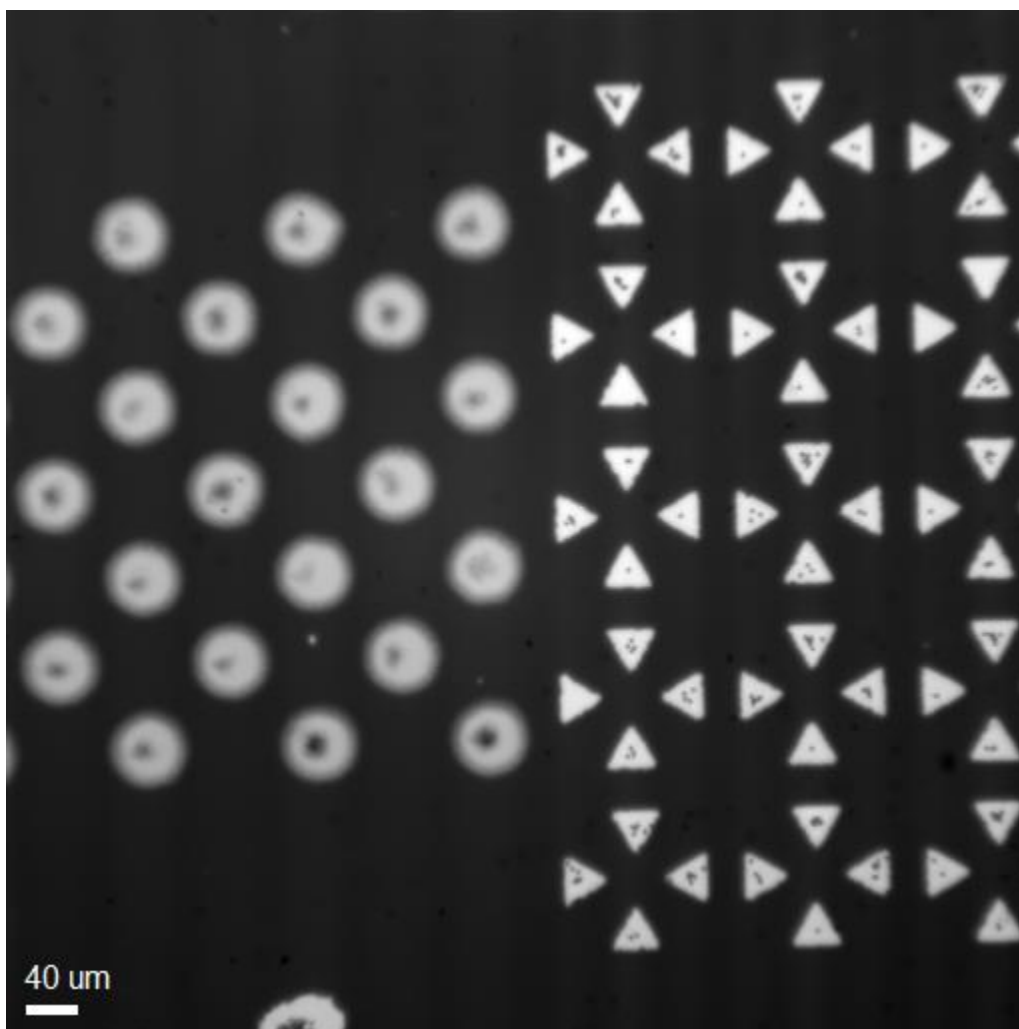
Figure 6.3 – Simultaneous trapping on both the top and bottom electrodes, focus is on top electrode. As evidenced by the image, corral trapping is even possible with triangles.

Since it is clear that patterns on both electrodes can affect beads, it might be possible to move a bead up and down along the vertical z axis. Based on the results in Chapter 5.9, if a bead is trapped with an invert corral, it is located on the surface of the electrode. Two inverted corrals, one on top of the other and with different diameters, could possibly move the bead up and down. The inverted corral with the smaller diameter would have a higher electric field density, while the inverted corral with the larger diameter would have a lower electric field density. By changing the AC frequency, the bead could

hypothetically move up and down. Figure 6.4 below shows the relative diameters of the

inverted corral and how they would be oriented.
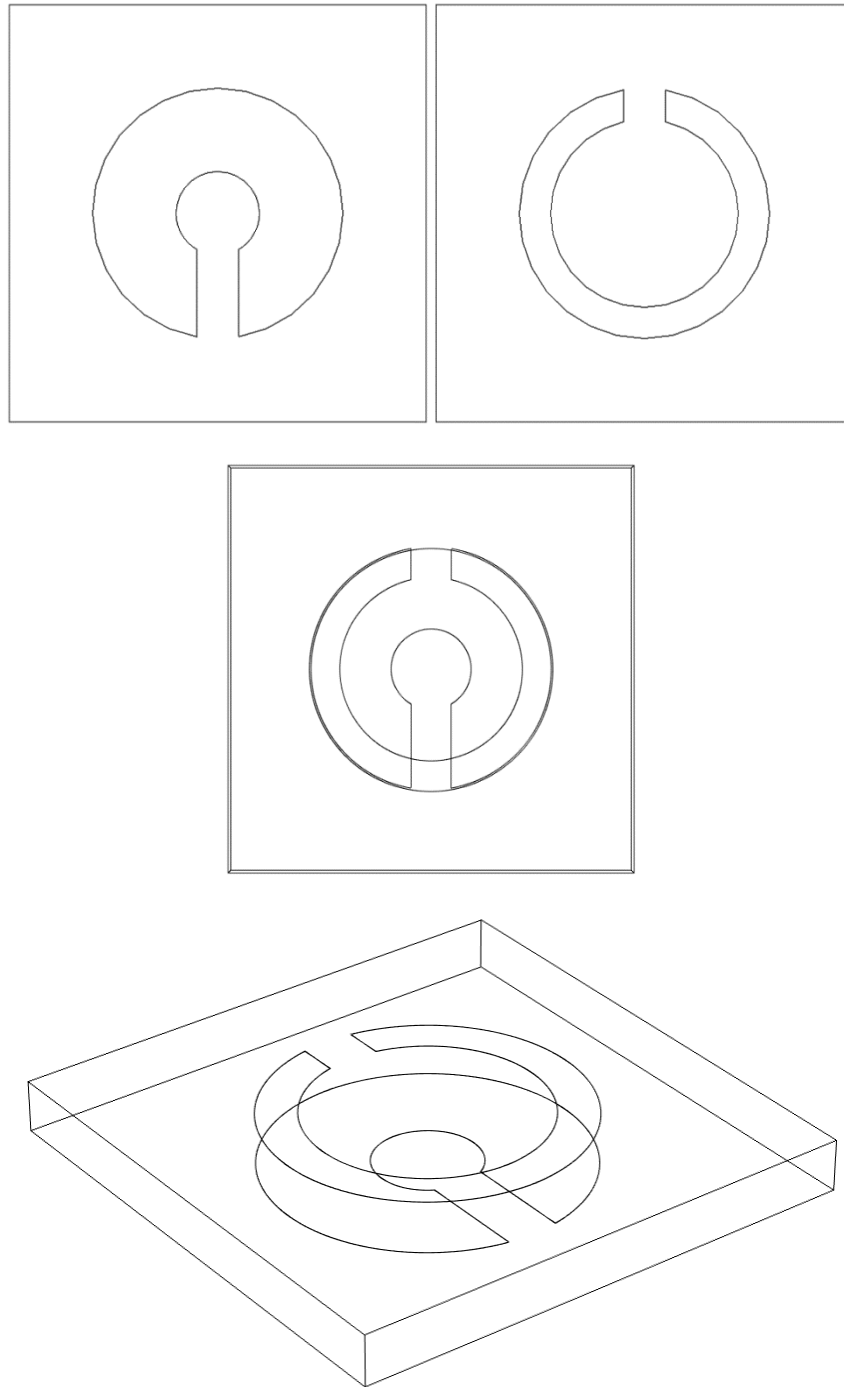
Figure 6.4 – Two inverted corral traps. The trap on the bottom electrode has a smaller inner diameter, and the trap on the top electrode has a larger inner diameter.

6.2 Spiral Patterns

The general trend for negative dielectroporesis is that a bead will go from areas of high electric field density to areas of lower electric field density. Theoretically, if a bead is located at the tip of a spiral that gradually widens as the pattern spirals out; the bead should follow the path of the spiral. While there wouldn't seem to be any practical uses for this at the moment, it could be pursued out of mere scientific curiosity. The left image in Figure 6.5 is a smooth spiral, which is basically a very long curved "V" shape. A curved "V" could be used to change the direction of a bead. The right image, while not gradual and smooth, would theoretically work since the width does increase the further out the spiral is. Also theoretically, a bead would move inward towards the tip of the spiral if it was under positive dielectrophoresis.

Figure 6.5 – Metal spiral patterns.

6.3 Continuous Electrokinetic Cycles

Figure 6.6 below shows the metal patterns that would be on the bottom and top electrodes. They would be lined up, one directly on top of the other. The patterns consist of four "V"s. Beads would first be pushed from the sharp end of a "V" to the wide end on one of the surfaces. The beads would then theoretically move towards the sharp end of the next "V" that is on the other electrode surface. The process would continue in a cycle as long as the voltage was on.
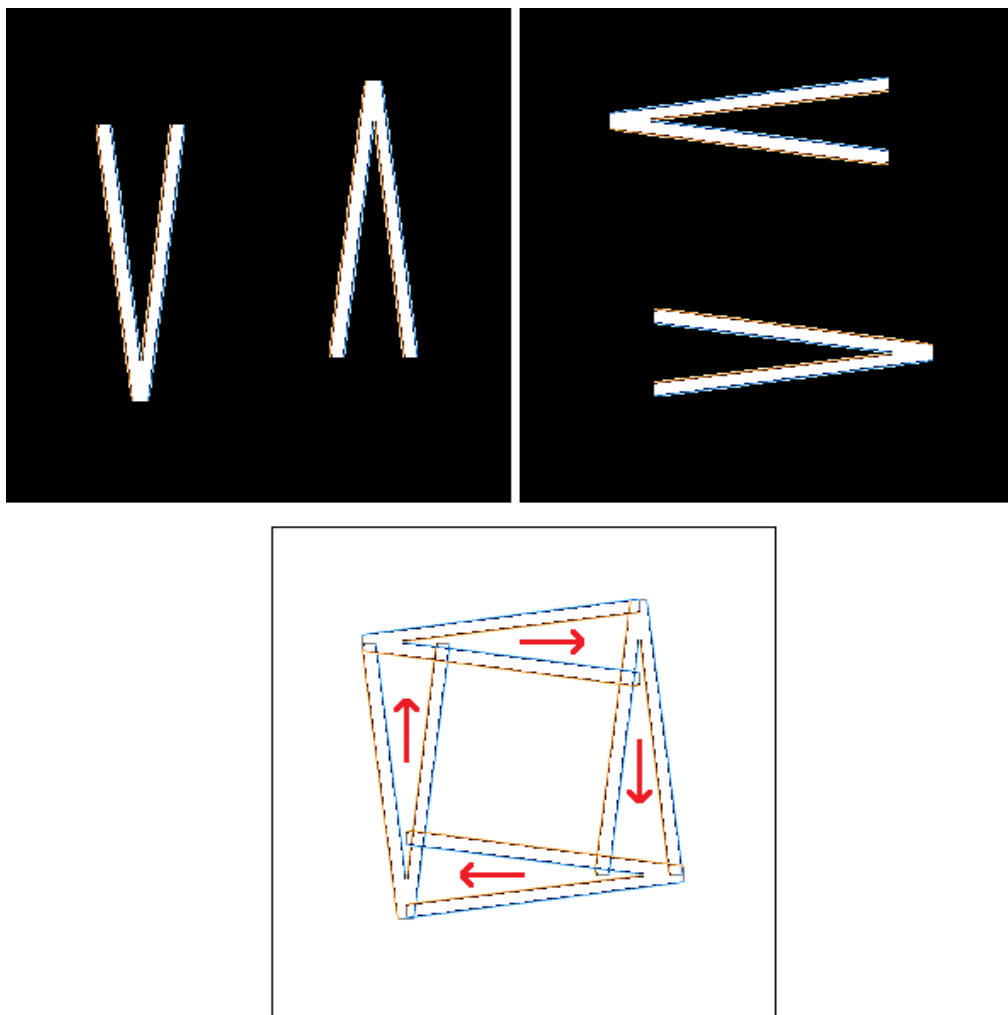
Figure 6.6 – Top images, metal patterns for the bottom and top electrodes. Bottom image, how the electrodes would line up. Red arrows indicate direction of bead flow.

6.4 Back and Forth Planar Bead Migration

This design is a slight modification to the inverted corral trap. The smaller circle would have a larger electric field density while the larger circle would have a smaller electric field density. Trapping would initially be achieved on one of the circles, then by changing the AC frequency, the beads would theoretically move back and forth between these two areas.
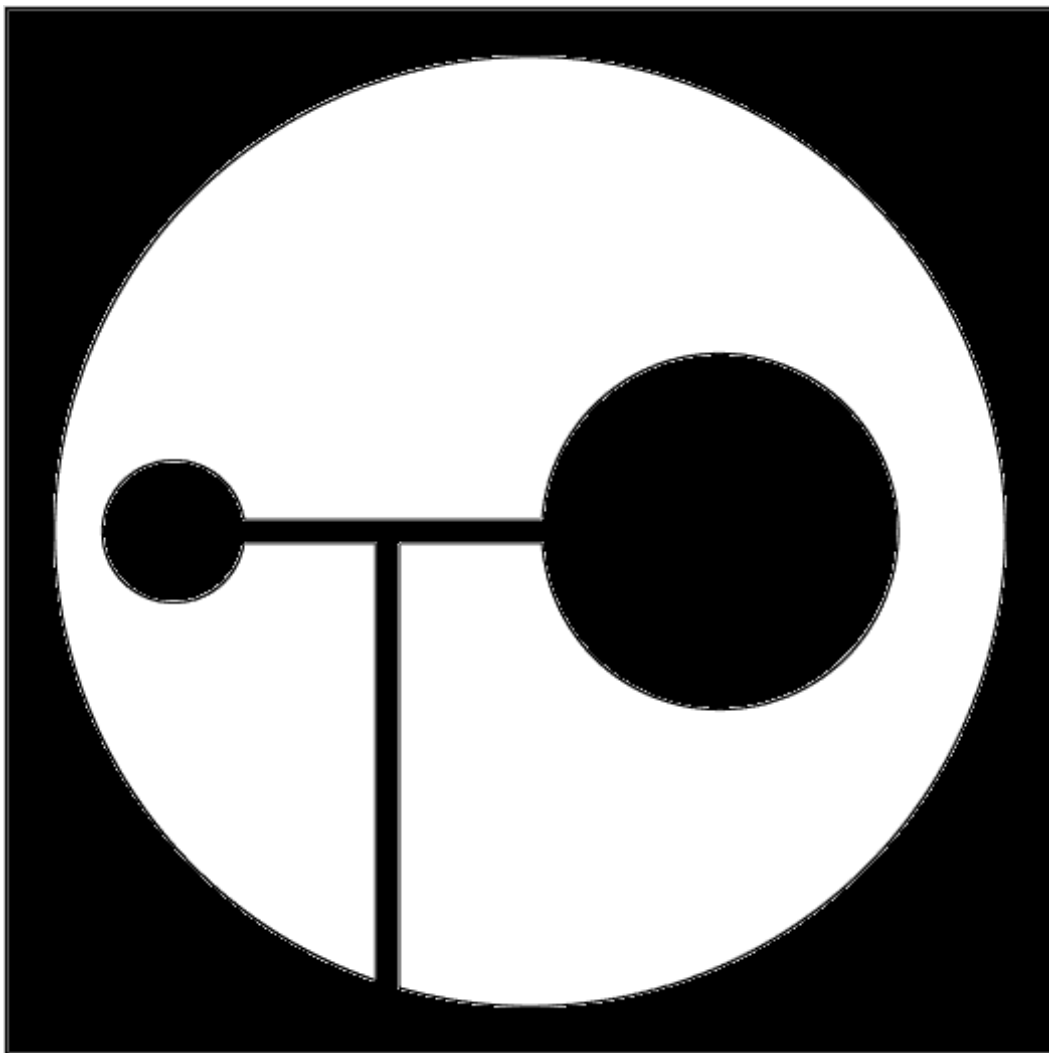
Figure 6.7 – Theoretical pattern for back and forth bead migration from one rounded end to the other rounded end.
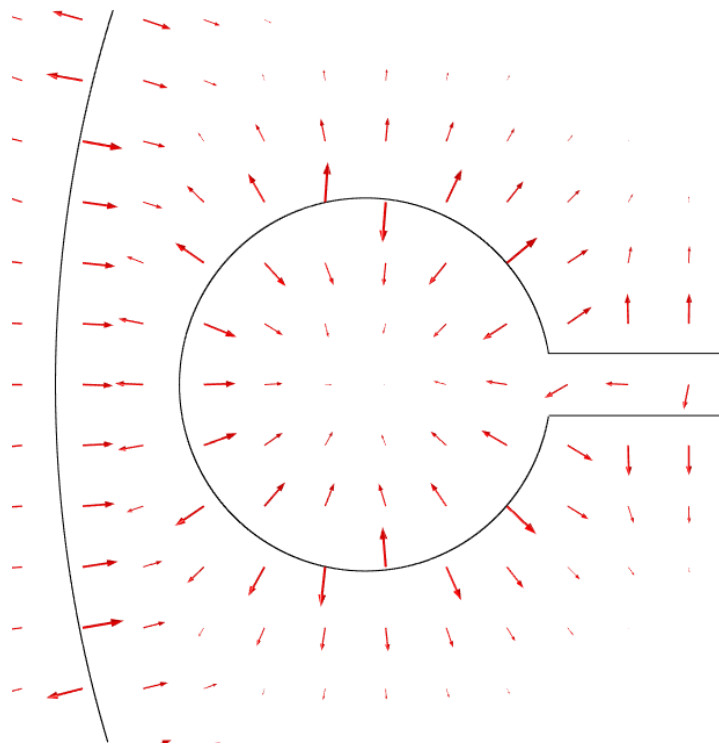
Figure 6.8 – Negative dielectrophoretic field of the smaller end.
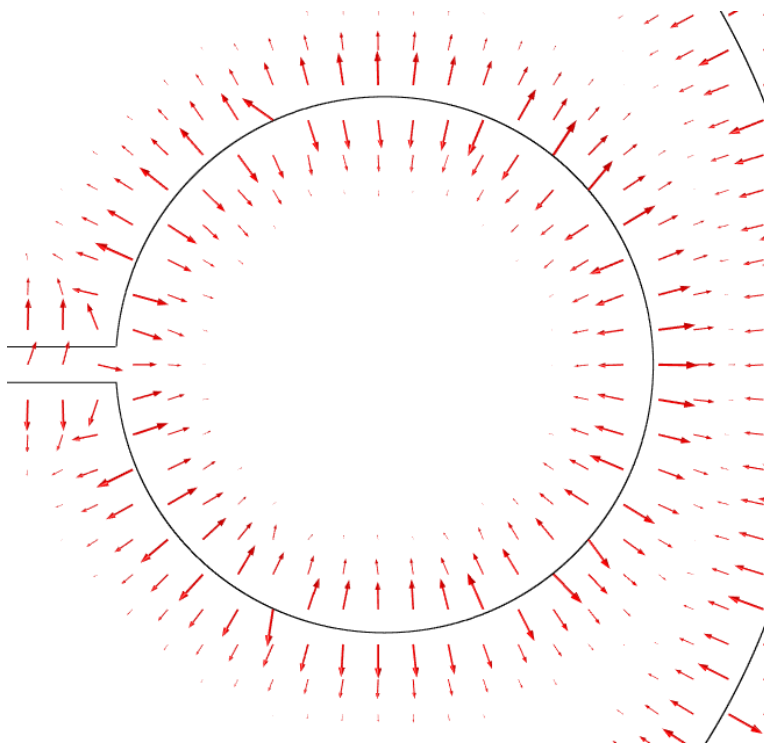
Figure 6.9 – Negative dielectrophoretic field of the larger end. This image is not scaled relative to the smaller end.

174

6.5 Tracks, Rails, Or Pathways For Beads To Follow

Tracks could be designed that would either be rectangular metal strips or rectangular voids. Figure 6.10 below shows three possible designs. Both would occur under negative dielectrophoresis. For the top images, the pathway itself is metal. This would only happen if the bead was directly on the surface of the metal. The colored beads indicate where beads would start and where they would end. For the bottom images, the pathway is a void. This would only happen if the bead was somewhere between the two electrodes.
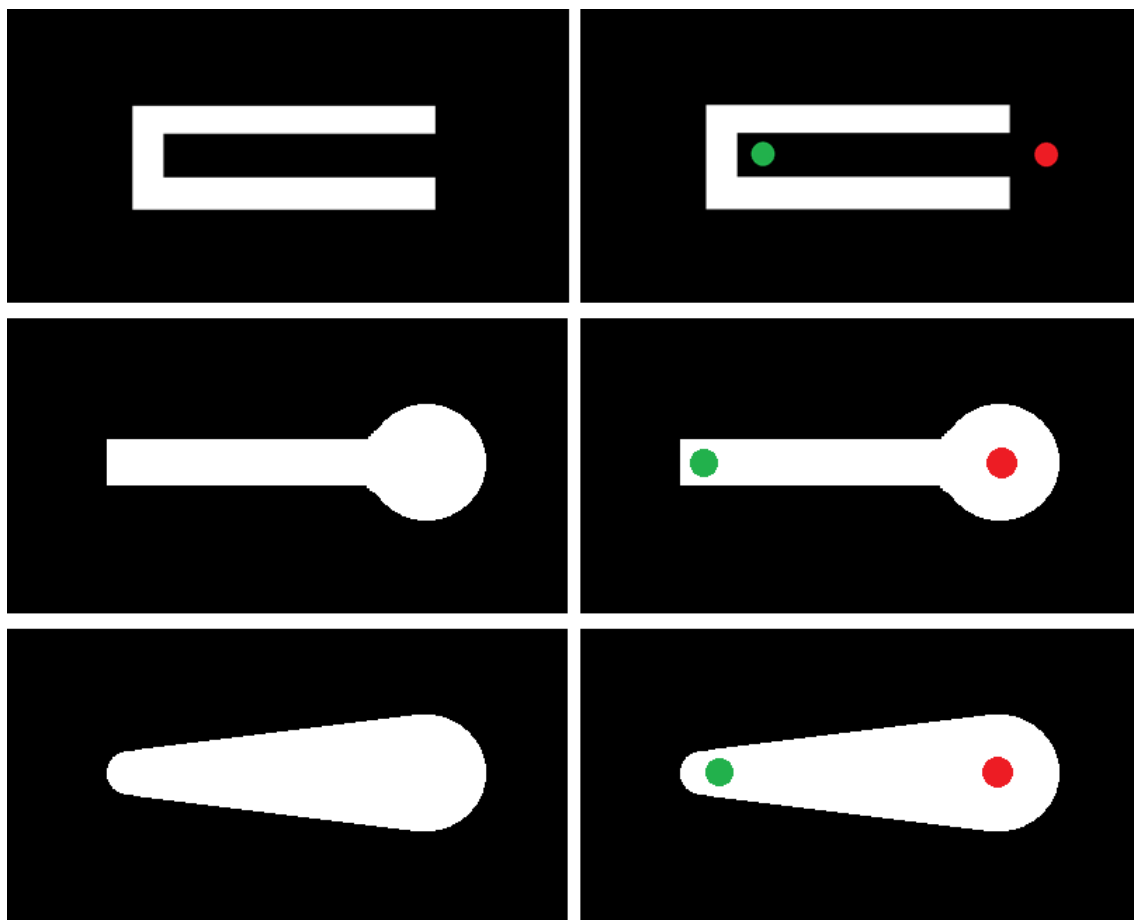
Figure 6.10 – Left images, possible designs for bead trails. Right images, green circle indicates where beads would start. Red circle indicates where beads would end up.
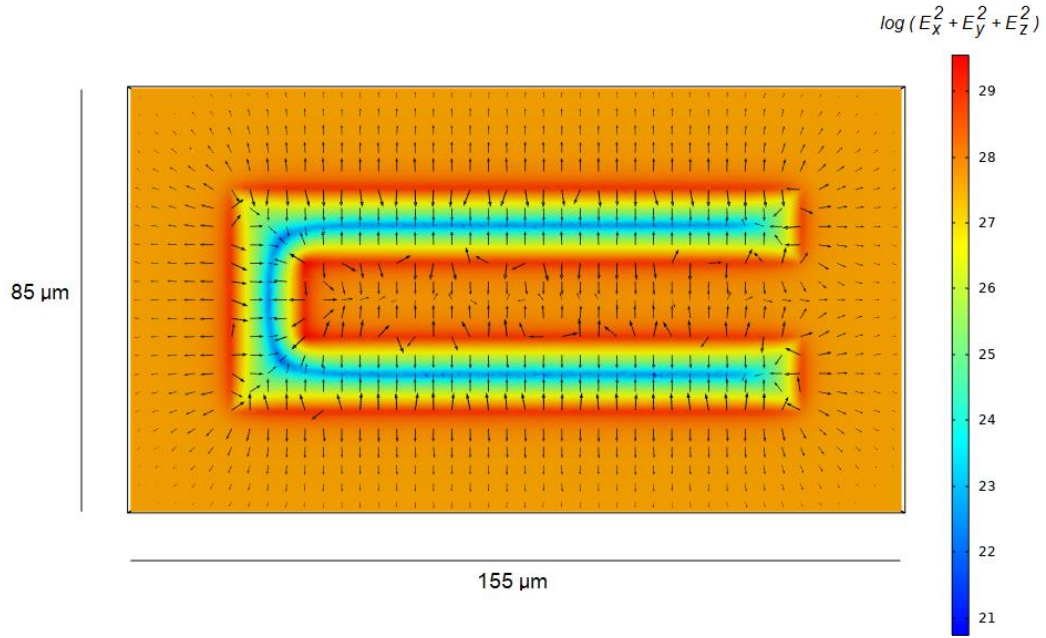
Figure 6.11 – Negative dielectrophoretic field of a "U' pattern 0.75 μm above the surface of the bottom electrode.
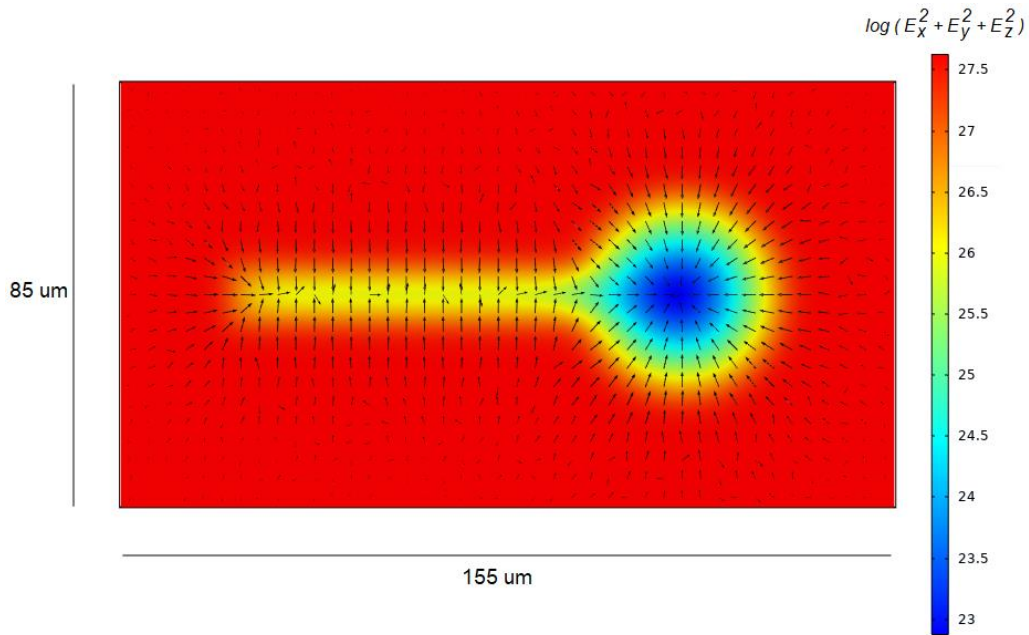
Figure 6.12 – Negative dielectrophoretic field of a thermometer pattern exactly midway between the top and bottom electrodes which are 10 μm apart.
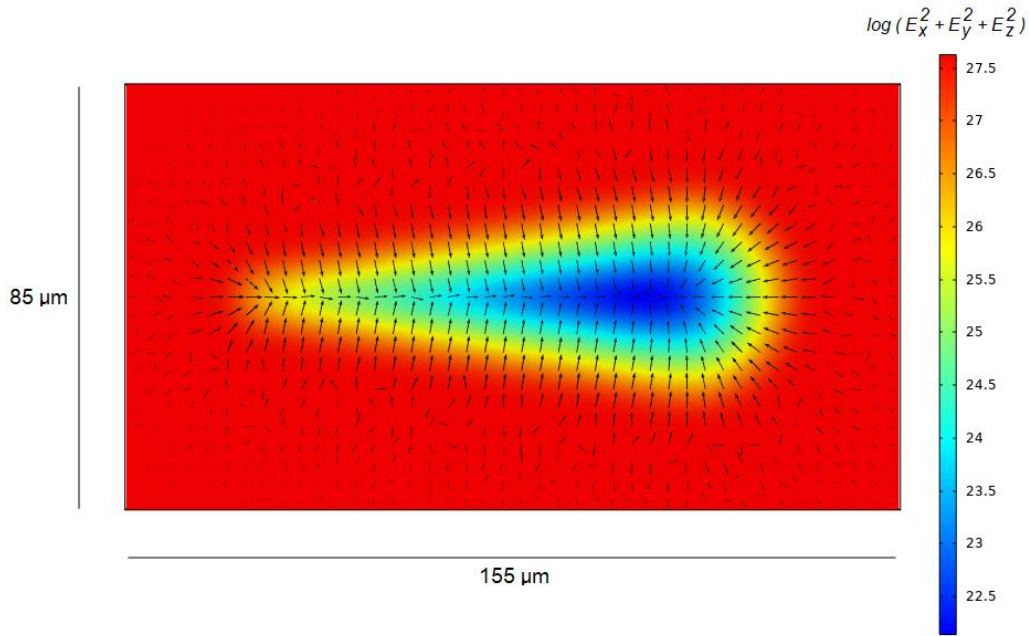
Figure 6.13 – Negative dielectrophoretic field of a teardrop pattern exactly midway between the top and bottom electrodes which are 10 µm apart.

When the dielectrophoretic fields of the three patterns are compared, the teardrop pattern clearly shows consistent forces that would push the bead from the smaller end to the larger end. The other two patterns could still potentially work due to the results of adjacent rectangles and the star trap patterns, but the bead would probably move at a slower velocity.

6.6 Linear Control of Beads
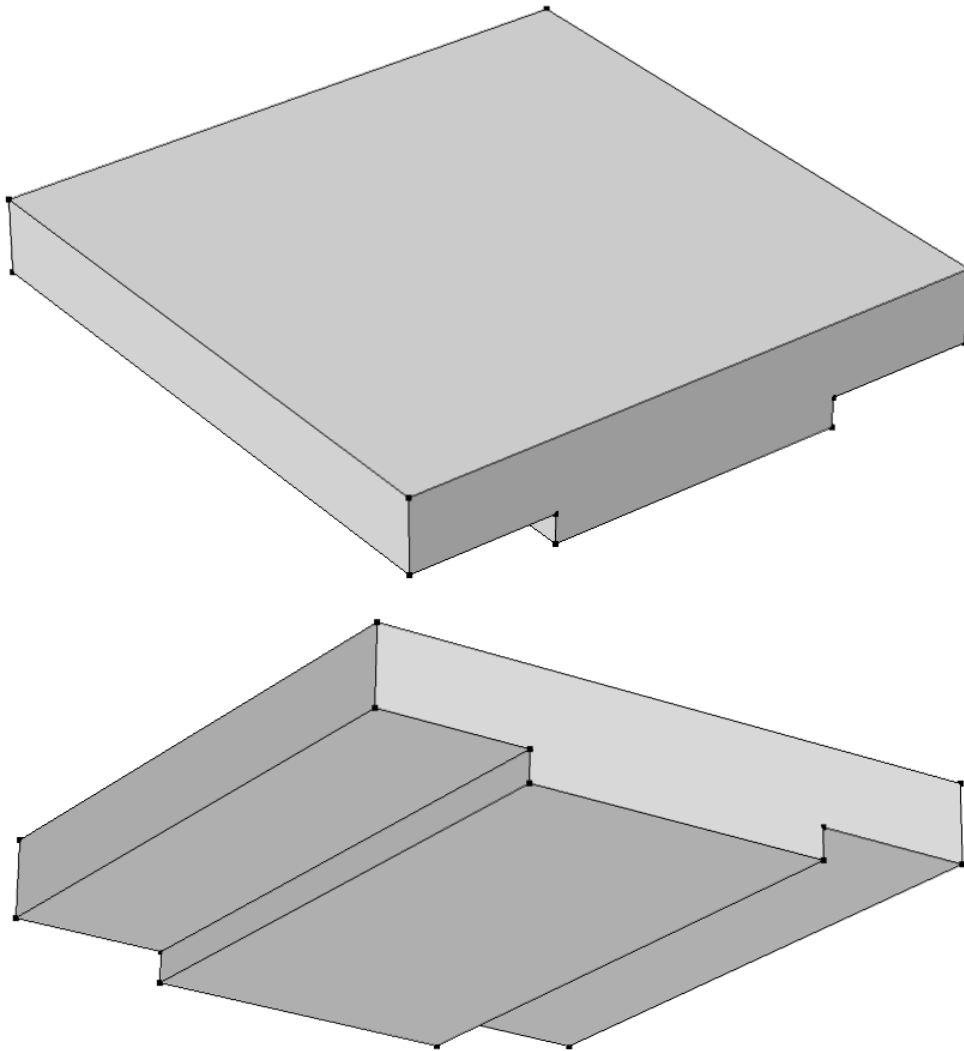
Figure 6.14 – Three dimensional geometry of the system.

Figure 6.14 above shows the exaggerated geometry of a system that consists of

two parallel metal strips that are electrically isolated from each other. The top view of the

system would be just like Figure 6.15 on the following page. The metal strips would not

be in electrical contact with each other. If voltage is turned on, beads in solution would line up midway between the two metal strips.
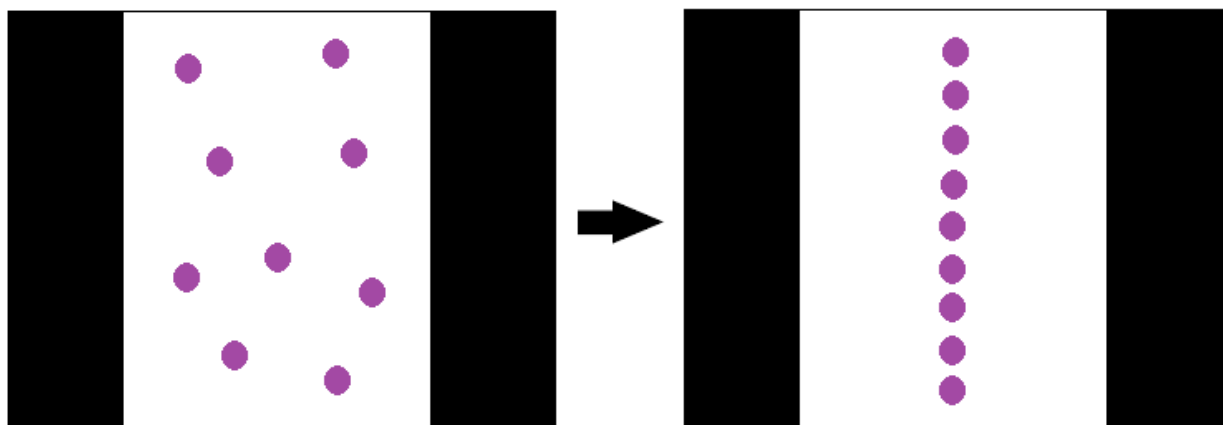
Figure 6.15 – Top view of two parallel metal strips electrically isolated from each other. The two metal strips are both bottom electrodes. Top electrode is not shown. Left, the system before voltage is turned on. Right, the system after voltage is turned on.

This should occur if the two metal strips were the exact same voltage. If the voltage of the two metal strips are changed, the left strip is changed to 10V while the right strip is changed to 0.5V, the beads would stay in a straight line but move closer to the left strip. By changing the voltages of the metal strips, the beads could be made to move back and forth between the two strips, shown in Figure 6.16 on the next page.
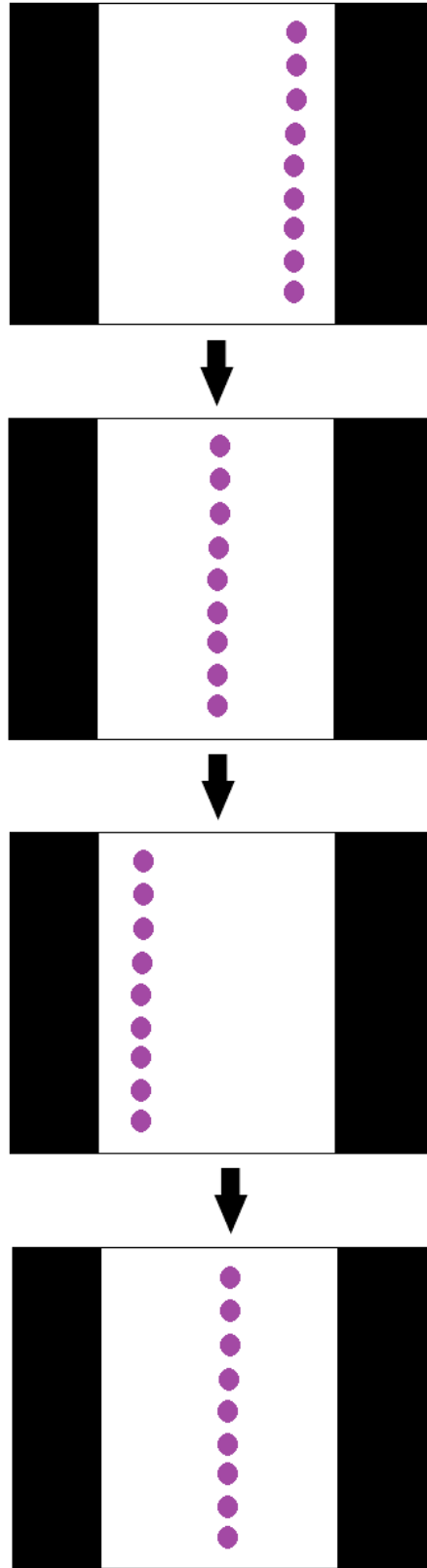
Figure 6.16 – Moving beads back and forth by changing the voltages of the metal strips.
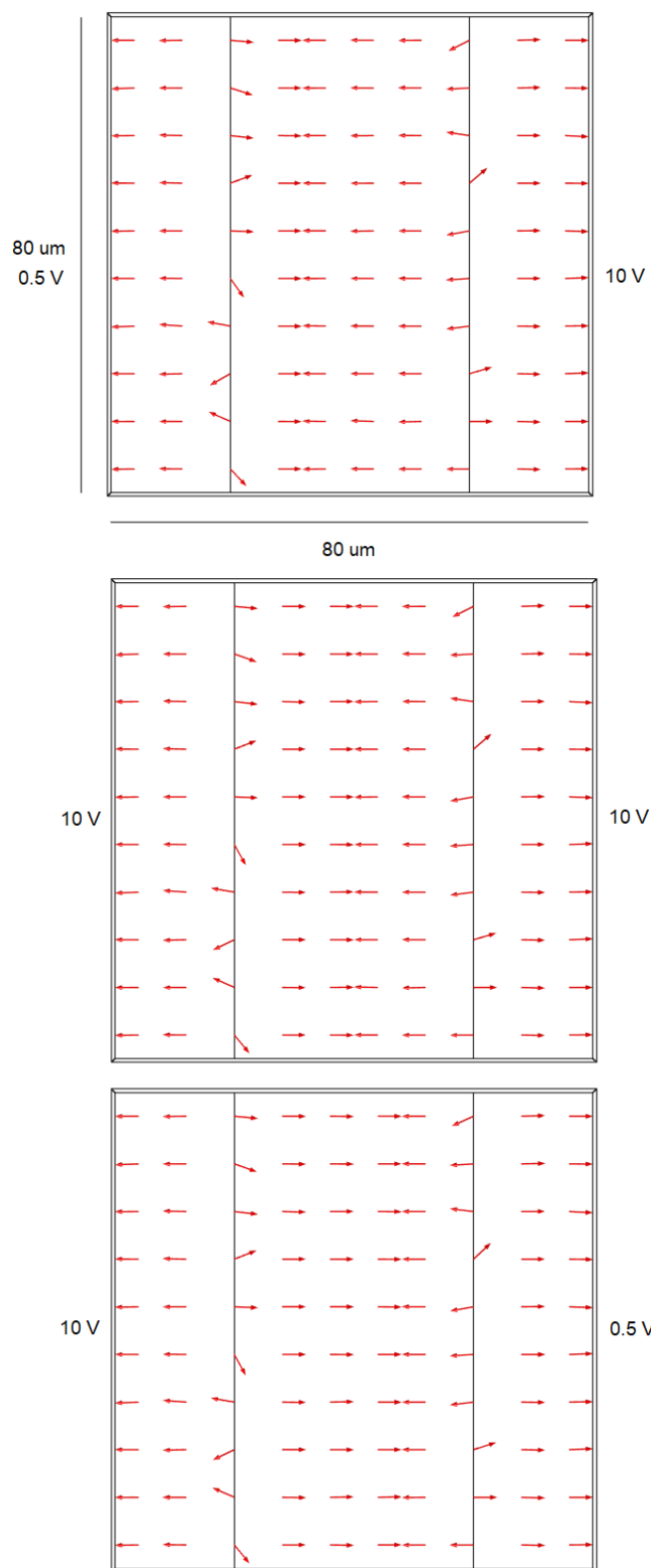
Figure 6.17 – Top view of the dielectrophoretic fields of the system with varying voltages of the metal strips. Field is 0.75 μm above the surface of the bottom electrodes.
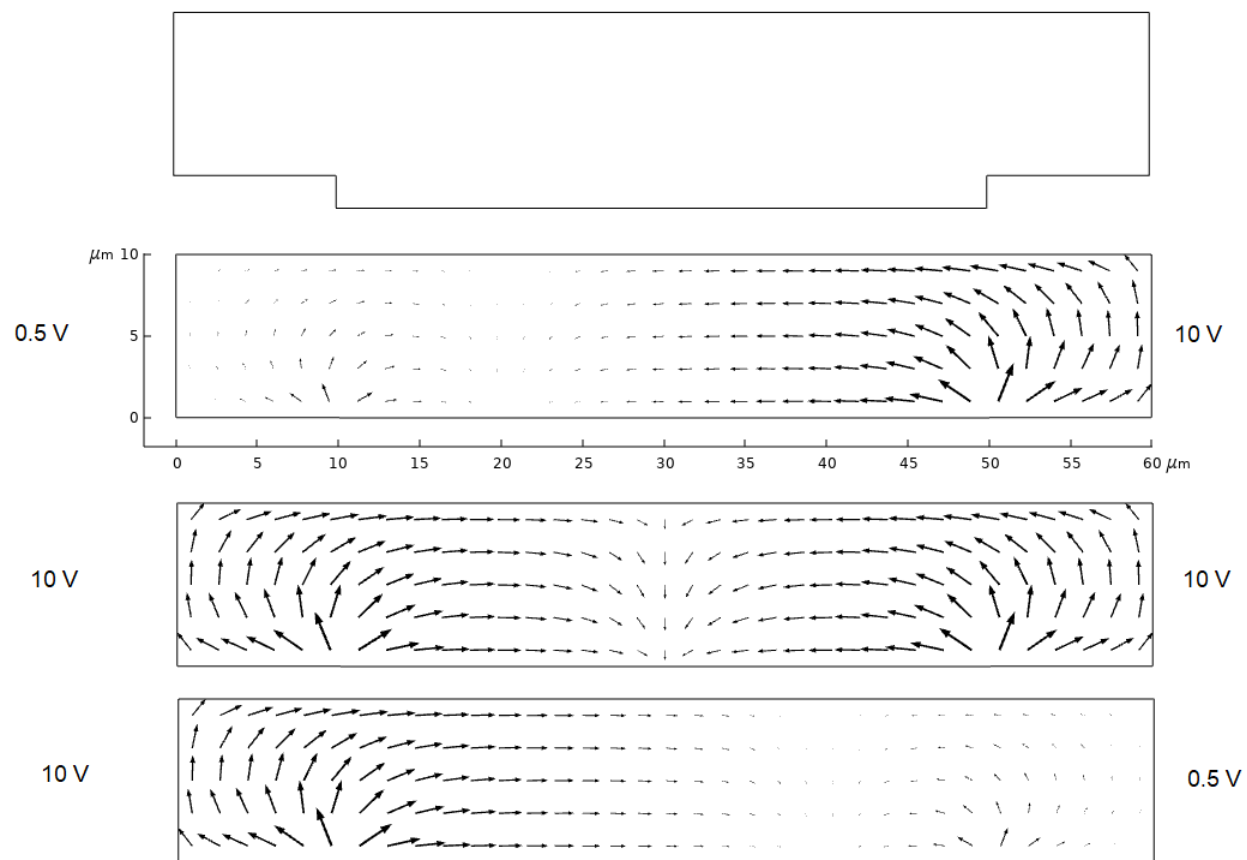
Figure 6.18 – Side view of the dielectrophoretic fields of the system with varying voltages of the metal strips.

References for Chapter 6

1. Michael J. Nasse, Jorg C. Woehl, "Realistic modeling of the illumination point spread function in confocal scanning optical microscopy", 2010, *Optical Society of America*, Volume 27, Number 2, Pages 295-302

Chapter 7

Conclusion

The main principles of this thesis are based on electric fields and how they can affect particles. There appear to be three significant forces: electrostatic forces, dielectrophoretic forces, and electro-osmotic forces. Electrostatics is the interaction between an electric field and charged particles, this leads to the phenomenon of electrophoresis. Dielectrophoresis is the interaction between a non-uniform electric field and polarizable particles. A non-uniform electric field will create a field gradient, it will have areas of high field density and areas of low field density. This field gradient is capable of polarizing particles. Electro-osmosis is the flow of solution caused by an electric field. Since electro-osmosis is solution flow, it will affect any type of particle. It doesn't matter if the particle is charged or uncharged, or polarizable or non-polarizable.

A dielectrophoretic field can only exist if the electric field is non-uniform or non-homogeneous. If the system consists of featureless flat metal surfaces, this creates a uniform electric field which can only affect charged particles. If there are voids in the metal surface, this creates a non-uniform electric field, which is then capable of generating a dielectrophoretic field. These voids can have different shapes; such as circles, rectangles, or stars. Each shape is capable of generating an electric field with its own unique geometry. Each electric field geometry can induce specific behaviors in particles. The simplest shape is a circle. The circle's geometry enables the trapping of particles because its geometry exerts symmetric and equal forces around the center of the circle. Other shapes can induce turns, push beads in a certain direction, or be used as pathways or trails. The theoretical simulations done with COMSOL all seem to correlate well with experimental observations. This means COMSOL can also be used to predict the behavior of untested geometries. The electro-osmotic velocity field, like the

185

dielectrophoretic field, is dependent on the geometry of the electric field. If the bead behavior seems to contradict the dielectrophoretic field, the behavior can generally be accounted for with electro-osmosis.

Corral trapping of charged particles with DC has still been inconsistent, however there have been isolated instances of success. The main problem has been the occurrence of electrolysis at high voltages, which degrades the electrodes. The electric field of two parallel plates is[1]

$$E = -\Delta V/d$$

ΔV is the potential difference between the two plates and d is the distance between the two plates. A strong electric field is possible with a low voltage as long as the electrodes are closer together. The key would be to get a strong enough electric field without exceeding 1.23 V, the voltage at which electrolysis occurs. This could be achieved by getting the electrodes as close as possible while still allowing the beads to be mobile. If the potential difference was 10 V and the electrodes were 25 µm apart, an equivalent electric field could be obtained with 1.2 V if the electrodes were 3 µm apart. So to corral trap a charged 2.0 µm diameter bead, the electrodes should probably be 3.0 µm apart at most in order to get the best results. Since the dielectrophoretic force is directly proportional to the cube of the radius of the particle, $F_{DEP} \propto r^3$, it is likely that trapping small particles on a molecular scale will be very difficult. On a small scale, electrostatics might be more advantageous than dielectrophoresis. So determining the optimal, consistent conditions for corral trapping with DC would still be beneficial.

Despite all of the interesting things that have already been achieved with dielectrophoresis, there doesn't appear to be an adequate fundamental study. A fundamental study would account for all possible physical phenomenon that occur during electrokinetic processes. All of the factors that must be considered would be electrostatics, dielectrophoresis, electro-osmosis, drag forces on the particle, thermal gradients, and fluid pressure gradients. As soon as a particle begins to move, a directionally opposing drag force is immediately produced. High potential differences between two electrodes would likely cause large temperature differences, so a temperature gradient might also be a key factor in observed bead behavior as well as fluid pressure gradients in the solution. Lastly, adequate "z" data, the particle's vertical height position, must also be acquired. The precise image of the bead at the surface of the bottom electrode and the image of the bead at the surface of the top electrode must be determined. The bead's size and appearance, or point spread function, could then be correlated to its height along the z axis.

The principle of using fields to manipulate and control particles can be done on a microscopic level. It is entirely possible these same principles could form the basis for nano-scale manipulation, possibly even on the single molecule level. Ultimately, a metal pattern that incorporates numerous geometries could potentially be used in a multi-step micro-scale manufacturing process.

References For Chapter 7

1.   Wayne E. Haven, Robert W. Pidd, *Physics*, 1965, Addison-Wesley Publishing Company, Inc., Reading, Massachusetts

Xavier Sacro Udad

University of Wisconsin-Milwaukee
Department of Chemistry
3210 N Cramer St
Milwaukee, WI 53211

Education

University of Wisconsin-Milwaukee, Milwaukee, WI - Current
PhD Student in Chemistry - Current

- Areas of Concentration or Major: Chemistry
- Pending Dissertation/Thesis:
    - Controlling and manipulating microscopic particles in solution by using various electric field geometries

DePaul University, Chicago, IL - 2011
MS in Chemistry - 2011

- Areas of Concentration or Major: Chemistry
- Dissertation/Thesis:
    - Investigating the process of fibril formation of the Iowa mutant of the Alzheimer's peptide

University of Illinois, Chicago, IL - 2001
BS in Chemistry - 2001

- Areas of Concentration/Major: Chemistry

College of Lake County, Grayslake, IL – 1998
AS – 1998

- Areas of Concentration/Major: Chemistry

Professional Skills

Fluorescence Microscopy	Photolithography
Confocal Microscopy	Metal Deposition
Scanning Electron Microscopy	Optical Systems

Teaching and Research Experience

- Fall 2011 – Present
Research Assistant, UWM

- Fall 2019
Teaching Assistant, UWM
Course: CHEM 100 – Chemical Science
    CHEM 105 – General Chemistry for Engineering

- Spring 2019
Teaching Assistant, UWM
Course: CHEM 104 – General Chemistry II
    CHEM 561 – Physical Chemistry I

- Fall 2018
Teaching Assistant, UWM
Course: CHEM 104 – General Chemistry II
    CHEM 562 – Physical Chemistry II

- Spring 2018
Teaching Assistant, UWM
Course: CHEM 104 – General Chemistry II
    CHEM 561 – Physical Chemistry I

- Fall 2017
Teaching Assistant, UWM
Course: CHEM 104 – General Chemistry II
    CHEM 561 – Physical Chemistry II

- Spring 2017
Teaching Assistant, UWM
Course: CHEM 104 – General Chemistry II

- Fall 2016
Teaching Assistant, UWM
Course: CHEM 104 – General Chemistry II
    CHEM 105 – General Chemistry for Engineering

- Summer 2016
Teaching Assistant, UWM
Course: CHEM 104 – General Chemistry II

- Spring 2016
  Teaching Assistant, UWM
  Course: CHEM 104 – General Chemistry II
          CHEM 561 – Physical Chemistry I

- Fall 2015
  Teaching Assistant, UWM
  Course: CHEM 104 – General Chemistry II

- Spring 2015
  Teaching Assistant, UWM
  Course: CHEM 104 – General Chemistry II
          CHEM 561 – Physical Chemistry I

- Fall 2014
  Teaching Assistant, UWM
  Course: CHEM 104 – General Chemistry II

- Fall 2013
  Teaching Assistant, UWM
  Course: CHEM 101 – Chemical Science for Nurses
          CHEM 562 – Physical Chemistry II

National Conferences

Poster Presentations

- "Immobilizing a DNA molecule within an electrostatic corral", Xavier S. Udad, Alaknanda A. Patel, Christine A. Carlson, and Jörg C. Woehl, SciX Conferenece, Milwaukee, WI – September 29, 2013

- "Trapping a single DNA molecule within an electrical field", Xavier S. Udad, Alaknanda A. Patel, Christine A. Carlson, and Jörg C. Woehl, SciX Conference, Kansas City, MO – September 30, 2012

Regional Conferences

Oral Presentations

- "Controlling and manipulating microscopic particles in solution by using various electric field geometries", Xavier S. Udad and Jörg C. Woehl, ACS Regional Meeting, Lisle, IL – May 2, 2019

Poster Presentations

- "Isolating a single DNA molecule inside a corral trap", Xavier S. Udad, Alaknanda A. Patel, Christine A. Carlson, and Jörg C. Woehl, ACS Regional Meeting, La Crosse, WI – 2013

<div align="center">

Departmental Symposiums

</div>

Poster Presentations

- "Controlling and manipulating microscopic particles in solution by using various electric field geometries", Xavier S. Udad, Quintus S. Owen, Erika R. Johansen, Christine A. Carlson, and Jörg C. Woehl, Chemistry Department Awards Day, University of Wisconsin-Milwaukee, Milwaukee, WI – May 2019

- "Electrokinetic trapping of particles with a corral trap that is implemented into a microfluidic system", Xavier S. Udad, Christine A. Carlson, and Jörg C. Woehl, Chemistry Department Awards Day, University of Wisconsin-Milwaukee, Milwaukee, WI – May 2018

- "Corral trapping of nanoparticles in solution", Xavier S. Udad, Christine A. Carlson, and Jörg C. Woehl, Chemistry Department Awards Day, University of Wisconsin-Milwaukee, Milwaukee, WI – May 2017

- "Fabrication of a glass microfluidic flowcell for single particle tracking", Xavier S. Udad, Quintus S. Owen, Richard Kellow, and Jörg C. Woehl, Chemistry Department Awards Day, University of Wisconsin-Milwaukee, Milwaukee, WI – May 2016

- "Confining charged particles in solution with an electrical field generated by a corral trap", Xavier S. Udad, Quintus S. Owen, Alaknanda A. Patel, Christine A. Carlson, and Jörg C. Woehl, Chemistry Department Awards Day, University of Wisconsin-Milwaukee, Milwaukee, WI – May 2015

- "Theoretical electrokinetics and possible applications for immobilized charged particles", Xavier S. Udad, Alaknanda A. Patel, Christine A. Carlson, and Jörg C. Woehl, Chemistry Department Awards Day, University of Wisconsin-Milwaukee, Milwaukee, WI – May 2014

Events

- Graduate Student Research Symposium, Organizer, University of Wisconsin-Milwaukee, Milwaukee, WI – October 28, 2016

Awards

- Chemistry Supplemental Instruction Award, Chemistry Department Awards Day, University of Wisconsin-Milwaukee, Milwaukee, WI – May 2018